EFFECT OF E-BEAM STERILIZATION ON POLYPROPYLENE/ETHYLENE PROPYLENE DIENE MONOMER AND ETHYLENE VINYL ACETATE THERMOPLASTIC ELASTOMER

ANAND BELLAM BALAJI

Thesis submitted to University of Nottingham

for the degree of Doctor of Philosophy

February 2018

ABSTRACT

Thermoplastic elastomer is one of the priority polymeric compound identified for promotion and further development, given the growing demand for a number of commercial industries such as automobile, construction, footwear, healthcare, medical and food packaging sectors. In this study polypropylene (PP)/ethylene propylene diene monomer (EPDM) based thermoplastic elastomers are preferred for improving their properties as it can serve as a good replacement for PP or EPDM material, bridging the gap between thermoset and thermoplastic materials. This study focuses to develop PP/EPDM which can resist changes or improve properties when exposed to E-beam radiation, as E-beam also offers sustainable sterilization at low cost.

The PP/EPDM blends with mixing ratios of 80/20, 50/50 and 20/80 were melt blended with the process parameters optimized using Design of experiments (DOE). The effect of E-beam on mechanical properties, thermal stability, crystallization and dynamic mechanical properties over the dose of 0 to 100 kGy were studied. The blends with high EPDM content (20PP/80EPDM) showed improvement in tensile strength up to 36% (at 40kGy and 60kGy) and resistant to impact strength up to 100 kGy, at the expense of elongation at break. On the other hand, the blends with high PP content (80 PP/20 EPDM and 50 PP/50 EPDM) showed detrimental effects on mechanical properties at all radiation dose studied and found to be not compatible for E-beam sterilization.

Further, ethylene vinyl acetate (EVA) was incorporated to PP/EPDM blends at 10EVA/40EPDM/50PP, 20EVA/30 EPDM/50PP, 30EVA/20 EPDM/50PP and 40EVA/10 EPDM/50PP ratios. The gel content analysis showed that the efficiency of crosslinking decreased with increase in EVA loading. However, the presence of EVA in ternary blend especially facilitated the induction of sufficient crosslinks leading to improvement in tensile strength (up to 29% at 60 kGy), impact strength (up to 15% at 80 kGy) and retention of stiffness and thermal properties under radiation at the expense of elongation at break.

In order to develop antibacterial ternary blends, silver nanoparticles (AgNP) were added by varying the loading from 0.3wt% to 1wt%. The Ag-ternary blends showed enhancement in impact properties (up to 9%) at the expense of decrement in tensile properties due to the agglomeration of AgNP. When, exposed to E-beam radiation, the mechanical and thermal

properties exhibited similar trend of increment and decrement across radiation dose similar to the blends without AgNP. While, 1% Ag blend composites showed bacteriostatic effect on Staphylococcus aureuson, no significant reduction of Pseudomonas aeruginosa bacteria was observed. All the blends, before and after sterilization showed no significant toxicity on HaCaT cells investigated using *in vitro* analysis. Thus, the blends showed an instinct that their application could be extended to manufacturing of healthcare products and food packaging sector, as they are biocompatible and can withstand E-beam sterilization as demanded by the respective application. Among all the blends ternary blends studied (that exhibited biocompatibility even after radiation), 20EVA/30EPDM/50PP without AgNP showed the highest tensile strength of 18.41 MPa and impact strength of 43.64 J/m. Only a slight increase in tensile and impact properties was witnessed upon addition of 20% EVA to PP/EPDM blend in comparison to the binary blend (50PP/50EPDM blend). However, unlike the binary blend (whose properties decreased upon radiation), the ternary blend (20EVA/30EPDM/50PP) showed improvement in tensile strength up to 29% at 60kGy and up to 15% increase in impact strength at 80kGy.

LIST OF PUBLICATIONS

Journal Publications

BALAJI, A. B., KHALID, M., RATNAM, C. T., MICHAEL, F. M. & WALVEKAR, R. 2017. Co-PP/EPDM Blend Optimization Using D-Optimal Design for Medical Applications. *Polymer-Plastics Technology and Engineering,* 56**,** 216-226.

BALAJI, A. B., RATNAM, C. T., KHALID, M. & WALVEKAR, R. 2017. Effect of electron beam irradiation on thermal and crystallization behavior of PP/EPDM blend. *Radiation Physics and Chemistry,* 141**,** 179-189.

BALAJI, A. B., RATNAM, C. T. & KHALID, M. 2018. E-beam sterilizable thermoplastics elastomers for healthcare devices: Mechanical, morphology, and in vivo studies. *Journal of Biomaterials Applications,* 32**,** 1049-1062.

Conference Presentations

BALAJI, A. B., KHALID, M. & RATNAM, C. T. 2016. Characteristics of E-beam Sterilized PP/EPDM blends for Medical Applications. *International Conference on Advanced Polymeric Materials [IUPAC PSK 40],Jeju,South Korea.*

BALAJI, A. B., KHALID, M. & RATNAM, C. T. 2018. Investigation of Ethylene vinyl acetate (EVA)/ Ethylene propylene diene monomer (EPDM)/Polypropylene (PP) ternary polymer mixture using simplex centroid design. *European Advanced Materials Congress,Stockholm,Sweden.*

I dedicate this thesis to my beloved parents,

Mr. Bellam Balaji and Mrs. Kavitha Balaji

ACKNOWLEDGEMENT

Firstly, I would like to express my deepest gratitude to **Dr. Mohammad Khalid Siddiqui** and **Dr. Chantara Thevy Ratnam** for giving me this opportunity, support, patience, encouragement and constant supervision throughout my research. Their scholarly advice and scientific approach has assisted me to a great extent in accomplishing my study. I also owe a deep sense of gratitude to **Dr. Lim Siew Shee** for her guidance on in-vitro studies and for her in evitable suggestions on completion of my thesis. I would also like to thank **Dr. Cheng Foh** for helping me on antibacterial studies.

I am extremely thankful to all the technicians at UNMC and Nuklear Malaysia, especially **Mr. Wan Ali, Ms. Fatihah, Mr. Fareez, Ms. Khairani** and **Mr. Hasnul** for their willingness to help on characterization techniques and equipment handling.

My thanks and appreciation also extends to **Dr. Suganti Ramrad**, **Dr. Feven Matthews Michael** and all my PhD colleagues who have willingly helped me with their abilities. And finally, I am thankful to all my friends and family who always believed in me and have been supportive during my study period.

TABLE OF CONTENTS

ABSTRACT i

LIST OF PUBLICATIONS iii

ACKNOWLEDGEMENT v

LIST OF FIGURES xii

LIST OF TABLES xviii

1 INTRODUCTION 1

1.1 Introduction 2

1.2 Problem Statement 3

1.3 Scope 3

1.4 Aims and Objectives 4

1.5 Significance of the Research 5

1.6 Thesis Outline 6

2 LITERATURE REVIEW 8

2.1 Introduction 9

2.2 PP/EPDM blends 10

2.3 Sterilization 16

2.4 Effect of Ionizing radiation on Polypropylene, PP/EPDM and PP/EVA blends 24

2.5 Overview on Antimicrobial Polymer composites 34

2.6 Summary 41

3 METHODOLOGY 43

3.1 Introduction 44

3.2 Materials 44

3.3 Blending 44

3.4 Compression Moulding 45

3.5 Electron Beam Irradiation 45

3.6 Gel Content 45

3.7 Tensile Properties 46

3.8 Impact Strength 46

3.9 Hardness Test 46

3.10 Thermogravimetric Analysis 47

3.11 Differential Scanning Calorimetry 47

3.12 Dynamic Mechanical Analysis 48

3.13 Fourier Transform Infrared Spectroscopy 48

3.14 Yellow Index 48

3.15 *In Vitro* Analysis 48

4 OPTIMIZATION OF PROCESSING PARAMETERS FOR PP/EPDM BLENDING USING DESIGN OF EXPERIMENT 53

4.1 Introduction 54

4.2 Design of Response Surface Methodology 54

4.3 Fit of Regression Model 58

4.4 Evaluation of Regression Model 58

4.5 Comprehensive investigation of the effect of blending parameters on the tensile strength and maximum elongation of PP/EPDM blends 63

4.6 Analysis of 3D Response curve 64

4.7 Optimization 67

4.8 Summary 69

5 EFFECT OF E-BEAM IRRADIATION ON POLYPROPYLENE (PP)/ ETHYLENE PROPYLENE DIENE MONOMER (EPDM) BLENDS 70

5.1 Introduction 71

5.2 Gel Content 72

5.3 Tensile Strength 75

5.4 Elongation at Break 77

5.5 Impact Strength 78

5.6 Hardness 80

5.7 Thermogravimetric Analysis 81

5.8 Differential Scanning Calorimetry 84

5.9 Dynamic Mechanical Analysis 87

5.10 Scanning Electron Micrographs 97

5.11 Fourier Transform Infrared Spectroscopy 101

5.12 Yellow Index 104

5.13 Summary 105

6 PREDICTION OF MECHANICAL PROPERTIES OF POLYPROPYLENE (PP)/ ETHYLENE PROPYLENE DIENE MONOMER (EPDM) AND ETHYLENE VINYL ACETATE (EVA) TERNARY BLENDS USING DESIGN OF EXPERIMENTS 106

6.1 Introduction 107

6.2 Experimental Design 107

6.3 Fitting of model and Analysis of Variance (ANOVA) 109

6.4 Tensile and Impact property profile of ternary blend obtained using Design of Experiments 114

6.5 Validation of mechanical properties of ternary Blend: 117

6.6 Summary 119

7 EFFECT OF E-BEAM IRRADIATION ON POLYPROPYLENE (PP)/ ETHYLENE PROPYLENE DIENE MONOMER (EPDM) AND ETHYLENE VINYL ACETATE (EVA) TERNARY BLENDS .. 120

7.1 Introduction 121

7.2 Gel Content 122

7.3 Tensile Properties 125

7.4 Impact Strength 127

7.5 Thermogravimetric Analysis 129

7.6 Differential Scanning Calorimetry 131

7.7 Dynamic Mechanical Analysis 138

7.8 Scanning Electron Micrographs 146

7.9 Visual Appearance 150

7.10 Summary 151

8 EFFECT OF E-BEAM ON POLYPROPYLENE (PP)/ ETHYLENE PROPYLENE DIENE MONOMER (EPDM) AND ETHYLENE VINYL ACETATE (EVA) TERNARY BLENDS CONTAINING SILVER NANOPARTICLES 152

8.1 Introduction 153

8.2 SEM and Elemental Analysis 153

8.3 Gel Content Analysis 155

8.4 Tensile Strength 156

8.5 Elongation at Break 157

8.6 Impact Strength 158

8.7 Thermogravimetric Analysis 160

8.8 Differential Scanning Calorimetry 163

8.9 *In-vitro* Analysis 169

8.10 Antimicrobial Studies 178

8.11 Visual Appearance 181

8.12 Summary 182

9 PRINCIPLE FINDINGS AND RECOMMENDATIONS FOR FURTURE WORK 183

9.1 Principal Findings 184

9.2 Future Prospects 186

REFERENCES 188

LIST OF FIGURES

Figure 2.1 Schematics of peroxide crosslinking (Aprem et al., 2005) 14

Figure 2.2 Cost of sterilization by E-beam, Gamma and X-ray technologies (Iba, 2014)..... 22

Figure 2.3 Mechanisms for the antimicrobial behaviour of polymer/metal nanocomposites with AgNP (Palza, 2015). 39

Figure 3.1 Procedures for cell fixing 50

Figure 4.1 Normal Plot for Tensile Strength 60

Figure 4.2 Normal Plot for Elongation at Break 61

Figure 4.3 Comparison of Predicted vs actual properties of (A) Tensile Strength and (B) elongation at break 62

Figure 4.4 Residuals Vs Run for (A) Tensile strength and (B) Elongation at break 62

Figure 4.5 Residuals vs Predicted plot for (A) Tensile strength and (B) Elongation at break 63

Figure 4.6 Perturbation plot for (A) Tensile strength and (B) Elongation at break 64

Figure 4.7 3D plot of D-optimal-RSM showing effect of time and composition ratio on tensile strength 65

Figure 4.8 3D plot of D-optimal-RSM showing effect of temperature and screw speed on elongation at break 66

Figure 4.9 3D plot of D-Optimal-RSM showing effect of time and composition ratio on elongation at break 67

Figure 5.1 Schematic showing inter and intra crosslinking between PP and EPDM before and after E-beam radiation 72

Figure 5.2 Gel content of PP, EPDM and PP/EPDM blends at varied radiation dosage.....73

Figure 5.3 Tensile strength of PP/EPDM as a function of radiation dose 76

Figure 5.4 Elongation at break of PP/EPDM blends as a function of irradiation dose 78

Figure 5.5 Impact strength of PP/EPDM blends as function of radiation dose.....80

Figure 5.6 Hardness of PP/EPDM blends as a function of irradiation dose 81

Figure 5.7 TGA thermograms of (A) PP/EPDM blends before radiation (B) 100% PP (C) 80% PP (D) 50%PP (E) 20%PP and (F) 100% EPDM.....82

Figure 5.8 DSC Thermo grams for PP/EPDM blends before radiation.....84

Figure 5.9 Temperature dependence of Tan delta curve – (A) PP/EPDM blends before radiation (B) 100% PP (C) 80% PP (D) 50% PP (E) 20% PP and(F) 100% EPDM.....91

Figure 5.10 Temperature dependence of storage modulus of (A) 100% PP (B) 80% PP (C) 50% PP (D) 20% PP and (E) 100% EPDM 94

Figure 5.11 Temperature dependence of loss modulus of (A) 100% PP (B) 80% PP (C) 50% PP (D) 20% PP and (E) 100% EPDM 96

Figure 5.12 SEM image for 100% PP (A) before radiation and (B) after radiation at 40 kGy97

Figure 5.13 Impact fractograph for 100% PP (A) before radiation (B) radiated at 40 kGy ...98

Figure 5.14 SEM images of blends before radiation (A) 80%PP and (B) 50%PP 98

Figure 5.15 Morphology of 50%PP blend (A) radiation dose 40 kGY and (B) radiation dose 80 kGy 100

Figure 5.16 Morphology of 20% PP blend (A) before radiation (B) radiated at 40 kGy..... 100

Figure 5.17 SEM micrographs of 20%PP (A) before radiation (B) 40 kGy..... 101

Figure 5.18 FTIR spectrum of 20PP/80EPDM blend at various radiation dose 104

Figure 5.19 Yellow index of PP/ EPDM blend with increasing radiation dosage 105

Figure 6.1 Three component simplex centroid design with extreme limits (augmented) (where A=EPDM, B=PP and C=EVA) 108

Figure 6.2 Normal Residual plots (A) Tensile strength (B) Elongation at break and (C) Impact strength 111

Figure 6.3 Residual vs runs plots (A) tensile strength (B) elongation at break and (C) impact strength 112

Figure 6.4 Actual vs. predicted plot (A) tensile strength (B) elongation at break and (C) impact strength 113

Figure 6.5 Tensile strength property chart for PP/EPDM/EVA blend 114

Figure 6.6 Elongation at break chart for PP/EPDM/EVA blend 115

Figure 6.7 Impact strength chart for PP/EPDM/EVA blend 116

Figure 6.8 SEM micrographs of (A) 30EPDM/20EVA/50PP ternary blend and (B) 50PP/50EVA 118

Figure 7.1 Schematic of inter and intra crosslinking of PP,EVA and EPDM 122

Figure 7.2 Gel content analysis of neat polymers, binary and ternary blends 123

Figure 7.3 Tensile strength of PP/EVA and PP/EVA/EPDM blends as a function of radiation dose 125

Figure 7.4 Elongation at break of PP/EVA and PP/EVA/EPDM blends as a function of radiation dose 126

Figure 7.5 Impact strength of ternary blends upon radiation 128

Figure 7.6 (A) TGA and (B) DTG thermograms of PP/EVA and PP/EVA/EPDM blends 130

Figure 7.7 (A) Cooling and (B) heating curves of ternary blends prior to radiation 132

Figure 7.8 (A) Cooling and (B) heating curves of 10 EVA/40 EPDM/50 PP ternary blend at various radiation dose 133

Figure 7.9 (A) Cooling and (B) heating curves of 20 EVA/30 EPDM/50 PP ternary blend at various radiation dose 134

Figure 7.10 (A) Cooling and (B) heating curves of 50 EVA/50 PP blend at various radiation dose 135

Figure 7.11 Tan delta curves of (A) ternary blends prior to radiation (B) 10EVA/40EPDM/50PP blend at various dose (C) 20EVA/30EPDM/50PP blend at various dose and (D) 50EVA/50 PP blend at various dose 141

Figure 7.12 Storage modulus of ternary and binary blends 143

Figure 7.13 Storage modulus (A) 10EVA/40 EPDM/50 PP blend at various dose (B) 20EVA/30 EPDM/50 PP blend at various dose and (C) 50EVA/50PP blend at various dose 145

Figure 7.14 SEM micrographs (A) 50PP/50 EPDM (B) 10 EVA/40 EPDM/50PP (C) 20EVA/30 EPDM/50PP and (D) 50PP/50 EVA 147

Figure 7.15 SEM of 20EVA/30EPDM/50PP blend at (A) 0 kGy (B) 60 kGy (C) 80 kGy and (D) 100 kGy 148

Figure 7.16 Surface morphology of cryo-factured 20EVA/30EPDM/50PP blend at (A) 0 kGy (B) 60 kGy 149

Figure 7.17 Visual appearance of polymer blends 150

Figure 8.1 SEM and elemental analysis (1) 0.3% Ag (2) 0.5% Ag and (3) 1% Ag in 20 EVA/30 EPDM/50 PP blends 154

Figure 8.2 Gel content of Ag/ternary blend nanocomposite as a function of radiation dose 155

Figure 8.3 Tensile strength as a function of radiation dose for Ag/ternary blend nanocomposite..... 157

Figure 8.4 Elongation at break as a function of radiation dose for Ag/ternary blend nanocomposite..... 158

Figure 8.5 Impact strength of Ag/ternary blend nanocomposite as a function of radiation dose 159

Figure 8.6 (A) TGA and (B) DTGA thermogram of ternary blend with different AgNP loading 162

Figure 8.7 (A) Cooling and (B) heating curves of ternary blends with Ag loadings prior to radiation 164

Figure 8.8 (A) Cooling and (B) Heating curves of ternary blend with 0.3 % Ag loading upon radiation 166

Figure 8.9 (A) Cooling and (B) Heating curves of ternary blend with 0.5 % Ag loading upon radiation 167

Figure 8.10 (A) Cooling and (B) Heating curves of ternary blend with 1 % Ag loading upon radiation 168

Figure 8.11 SEM images showing the morphology of the cells on 50PP/50EPDM blends at different radiation dose after 4 h, 3 days and 7 days of culture..... 170

Figure 8.12 SEM images showing the morphology of the cells on 20 EVA/30 EPDM/50 PP blends at different radiation doses after 4 h, 3 days and 7 days..... 171

Figure 8.13 SEM images showing the morphology of the cells on 20 EVA/30 EPDM/50 PP blend with 0.3 wt% Ag 172

Figure 8.14 SEM images showing the morphology of the cells on 20 EVA/30 EPDM/50 PP blend with 0.5 wt% Ag 173

Figure 8.15 SEM images showing the morphology of the cells on 20 EVA/30 EPDM/50 PP blend with 1 wt% Ag 174

Figure 8.16 Proliferation of HaCaT cells on 50PP/50EPDM blend 175

Figure 8.17 Proliferation of HaCaT cells on 20 EVA/30 EPDM/50PP blend 176

Figure 8.18 Proliferation of HaCaT cells on 20 EVA/30 EPDM/50PP blend with 0.3% Ag loading 176

Figure 8.19 Proliferation of HaCaT cells on 20 EVA/30 EPDM/50PP blend with 0.5% Ag loading 177

Figure 8.20 Proliferation of HaCaT cells on 20 EVA/30 EPDM/50PP blend with 1% Ag loading 177

Figure 8.21 Proliferation of Staphylococcus aureuson on ternary blend with or without AgNP radiated at 60 kGy 179

Figure 8.22 Proliferation of Pseudomonas aeruginosa on ternary blend with or without AgNP radiated at 60 kGy 179

Figure 8.23 Growth of Staphylococcus aureuson after 6x dilution on different polymer blends 180

Figure 8.24 Growth of Pseudomonas aeruginosa after 6x dilution on different polymer blends 180

Figure 8.25 Colour of ternary blends with AgNP 181

LIST OF TABLES

Table 2.1 Summary of various sterilization technologies 19

Table 2.2 Comparison of Gamma, E-beam and X-ray sterilization 23

Table 2.3 Effect of additives in improving PP under radiation 27

Table 2.4 Statistics on CAUTI affected patients in few countries 35

Table 2.5 Metal nanoparticles for biocidal action 36

Table 4.1 Independent variables chosen in RSM study 55

Table 4.2 Actual and Predicted values 56

Table 4.3 Regression Model Characteristics using ANOVA 60

Table 4.4 Correlation factor of individual factors 64

Table 4.5 Goals for Optimization 68

Table 4.6 Optimized Parameters 68

Table 5.1 Experimental and theoretical values of po/qo ratios 74

Table 5.2 Maximum degradation temperature of PP, PP/EPDM and EPDM obtained from TGA analysis 83

Table 5.3 Melting temperature (T_m), crystallization temperature (T_C), heat of fusion (ΔH_f) and crystallinity (Xc) of PP/EPDM blends before and after radiation 85

Table 5.4 Glass transition temperatures and tan delta values for PP/EPDM blends before and after radiation 89

Table 5.5 Absorbance ratio and functional groups of 20% PP blend 102

Table 6.1 Blend proportion designs generated by DOE..... 109

Table 6.2 Actual and predicted values of mechanical properties for PP/EPDM/EVA blends 117

Table 7.1 Crosslinking to scission ratio of the blends using Charles Pinner equation 124

Table 7.2 Effect of degradation temperatures of binary and ternary blends 131

Table 7.3 Melting temperature (T_m), crystallization temperature (T_c) and extent of crystallinity of ternary blends before and after radiation 137

Table 7.4 Tan delta peaks of ternary blends before and after radiation 139

Table 8.1 Degradation temperatures of ternary blends with different Ag loading..... 161

Table 8.2 Melting temperature (T_m) and crystallization temperature (T_c) of ternary blends with AgNP before and after radiation 165

1 INTRODUCTION

1.1 Introduction

Thermoplastic elastomers (TPE's) are a class of polymers whose market is valued at 3.82 million tons and the demand increasing at a rate of 7.6% from 2014 to 2020 (TPEmarket, 2016). TPEs are gaining limelight focus mainly due to the melt process-ability like thermoplastic while providing rubber like properties. Designers increasingly use TPEs due to the significant cost savings possible because their ability to be processed on plastics machinery and high chemical resistance. This unique combination of properties is a result of the two-phase morphology of these materials. PP/EPDM is one of the important commercially used TPE mainly used in the automobile sector. These polymers are extensively used in manufacturing of grommets, sleeves, door sills, over moulded films, shift knobs, lamp seals, slush moulding, wire/cable in automobile industries. Though automobile industries are driving force for boosting its consumption, in recent years, their applications are being explored in other industrial arenas such as footwear, consumer goods, electronics, medical, healthcare devices, food packaging and construction.

PP/EPDM are non-homogeneous blends usually produced by melt blending technique. The processing conditions of these blends greatly affect the properties of the blend. Thus, this work focuses on optimization of process conditions for effective commercial processing of these blends in the above mentioned industrial applications. The optimization was carried out using Design of experiment methodology.

Radiation processing of the polymeric blends are sustainable process usually used in modification of the blend properties. The high energy ionization modify the properties of the material as they are subjected to crosslink and degradation due to scission and oxidation. Apart from improving the properties, E-beam radiation also offers an added advantage of sterilizing the final products. Sterilization is a mandatory process in manufacturing of few crucial applications such as food packaging and healthcare sectors. Thus in this study, the effect of E-beam on the material properties of the PP/EPDM based thermoplastic elastomers are investigated and described in detail, which enables us to explore the potential strategy to improve the blend properties using E-beam radiation. Further, EVA a ternary co-polymer (with ethylene and vinyl content) is blended with PP/EPDM blends, as EVA could act as a compatibilizing and crosslinking agent in order to improve the property of the ternary TPE.

The efficiency of EB irradiation in improving the properties of PP/EPDM/EVA blends has also been reported.

As an initiative to extend the application of the ternary blends to healthcare and food packaging sectors, Ag nanoparticles are incorporated. It is a well-known fact that silver ions and silver-based compounds are highly toxic to various microorganisms. This aspect of silver (Ag) makes it an excellent choice for multiple roles in the medical field (Prabhu and Poulose, 2012). A brief insight on the effect of mechanical and thermal properties before and after E-beam radiation of the PP/EVA/EPDM/Ag polymeric blend was also included in the study.

1.2 Problem Statement

It is important to notice that the properties of PP/EPDM blends also depends upon processing conditions such as blending temperature, time and screw speed. Improper blending of PP/EPDM will lead to detrimental mechanical properties due to poor interfacial adhesion, poor morphology and mixing due to varied viscosities, thermal degradation and so on. Literature still lacks a clear study on effect of these parameters and optimizing these conditions.

Also, in recent years, the properties of PP/EPDM blends are improved drastically using various crosslinking strategies and additions of fillers. Though improvement in properties were achieved, each system has its own demerits such as change of hygroscopicity, dark colour formation, blooming effects and so on. Sustainable alternative cross-linking technologies like ionization radiations are gaining its importance in recent use for improving the properties of final products. However, though the proof of concept of improving the blend properties by E-beam is evident in the literature, the effect of E-Beam in improving properties the blends greatly depends on material grade, blend ratio and optimization dose. A clear strategy is still required to improve the properties of PP/EPDM and PP/EPDM/EVA blends to expand its potential applications.

1.3 Scope

The scope of the research was to optimize and study the effect of E-beam radiation on blend properties of PP/EPDM and PP/EPDM/EVA thermoplastic elastomer. The effect of radiation

on PP/EPDM/EVA blends are studied in the range of 0-100 kGy radiation dose, as the minimum dose of E-beam required for sterilization is 25-40 kGy. Further irradiation dose is considered in the study in perspective to improve its properties, by making use of the ability of E-beam radiation to induce crosslinks in the polymeric blends. In short, E-beam radiation is used for dual purpose-1) sterilization during packaging and 2) enhancement of polymer blend properties. As a step ahead, the anti-microbial property is introduced to the blend via an incorporation of AgNP to dodge wellbeing dangers related to restorative consideration. The effect of dosage of E-beam on the blend with AgNP will also be examined. Monograms or instant property charts were also generated for PP/EPM/EVA blends as different blend compositions can provide different mechanical properties.

1.4 Aims and Objectives

The overall aim of this study is to improve the properties of PP based TPE blend without addition of fillers or chemical additives. Hence, a sustainable approach namely E-beam radiation is used to improve the blend properties which simultaneously provides an additional advantage of sterilization. The study facilitates to bring an insight that the newly developed thermoplastic blend could maximize the use of PP/EPDM/EVA TPE blends across various sectors.

To achieve the aforementioned aim of this research, the following objectives were concentrated in this work:

- To formulate, characterize and optimize the processing parameters of PP/EPDM blend using design of experiment (DOE).
- To assess the effect of E-beam sterilization on the physical, mechanical and thermal properties of PP/EPDM blends.
- To study and generate instant property charts for the mechanical properties of PP/EPDM/EVA ternary blend using DOE
- To evaluate the effect of EVA addition, in terms of improvement in properties of the PP/EPDM/EVA ternary blend under E-beam radiation
- To evaluate the feasibility of AgNP addition in ternary blend and their effect under E-beam radiation for anti-microbial enrichment studies.
- To evaluate the biocompatibility of the polymer blends after radiation.

1.5 Significance of the Research

This study contributing in development of E-beam sterilisable PP/EPDM/EVA ternary blends helps them to be potentially used in various industrial and consumer applications, especially, in medical and food packaging sector. Apart from sterilization, stiffness, tensile and impact properties are also improved by exposing the ternary blends to E-beam radiations. The improvement of these properties will aid the materials to meet various end products requirements, as different products require different mechanical properties based on the nature of their use. For instance, it is important to improve tensile strength, as the products can have higher resistance from breaking under tension. The blood bags needs higher tensile strength to sustain centripetal force of centrifugation when used for plasma separation. The tensile strength of current blood bags ranges from 10-25 MPa, however a maximum of 40 MPa is desirable. To ensure flexibility when the bag is squeezed, the Young's Modulus should be as low as 0.1 GPa (Iverson et al., 2004). They also need to have high impact strength to bear shock/drop resistance. An indwelling catheter needs higher tensile strength and elongation at break to avoid fracture upon removal or insertion (Fiol et al., 2016). In general, soft materials (low hardness) are considered for all types of catheters and drainage tubes to ensure patients' cosiness. Higher tensile strength leads to rise in radial strength and also permit the usage for lower profile and thus providing better deliverability and access to narrow areas (Shrivastava, 2004). With respect to packaging products such as packaging tape, stretch film, materials with higher tensile and impact strength is preferred to reduce shipping damages and increase load stabilization (Shin, 2014).

1.6 Thesis Outline

This thesis contains eight chapters whose outlines are as follows:

Chapter 1: Introduction

This chapter will discuss the research background, problem statement, aim, objectives and the importance of this project.

Chapter 2: Literature Review

This chapter will cover the current knowledge in improving the properties of PP/EPDM based TPE, their advantages and disadvantages. The effect of ionization radiation on these polymers in prospects of their mechanical and thermal properties will be elaborated. Also, the effect of different nanoparticles and compounding methods used to improve antimicrobial properties of the material will be discussed. This chapter will introduce the state of the art of the current project.

Chapter 3: Materials and Methodology

The materials used and the methodology for the compounding and characterizations of the polymer blends will be elaborated in detail.

Chapter 4: Optimization of processing parameters of PP/EPDM blend

Optimization of processing parameters for PP/EPDM binary blends were carried out by using Design of Experiment (DOE). The blends synthesized with optimum parameters were used throughout the research. The blending parameters including temperature, time and rotor speed were studied and optimized.

Chapter 5: Effect of E-beam irradiation on PP/EPDM blends

This chapter focuses on the characteristics of PP/EPDM binary blend and the effect of E-Beam radiation on their mechanical and thermal properties.

Chapter 6: Properties of PP/EVA/EPDM ternary blends predicted using DOE

This chapter will be discussing on the property profile charts of ternary blends generated using DOE. The mechanical properties of the blend over the entire possible combinations of the polymeric blends were predicted.

Chapter 7: Effect of E-beam irradiation on PP/EPDM/EVA ternary blend

This chapter is regarding the characteristics of PP/EPDM/EVA ternary blend and their mechanical and thermal properties upon E-beam radiation.

Chapter 8: Effect of E-beam irradiation on PP/EPDM/EVA/Ag nanoparticles

Ag nanoparticles were added to the optimum ternary blend with high tensile strength for enhancing its anti-microbial properties. This chapter discusses their synthesis and effect of E-beam radiation on its mechanical and thermal properties. The biocompatibility and the effect of AgNP on Pseudomonas aeruginosa and Staphylococcus aureus strains were carried out and discussed.

Chapter 9: Future Prospective and Conclusion

This final chapter will conclude the changes in the thermal, mechanical, antimicrobial and biocompatibility properties of PP/EPDM/EVA/Ag thermoplastic elastomer. Some future work required for the commercialization of these materials will be addressed to attend problems which were not covered in our study.

2 LITERATURE REVIEW

2.1 Introduction

The progress in advancements of thermoplastic processing technology, complexity in designs and advancements in machinery equipment for moulding has opened the roads for replacement of conventionally used material with thermoplastic elastomers in various applications. PP/EPDM is one of the most commonly preferred TPE in today's industry which often bridges the gap between thermoplastics and thermoset rubbers. This chapter presents a review of literature on the PP/EPDM based thermoplastic elastomer compounded by melt blending technique and the effects of additives used in improving the properties of such blend. Also, an overview of the effect of ionizing radiations on PP and PP/EPDM blends are studied. Further, the effect of ionizing radiations on PP/EVA blends are also studied. EVA is a thermosetting elastomer which is a copolymer of ethylene and vinyl content. Though EVA is a co-polymer, in many cases, acts like a compatibilizer between PP and its blends (Abolhasani et al., 2010). EVA offers compatibilizing effect in PP blends similar to the chemical additives as discussed in section 2.2 and 2.4. For instance, EVA improved the compatibilization between PP and Polyethylene terephthalate (PET) by providing a core shell morphology and multi core morphology leading to enhancement of the mechanical properties of the ternary blend (Abolhasani et al., 2009). However, EVA (being a co-polymer) improves compatibilization of PP with other polymeric materials avoiding the disadvantages such as leaching, discoloration and blooming effects caused by the chemical additives that are used as compatibilizers (discussed in section 2.4). Upon radiation, they also crosslink with the secondary polymers blended along with them and improves the properties of the blend on the whole. A review on the effect of crosslinking upon radiation of PP/EVA blends have been included in this study to aid the development of PP/EPDM/EVA based ternary thermoplastic elastomer and improve their properties/radiation stability under E-beam radiations. Further, a detailed comparison of various sterilization methods and their current technologies are briefed as E-beam offers sterilization advantage apart from improving the properties of the polymeric blends. Finally, the effect of metal nanoparticles, especially AgNP in polymer composites to introduce antimicrobial properties in the blend is reviewed.

2.2 PP/EPDM blends

Price pressures and the trend towards commoditization of standard TPEs have led suppliers to develop new materials with enhanced properties that can add value to the end products (Markarian, 2008). PP/EPDM is one of the well-established blends used in a variety of applications such as roofing, cable and wire insulation, footwear and also has shown potential to be used in manufacturing of healthcare devices. These blends do not contain leachables, extractables (like PVC) or do not emit nitrosamine, mercapto benzo thiazole (like few thermoset polymers) that are classified as toxic and irritants (Varma, 2007), making them safe to be used in medical applications. PP and EPDM individually have exhibited good biocompatibility (Simmons, 2012, Naderi et al., 2007). Positive biocompatibility were shown by PP, when *in vivo* tests were carried out in sheep specimens (Kelly et al., 2017). Fischer et al. (1979) showed that both PP and EPDM have exhibited good blood compatibility when evaluated under citrated human plasma.

PP and EPDM are blended together due to their similarity of the chemical structure to yield a polymeric blend of varied properties and extend their applications. The PP/EPDM blends are generally produced by melt mixing method. PP and EPDM are melted together at temperature usually slightly higher than the melting point of PP. Nevertheless, the temperature of blending is subjected to the PP and EPDM grades and needs to be optimized each time before used for the study. The polymers are melt blended under the presence of shear force to enhance uniform distribution for a certain period of time, usually 5-15 min. Like the blending temperature, the shear rate (rotation per minute) and the time of blending must also be optimized based on the requirements of the product and material. Although solvent blending is another option for producing PP/EPDM blends, they are not preferred by researchers or industrialists due to the difficulties in processing and non-eco friendliness (Nwabunma, 2008). However, PP/EPDM blends are generally immiscible blends where PP and EPDM phase exist separately. The properties of PP/EPDM largely depend on various parameters such as morphology (particle size and inter particle distance of dispersed phase), blend composition, viscosity ratio, interfacial tension, shear rate/shear stress, elasticity ratio, molecular weight and processing conditions (Ning et al., 2017). Apart from optimizing the aforementioned parameters, the properties of the blends are also improved by numerous techniques such as enhancing compatibilization and introducing crosslinking between

PP/EPDM matrices. A brief overview of the methods to improve PP/EPDM blends will be elaborated in the following sections.

Effect of Compatibilization:

One of the most common methods to improve the properties of the PP/EPDM blend is through the use of compatibilizer during blending. Though PP/EPDM are immiscible blends, some extent of partial compatibility was still found in the blends due to the penetration of EPDM into amorphous phase of PP during blending of the polymers (Krause, 1972, Xiao et al., 2002). In general, compatibilization aids the polymeric blend to improve adhesion between PP and EPDM phase by reducing their interfacial tension and also aids in the stabilization of morphology during processing and servicing (Ramarad et al., 2015a).

For instance, the tensile properties of PP/EPDM blends were improved by reducing the interfacial tension between the two phases upon the addition of olefin block copolymer (OBC) as compatibilizer. The tensile strength of the 50 PP/50 EPDM blends increased by 15% and elongation at break by 27% by addition of 5 phr OBC. Further, the young's modulus increased by 25% with addition of 15 phr OBC (Zhang et al., 2015).

Ezzati et al. (2008) used maleic anhydride (MAH) grafted either to PP or EPDM as a compatibilizer in PP/EPDM blends . The maleated polymers were able to increase the interfacial adhesion between the PP and EPDM phases. Purnima et al. (2006) also showed an improvement in yield strength and young's modulus in all the blend compositions of PP/EPDM. A maximum improvement of 20 MPa in young's modulus was observed in the blends with 33.3% EPDM, when 0.3% MAH was used. Improvements in storage modulus and rheological properties were also reported, when 6 phr PP-g-MAH was used (Ezzati et al., 2008). Bouchart et al. (2008) showed a good improvement in the tensile properties of PP/EPDM blends when 7% maleated PP was incorporated into the blends along with ionomer compatibilizer such as surlyn (ethylene-co-methacrylic acid neutralized by sodium ion).

Kim et al. (2000) studied the effect of (PP-g-MAH)-co-[PA-6, 6]-co-(EPDM-g-MAH) (a triblock compatibilizer) in 65% PP/35% EPDM blend. The authors reported that 0.5 wt% was the optimum dose of the compatibilizer in enhancing the impact strength to 13%, where further

increase in the amount of compatibilizer did not show any significant effect. The compatibilizer improved the impact strength by the induction of β-crystallization in PP matrix. Further, no improvement in interfacial adhesion was reported except the dispersion of EPDM was improved along with its uniform distribution. Their study significantly demonstrated that the triblock copolymers acted as an auxiliary compatibilizers in the PP/EPDM blends.

Effect of crosslinking:

Another common method of improving the properties of PP/EPDM is by crosslinking. During this process, the polymeric chains are linked with each other by induction of crosslinks. The crosslinks usually involve the formation of new chemical bonds which will result in enhancing the interfacial adhesion and thus improving the mechanical and thermal properties of PP/EPDM blends.

Sulphur crosslinking also termed as vulcanization is used for improving polymeric blends. Sulphur serves as crosslink bridging between carbon chains (C-Sx-C). Coran and Patel (1980) showed improvement in the properties of PP/EPDM blend by static vulcanization using sulphur as crosslinking agent and other additives such as zinc oxide and stearic acid activators, dibenzothiazole disulfide (MBTS), tetramethyl thiuram disulfide (TMTD) accelerators. The tensile strength increased by 20 MPa, elongation at break increased from 190 to 530% and decrease in tension set by over 100 times were reported in 40 PP/60 EPDM blend when up to 2 phr sulphur was used. The improvement in property was due to the crosslinking mechanism initiated by the additives.

Further, Lopez-Manchado et al. (2001) studied the crosslinking of PP/EPDM with same set of additives under both static and dynamic vulcanization. He concluded that the modification

of EPDM- dispersion particle system, caused by dynamic vulcanization along with crosslinks formed by sulphur additives enhanced the improvement of properties in comparison to static curing. The dynamic vulcanization of PP/EPDM in the presence of sulphur alone was studied by Prut et al. (2006). A 10-time improvement in the viscosity of the cured PP/EPDM blends was observed. The un-deformable elastomeric dispersion hampered the flow of the blends. As the sulphur content was increased to 2 phr, the viscosities increased three times. Moreover, the blends showed an improvement in tensile properties which was attributed to the rigid 3- dimensional (3D) network initiated by crosslinking. However, sulphur crosslinked PP/EPDM is not preferred for commercial uses due to the poor thermal stability of the crosslinks. Moreover, it led to stench issues during production and processing (Naskar, 2007).

Inoue and Suzuki (1995) used 0.2 phr N,N'-m-phenylene-bismaleimide and 0.3 phr poly-(2,2,4-trimethyl-1,2-dihydroquinoli as crosslinking agent. The crosslinking increased the interfacial adhesion without changing morphology and increased the impact strength from 12.6 to 60 (kg-cm/cm) in 80 PP/20 EPDM blend. The improvement in interfacial adhesion was very much evident in shift of glass transition temperature (T_g)to 5°C, indicating increase in free volume of PP under distortion (Inoue and Suzuki, 1996).

López Manchado and Kenny (2001) used benzene-1,3-bis(sulfonyl) azide to enhance the interaction between the C-H bonds of EPDM and PP phase. The young's modulus increased from 145 to 290 MPa in 50 PP/50 EPDM blends. Further, flexural stress increased from 6.5 to 11.9 MPa, hardness from 45 to 55 shore A and resilience from 47 to 55%. Zielińska et al. (2011) compared the effects of 4,4′-isopropylidenediphenyl azidoformate (4,4′DAF), tri(ethylene glycol)-di(azidoformate) (GDAF) and 1,3-benzenedisulfonyl azide (1,3BDSA) diazide as crosslinking agents on the performance of PP/EPDM. They showed that 1,3BDSA aided the polymer blend to show the highest tensile strength, impact strength and compression sets in comparison to the other two.

Peroxide crosslinking is another method to improve the PP/EPDM blends where the haemolytic decomposition of peroxides causes generation of free radicals. The free radical further abstracts hydrogen atom from the polymer chains leading to creation of stable peroxide decomposition products and macromolecular radicals. The free macromolecular radicals from the combination two polymers undergo coupling and form crosslinks between

C-C chains. The efficiency of crosslinks also depends on the type of crosslinking agent used and polymer radical generation from polymeric chains (Naskar, 2007). Various side reactions may also interfere the crosslinking process, either by consuming the peroxide in non-productive ways or simply degrading the polymer. The polymer degradation takes place when the free radicals react with atmospheric oxygen which leads to oxygenation. A schematics for general crosslinking and degradation mechanisms is shown in **Error! Reference source not found.**1. To reduce the degradation and improve the crosslinking efficiency, the peroxide crosslinking is always carried out with additional co-agents such as antioxidants, stabilizers and accelerators.

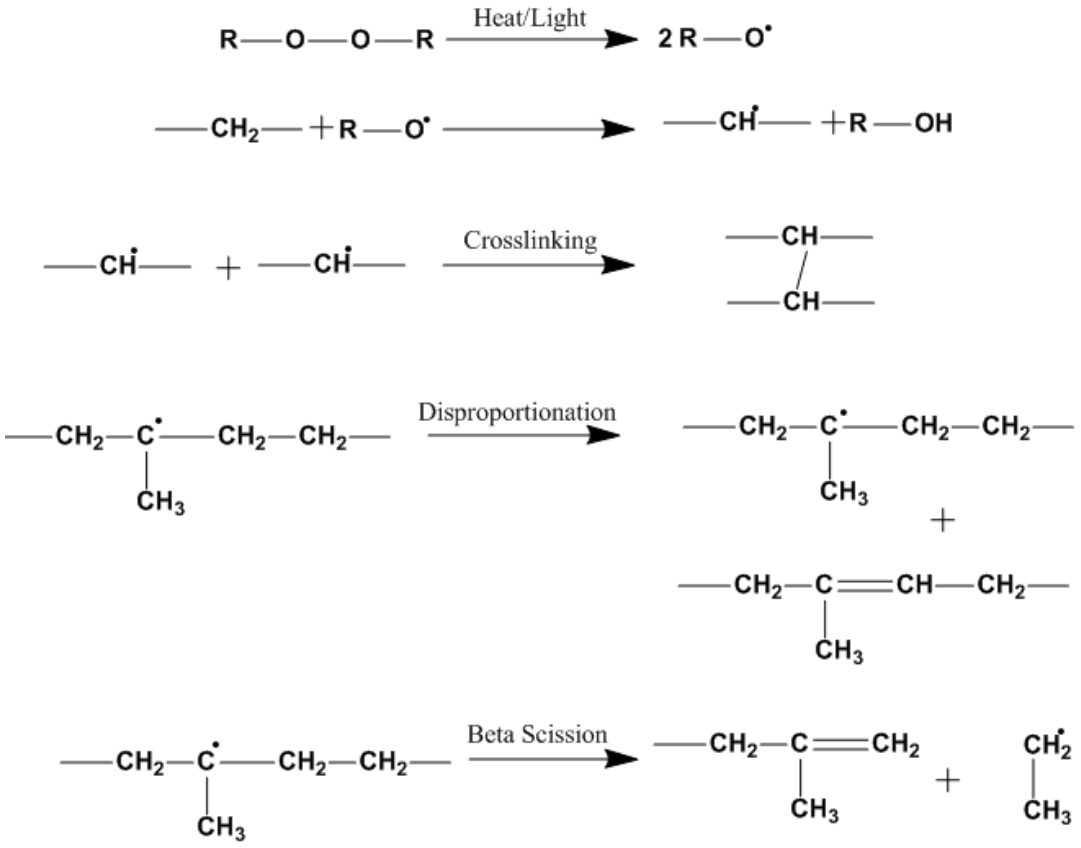


Figure 2.1 Schematics of peroxide crosslinking (Aprem et al., 2005)

Dicumyl peroxide (DCP) is one of the most commonly used peroxide agent for inducing crosslinks in PP/EPDM blends. Chen et al. (2013) performed dynamic vulcanization of PP/EPDM in the presence of DCP peroxide and zinc dimethacrylate (ZDMA) as co-agent. DCP of 1 wt % was used in different composition of PP/EPDM blends. A significant improvement in impact strength (five times) and elongation at break (seven times) was observed. De Risi and Noordermeer (2007) also studied the effect of DCP in the presence of few curing agents such as ethylene glycol dimetaacrylate (EDMA), trimethylol propane trimethyacrylate (TMPTMA) and zinc dimethacrylate (ZDMA). They found that more stable free radicals were formed by positioning the radicals on the co-agent molecules. This stable positioning prevented the chain fragmentation of the PP, which indicated that the drawbacks of using peroxides could be partially overcome by the employment of suitable (meth) acrylate co-agents.

Multifunctional peroxides such as 1-(2-tert-butylperoxyisoprpyl)-3-isopropenyl benzene (TBIB), 2,4-diallyloxy-6-tert-butylperoxy-1,3,5-triazine (DTBT) and tert-buty cumyl peroxide (TBCP, Trigonox T) improved young's modulus of PP/EPDM blend by approximately 2 times, hardness from 60-65 shore A and increase in tensile strength of 5 MPa (Naskar and Noordermeer, 2004).

Naskar et al. (2004) stabilized the mechanical properties of PP/EPDM blends which degraded against ageing using DCP/ triallyl cyanurate (TAC) curing system with stabilizers such as octadecyl-3,5-di-tert-butyl 1-4 hydroxyhydrocinnamate (Irganox 1076), tris(2,4-di-tert-butylphenyl)phosphite (Irgafos 168), Chimassorb 944 LD and bis(hydrogenated tallow alkyl)amines (Irgastab FS 042). Nicolini et al. (2008) compared the crosslinking efficiency of PP/EPDM induced by two peroxide systems- peroximon and bismaleimide (BMI)/DCP in 35 PP/65 EPDM blends. The authors showed that even 1.2 phr of peroximon gave better crosslinking efficiency than 2.5 phr BMI/DCP. However, both systems showed only a slight improvement of 5 MPa in tensile strength.

Expensive crosslinking and co-agents, high curing time, high temperature requirement for curing and poor resistance to flex fatigue are some of the disadvantages of peroxide crosslinking (Aprem et al., 2005). However, apart from crosslinking the carbon radicals can oxidize and produce decomposed products. The traces of decomposed products could lead to rise of blooming effect, smell and gets extracted and leached in contact with solvents (Datta

et al., 2005). This leads to the uncertainties in toxicity when proposed to be used for medical applications.

PP/EPDM was also crosslinked using phenolic resols. The phenolic resols are a class of chemicals that generally, consists of methylol groups and dimethylene-ether units. The resols in presence of activators such as $SnCl_2$ initiate ether scisson and forms benzyl cations. These cations formed chromans and methylene bridged intermediates (mono-phenolic crosslinks) with EPDM phase (van Duin, 2006). Jain et al. (2000) showed an improvement of PP/EPDM blends by using dimethylol phenolic resin in varied blend compositions of PP/EPDM blends. A maximum improvement in elongation at break (from 285% to 350%) and impact strength (from 190 to 1150 J/m partial breaking) was achieved in 60 PP/40 EPDM blends. An improvement of 26% in flexural modulus was achieved in 70 wt% and 80 wt% PP blends. Only a limited works involved resol curing of PP/EPDM blends because of its discoloration and hygroscopicity. The method requires a long and high temperature drying in order to avoid any defects caused by its hygroscopic nature. Also, the blends turned to dark brown which would be a limitation for medical devices as it hinders masking and monitoring of fluids (Naskar and Noordermeer, 2004).

The advantages and disadvantages of the methods used in improving the PP/EPDM blends for various applications were discussed previously. Apart from the disadvantages such as blooming, high cost of additives and discoloration mentioned above, it is to be noted that all the methods discussed used additives as source for improving the overall properties of PP/EPDM blends. However, it could be highly possible that these additives will be leached by the fluids when used as healthcare devices. The data on leaching studies and the cytotoxicity of these additives are scanty in the literature. This leads to the uncertainty in adopting these methods for improving PP/EPDM blends that is proposed to be used in manufacturing of healthcare devices.

2.3 Sterilization

Sterilization is a necessary quality control technology in the manufacturing of medical care devices and food packaging. Sterilization is necessary for the complete destruction or removal of all microorganisms (including spore-forming and non-spore-forming bacteria, viruses, fungi, and protozoa) that could contaminate materials and thereby constitute a

health hazard. Many health organizations and authorities propose that the requirements for Good Manufacturing Practice (GMP) should be observed throughout all stages of manufacture and sterilization. With this concern in mind, researchers have established many sterilization methods. Heat sterilization, sterilization using chemicals, UV, irradiation and plasma sterilization are common technologies used in need for prevention of patient exposure to infections caused by organisms on instruments and devices used during their health care and usage of food packages. Table 2.1 briefly describes the new technologies, their advantages and disadvantages over the polymers used in manufacturing of healthcare devices and packaging.

Dry heat sterilization is usually carried out by exposing the products to extreme temperatures. The temperatures usually lies between 140 to 170°C. However, such high temperatures are not suitable for materials whose melting temperatures coincides at such processing temperatures. Also, dry heat sterilization has low penetration power providing only superficial sterilization (Sultana, 2007). The heat leads to destruction of endotoxins serving as the lethal factor for bacterial stains.

Apart from heat sterilization, the sterility of the medical products can be achieved using chemical sterilants such as ethylene oxide (EtO), vaporized H_2O_2, Ozone, formaldehyde, aqueous gutraldehyde, chlorine dioxide and peracetic acid solutions. All these chemicals are used in gaseous form to kill the microbes found on the products. Amongst the afore mentioned chemical sterilants, EtO sterilization is the most preferred in today's industry. Low temperature process, high efficiency, large sterilizing volume/capacity and its non-corrosiveness towards plastics and metals make it more favourable than other sterilants. On the other hand, it requires a long processing time of up to 14 h and high cost of processing. It also leads to potential acute health hazard such as irritations to skin, eyes, gastrointestinal or respiratory tracts and central nervous system depression. Chronic inhalation could lead to the formation of cataracts, cognitive impairment, neurologic dysfunction, and disabling polyneuropathies. Occupational exposure in healthcare facilities has been linked to hematologic change and an increased risk of spontaneous abortions and cancer. The waste discharge from EtO could be a source of pollution, which also urges the industrialists to look for other sterilization options.

UV sterilization is a non-ionizing sterilization method where, the UV lights absorbed by the nucleic acids prevents the bacteria to be replicated and also discontinues the transcription process. Though they are relatively fast and safer to be used, the cost of bulk sterilization hinders them to be preferred by manufacturers. They are also found to be impervious to many materials especially PP.

Gas plasma sterilization is usually performed by generation plasma from various gaseous sources such as nitrogen, helium, neon, argon and xenon (Gas plasma sterilization of microorganisms and mechanisms of action). The plasma devoids C, H, N, O atoms of the microbes leading to their devastation. Rapid processing and low toxicity are few advantages of gas plasma sterilization. On the other hand, they are not suitable for sterilization of many flexible materials due to low pressure working conditions.

Ionizing radiations such as gamma, E-beam and X-rays are gaining attention in the current industry mainly due to their sustainability and low cost. Unlike other sterilization methods, no toxic waste is generated and can minimize the waste management system. Also in these technologies there is no requirement for post treatment quarantine period. The radiations destruct the microbes on the products in the manufacturing procedures. Ionizing radiation can influence DNA either directly or in a roundabout way. Water molecules around the bacterial cell when exposed to radiation free radicals (hydrogen ions, hydroxyl radical and solvated electron e^-) are formed, that can diffuse sufficiently far to reach and harm DNA. Free radicals framed in the hydration layer around the DNA particle are in charge of 90% of DNA harm (Hammad, 2008). Typically, a sterilization dosage of 20-40 kGy is required to reduce the microbial burden on the healthcare products. On the off chance, if there is no data about the number and protection of the microbial bioburden, the item has to be radiated with 25 kGy (KARPUZ and ÖZER, 2016). However, when polymers are exposed to ionizing radiations, the free radicals formed within the polymeric chains leading to simultaneous crosslinking and scission mechanisms altering the properties of the polymeric material. A brief overview on the effect of ionizing radiation on polypropylene, EPDM and their blends are discussed section 2.7.

Table 2.1 Summary of various sterilization technologies

METHOD	PROCESS	Advantages	Disadvantages	References
Dry heat sterilization	Conduction using dry air. The heat penetrates to interior of the material until temperature required for sterilization is achieved.	Non-toxic	High temperature and time consuming. Up to 160-170^{o}C for 1 -2 h. Not suitable for heat sensitive materials	(Rutala et al., 2008)
Pressured vapor sterilization	Pressurized steam with the generation of heat acts as sterilization agent. Parameters required: 3 min at 110-160°C	Economic and short processing time.	Not suitable for many polymeric material due to high temperatures. Standard cycle is limited to polymers having softening point above this temperature	(Silindir and Ozer, 2009)
Ethylene oxide (EtO)sterilization	Exposure of ethylene oxide gas at 55 °C for 3 hrs.	Low temperature process and complete penetration can be obtained. Suitable for most polymers and used in 70% of the market.	Critical and lengthy procedures for de-gassing of the gas and more safety concerns required. EtO is toxic, cancerogenic, flammable and explosive.	(Mendes et al., 2007)

Formaldehyde Sterilization	In formaldehyde processes formaldehyde and steam are combined at temperatures of 55 °C to 75 °C for microbicidal action	Neither flammable nor explosive. Simple procedure.	Should be carried out only with the combination of steam. Unlike EtO, Only superficial sterilization can be reached.	(Miorini)
Gas plasma sterilization	Electric discharge is applied to hydrogen peroxide gas. The resultant free radicals called plasma acts as sterilizing agent.	Rapid time cycles and can be achieved at low temperatures. Less toxic.	Weak penetration in presence of organic residues, bulk sterilization and complex geometries. Not suitable for low pressure resistant polymers.	(Krebs et al., 1998, McDonnell, 2012, Silindir and Ozer, 2009)
Radiation sterilization	Gamma, E-beam and X-ray rays acts as sterilizing agent	Precise dosing, Rapid processing, uniform distribution, immediate availability of product after processing	No flexibility of dosing parameters. Long residence time required.	(Lee and Chu, 1996)
Dielectric Barrier Discharge	plasma generation characterized by high AC voltage induced gaseous discharges created at near atmospheric pressure	Low temperature operation, time-saving and non-toxicity over the conventional methods	low penetrability during bulk sterilization	(Eto et al., 2008, Sirajuddin and Foster, 2007)

UV Sterilization	UV light sterilizes having a wavelength of that breaks the molecular bonds in microbe DNA acts as sterilizing agent.	Fast time cycle, bulk sterilization possible, green technology	High dosage and maintenance required. Not cost effective.	(Dai et al., 2011, Bak et al., 2009, Kaldany, 1993)

E-beam radiation is currently the most preferred method among other radiation sterilization methods. E-beam is electricity dependent and dose-rates are substantially higher than gamma bringing about fundamentally diminished exposure times. From Figure 2.2, it can be noticed that E-beam is the most financially savvy cleansing procedure due to being normally 30% to 40% more affordable than gamma treatment. For every sterilization cycle, E-beam is proficient in seconds rather than minutes or hours for different advances, diminishing impacts on delicate materials. Such short treatment time enables makers to apply "in the nick of time" producing systems, in this manner reducing the storage of items after treatment. E-beam has the potential of probing through card board bundling and offering the products to be sterilized at the end after packaging. With a vitality of 10 MeV, E-beam can penetrate through thicknesses of around 20-25 cm in a single pass and 60 cm in a two-fold side pass (Mohammad et al., 2012). Since the penetration time is also short, potential effect of radiation on medicinal gadgets is exceptionally constrained. The advantages and disadvantages of E-beam, Gamma and X-ray sterilization systems are summarized in Table 2.2.

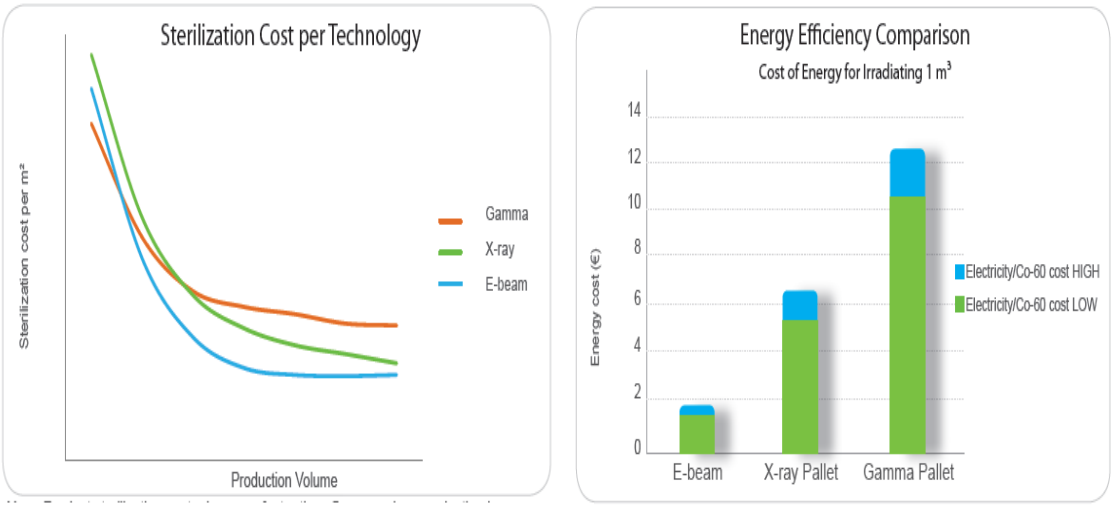


Figure 2.2 Cost of sterilization by E-beam, Gamma and X-ray technologies (Iba, 2014)

Table 2.2 Comparison of Gamma, E-beam and X-ray sterilization

	Gamma Sterilization	**E-Beam Sterilization**	**X-ray sterilization**
Energy Source	Cobalt	Electricity	Electricity
Energy Competence	High energy requirement	Low energy requirement	Higher than E-beam
Product Penetration	Capability of high penetration	Lower than Gamma	Comparatively good penetration
Ability to stop source irradiation	No	Yes	Yes
Dose Uniformity	High	Very high	Low
Dose rate	Low	Very high	Good
Time for treatment	Very long (hours)	Very short (seconds)	In minutes
Cost Efficiency	Expensive than E-beam	Cheaper than Gamma and X-ray sterilization	Cheaper than Gamma sterilization
Development of Heat	A maximum rise of 20°C	~ 0.5°C / kGy	Less than gamma and E-beam
Availability and growth in market	widely adopted	being widely adopted	very new technology

2.4 Effect of Ionizing radiation on Polypropylene, PP/EPDM and PP/EVA blends

Polymers when exposed to ionizing radiations, absorbs high energy within them. The high energy causes hydrogen abstraction from the polymer backbone creating free radical species. The chain propagates creating addition of reactive species. These free radicals are usually entrapped within the crystalline part of the polymer disrupting its molecular structure. The free radicals can lead to crosslinking, scission and also oxidation mechanisms. All these mechanisms are spontaneous and random reactions. These simultaneous mechanisms alter the mechanical and thermal properties of the polymer to a greater extent. To develop PP/EPDM/EVA blends that are suitable for E-beam sterilization, it is important to understand and review the current state-of-art of these polymers. Though the source of E-beam is different from gamma and x-rays, the chain scission and crosslinks follow similar mechanisms. However, the extent of chain scission and crosslinking varies based on the source of ionizing radiations. An overview of the current literature regarding the mechanism, parameters affecting the material properties, methods and additives used to improve the material properties are elaborated in following sections.

Polypropylene under ionizing radiations:

The study of effect of radiation on the properties of the PP is generally carried out by the researchers by melt blending raw PP and moulding into required shape and sizes as per the test standards. The sample specimens will then be exposed to ionizing radiations. The net properties of the PP after radiation depends on the dominating reactions which include crosslinking, scission or oxidation reaction. The rate of crosslinking, scission or oxidation depends on molecular weight of PP, radiation atmosphere, dosage rate, tacticity of PP and presence of additives.

Generally, crosslinking occurs in amorphous phase and scission is favoured in crystalline phase. Isotactic PP and random PP are copolymer and have higher amorphousness than homo polymer PP. Presence of more amorphosity encourages crosslinking. Gao et al. (2002) compared the effect of gamma radiation on homopolymer PP, random polymer PP and isotactic PP (IPP). Even though degradation occurred in PP, authors concluded that IPP showed higher potential of crosslinking than the other two. The crosslinking and chain

scission also depend on the stereosphecificity of the PP. Most of the commercial PP is isotactic, which is semi-crystalline and has pendant methyl groups arranged on same side. Whereas, atactic is mainly amorphous and randomly arranged. Hence, atactic shows lower p_o/q_o value than isotactic indicating that crosslinking is favoured more in atactic PP. If the radical is formed on the pendant methyl, the resulting reaction is cross-linking. However, if the radical is formed in the main chain, the chain end may react with hydrogen thus causing an irreversible scission (Drobny, 2012).

PP, in general, undergoes degradation at gamma dosage range of 10-100 kGy at ambient room conditions. This was mainly attributed to the domination of scission over crosslinking (Busfield and O'Donnell, 1979). On the other hand, Otaguro et al. (2010a) demonstrated that radiation in inert conditions and at dose rate of 12.5 kGy, the concentration of newly formed free macro radicals was too great to be neutralized and so some macro radicals attacked neighbouring chains leading to chain branching and ultimately to cross-linking. Formation of chain branching was analysed using molecular weight distribution and Chain Scission Distribution Function (CSDF) with the aid of rheological characteristics and gel fractions. PP radiated in acetylene atmosphere (with branch promoters) and thermal treatment at a dosage of 5-20 kGy showed crosslinking effects (Oliani et al., 2013). The effect of crosslinking was confirmed by the formation of micro gels. Upon radiation, microgels are formed as spherulites in the border linked by fibrils constituting the phases amorphous and crystalline. These gels are direct indication of formation of 3D network upon crosslinking (Funke et al., 1998, Rosiak et al., 2005). However, there was no gel formed when PP was radiated in air even up to dosage of 150 kGy (Krupa and Luyt, 2001). This again confirms that the degradation due to scission is favoured when PP is radiated under ambient atmosphere. Krupa and Luyt (2001) also reported that apart from mechanical properties, the thermal and crystalline properties of PP also decreased with increase in radiation due to degradation. Lugão et al. (2000) radiated PP in nitrogen, hydrogen and acetylene atmospheres to understand the effect of crosslinking, branching and scission mechanisms in these atmospheres. PP showed degradation below 3 kGy in all the conditions. However, between 3-15 kGy, double bond formation was confirmed. It is interesting to note another claim of the author that the crystallization kinetics and temperature of PP were affected only by the long branching induced by radiation and formation of double bonds didnot affect the crystallization of PP. In the presence of N_2O atmosphere, crosslinking was very slightly

improved by accompanying scission, as N_2O acted as radical scavengers (Kondo and Dole, 1966).

Though PP shows possibility of crosslinking in different atmospheres, mostly degradation is favoured in air. Most of the healthcare devices and materials used in food industries are usually sterilized only in ambient conditions. Hegazy et al. (1981) reported decrement in tensile properties of PP based medical devices after sterilized under room condition. Further, Sevil and Güven (1995) demonstrated up to 60% decrement in compression strength of PP based syringes. Recently, Fintzou et al. (2006) also reported detrimental effects of radiation on PP based surgical syringes, where up to 57% reduction in compression strength and elongation at break. The work was extended to comparison of effect of E-beam and Gamma radiation on disposable syringes. The authors reported that the effect of degradation was less in products radiated by E-beam in comparison to products radiated by gamma (Fintzou et al., 2007). Electron-beam irradiation requires less time than gamma irradiation to achieve the same dose, due to its high dose rate. Thus indirectly electron-beam irradiation limits oxygen diffusion into the sample. It is the radiation-induced oxidative degradation of polymers in the presence of air that causes the deterioration in mechanical properties. On the other hand, Woo and Sandford (2002) showed that PP based medical packages radiated at dose rates beyond 100 kGy and due to temperature rise, some extent of stability was observed due to higher termination effects than free radical initiation leading to increase of crosslinks. Other properties of PP based syringe barrels including tensile modulus, creep to decrease and discoloration was reported when radiated at e-beam dosage range of 20-80 kGy (Abraham et al., 2010).

Apart from the problem of degradation at the time of radiation, PP also poses post radiation syndromes. It is important to study the post radiation effects to analyze the potentiality of the stability of the products during their storage. The oxidation of gamma-irradiated polymers continues for a long time after exposure. In most cases, the degradation during storage is related to the residual free radicals that existed in crystalline region after radiation. These radicals persist to migrate from the crystalline and amorphous areas to interface area. At the interface, in the presence of oxygen the free radicals undergoes oxidation reactions. Additionally, slow decomposition of hyperoxide formed during oxidation propogates leading to degradation polymer properties (Suljovrujic, 2009, Sonnier et al., 2010). Various oxidative

species such as alcohols, ketones and carboxylic acids were formed during post radiation storage which contibutes to the degradation of PP (Rivaton et al., 2004).

Prevention of PP degradation during the radiation and storage after radiation is mostly performed by termination of the free radicals inititiated in the polymeric backbones. Addition of various additives such as antioxidants and mobilizers that work in synergistic manner to reduce the degradation properties is a common method. Apart from direct additive incorporation, grafting of chemical onto PP is also employed in stabilizing PP after radiation (Lugão et al., 2003). Various additives and mobilizers used in the prvention of PP degradation are listed in Table 2.3:

Table 2.3 Effect of additives in improving PP under radiation

Additive Type	**Additives used**	**Dosage**	**Advantages**	**References**
Mobilizer	Dioctyl phtallate	0.1 pphr	Stable mechanical properties up to 7 months	(Shamshad and Basfar, 2000)
Antioxidant	Hindered amines (Chimmassorb 944 and Tinuvin 622)	0.1 pphr		
Nucleating agent	Bemzoic acid	0.2 pphr		
Antioxidant	Tinuvin 328	0.1 wt%	Better retention of mechanical properties under radiation	(Jia et al., 2007)
Co-polymers	1,2,2,6,6-pentamethyl-4-piperidinyl methacrylate (PMPM), and the copolymers of 2,2,6,6-tetramethyl-4-piperidinyl methacrylate (TMPM) with styrene	NA		
Grafting of stabilizers	PMPM and TMPM	Upto 10%	Improvement in thermal stability	(Wang and Chen, 2006)

Grafting of stabilizers	acrylic acid (AAc) and thermosensitive *N*-isopropylacrylamide (NIPAAm)	NA	Improvement in thermal stability	(Ramírez-Fuentes et al., 2007)
Stabilizers	*tert*-butylcalix[n]arene (*n*=4, 6, 8)	0.3 wt%	Stability of mechanical up to 4 months	(Feng et al., 2000)
Antioxidant	calix[4]arene	NA	Improvement in thermal stability	(Chennakesavulu et al., 2011)
Stabilizer	Fullerene with methyl levopimarate	0.25 wt%	Reduces oxygen uptake	(Zaharescu et al., 2002)
Antioxidant	Irganox 1076 or Topanol OC	0.25 wt%		
Stabilizers	2,2,6,6-tetramethyl-4-piperidyl sebacate	0.5 wt%	Reduces molecular weight, reduces discoloration, Retention upto 6 months at 2.5Megarads	(Klemchuk, 1993)
Stabilizers	tris(2,4di-ferr-butyylphenyl) phosphite	0.5 wt%		
Stabilizers	distearyl thiodipropionate,	0.5 wt%		
Antioxidant	2,6-di-t-butyl-p-cresol	0.2 wt%	Stability up to 25 months	(Yousefi and Katbab, 1994)
Grafting of Stabilizer	HDDA (1,6-hexanediol diacrylate) and TPGDA (tripropyleneglycol diacrylate)	1 wt%	Improvement in melt visocity	(Han et al., 2006)

Nucleating agent	p-(t-butyl) benzoic aluminium	0.1-2%	Improving the crosslinking efficiency by decreasing the crystallinity	(Nhan et al., 2014)

Though these additives enhance the stability of the PP for longer time, there exists a serious threat of migration of the additives from PP into human body through leaching by the fluids. Dopico-García et al. (2007) reported the possibility of migration of several antioxidants including BHA, BHT, AO 2246, AO 425, Ethanox 330, Irganox 1010, and Irganox 1076 from PP. This in turn causes various potential health hazards towards patients (Bourges et al., 1993). The effect is similar to the leaching of plasticizers from PVC. Further, over a longer time the antioxidants and stabilizers also undergo degradation due to their exposure to ionizing radiations. The additives degrade and contribute to additional hyper-peroxides, ketones and carboxylic groups which induce discoloration as well as toxicity. Biedermann et al. (2014) reported the presence of over 70 additives and their resultant degradation products due to radiation in commercial polypropylenes using comprehensive two-dimensional gas chromatography. The degraded compounds if leached from the products could lead to potential health hazards.

PP/EPDM blends under ionizing radiation:

The degradation of PP under ionizing radiation can also be controlled by blending of PP with cross- linkable elastomers such as EPDM. Only very few works were published on the effect of PP/EPDM blends under Gamma and E-beam radiations. A brief of state-of-art of PP/EPDM blend under ionizing radiation is detailed in the following sections.

PP/EPDM is generally an immiscible blend often exhibiting two phase system (Patermann and Altstädt, 2014). Researchers utilized the effect of crosslinking induced by high energy ionization for enhancing the compatibility of the blends, which in turn improved their mechanical and physical properties. However, similar to PP and other polymeric blends, PP/EPDM also undergoes scission and oxidation mechanisms along with the crosslinking.

However, the change in properties of the blend caused by the reaction mechanisms depends on the type of radiation source, absorbed dosage, blend composition and nature of the raw materials (Grosu et al., 2003).

PP/EPDM with blend composition of 90 PP/10 EPDM, 80 PP/20 EPDM and 70 PP/30 EPDM blends irradiated under gamma radiation with a dose range of 5-20 kGy were studied by Cardoso et al. (2016). At these low dosages no significant change in tensile properties, impact strength and structural changes were observed. This indicates that the blend can retain afore mentioned mechanical properties and resist radiation degradation. Grosu et al. (2003) studied the radiation effects on 50 PP/50 EPDM and 25 PP/75 EPDM blends at dose of 50 and 150 kGy for medical uses. Authors reported that the blends with 50% EPDM showed slight decrease in tensile strength and elongation at break up to 150 kGy. On the other hand, the blend with 75% EPDM showed increase in tensile strength at both 50 and 150 kGy. This again was attributed to crosslinking in the polymer blend due to high amorphousness of EPDM favouring crosslinking. The simultaneous crosslinking, scission and oxidation reactions in 50 PP/50 EPDM blends at low dosages of 0-50 kGy were reported by using gel content analysis (Zaharescu and Budrugeac, 2002). It was observed that crosslinking between PP and EPDM below 50 kGy was less favorable than the reaction between free radicals and the oxygen present in atmosphere leading to degradation (in this case thermal properties). This highlighted that EPDM did not protect the blend from degradation at low gamma radiation dosage. EPDM/PP showed low gelation when radiated up to 50 kGy. As a result, reduction of the tensile properties and elongation at break were observed (Zaharescu et al., 1999).

Similar to gamma radiation, the effects of electron beam radiation on PP/EPDM were also carried out only by very few researchers. The tensile strength in PP/EPDM was reported to decrease slightly at 25 kGy, 50 kGy and 75 kGy and severe decrease at 100 kGy and 200 kGy. The material fragility increased due to the domination of chain scission in crystalline region of the blend (Scagliusi et al., 2016). It is noted that at a given dosage range the PP/EPDM exhibits variations in the trend of mechanical properties. One of the possibility is mode of radiation (weather E-beam or gamma). Another factor is that the type of EPDM used, as it also exhibits different ratios of crosslinking and chain scissions. It depends on the ternary monomers like 1,4 hexadiene, dicyclopentadiene and norbene. The effect of radiation on the properties of polymer blend also depends on the ethylene and propylene ratio as well

(O'Donnell and Whittaker, 1985). Among the variety of EPDM grades, those containing ethylidene norbornene exhibit the fastest rate of radiation cross-linking (Drobny, 2012).

In recent years, the radiation of PP/EPDM blends have been carried out in presence of antioxidants, fillers and stabilizing agents. These studies focused on ageing properties and toughening mechanisms targeted for various applications such as automobile, weathering and insulation cables. Many antioxidants and stabilizers used in stabilizing PP are more commonly used for PP/EPDM blends also. They include styrene–ethylene/butylene–styrene elastomer grafted with maleic anhydride, trimethylol propane trimethacrylate (TMPTA) (Żenkiewicz and Dzwonkowski, 2007), stearin and zinc oxide (Scagliusi et al., 2016), alkyl diphenyl ether/ octoxybenzenophenone/ diaryl-p-phenylenedamines (Ueda et al., 1992). However, these studies cannot be co-related with medical devices due to the unavailability of toxicity data on addition of additives to PP/EPDM blend.

Though radiation of PP/EPDM is a well-known process and several reviews and commercial reports (Rogers, 2012, Simmons, 2012) testified the sterilization of PP/EPDM blends by gamma and E-beam radiation, there lies a scarcity of complete data in literature. It is surprising to note that the technical details of PP/EPDM blends such as effect of radiation around sterilization dose of 25-40 kGy is scanty in literature (Balaji et al., 2016). It is important to optimize various factors such as material structure, absorption dose and other radiation conditions, as crosslinking and scission mechanism are rather random processes which cannot be generalized for all materials (Fintzou et al., 2007). The structure and mechanical property relationship, morphological studies, hardness, stiffness, thermal stability, extent of crystallinity of polymer blends are also not available in literature. Moreover, literature also lacks of toxicity data evaluating the biocompatibility of the blend after radiation.

PP/EVA blends under ionizing radiation:

PP/ EVA blends are type of thermoplastic elastomers, whose applications have recently been focused on medical care devices (Shishido et al., 2000, Wagner, 2016, Levernier, 2010). When these polymers are subjected to ionizing radiations for sterilization purpose, they undergo structural changes due to crosslinking and scission induced by hydrogen abstraction from the polymer backbone like any other polymers. To ensure the stability or to improve the

properties of PP/EVA when sterilized under radiation, it is necessary to understand the basics of micro and macro effects of these changes.

At lower dosage of 20 kGy, 60 EVA/40 PP showed reduction of tensile strength from 4.9 MPa to 2 MPa. The EVA did not shield the degradation of PP when radiated under 20 kGy. The storage modulus of the blends also decreased upon radiation. The degradation in crystalline phase was supported by the DSC studies. However, the PP/EVA blend showed better flow characteristics and good reprocess ability of the blends when radiated under 20 kGy (Chattopadhyay et al., 2001).

A detailed study on radiation of PP/EVA at higher dosage range of 1-100 Mrad was reported by Thomas et al. (1987). It was reported that chain scission was dominant in the blends with PP concentration of more than 50%. On the other hand, crosslinking was more dominant in blends with more than 50% EVA. The tensile strength of blends up to 50 EVA decreased in dose range of 10-50 Mrad, due to oxidation of PP resulted from chain scission. In case of blends with 70% EVA, the tensile strength decreased when exposed up to 1 Mrad and has no effect in further increase of dosages. The elongation at break depends on the morphology of each blend. The author reported that net results of simultaneous crosslinks and scission mechanisms caused extensibility in blends, when the blends exhibit co-continuity at 50 PP/50 EVA. However, when particles were found in dispersed phase of rubber in plastic phase, the co-continuity effect is negligible decreasing the elongation at break. In prospective of hardness, only EVA rich blend showed slight increase with increase of radiation dose. For other blends, no significant change was observed.

The radiation improved the compatibility of the blend further by enhancing the interfacial adhesion and providing better morphology. An interfacial region was created between the immiscible blends when radiated at a higher dose of 100 kGy. The formation of interfacial adhesion improves the compatibility of the blend (MIHAYLOVA et al., 2001). The compatibility at 100 kGy between the PP/EVA phase was increased which was evident from single T_g peak transition and single jump of storage modulus. However, the compatibility was improved due to interaction between amorphous regions of PP and EVA only, while they still crystallized separately (Mittal, 2016). A similar effect was reported at a dosage range of 10-100 kGy, where with increase in EVA content and increase in radiation dose, the compatibility of the blends improved (Dalai and Wenxiu, 2002b). A step investigation using

thermogravimetric analysis was attempted to study the effect of reaction mechanisms involved in the crosslinking of PP and EPDM that improved the compatibility of blend in amorphous region. The mobile radicals from PVA chain of EVA combined with the active sites of alkyl radicals from PP to form crosslinks. This result highlighted that PP contributed to the crosslinking in PP/EVA blends and that PP degradation was prevented in PP/EVA blends; that is, methyl radicals in EVA chains are active sites for enhancement of radiation crosslinking in PP/EVA. Apart from crosslinking, the active sites also could form scission and lead to oxidation. It was reported that elongation at break for high EVA content increased till 40 kGy and stabilized with further radiation dose up to 100 kGy. The trend where crosslinking was dominating in EVA rich PP blends was again confirmed by positron annihilation technique implied on radius of free-volume holes that were formed in amorphous phase of the PP/EVA thermoplastic elastomer on radiation (Misheva et al., 2000).

Similarly, Mihailova et al. (1999) showed an evidence of interpreting layer between the amorphous chains of two components and the crystals using X-ray studies. He also reported that the formation of interface layer increased in PP/EVA blend up to 100kGy. The presence of high energy due to radiation caused the shortening of chains and reduced the difference in surface tension between crystalline and amorphous phase, affecting the stability of the phase boundary. At this point the thickness of the interfacial layer grows upon radiation improving the compatibility.

Though EVA deters the oxidation in PP/EVA blends at instance of radiation, during post radiation storage up to 6 months, the total effect or intensity of oxidation degradation was higher in PP/EVA blends rather neat PP polymer (Przybytniak et al., 2007). The authors investigated the free radical process and elaborated the nature and degradation kinetics of PP/EVA blends irradiated at 25 kGy. The effect of degradation of blends was also reported to be higher in terms of rheological properties and mechanical properties during storage. It was shown that in the blends with less EVA content, EVA can also contribute to the worsening of properties during storage. The author also reported that such degradation effect can be minimized when EVA with high VA (more than 25%) content could be used for manufacturing of PP/EVA blends.

2.5 Overview on Antimicrobial Polymer composites

A number of infections and disease caused by microbial/bacterial formation on the medical tubing (especially in urinary catheters) and blood transfusion medical care products were reported (Zimlichman et al., 2013) (Health care-associated infections FACT SHEET, WHO). Catheter-associated urinary tract infection (CAUTI) is a sort of urinary tract disease (UTI) infecting the urinary framework, including urethra, bladder, ureters, and kidney. At the point when a urinary catheter is not inserted accurately, not kept clean, or left in a patient for a really long time, germs can go through the catheter and taint the bladder and kidneys (Arnold et al., Tambyah et al., 1999). Besides, CAUTI can also be induced by improper synthesis of non-biocompatible polymer blends without proper sterilization. CAUTI is the second most normal reason of nosocomial circulatory system disease, and studies recommend that patients with CAUTI have an expanded institutional passing rate, irrelevant to the advancement of urosepsis (UTI not caused by medical care products) (Maki and Tambyah, 2001). Concern over the magnitude of infection due to microbial contamination in blood transfusion tubes and bags was showed in various studies and health organization reports (Hillyer et al., 2003, Eder et al., 2007, Schrezenmeier et al., 2007, Makuni et al., 2015). The whole-blood components are usually stored at 1 to 6°C and platelets are stored at 20 to 24°C to preserve function and survival. Storage at these conditions makes them an excellent growth medium for a broad spectrum of bacteria (Adjei et al., 2009). Multiple aerobic-culture surveillance studies demonstrated that, in 1,000 to 2,000 platelet units are bacterially contaminated (Brecher and Hay, 2005). A detailed study of platelet adhesion and bacterial/fungal adhesion on the polymer blend was well documented by Acton (2013). The study shows that each year more than 1 million patients in U.S. acute-care hospitals and extended-care facilities acquired CAUTI infections (Maki and Tambyah, 2001). As per the reports of Public Health Agency in Canada, 200,000 patients got infections every year while receiving healthcare (Zoutman et al., 2005). Table 2.4 shows the increase in percentage of CAUTI and health care associate infections.

Table 2.4 Statistics on CAUTI affected patients in few countries

Countries	Year recorded	% Increase in CAUTI patients	Reference
USA	2006	14.4	Joint Commission Report,2011
India	2014	10.5	(Datta et al., 2014)
China	2011	15.8	(Xie et al., 2011)
Malaysia	2016	13.9	Joint Commission Report,2011
Morocco	2016	17.8	Joint Commission Report,2011

Various methods such as enzyme coating, medical solution coatings, hydrogel coating and incorporation of metal nanoparticles are adopted in order to combat the issues. However, these methodologies have limitations in their instability and difficulties of immobilization of these coating solutions on polymers.

Incorporation of metal nanoparticles into polymeric matrix is one of the most commercially preferred methods to introduce antimicrobial properties due to cost efficiency and ease of manufacturing. Few metals are greatly toxic to microbes (especially bacteria) at uncommonly low concentrations. On account of this biocidal movement, metals have been broadly utilized as antimicrobial operators in health care industry. Unlike other antimicrobial operators, metals are stable under most of the conditions as of now found in the business permitting their utilization as added substances. One recent route to further extend the antimicrobial applications of these metals is via their incorporation as nanoparticles into polymer matrices (Palza, 2015). Over the years, a number of studies have been published on the different metal nanoparticles used as antimicrobial agents. Metal and metal oxide nanoparticles such as magnesium oxide, gold, titanium, aluminium, copper oxide, copper nanoparticles and zinc are highly stable and show biocidal action against various gram negative and gram positive bacterial stains (Stoimenov et al., 2002). The effect of biocidal activity depends on exposure method, concentration of nanoparticles and size of the nanoparticles. Different nanoparticles have different mechanism against the bacterial exposure. The nanoparticles usually are

considered to follow one of the following generalized mechanisms: oxidative stress induction, metal ion release or non-oxidative mechanisms. Sometimes, all 3 types of mechanisms can also occur simultaneously (Wang et al., 2017). The mechanism of action against few targeted microbes of gold, magnesium oxide, zinc oxide, copper oxide, aluminium and AgNP are summarized in Table 2.5. Among the metal nanomaterials listed in Table 2.5, Ag nanoparticles are most preferred to business commercial enterprises. It is because of its efficacy of toxicity over a wide range of microbes (Dowling et al., 2001). Syed et al. (2009),Meenakumari et al. (2013), Agarwala et al. (2014) and many others have studied the biocidal action of AgNP on pathogens, providing protection against the CAUTI infections. Also, various studies on the mechanism of action of AgNP over the microorganisms and their dispersion in polymers were studied to manufacture engineered polymers for health arena (Furno et al., 2004, Knetsch and Koole, 2011).

Table 2.5 Metal nanoparticles for biocidal action

Metal Nanoparticles	Mechanism of Action	Targeted Microbes	References
Gold	On near infrared (NIR) irradiation the Au-based nanomaterials destroy bacteria	Staphylococcus aureus, Gram-positive and Gram-negative bacteria,	(Pissuwan et al., 2010)
Magnesium oxide	Active oxygen generated from MgO was related to its antibacterial activity	Bacillus megaterium, Bacillus subtilis	(Jones et al., 2008, Sawai et al., 2000)
Zinc oxide	The generation of hydrogen peroxide from the surface of ZnO inhibits bacterial growth	Listeria monocytogenes, Salmonella enteritidis, Salmonella typhimurium and Staphylococcus aureus,	(Ravishankar Rai and Jamuna Bai, 2011)

		E.coli, Campylobacter jejuni	
Copper oxide	Copper ions released may also interact with DNA molecules and intercalate with nucleic acid strands. The exact mechanism behind bactericidal effect of copper nanoparticles is not clear.	Pseudomonas aeruginosa, Proteus spp., B. subtilis	(Wei et al., 2014)
Aluminium	Free-radical scavenging properties of the particles might have prevented cell wall disruption and drastic antimicrobial action	E. coli cells	(Mukherjee et al., 2011)
Silver	Silver ions (particularly Silver ions released from interact with Phosphorous moieties in DNA to inactivate DNA replication, or react with sulfur-containing proteins, leading to the inhibition of enzyme functions	Staphylococcus aureus, Staphylococcus epidermidis, Enterococcus faecium, Klebsiella pneumonia, Staphylococcus epidermidis, Streptococcus pyogenes, Salmonella typhi	(Dallas et al., 2011)

There are many possible mechanisms being put forward on the biocidal action of AgNP on microbes. However, the most common theory is that AgNP bind to the cell wall of the bacterium. They pass through the cell membrane and causes structural changes in bacterium leading to toxic effects on bacterium. Sondi and Salopek-Sondi (2004) proposed that tightly packed lipopolysaccharide (LPS) molecules in the outer cell acts as permeable membrane enabling the penetration of AgNP. Additionally, the morphological images show that a "pits" are being formed in surface where more AgNP accumulated and enhanced the destruction of cell membranes. On the other hand, Kim et al. (2007) showed that free radical formation of AgNP is the main cause for destruction microbe cell membrane. Further, another theory states that ions released from Ag nanoparticles could also be the main cause for cell destruction. Though, the mechanism is not clear the Ag nanoparticles were impregnated in a number of polymer matrix to introduce antibacterial properties to the material (Palza, 2015). A general mechanism of biocidal action of AgNP is illustrated in Figure 2.3.

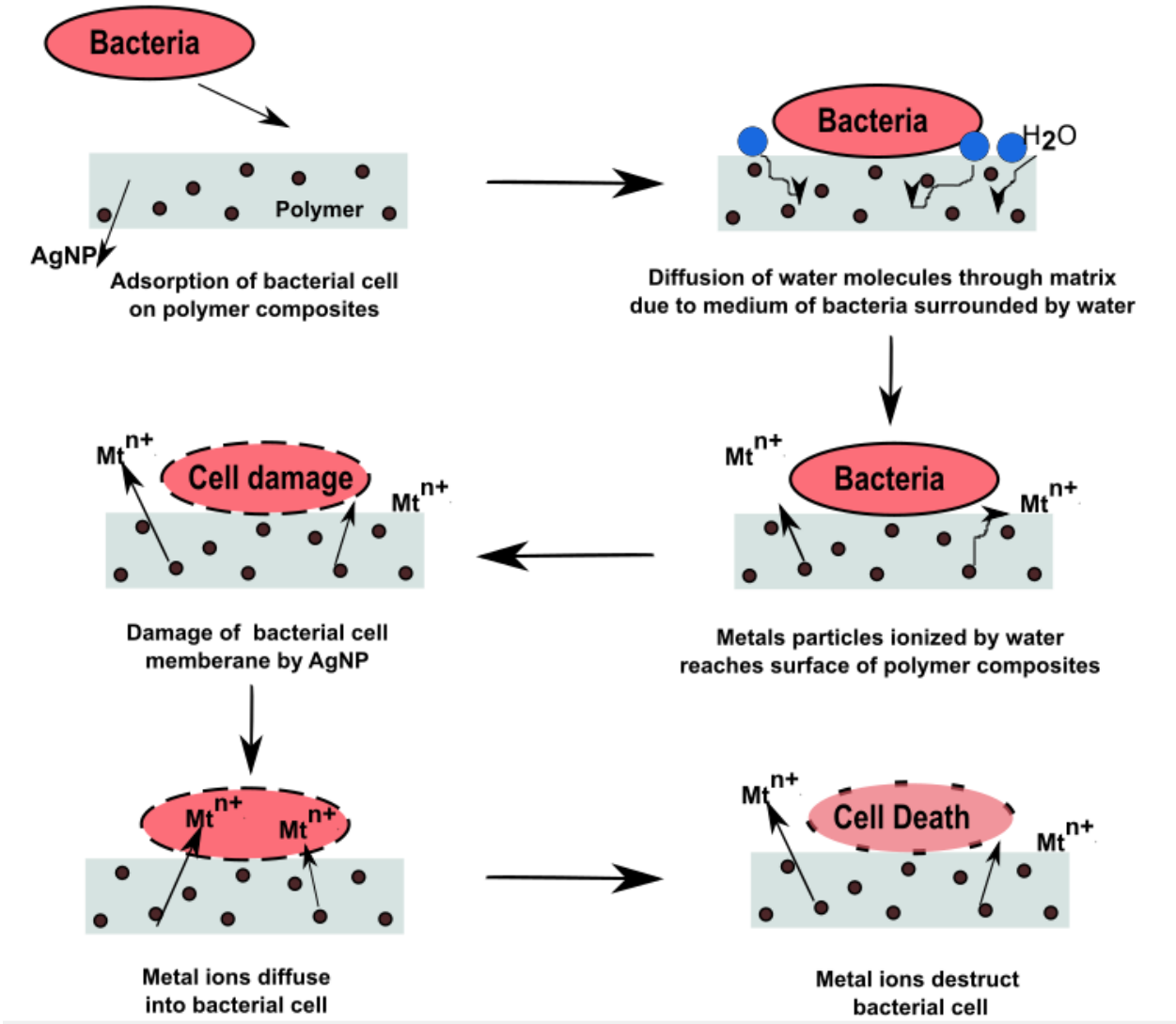


Figure 2.3 Mechanisms for the antimicrobial behaviour of polymer/metal nanocomposites with AgNP (Palza, 2015).

The Ag nanoparticle-polymer composite was synthesized either by in-situ or ex-situ methods. In-situ method is carried out by dissolving a metal precursor in the polymer and decomposed either by thermal or radiation source. During the decomposition, the Ag atoms diffused into polymer matrix which is in contact with microbes executes its biocidal effect. A number of works based on in-situ synthesis of Ag nanoparticle composites were carried out in various polymers such as polystyrene (Voronov et al., 2007), polyurethane(Triebel et al., 2011), polyamides and polypropylene (Muñoz-Bonilla and Fernández-García, 2012) for various

medical, food packaging, textiles and healthcare applications. The antibacterial properties are usually evaluated using quantitative methods such as agar diffusion tests and broth dilution tests (following the JIS Z 2801 standards). Different studies showed the biocidal effect of Ag on various strains of bacteria, fungi and yeast. However, *Escherichia coli* and *Staphylococcus aureus* are the commonly used strains for the preliminary evaluation of antibacterial effects of AgNP polymer composites.

Ex-situ method involves melt blending or extrusion of AgNP along with polymeric raw materials. AgNP exhibit biocidal property mainly because of the ions released by the nanoparticles in contact with water from the bacterium medium. Though PP and polyethylene is hydrophobic, some extent of water diffusion was still shown possible due to their trans-crystallinity nature (Ton-That and Jungnickel, 1999). Radheshkumar and Münstedt (2006) studied the mechanism of Ag ions in a PP matrix using anode stripping voltammetry. He showed that Ag ion migration was not only surface property but also occurred through layers in bulk polymer system. The water molecules diffused into bulk system and caused corrosion or dissolution of AgNP leading to release of Ag ions. These Ag ions migrated to the surface of PP and served as the main source of biocidal action against microbes attached to its surface (Palza, 2015). Radheshkumar and Münstedt (2006) also showed that quenching and use of coatings such as zeolites, TiO_2 and sodium hydrogen zirconium enhanced the antimicrobial efficiency of polymer nanocomposites as well.

When AgNP were added to polymer composites by melt blending or extrusion technique, the properties of the polymer alters depending upon the type and loading of AgNP. Ghosh and Maiti (1996) evaluated the mechanical properties of PP after the incorporation of Ag nanoparticles. The authors reported that tensile strength showed decreasing trend when 0-5.6% AgNP were added. The Ag nanoparticles agglomerated in the matrix and acted as weak points that initiated cracks and reduced their strength. Moreover, impact strength also decreased due to the agglomerates of Ag nanoparticles acting as stress concentrators. On the other hand, flexural properties increased due to increase in rigidity, as AgNP do not provide any space for deformation. Yeo and Jeong (2003) showed that the crystallinity of PP was reduced as AgNP did not act as nucleating agents but was found to be present in matrix as impurities. Tjong and Bao (2007) studied the effect of 0.1-1.0% AgNP in isotactic PP. The authors reported that AgNP induced formation of β-phase melt peaks in crystalline region when studied under DSC. The formation of β-crystalline melt peaks in addition to α-

crystalline peaks was witnessed. He also concluded that such crystallinity induction upon addition of AgNP improved the ductility and impact properties of the polypropylene composites.

It is important to remark that AgNP have a great tendency to form micro-aggregates and the presence of a surfactant enhances better dispersion (at a nano-scale range) despite it is difficult to achieve total dispersion of individual particles even when using shear forces in the extrusion process (Fages et al., 2011). The authors improved the mechanical properties by improving the dispersion of nanoparticles by coating AgNP with 2% oleic acid, PVP and addition of 0.4% PP-g-MA stabilizer. Though dispersion was improved, AgNP was not dispersed completely as agglomerates could still be viewed under TEM. Jokar et al. (2012) showed an insignificant difference change in tensile strength, elongation at break and young's modulus of LDPE nanocomposites when Ag nanoparticles were dispersed with 5% of PEG 200. Oliani et al. (2015) showed an improvement in de-agglomeration when AgNP were coated with PVP in PP matrix. However, studies on the effect of mechanical properties by addition of AgNP by melt blending are limited to only few polymer matrices.

2.6 Summary

From the literature, it can be understood that researchers have devoted more attention on developing new materials for manufacturing of PP/EPDM blends. Extending the trend, number of works have been performed to improve the various properties of PP/EPDM using chemical additives for numerous applications. It is also noteworthy to notice that the ionizing radiations, especially E-beam radiation can be an effective tool to improve the properties of the blend in addition to its advantage of providing sterilization of the materials at low cost and sustainable method. However, the ionizing radiations causes change in mechanical and thermal properties due to simultaneous chain scission and crosslinking mechanisms. The literature lacks a clear picture on the effect of E-beam radiation on PP/EPDM blends at low dosage of 20-100kGy. Also researchers aimed at improving the properties of the blends under radiations only with chemical additives, which again leads to toxicology uncertainties. Hence, this study aims to develop a strategy to improve the properties of PP/EPDM or at least make them resistible to E-beam radiation (without losing properties) by introducing a thermoplastic polymer-EVA. Characterization should be thoroughly conducted to identify and emulate ways to empower the newly developed ternary blend to explore its application

in various applications. Further, there is an urge for developing antibacterial materials to combat the infections caused during healthcare and food packaging. This is to be addressed by incorporating AgNP to the ternary blend. Clearly the magnitude of research on effect of incorporating Ag nanoparticles on the properties of the ternary blends is limited and hence is addressed in this study. Also, the novel blend compounded with Ag nanoparticles, must be characterized thoroughly to analyse their effects when exposed to E-beam sterilization.

3 METHODOLOGY

3.1 Introduction

This chapter details the materials and methods used in this study. The details of methodologies adopted were clearly documented here.

3.2 Materials

Isostatic polypropylene (Grade Globalene 8661) was purchased from LCY Chemical Corp, USA. The melt flow index, MFI, density and melting point of the polypropylene are 18 g/10 min, of 0.9 g/cm^3 and of 78°C, respectively. Ethylene propylene diene terpolymer of grade 3092PM (EPDM) having 65% ethylene and 6.4% diene monomer of Mooney Viscosity- 61(at 125°C) was purchased from Mitsui chemicals, Shanghai. Medical grade of ethylene vinyl acetate (EVA, Elvax 250) was purchased from DuPont, USA. EVA consisted of 28 wt% vinyl acetate with density of 0.95 g/cm^3 and melt flow rate of 25 g/10 min (190℃/2.16 kg). Ag nanoparticle powders of particle size <100 nm containing 99.5% trace metals and poly (vinyl pyrrolidone) (PVP) dispersant was purchased from Sigma Aldrich, USA. Materials for in-vivo tests including MTT (a tetrazolium dye, 3-(4,5-dimethylthiazol-2-yl)-2,5-diphenyltetrazolium bromide) was purchased from Gibco, USA and DMSO was purchased from Sigma Aldrich, Germany.

3.3 Blending

The polymer blends were prepared by melt blending in an internal melt mixer (Haake Remix Polydrive R600/610 of volumetric capacity of 44 cm^3). For the optimization of process parameters using DOE, various batches of different experimental runs were blended at different processing time, temperature and screw speed based on the design sheet listed in chapter 4, Table 4.2. For further studies, all the blends were prepared at temperature set of 165°C (obtained from optimization study chapter 4). The EPDM, PP and EVA were loaded at pre-determined ratio simultaneously and the total mixing time was kept constant to 10 min for all the blends to ensure similar thermal history. For Ag composite blend, the AgNP were premixed with polymers by manual mixing and loaded into the blender. The rotor speed was fixed at 50 rpm. The resultant materials were immediately cut into smaller pieces and kept in sealed plastic bags for compression moulding.

3.4 Compression Moulding

Materials collected from internal mixer were compression moulded to obtain rectangular slabs. The compounded materials were placed with a slight excess into a steel frame flash mould (200 mm x 200 mm) covered by disposable polyester sheets (200 mm x 200 mm x 0.1 mm) and aluminium plates (200 mm x 200 mm x 2 mm) on both sides . The thickness and shape of test specimens determine the thickness and cavity size of the flash mould. Disposable polyester sheets were used to ease the release of slabs from the flash mould, by avoiding the slabs from adhering to the aluminium plates.

The filled mould was positioned in between the platens of an automated hydraulic heated press (LP-S-50 Scientific Hot and Cold Press, Thailand). The platens were pre-heated to 160 °C. The heat reached the mould and compounded materials via conduction. The moulding cycles involved 4 min of preheating without pressure to melt the materials; followed by 20 sec of pressure cycling (also known as venting) between 0 to 10 MPa to distribute the melted material in the cavity and dislodge any air bubbles; and 4 min of holding pressure at 10 MPa.

Following the holding time, cooling procedure was imposed by carefully removing the mould from the heated press to the adjacent cooling press equipped with water circulating channels pumped with chilled water at 20°C. Cooling procedure was done for 4 min at 10 MPa to eliminate non-uniform cooling and warping of the slabs. The cooling rate of the mould was estimated to be between 40 and 50 °C/min. The slabs were then carefully removed from the mould cavity and excess/flash on the slabs was trimmed with a sharp knife.

3.5 Electron Beam Irradiation

The moulded slabs were irradiated using 3.0 MeV electron beam accelerator (model NHV-EPS-3000, Malaysia) at doses 20, 40, 60, 80 and 100 kGy. The acceleration energy, beam current and dose rate were 2 MeV, 5 mA, and 20 kGy per pass, respectively.

3.6 Gel Content

Gel content analyses were measured according to ASTM D2765. The binary/ternary polymer samples were extracted for 24 h in boiling xylene using a Soxhlet extraction set. The resulting

samples were then dried in oven at 70°C until a constant weight was obtained. Gel content was determined as per Eq. (3.1) below:

$$\text{Gel Content (\%)} = \frac{w_1}{w_0} \text{ x } 100 \qquad (3.1)$$

where, w_0 and w_1 are the dried weight of sample before and after extraction, respectively.

3.7 Tensile Properties

The samples subjected to tensile test were cut into dumbbell shape with dimensions (gauge length of 10 mm, thickness 1 mm and width of narrow section as 3.18 mm) in accordance with ASTM D638, specimen type V standard. The tensile properties of polymer blends were tested using a computerized tensile tester (Toyoseiki, Japan) with a load cell of 10 kN. The crosshead speed was set at 50 mm/min for all samples. Data for tensile strength, and elongation at break were recorded. At least 7 specimens were used for each set of blend and average results were taken as the resultant value. Standard deviation of the results was less than 10%.

3.8 Impact Strength

All impact samples were cut into rectangular specimens and notched. The Izod impact tests were conducted according to ASTM D256 using CEAST (Model CE UM-636, USA) Impact Pendulum Tester, with a 4 J hammer. The specimen dimensions were 6 mm wide and 3 mm thick with a notch of 2.59 mm. The samples were dipped in liquid nitrogen for 1 min and their impact energy was measured after cryo-treatment. Seven samples were tested and at least five replicate specimens were presented as an average of tested specimens.

3.9 Hardness Test

Hardness test specimens were compression moulded according to ASTM D2240 (Type Shore A) samples. The test pieces had a length of 100 mm, width of 100 mm and thickness of 5 mm. This test was conducted at ambient temperature using hardness tester with the blunt indenture (Durometer Hardness model Zwick 7206, Netherlands). A minimum of 7 hardness

readings was recorded for each sample and average results were taken as the resultant value. Standard deviation of the results was less than 10%.

3.10 Thermogravimetric Analysis

The thermal stability measurements were carried out by using approximately 10 mg of the blend at a heating rate of 10˚C/min from room temperature to 600˚C using a thermogravimetric analyzer (Perkin-Elmer Pyris TGA, USA). The mass loss versus temperature thermographs were obtained with the compounds placed in high quality nitrogen (99.5% nitrogen, 0.5% oxygen content) atmosphere with a flow rate of 20 mL/min, in order to avoid oxidation.

3.11 Differential Scanning Calorimetry

The samples were subjected to DSC analysis using Mettler Toledo DSC 1/700 equipped with STARe System (USA). All samples were subjected to a heating rate of 10 °C/min and a cooling rate of 20 °C/min. The samples were initially heated from room temperature to 200 °C and held for 10 min to erase the thermal history. Following the first heating, the samples were cooled to -100 °C. Then, the samples were subjected to second heating cycle up to 200 °C. The results were analyzed using STARe System software. The first heating rate was omitted from data analysis. T_c and T_m were defined as crystallization and melting temperature obtained from peak of crystallization and melting curve using the thermograms obtained, respectively. ΔH_f is the heat of fusion of the sample determined from the area under the peak of the melting curve. The percentage of crystallinity, X_c, of PP in the blends was calculated as per Equation (3.2) below:

$$X_c(\%) = \frac{\Delta H_f}{\Delta H_f^{\circ}} \text{ x } 100 \qquad (3.2)$$

where ΔH_f is the heat of fusion of the sample, ΔH_f° is the heat of fusion of a 100% PP crystalline which is 209 J/g (Manchado et al., 2000).

3.12 Dynamic Mechanical Analysis

DMA was performed in dual cantilever mode using a dynamic mechanical analyzer (Perkin ElmerUSA). The temperature interval was - 80 to 100 °C with a heating rate of 5 °C/min, using a frequency of 1 Hz. The samples were cut into a dimension of 25 x 6 x 2 mm from compression moulded slabs. The sample dimensions were kept as similar as possible in order to obtain an accurate comparison. Variation of storage modulus and tan δ values with temperature were recorded. Peak of tan δ was taken as the glass transition temperature (T_g) of the sample.

3.13 Fourier Transform Infrared Spectroscopy

The chemical functional group of the sample polymer blends was characterized using Fourier transform infrared spectroscopy (FTIR, Perkin Elmer Spectrum 2000, USA). The spectrometer was operated with 50 scans at 4 cm^{-1} resolution and within the range of 4000-400 cm^{-1} for each sample. All FTIR spectra were recorded in absorbance unit. The test was conducted by preparing a thin film of PP/EPDM pressed by compression moulding.

3.14 Yellow Index

The yellowness index (YI) values of irradiated and unirradiated samples was measured by using the Hunterlab Colourquest Spectro-Colorimeter (USA) in accordance with ASTM D1925. The control samples prior to radiation were used as blanks for the respective blends.

3.15 *In Vitro* Analysis

3.15.1 Cell culturing Process

The *in-vitro* biocompatibility of polymer blends was evaluated using HaCaT (human keratinocyte) cells. The cells were cultured in a complete MEM medium consisting of 5% fetal bovine serum (FBS). The cells were maintained at 37°C for incubation in 5% CO_2 atmosphere. The medium was changed every 2-3 days. The cells reached confluency in 7-9 days. Upon confluency, the complete medium was removed and washed with phosphate buffered saline (PBS) solution. The cells were detached from 75-mL flask by addition of 2 mL of 0.25%

trypsin. To facilitate the detachment (trypsinization process), the flasks were incubated at 37°C for 10-15 min in incubator. The detached cells were centrifuged at 1800 rpm for 8 min to separate the cells from the medium. Further, the cells were re-suspended in complete medium before seeding.

3.15.2 Cell fixing for FESEM analysis

The polymer samples prepared by compression moulding, with 0.5 mm thickness and 0.6 mm in diameter were used for the tests. The samples were sterilized in 96-well plate for 15 min by UV radiation before cell seeding. Approximately 2.5 x 10^5 cells were seeded into each well containing circular samples. Each well containing cells and polymer sample was filled to 1 mL with complete medium after seeding and incubated under standard cell culture conditions for different incubation periods (4 h, 1 day, 3 days and 7 days). The culture medium was changed every 3 days. After the pre-determined incubation period, the following steps (Figure 3.1) were performed for cell fixing before FESEM viewing. The majority of the cells was fixed on the upper side of the samples. The samples were taped onto stubs on the lower face using carbon tape for viewing. The morphology of the cells cultured on polymer samples was examined using FESEM at an accelerating voltage of 10 kV, at a magnification of 10000x and a working distance of 10 mm.

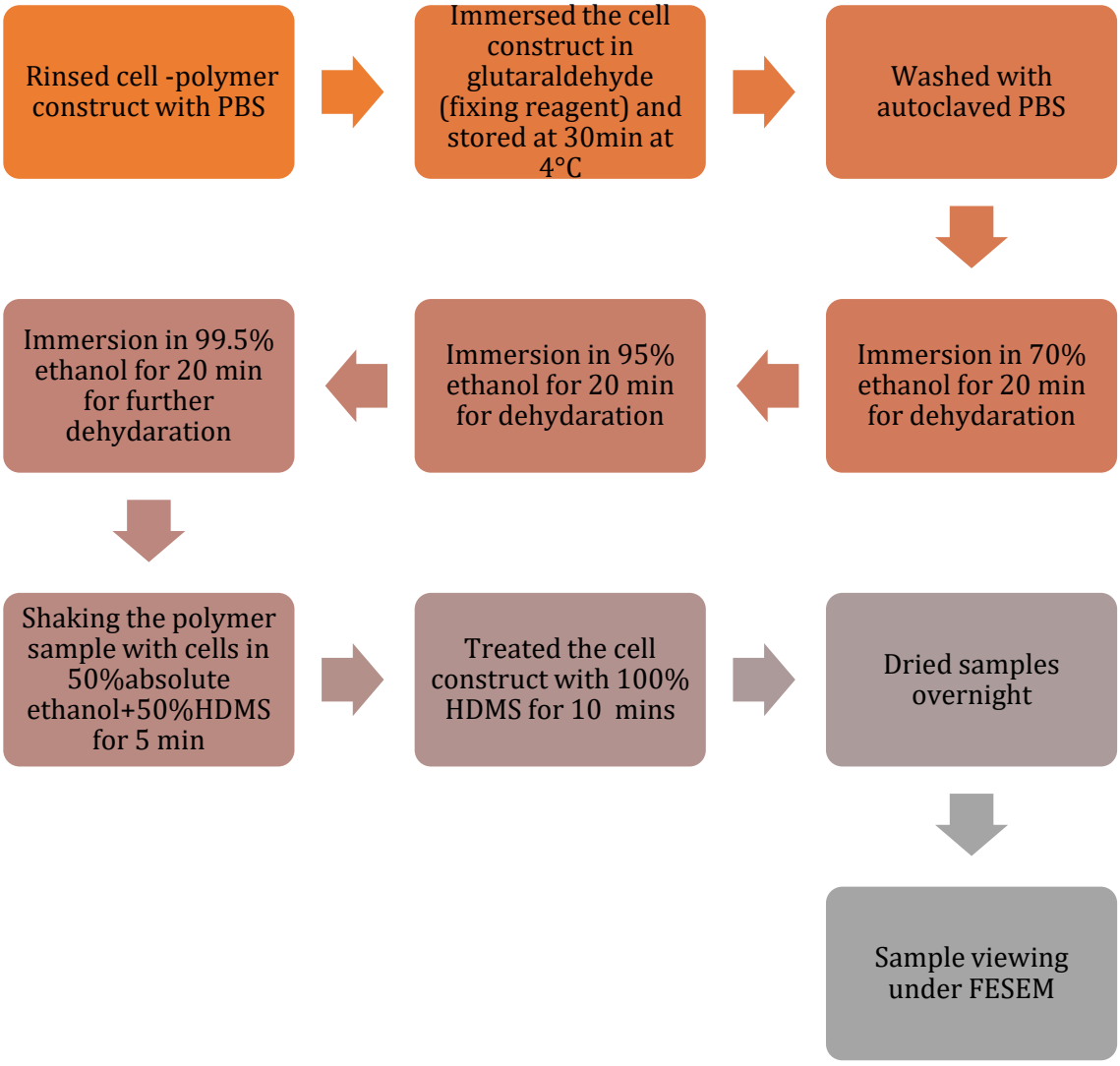


Figure 3.1 Procedures for cell fixing

3.15.3 Cytotoxicity Test

The toxicity of polymer blends was performed by using MTT (a tetrazolium dye, 3-(4,5-dimethylthiazol-2-yl)-2,5-diphenyltetrazolium bromide) assay. The MTT assay was performed after 1, 3 and 7 days of incubation. After incubation period, old medium was discarded and each well was refilled with 100 µl of pure MEM and 10 µl of MTT solution (containing 5 mg/ml MTT powder). The plates were incubated at 37°C for 4 h. MTT was reduced by mitochondrial succinate dehydrogenase of viable cells and formed insoluble and dark purple formazan. The formazan formed was dissolved by using 100 µl of dimethyl sulphoxide (DMSO). The optical density of the resulting solution of 200 µl was measured at 570 nm using Varioskan™ Flash multimode reader (Thermo scientific, USA). Triplicates were performed for each experiment at prescribed incubation period. The percentage of survival was calculated by regarding the optical density of resultant sample with the optical density of the solution in control well (well without polymeric sample).

3.15.4 Antimicrobial Test

The bacterium strains Pseudomonas aeruginosa ATCC27853 and Staphylococcus aureus ATCC29213 were cultured in brain heart infused broth incubated at 37°C for 24 h under 5% CO_2. Direct suspension of the colonies was made in cationically-adjusted MHB (CAMHB) and adjusted to OD625 0.08–0.1 which corresponded to 1-2 x 10^8 CFU/ml. The cells were maintained at approximately 5 x 10^4 CFU/ml by serial dilution. Sterilized rectangular polymer samples of 3 mm thickness were used in the study. 10 µl of the bacterial suspension was pipetted on polymer slab. A sterilized glass plate was placed on the top. The polymer-glass construct was placed in a circular plate. The circular plate was covered and sealed (using parafilm) with water spread on sides to prevent evaporation of the suspension and drying of the bacterium strain when incubated. The sealed circular plate was incubated at 37°C for 24 h under 5% CO_2. After 24 h, the polymer slab and glass were washed with 2 ml of PBS by mild shaking for 2 min. The diluted bacterial strain was further subjected to 6-fold dilution. One hundred µl of diluted medium and the medium before dilution were aliquoted onto agar plates separately. The aliquoted medium containing bacterium strain were spread evenly using a sterilized glass spreader. The agar plates were incubated for 24 h at 37°C under 5% CO_2. The bacterium colonies grown were counted after 24 h. Three experimental trials

were performed for each sample with each bacterium strain. The average of three trials were determined for the study.

4 OPTIMIZATION OF PROCESSING PARAMETERS FOR PP/EPDM BLENDING USING DESIGN OF EXPERIMENT

4.1 Introduction

The current chapter addresses the first aim of this study which was to optimize the process conditions for blending PP/EPDM. Processing time, temperature, rotor speed and blend composition were the parameters considered in this study for optimization. The trials to achieve optimized blend were constructed in specific order using a software called Design of Experiment R 8.0 by Stat-Ease Ltd. The optimized parameters were obtained with the target of achieving the blend with the highest tensile strength and maximum elongation at break. The content of this chapter was published in Journal of Polymer Plastic Engineering technology (DOI: 10.1080/03602559.2016.1211695).

4.2 Design of Response Surface Methodology

A Response Surface Methodology (RSM) design package was selected for the study, as they assist to explore the relationship between several input variables and one or more response variables. The analysis was based on D-Optimal design model. The advantage of D-optimal design over the other designs, such as central composite design, box-benken method and factorial method, is that the effect of factor estimates can be co-related at the same time with reduced number of runs. D-optimal includes the best subset of all possible experiments. It also provides a wide range of property profile based on the factors considered, easing one to choose the blend ratio and the processing conditions that suit the requirement of the product. The other advantages include combination of process and mixture factors which can be used in same time, even irregular/constrained design space which can be modelled, the opportunity to modify the underlying model in different regression models. The analysis was based on D-Optimal design model with 4 factors and 2 responses. The blending parameters studied known as factors in RSM included temperature (A), blending time (B), screw speed (C) and composition ratio (D). Parameters A, B and C were continuous type factors with two levels (high and low), while the factor D was discrete type with 7 levels. Table 4.1 shows the range of factors used. The effect of these factors on the PP/EPDM blend was studied in terms of two responses: tensile strength (Response 1) and elongation at break (Response 2). Table 4.2 shows the 25 experimental runs generated by the RSM software. Runs 6, 10, 16, 20 and 25 were replicated runs which were used to study the lack of fit and pure errors.

Table 4.1 Independent variables chosen in RSM study

Coded Name	**Factors**	**Type**	**Range**		**Units**
A	Blending Temperature	Continuous	Level 1/ Low	140	˚C
			Level 2/ High	180	
B	Blending Time	Continuous	Level 1/ Low	5	min
			Level 2/ High	15	
C	Screw Speed	Continuous	Level 1/ Low	50	rpm
			Level 2/ High	100	
D	Blend Ratio	Discrete	Level 1	100 EPDM	%
			Level 2	80:20 PP:EPDM	
			Level 3	70:30 PP:EPDM	
			Level 4	50:50 PP:EPDM	
			Level 5	30:70 PP:EPDM	
			Level 6	20:80 PP:EPDM	
			Level 7	100 PP	

Table 4.2 Actual and Predicted values

Run	Factor A (Temperature) (°C)	Factor B (Time) (min)	Factor C (Screw speed) (rpm)	Factor D (Blend Ratio) (%)	Response 1		Response 2	
					Actual	Predicted	Actual	Predicted
1	180	10	82	100% EPDM	4.350	1.68	703	766.90
2	159	5	82	100% PP	28.235	28.00	692	686.76
3	140	5	100	100% EPDM	5.029	3.14	1078	1069.02
4	140	13	50	100% EPDM	4.673	3.86	1128	1141.80
5	180	15	50	100% EPDM	2.565	2.27	752	754.17
6	180	15	50	100% EPDM	2.647	2.28	956	958
7	177	10	79	70:30% PP:EPDM	14.676	20.41	722	753.98
8	140	10	100	100% PP	30.942	29.57	666	682.93
9	180	5	50	100% PP	28.739	30.87	638	701.12
10	140	13	50	100% EPDM	5.353	3.86	1108	1141.80
11	158	9	94	30:70% PP:EPDM	11.993	10.851	966	965
12	180	5	100	50:50% PP:EPDM	13.613	14.79	808	796.77
13	140	5	50	80:20% PP:EPDM	20.876	21.94	774	801.07
14	165	14	72	30:70% PP:EPDM	8.755	10.47	952	801.78
15	171	5	50	100% EPDM	2.753	4.19	966	1031.18

16	180	5	50	100% PP	35.566	30.87	776	701.12
17	180	15	100	100% PP	29.379	25.87	763	730.85
18	161	15	100	100% EPDM	2.238	2.00	686	697.71
19	140	15	82	50:50% PP:EPDM	14.917	18.21	826	859.46
20	171	5	50	100% EPDM	5.125	4.19	1100	1031.18
21	141	7	67	20:80% PP:EPDM	5.337	7.80	1088	1058.52
22	165	11	50	70:30% PP:EPDM	23.48	22.03	862	82.14
23	140	15	50	100% PP	32.950	31.36	886	863.29
24	180	15	65	100% PP	26.54	28.70	700	774.43
25	159	5	82	100% PP	31.346	30.646	492	490

4.3 Fit of Regression Model

Fit of regression model enables values on one variable to be predicted from one or more actual variables (Triacca et al., 1993). Hence, the actual experimental data obtained after conducting the mechanical property tests was fitted into the most suitable mathematical regression model in order to generate the predicted values presented in Table 4.2. In this study, the data was fitted into 2FI (two factor interaction) regression model using the QR (orthogonal matrix Q and an upper triangular matrix R) decomposition algorithm adapted by the Design Expert software. The advantage of 2FI model is that the interaction between two factors and their effect on the responses is considered simultaneously.

4.4 Evaluation of Regression Model

The regression of the fitted model was first evaluated using Analysis of Variance (ANOVA). The polynomial equation for the fitted 2FI regression model for each responses tensile strength (Y1) and elongation at break (Y2) were expressed in coded factors as shown in Eq (4.1) and Eq (4.2), respectively.

Y1 = 15.91 + 00.30*A - 0.60*B - 0.65*C- 13.05*D - 1.33*AB - 0.13*AC - 0.42*AD - 1.04*BC - 0.17*BD + 0.19*CD

Eq(4.1)

Y2 = 831.34 – 32.37*A – 68.43*B – 60.22*C + 97.37*D – 20.47*AB – 22.30*AC – 76.54*AD + 18.94*BC -72.75*BD – 32.44*CD

Eq (4.2)

In the regression equation, the negative sign assigned for coefficient indicates an inverse effect between the factor and the response variables. Alternatively, the positive sign indicates the synergistic effects (Dubey et al., 2006b). Some of the characteristic terms that aid ANOVA to validate the significance of the fitted model are coefficient variation (CV), predicted residual sum of squares (PRESS), multiple correlation coefficient (R^2), adjusted R^2 (Adj R^2), and adequate precision. Table 4.3 shows the summarized ANOVA results for both the responses. In this table, the multiple correlation factor R^2 for both tensile and elongation at break were found to be 0.9581 and 0.8947, respectively. Given that these values are

approaching the integrity (≈1) indicated good degree of fitness. R^2 is optimized to the integrity by adjusting the PRESS factor to 695.01 for tensile and 1895 for elongation at break. These high values of PRESS for both responses shows the possibility of each experimental run considered to fit the model is higher. Further, from the same table, adjusted correlation factor (Adj R^2) were found to be 0.9200 and 0.7990 for tensile and elongation at break, respectively. These values were close to optimum limit of 1 indicating a high degree of variations of adjusted parameters considered for the fit along the mean of the regression. In other words, only 8% (for tensile) and 20% (for elongation at break) of the adjusted parameter variations are not considered for the fit of the regression model. Similarly, the predicted R^2 of tensile and elongation at break being 0.7612 and 0.668, signified the predicted parameters (Predicted R^2) were also considered with high degree of variations. Additionally, predicted R^2 was in reasonable agreement with Adj R^2, as their difference is less than the upper limit of 0.2. This result is in agreement with the principle of ANOVA, as this analysis works by comparing the variations due to the treatment, with the variation due to the random errors that were inherited along with the dimensions of generated responses (Triacca et al., 1993). Additionally, the relatively low CV% for tensile strength (21.1%) and elongation at break (8.6%), ensures that the reliability and correlation between the actual and predicted are considerably higher. Furthermore, the standard deviation of the model was as low as 3.33 and 7.36 for tensile strength and elongation at break, respectively. Adequate precision can be related inversely with standard deviation and is used to measure the signal to noise ratio. From Table 4.3, it can be observed that the adequate precision of both the responses was higher than the required value of 4, indicating that the model was designed with least errors possible.

Other factors that can be used in ANOVA are p-value and F-values. The p-value for the models of both responses was in Table 4.3 within the reference value of 0.05, denoting that the fitted models were significant. The low p-values (< 0.0001) for both tensile strength and elongation at break advocates for evidence that the null hypothesis are rejected through the entire model (Sellke et al., 2001). Moreover, the F-values imply lack of fit is not significant relative to pure error. The desired non-significance ensures the validation of fitted model in addition to the ANOVA. The F-test is validated by ANOVA with the assumption that the data follows normal distribution (Zou et al., 2004, Anderson, 2001). The assumption is validated using the normal

plot of residuals (Figures 4.1 and 4.2). In both the plots, the residuals were found along the straight line which ensures that the model data points follow normal distribution.

Table 4.3 Regression Model Characteristics using ANOVA

Respo-nse	Model Type	F value	p-value	Lack of Fit	Std. Dev	C.V %	PRESS	R^2	Adj R^2	Predicted R^2	Adequate Precision
Tensile Strength	2FI	25.15	< 0.0001	11.95	3.33	21.1	695.01	0.9581	0.920	0.7612	12.608
Elongation at Break	2 FI	9.35	< 0.0001	0.81	7.33	8.6	189500	0.8947	0.799	0.6628	8.846

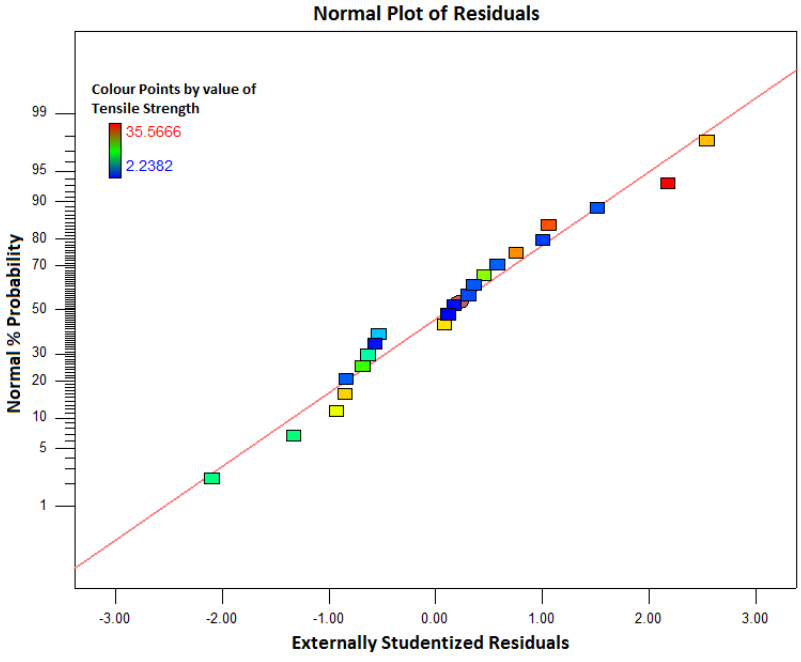


Figure 4.1 Normal Plot for Tensile Strength

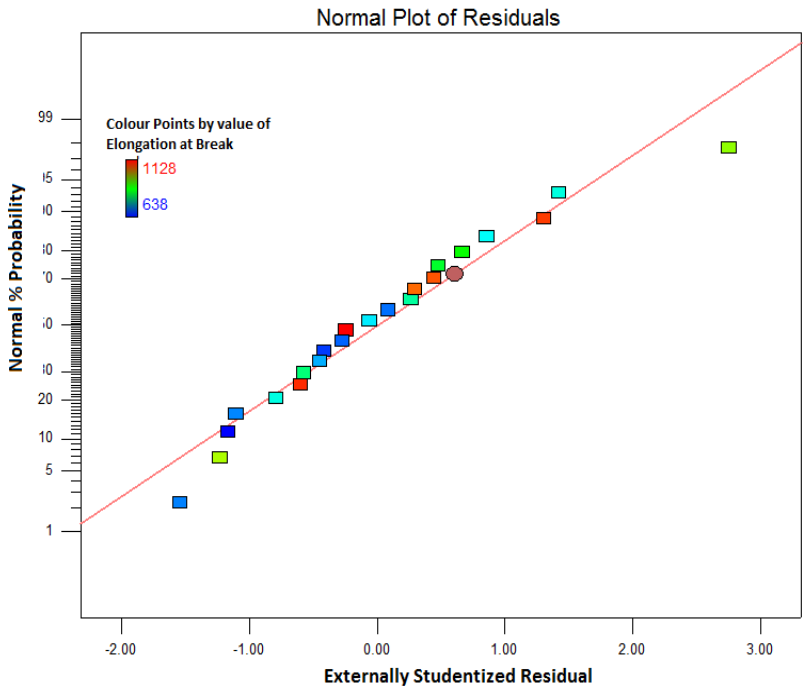


Figure 4.2 Normal Plot for Elongation at Break

In addition, the design expert software provides graphical forms of diagnostics to analyze the accuracy of the model fit. Figures 4.3 (A-B) denote the accuracy of predicted vs. actual values for each experimental run. From these figures, it can be observed that all the values (both actual and predicted) were fitted around the regression line. Further, Figures 4.4 (A-B) depict the relationship between the residuals and the experimental runs. From these figures, the residuals (experimental error obtained by subtracting the observed responses from the predicted responses) were randomly scattered in irregular trend. This indicates that the model is efficient, as the D-Optimal design and the regression model had predicted the values, higher than actual values and lower than actual values with equal probability (Pham, 2006) . Also, all the data points fitted within the limits of ± 4, which advocates for the 95% confidence limits depending upon the number of runs. This indicates that there are no outliers found when the data points are fitted using 2FI design model. Figures 4.5 (A-B) represent the internally studentized residuals versus predicted values for tensile strength and elongation at break, respectively. The randomly scattered data points in both the plots were used to confirm the constant variance assumption. The data here exhibited that the residuals increased in size with the predicted values. This ensures the constant variance along the hypothesis.

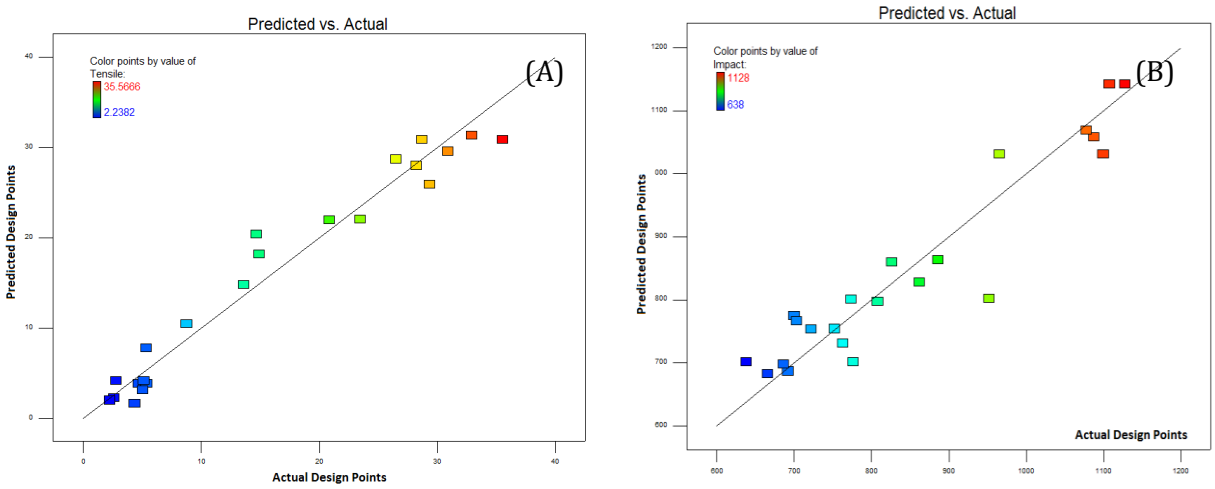


Figure 4.3 Comparison of Predicted vs actual properties of (A) Tensile Strength and (B) elongation at break

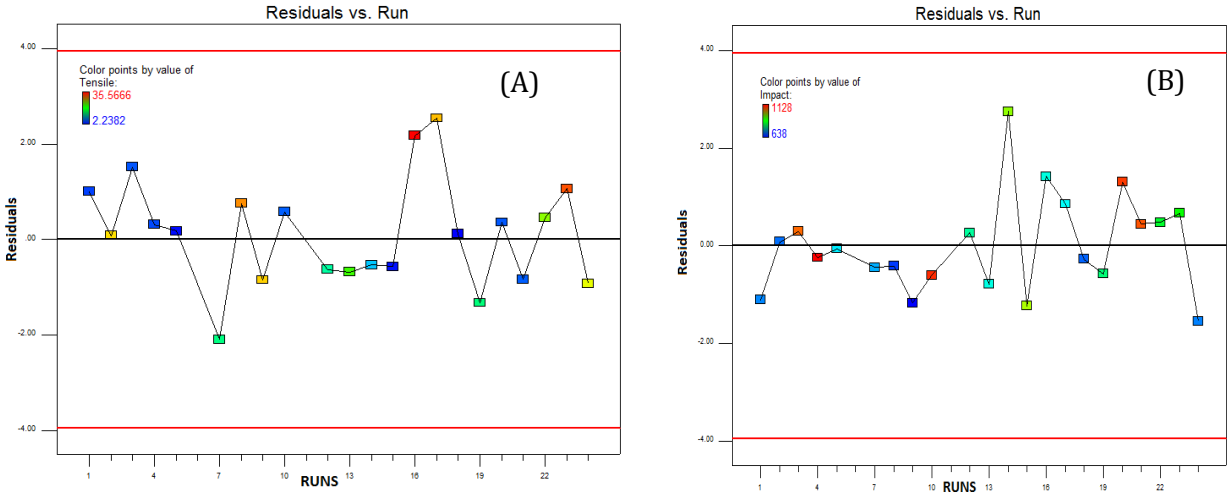


Figure 4.4 Residuals Vs Run for (A) Tensile strength and (B) Elongation at break

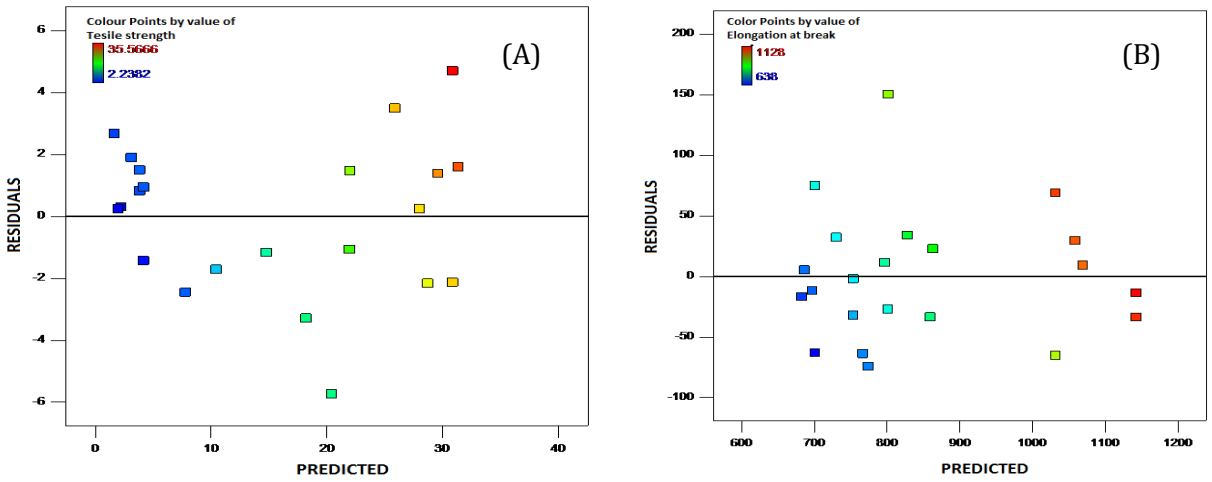


Figure 4.5 Residuals vs Predicted plot for (A) Tensile strength and (B) Elongation at break

4.5 Comprehensive investigation of the effect of blending parameters on the tensile strength and maximum elongation of PP/EPDM blends

The effect of the blending parameters; time, temperature, screw speed and the blend composition ratio on the tensile strength and maximum elongation at break of polymer blends was investigated with the aid of graph column tools provided by the Design expert. The level of significance of each parameter on the individual response was studied between the ranges of -1 to 1. The parameters with correlation factor close to zero were considered to have least significance on the response. While, the parameters ranging closer to -1 and 1 were considered to have profound effect on the response(s). Table 4.4 lists the correlation of each parameter over each response. Furthermore, Figures 4.6 (A-B) display the simplified version of effect of blending parameters on both the responses. From Table 4.4 and Figure 4.6, it can be observed that composition ratio had the most significant effect on both the responses. Nonetheless, blending time showed a considerable influence on the tensile strength. Temperature and screw speed had affected the elongation at break to a less significant extent. These results were in line with the outcomes of a previous work (Svoboda, 2015).

Table 4.4 Correlation factor of individual factors

Response	Factor			
	Time	**Temperature**	**Screw Speed**	**Composition Ratio**
Tensile Strength	-0.158	0.031	0.051	-0.974
Elongation at Break	0.051	-0.373	-0.302	0.648

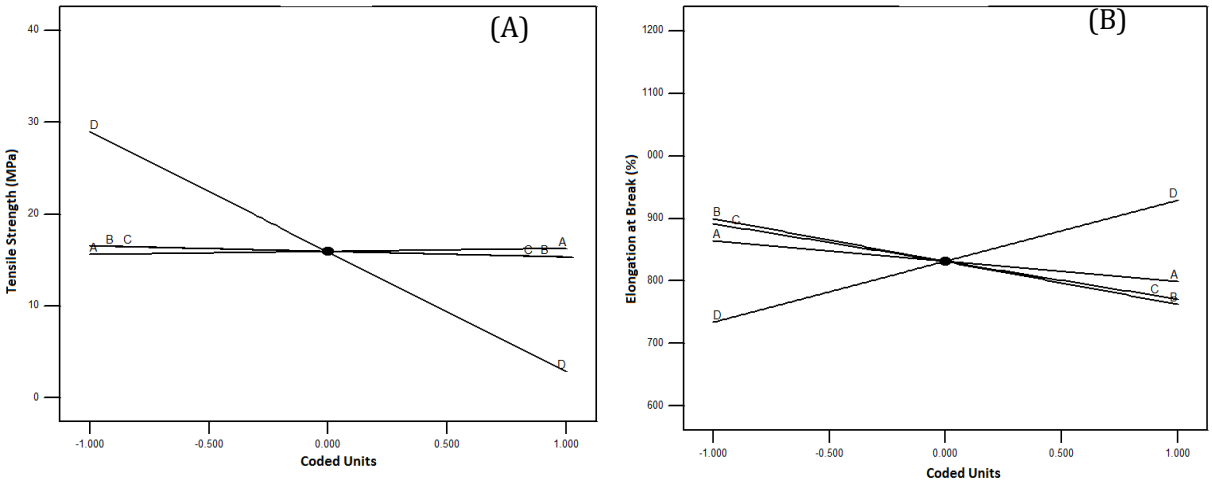


Figure 4.6 Perturbation plot for (A) Tensile strength and (B) Elongation at break

4.6 Analysis of 3D Response curve

The analysis of the 3D response curve was carried out based on the most significant factors in relation to the responses. As a result, Figure 4.7 shows the 3D response plot of blending time vs composition ratio in respect to the tensile strength, keeping the temperature and screw speed constant. From the Figure, it can be observed that increasing the composition ratio of EPDM caused the tensile strength to decrease. In contrast, a marginal increase in tensile strength can be detected with increase in blending time.

Figure 4.8 represents a 3D response plot of blending temperature vs screw speed with time and composition kept constant in respect to the elongation at break. In this Figure, it can be seen that elongation at break favoured lower blending temperature and screw speed.

In addition, Figure 4.9 displays a 3D response plot of blending time vs composition ratio at constant blending temperature and screw speed in respect to the elongation at break. From the Figure, higher composition ratio and lower blending time favoured for elongation at break response.

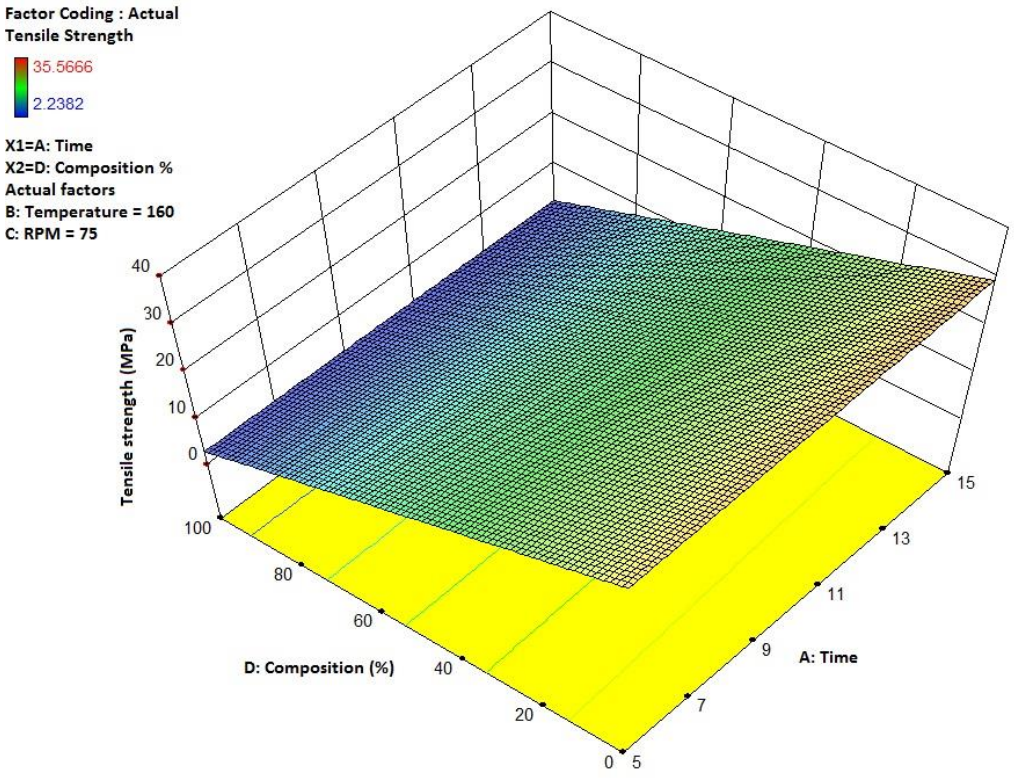


Figure 4.7 3D plot of D-optimal-RSM showing effect of time and composition ratio on tensile strength

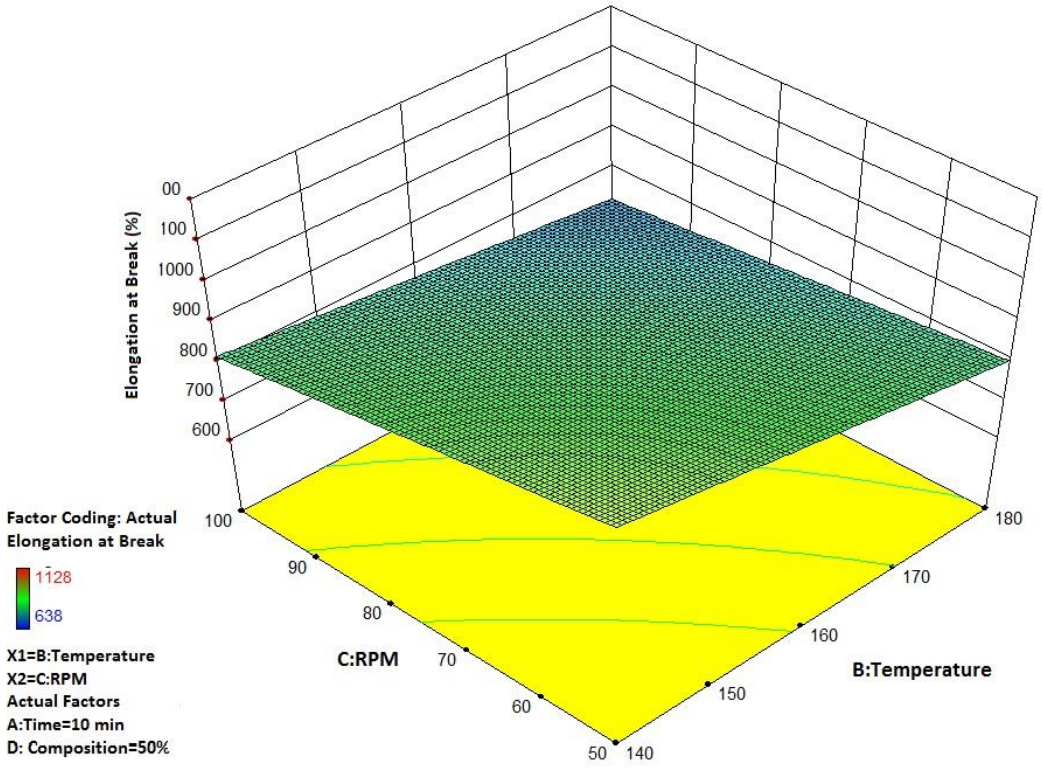


Figure 4.8 3D plot of D-optimal-RSM showing effect of temperature and screw speed on elongation at break

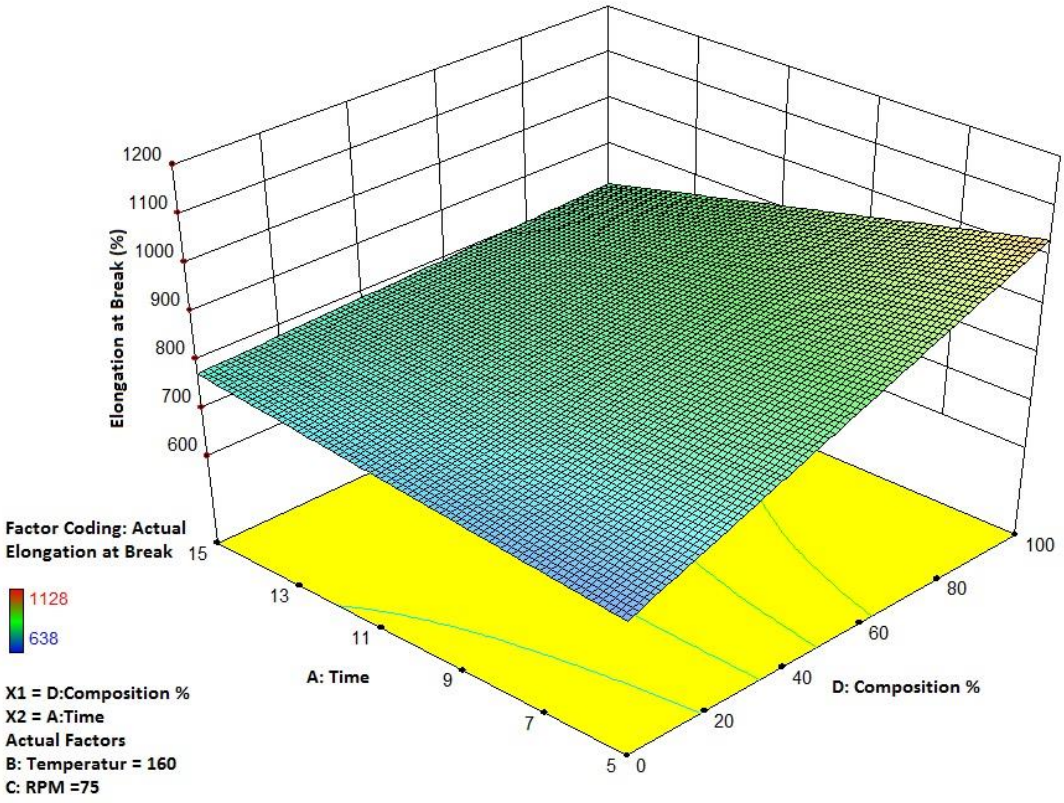


Figure 4.9 3D plot of D-Optimal-RSM showing effect of time and composition ratio on elongation at break

4.7 Optimization

The previous sections provided some insights into the significance of the studied factors, as well as the interaction between them. However, the optimization of the best blending process parameters was still difficult to conclude, as a result of one factor having the potential to influence positively to one of the responses, while influencing negatively to the second response. Hence, a statistical approach adapted by the Design expert software eases the derivation of desired optimum conditions of the factors and the response. It could be noticed that the elongation at break and tensile strength were two opposite mechanical properties greatly affected by the increase in content of EPDM ratio. In this study, optimization was performed to achieve both maximum tensile strength and maximum elongation at break. The factors and responses constrains are tabulated in Table 4.5.

Table 4.5 Goals for Optimization

Variables	Goal	Ranges
Time	In range	5-10 min
Temperature	In range	140-180 ^{0}C
Screw speed	In range	50-100 rpm
Blend ratio	In range	All the ratios considered
Tensile strength	Maximize	2.238-35.566 MPa
Elongation at break	Maximize	638-1128 %

Table 4.6 summarizes the optimized parameter combinations and the predicted responses obtained from Design of expert. The compromise between the two opposite responses (tensile strength and elongation at break) was offered with a high desirability of 87.6%. The actual experimental values of the tensile strength and elongation at break of the optimized blends were 25.28 MPa and 730.207 %. The results obtained based on the modified process parameters were almost similar to the predicted values as the percentage errors were less than 10% and 3.2% respectively.

Table 4.6 Optimized Parameters

Variables	Optimized Conditions	Units
Time	10	min
Temperature	165	^{0}C
Screw speed	50	rpm
Blend ratio	80:20 PP/ EPDM	%
Tensile strength	25.28	MPa
Elongation at break	730.207	%

4.8 Summary

The D-Optimal design yielded a comprehensive analysis on the effects of blending parameters and composition ratio over the blend. The study revealed that, as the EPDM content increased the tensile strength of the blend decreased. However, a marginal increase in tensile strength was achieved with increasing the blending time. The temperature and screw speed had the least effect on the tensile strength of polymer blends within the limits considered, while the elongation at break increased with increasing EPDM content. Further, the blend was optimized to have a property profile of maximum tensile strength and maximum elongation at break. The optimum process parameters is obtained at 10 min blending time with mixing temperature of 165˚C and mixing speed of 50 rpm.

5 EFFECT OF E-BEAM IRRADIATION ON POLYPROPYLENE (PP)/ ETHYLENE PROPYLENE DIENE MONOMER (EPDM) BLENDS

5.1 Introduction

In this chapter, the second aim of the study was addressed, whereby the characteristics of PP/EPDM blends and the effect of E-beam radiation were investigated and discussed. The PP/EPDM blends with mixing ratios of 80/20, 50/50, 20/80 and the individual components were prepared under the optimized conditions obtained from the previous chapter. The blends were prepared in a laboratory internal mixer at 165°C and a rotor speed of 50 rpm for 10 min followed by compression moulding. The blends and the individual components were irradiated by using a 3.0 MeV electron beam (EB) machine at doses ranging from 0-100 kGy in air and room temperature. Polymers when exposed to E-beam radiation experienced hydrogen abstraction which creates free radicals. These free radicals undergo crosslinking, scission and oxidation mechanisms depending on the blend composition and radiation dose (shown in Figure 5.1). The crosslinking can occur either within the individual polymer or between the two polymeric phases (PP and EPDM). Mechanical, structural, thermal and dynamic mechanical properties of the PP/EPDM blends before and after irradiation are elaborated here. The first part of this chapter related to the effect of E-beam sterilization on mechanical properties of PP/EPDM was published in Journal of Biomaterials applications (DOI: 10.1177/0885328217750476) and the second part on the effect of E-beam on thermal properties of the blend was published in Journal of Radiation Physics and Chemistry (DOI: 10.1016/j.radphyschem.2017.07.001).

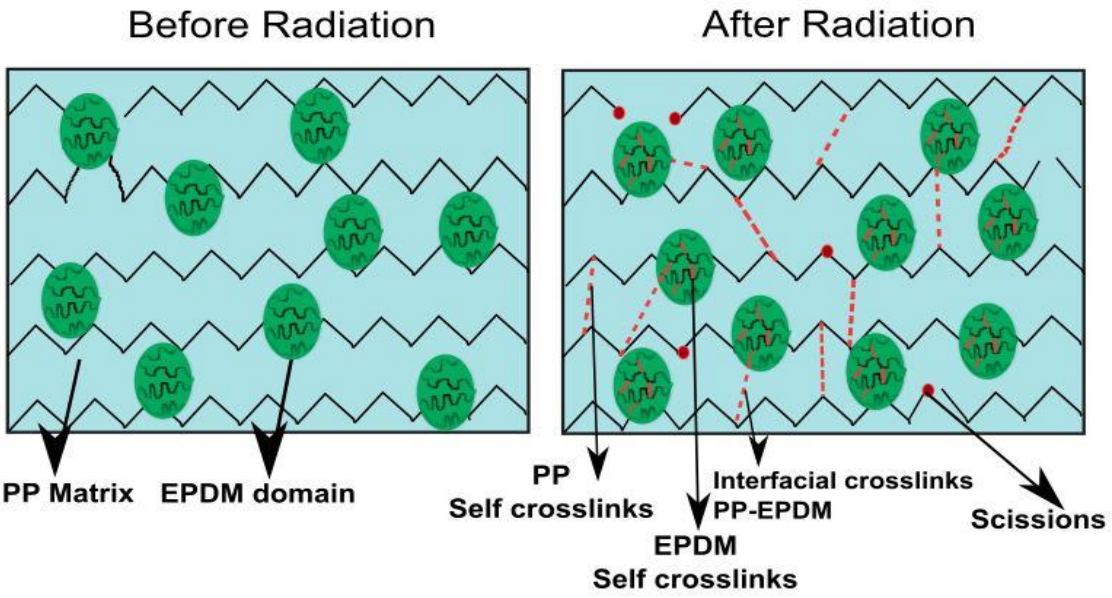


Figure 5.1 Schematic showing inter and intra crosslinking between PP and EPDM before and after E-beam radiation

5.2 Gel Content

Figure 5.2 shows the gel content of PP, EPDM and their blends at varied radiation dosage. Generally, the gel content formation of polymer is a direct reflection of the degree of crosslinks induced by the radiation (Kampouris and Andreopoulos, 1989). It is clear from Figure 5.2 that the un-irradiated blends (used as controls) showed negligible amount of gel formation. Prior to radiation, the 100% and 50% PP blends showed gel content of approximately 1%, while 20% PP blends and 100% EPDM revealed up to 4.9% and 6.2% respectively. The presence of such negligible amount of crosslinks could be caused by the thermally induced crosslinking during the blend preparation (Ha et al., 1986, Deepalaxmi and Rajini, 2014). Figure 5.2 also indicates that for PP dominant blends (100% PP and 80% PP), their gel content show only a marginal increase with increase in radiation dosage up to 40 kGy. Such observation was associated with the lower probability of recombination of free radicals in PP phase (Antunes et al., 2012). However, upon higher radiation dosage the virgin PP and the 80% PP blend showed a decrease in gel content. This can be attributed to the domination of chain scission reaction over crosslinking reactions in PP matrix upon exposure to higher radiation doses (Davenas et al., 2002b). A similar effect was reported by Otaguro et al. (2010b), where the gel content of PP decreased upon 50 kGy radiation dosage.

Meanwhile, the virgin EPDM exhibited a sharp increase of gel content up to 60 kGy and then stabilized as the irradiation dosages increased further. The amorphous nature of the EPDM and the diene content within the polymer enhanced the formation of crosslinking upon the exposure to radiation (Geissler et al., 1978). Likewise, for the blends with higher EPDM loading, the gel content upon radiation increased remarkably due to the formation of a three-dimensional network (Dubey et al., 2009). The 50% PP and 20% PP blends registered a steady increase of gel content up to 80 kGy, and decreased slightly at 100 kGy. The comparable results of various rubber/plastic blends like EPDM/LDPE are available in the literature, showing an increasing crosslinking degree with higher rubber content and at higher radiation dosages (Abou Zeid et al., 2008).

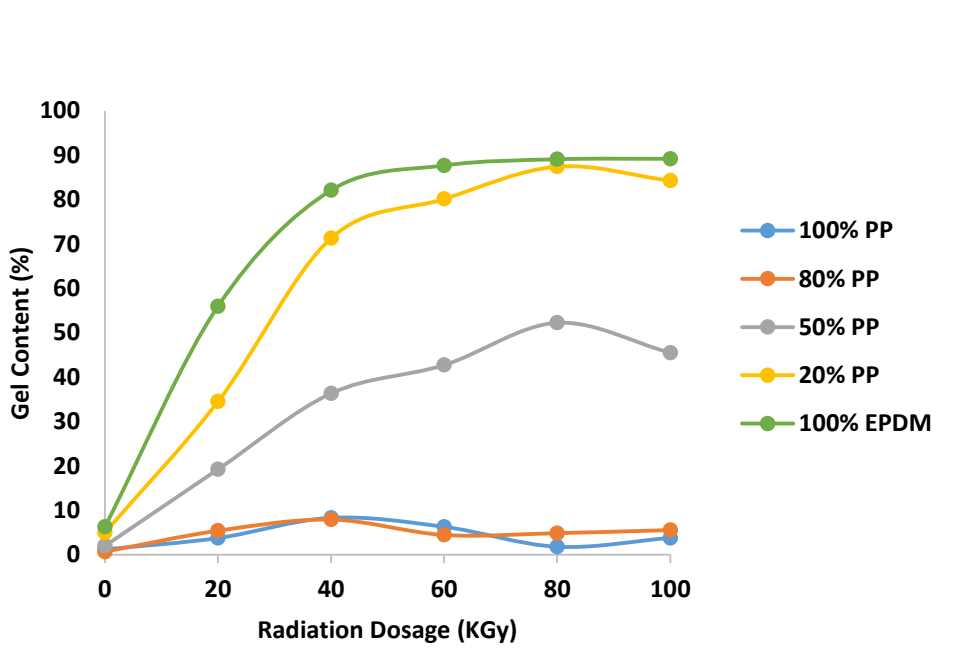


Figure 5.2 Gel content of PP, EPDM and PP/EPDM blends at varied radiation dosage

It is well documented that crosslinking and degradation proceed simultaneously for any polymer during irradiation. The net effect seen is as the resultant of the predominant process between the two (Zaharescu et al., 2000). Charlesby-Pinner equation (Eq 5.1) was used to quantitatively evaluate crosslinking and chain scission yields of irradiated PP/EPDM blends (Rosiak, 1998).

$$S + S^{1/2} = \frac{p_0}{q_0} + \frac{10}{q_0 D u_1} \qquad \text{Eq (5.1)}$$

Where, S is the sol fraction, u_1 the number averaged degree of polymerization, D radiation dose, p_o & q_o are degradation and crosslinking units per unit dose. By regression analysis, plots of $S+S^{1/2}$ vs 1/D were drawn to determine the p_o/q_o and listed in Table 5.1.

Table 5.1 Experimental and theoretical values of po/qo ratios

Blend	**p_0/q_0 values**	
	Experimental (Charlesby-Pinner equation)	**Theoretical (Additive rule)**
100% PP	1.9326	-
80% PP	1.9201	0.7946
50% PP	0.9865	0.5371
20% PP	0.2399	0.2796
100% EPDM	0.2160	-

From the Table 5.1, the reduction in p_0/q_0 ratio with the increasing EPDM content indicates the increase in efficiency of crosslinking over chain scission. The 100% EPDM showing the lowest p_0/q_0 value of 0.2160 has highest density of crosslinking. This is due to the extensive amount of tertiary carbon atoms present in the EPDM chain along with the radicals on a main chain or on a diene branch being generated (Svoboda, 2015). In the contrary, PP despite having a significant amount of tertiary carbon has the highest p_o/q_o value of 1.9201. This confirms that cumulative random chain scission due to various possibilities dominates over the crosslinking of PP. The blends, on the other hand, show an intermediate p_0/q_0 ratio value. It is interesting to note that the blend with 80% PP also has a crosslinking to scission ratio value of larger than one, which leads to the assumption of chain scissions domination over crosslinking (Dubey et al., 2006b).

The theoretical values for p_0/q_0 ratio calculated using rule of mixtures were listed in Table 5.1. For non-interacting type of system, gel faction values for the blends are expected to follow

rule of mixtures i.e. it should vary in proportion to the two components present in the matrix (Fraga et al., 2005). However, the blends of 80% PP and 50% PP showed a positive deviation while 20% PP shows a negative deviation. This observation could be due to the morphological variation and poor PP-EPDM interaction, which suggests that the presence of PP decreases the interaction probability between close lying macro radicals. Similar trend was also observed in LDPE/EVA blend and SBR-EPDM blends (Dubey et al., 2009).

5.3 Tensile Strength

Figure 5.3 shows tensile strength of PP / EPDM blend as a function of radiation dose ranging from 0-100 kGy. From the Figure 5.3, tensile strength of 80% PP blend was 25.28 MPa, 50% PP blend was 19.59 MPa and of 20% PP blend was 14.53 MPa respectively. Tensile strengths of all the blends fell within 100% PP (31.59 MPa) and 100% EPDM (9.92 MPa) controls. It can be noticed that prior to radiation, the tensile strength of PP decreases with increasing EPDM content. The decrease in tensile properties is simply due to the addition of EPDM which has relatively lower tensile strength in comparison to PP. The lower tensile strength of EPDM can be attributed to its amorphous nature.

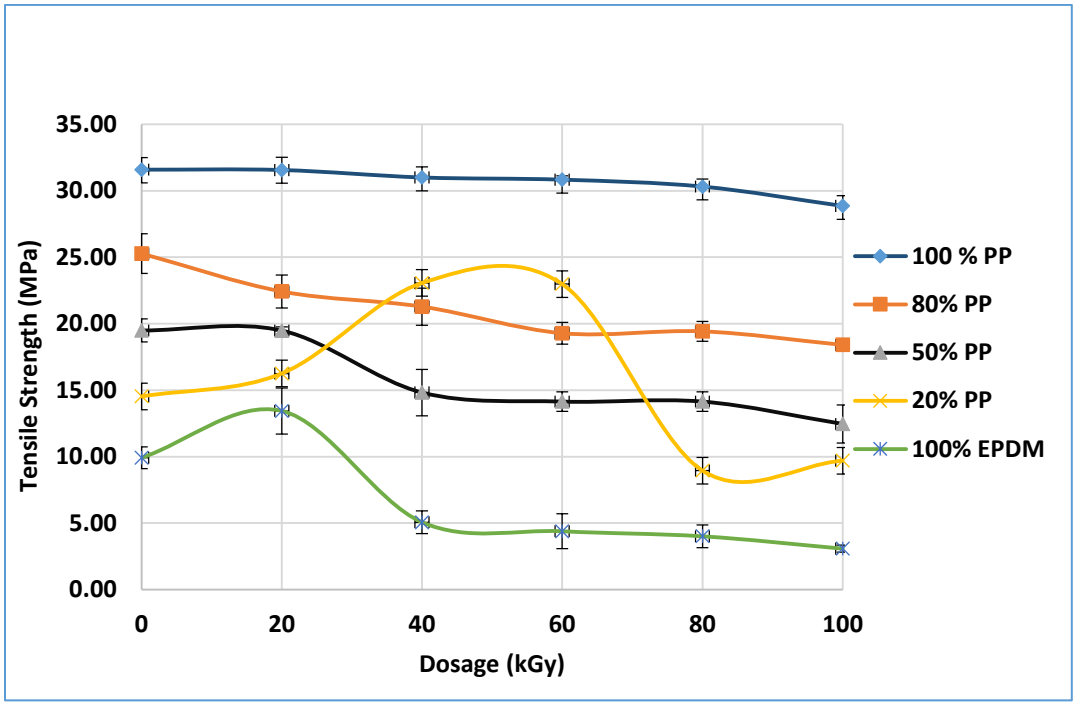


Figure 5.3 Tensile strength of PP/EPDM as a function of radiation dose

From Figure 5.3, it can be noticed that upon radiation the tensile strength of 100% PP showed a gradual decrease with increasing the radiation dose. Such a decline in tensile strength upon radiation is attributed to the radiation-induced scissions in PP chains as observed from the gel fraction results in section 5.2. Besides that, upon radiation the free radicals formed from PP undergoes oxidative degradation also resulting in the decreased tensile strength (Abiona and Osinkolu, 2010). Similarly, 80% PP blend also showed a considerable decrease in tensile strength with increasing radiation dose due to scission mechanism. The blends with 50% PP showed good retention till 20 kGy and showed a gradual decrease with increasing radiation up to 100 kGy. However, 50% PP can withstand radiation up to 20 kGy and the reduction in tensile strength was evident beyond 20 kGy.

On the other hand, it can be noted that the tensile strength of 20% PP blend reached an optimum in the range of 40-60 kGy radiation doses before a drop at 80 kGy. Such observation implies that exposing 20% PP blend to 40-60 kGy was able to increase the radiation stability with concomitant enhancement in tensile strength of the blend. The increased tensile strength of 20% PP blend up to 23.06 MPa at 40 kGy could be attributed to the intense crosslinking induced by radiation. In fact, the tensile strength of 20% PP blend in this range

yielded strength close to 80% PP having tensile strength of 25 MPa. Similarly, 100% EPDM shows increase in tensile strength of 20 MPa at 20 kGy followed by a drop. The crosslinks induced by E-beam radiation reduces the segmental rotation and the mobility of the polymer chains which restricts its free movement, adding strength to the materials (Manshaie et al., 2011). Hence, the presence of crosslinks increases the tensile strength. The drop in 50% PP, 20% PP and 100% EPDM in term of tensile strength after optimum is associated with the embrittlement of EPDM caused by excessive formation of crosslinks, at above 60 and 20 kGy for 20% PP and 100% EPDM, respectively. In the initial state of radiation, larger network system is framed by radiation actuated crosslinking bringing about an increase of tensile strength. However, later at higher radiation doses, additional crosslinks are formed between the promptly crosslinked chains contravening the larger network structure into smaller networks. This results in the decrease of tensile strength. A similar trend was observed by both Ratnam et al. (2001b) and Ramarad et al. (2015b) in radiation processing of poly (vinyl chloride), PVC/epoxidized natural rubber and, ethylene vinyl acetate (EVA)/waste rubber blends . It can also be inferred that, upon loading force, the energy is utilized to break the networks and only minimal energy is indulged in the polymer matrix (Frounchi et al., 2006)

5.4 Elongation at Break

Figure 5.4 shows the elongation at break of PP/EPDM blends with increasing radiation dose. Prior to radiation, while 80% PP blend exhibited 730% elongation, 50% PP blend exhibited 800% elongation and 20% PP blend showed up to 900% elongation. The elongation at break of all the blends fell within the limits of PP and EPDM blend. In particular, 100% PP exhibited up to 600% elongation. On the other hand, 100% EPDM exhibited as much as 1000%. This implies that the elongation at break of PP blends increased upon the addition of EPDM due to the amorphous nature of the later.

Further, upon irradiation the elongation at break for 100% PP and 80% PP decreased constantly up to 40 kGy. Under radiation dose above 60 kGy, the blends did not show any elongation. This was due to the scission mechanism dominating in the polymer blends at these doses, as discussed earlier. Similarly, the blends with 50% PP and 20% PP showed a gradual decrease in elongation at break up to 100 kGy. 100% EPDM also showed a progressive decrease in elongation at break with increase in the radiation dose. The radiation- induced crosslinks causes the embrittlement of EPDM, hindering the movement

of the rubber chains (Ratnam et al., 2000). This in turn reduced the ability of blend to plastically deform resulting in the reduction of elongation at break with increased dose.

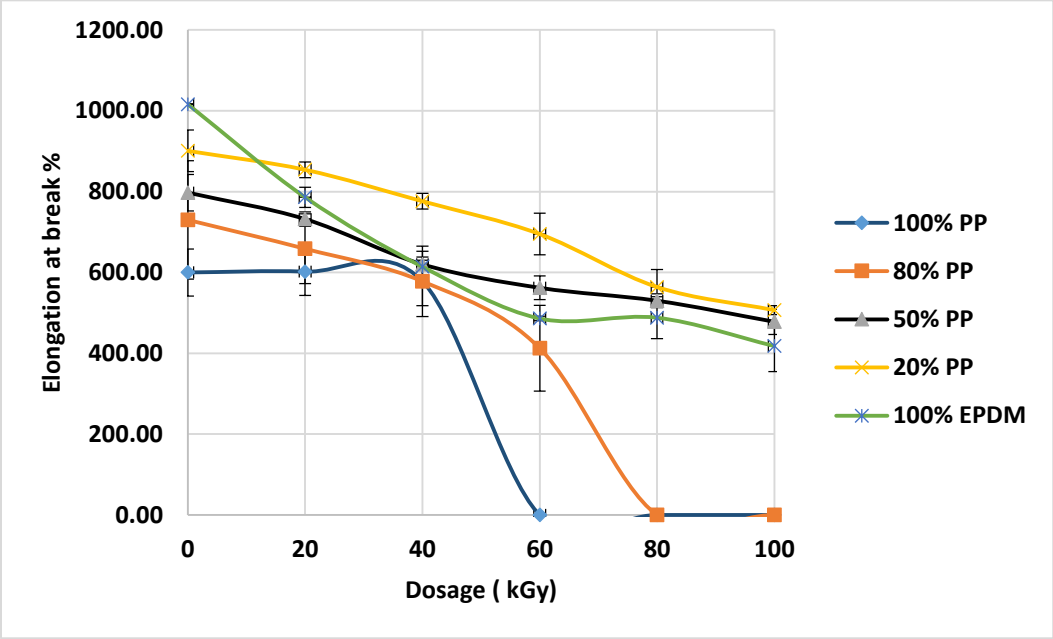


Figure 5.4 Elongation at break of PP/EPDM blends as a function of irradiation dose

5.5 Impact Strength

Figure 5.5 indicates the changes in the impact strength of PP/EPDM blends with the function of radiation. The impact strength of 80% PP increased up to 38.13 J/m (in comparison with 100% PP with 28.43 J/m impact strength) upon the addition of EPDM. The addition of EPDM increased the impact strength of PP .This observation implies the toughening effect EPDM which served as a soft elastomer in rigid PP matrix. However, with further increase in the EPDM loading up to 50%, there was a slight decrease in impact strength. The impact strength of 50% PP blend slightly decreased to 36.59 J/m. This is in accordance to other works, which stated that the optimum EPDM loading into PP for better impact strength is 20-40%. At lower EPDM loading (20-40% EPDM), the EPDM was a dispersed rubber domain in continuous PP matrix (Da Costa et al., 2006). The dispersed EPDM domains absorb energy and deforms. These deformed particles further initiates shear yielding and crazes in the polymer matrix, which further absorbs impact energy (Jafari and Gupta, 2000). Additionally, a number of

voids were found in 20% PP blend (Figure 5.14). The voids suppressed the nucleation of cataclysmic cracks at the location of crazes or matrix deformation and improved the impact strength of blends (Jain et al., 2000, Borggreve et al., 1989, Ramsteiner et al., 2002). However, at 50% EPDM loading, the voids and the dispersed rubber particles were less comparatively to the 20% EPDM blend and tended to form co-continuous phase, which was witnessed in leading to slight decrease in impact property. Upon further addition of EPDM, impact strength increased significantly to 87.1 J/m (for 20% PP blend). This was again attributed to the toughening mechanism of EPDM, as the major part of this blend was in amorphous form. However, all the impact strength of all the blends lies with the range of PP having the least impact strength of 28.3 J/m and EPDM having the highest of 92.35 J/m.

The blends up to 50% EPDM showed minor or no changes in impact strength upon increasing radiation dose. However, the EPDM rich blend with 20% PP and 100% EPDM showed a steady decrease in its impact strength with increasing dose. There is decrease of up to 25% and 37% in impact strength of 20% PP and pure EPDM blends at 100 kGy, respectively. This can also be attributed to the extensive crosslinking of the EPDM elastomer as mentioned earlier (McKeen, 2012). It can also be inferred that the larger networks formed upon radiation deters the energy to be dissipated into the polymer matrix, thus reducing the impact strength.

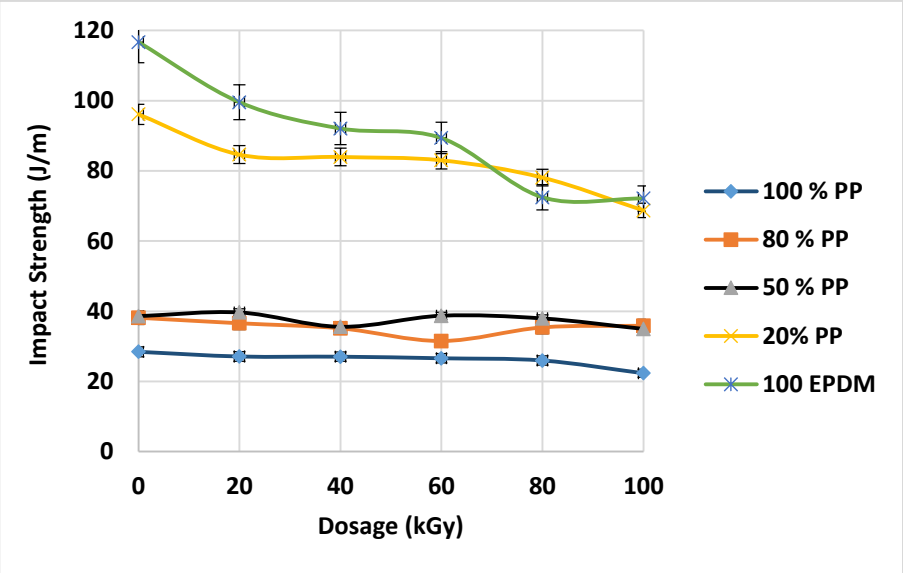


Figure 5.5 Impact strength of PP/EPDM blends as function of radiation dose

5.6 Hardness

Figure 5.6 shows the hardness of PP/EPDM blends before and after radiation. The 80% and 50% PP prior to radiation showed a closer values of hardness around 95 shore D. The addition of EPDM up to 50% did not show any significant change in the hardness value. The hardness of these blends was close to the hardness of the 100% PP. However, the EPDM rich blend of 20% PP showed a significant decrease to 65.25 shore D. This is due to the low hardness value of EPDM, where 100% EPDM with amorphous phase showed only 57.9 shore D.

From Figure 5.6, it can be noted that 100-50% PP blends showed a downward trend in hardness upon radiation from 20-100 kGy. Such a decline is contributed by the reduction in resistance to deformation of the blends as a results of to radiation-induced chain scission of PP. However, the hardness of 20% PP increased by 5% upon a radiation dose of 20 kGy, due to crosslinking in the blend induced by radiation. Upon further radiation, no increment in hardness was observed. Similarly, the crosslinking due to E-beam radiation did not cause a significant effect to the hardness of 100% EPDM, even at the highest dose of 100 kGy, implying the degree of crosslinking achieved at 20-100 kGy is inadequate to cause enhancement in the hardness of the 100% EPDM and 20% PP blend.

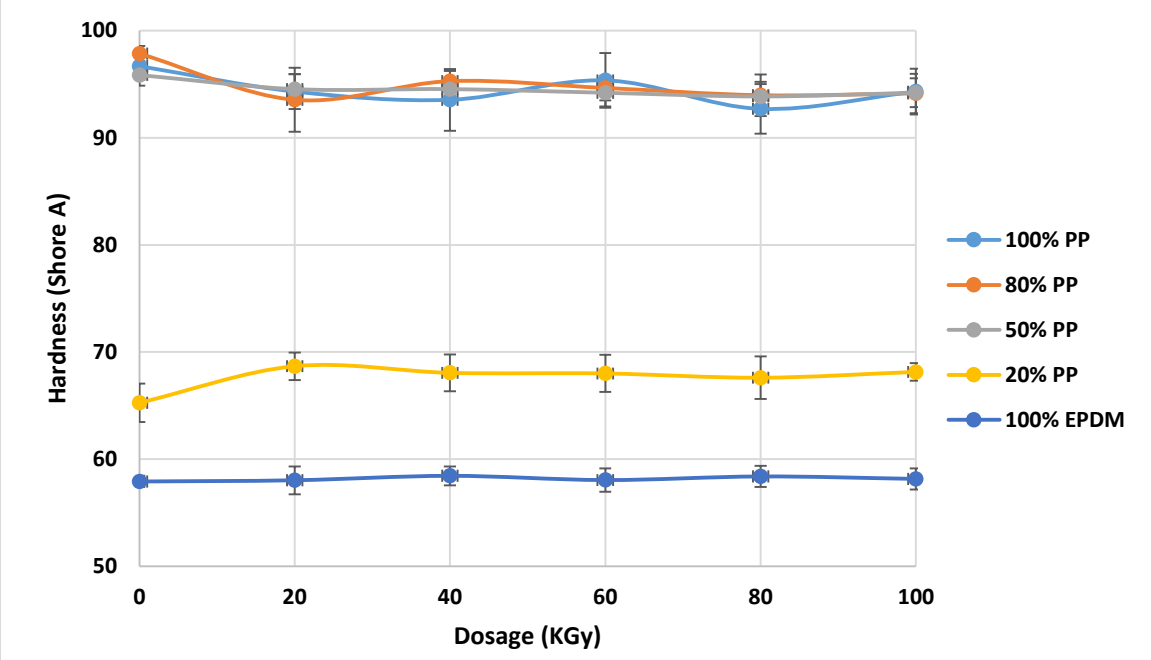


Figure 5.6 Hardness of PP/EPDM blends as a function of irradiation dose

5.7 Thermogravimetric Analysis

The effect of irradiation on the TGA themograms of PP/EPDM blends and the respective virgin polymers are shown in Figure 5.7. It is clear from Figure 5.7(A) that the 100% PP is thermally stable up to 395°C and majority of degradation occurs between 395°C to 456 °C. While, the 100% EPDM is thermally stable up to 440°C and completely degrades at 464.79°C (Figure 5.7(A)). The thermal degradation of EPDM and PP at high temperature is attributed to the random chain scission and hydrogen abstractions from the tertiary carbon involved in intermolecular transfer (Khalid et al., 2009). All the blends showed single-step degradation due to the similarity in the chemical structure of these polymers (Lopez-Manchado et al., 2000). The maximum degradation temperature (T_{peak}) obtained from the DTG thermo grams are listed in the Table 5.2, for further discussion.

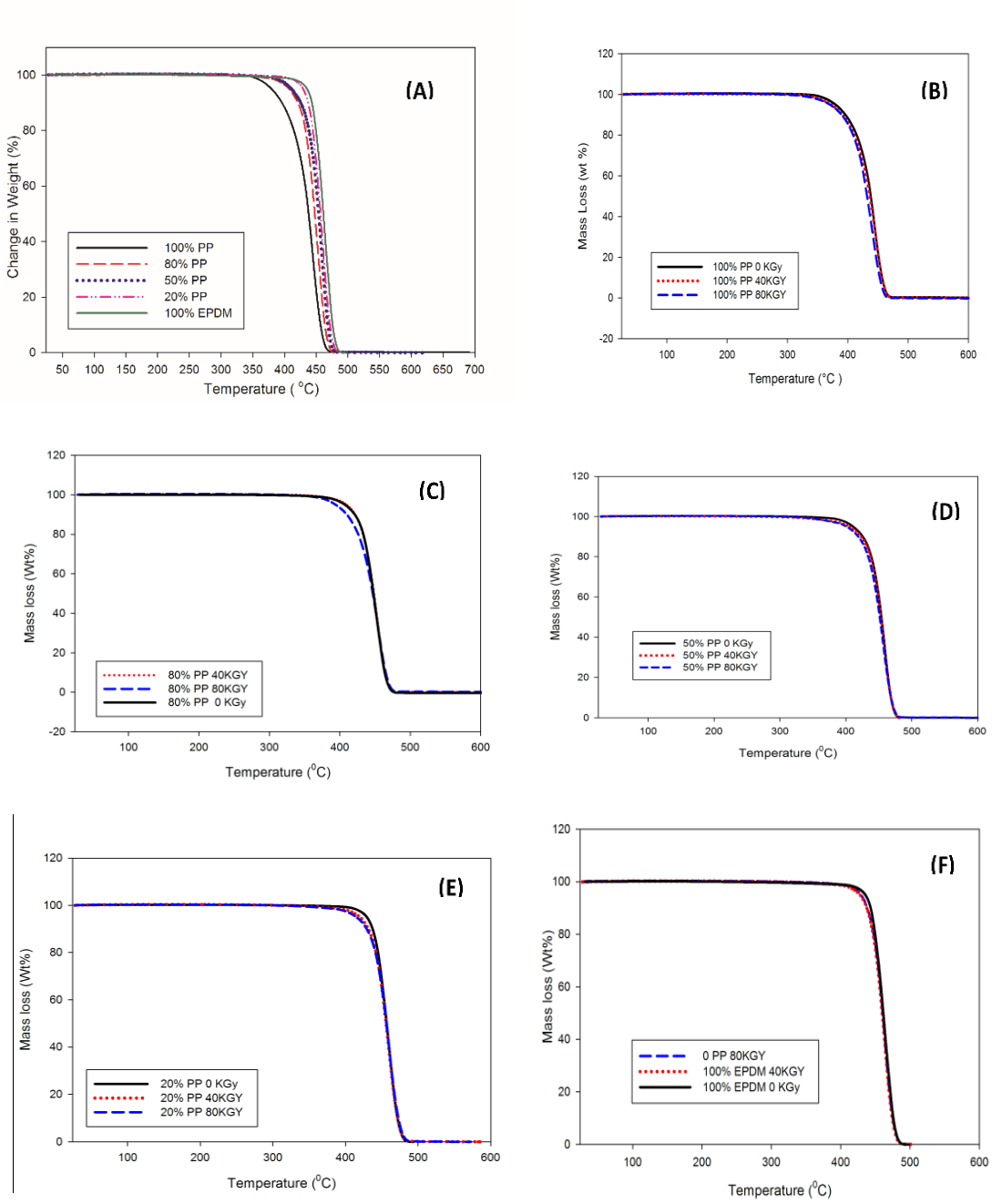


Figure 5.7 TGA thermograms of (A) PP/EPDM blends before radiation (B) 100% PP (C) 80% PP (D) 50%PP (E) 20%PP and (F) 100% EPDM

Table 5.2 Maximum degradation temperature of PP, PP/EPDM and EPDM obtained from TGA analysis

Samples	**Degradation Temp (T_{dmax}) °C**
100% PP	
0 kGy	446.72
40 kGy	447.38
80 kGy	442.59
80% PP	
0 kGy	457.01
40 kGy	453.12
80 kGy	454.83
50% PP	
0 kGy	460.01
40 kGy	460.11
80 KGy	458.83
20% PP	
0 kGy	462.84
40 kGy	463.81
80 KGy	461.13
100% EPDM	
0 kGy	464.79
40 kGy	466.50
80 kGy	463.99

It is evident from Table 5.2 that the thermal stability of the PP/EPDM blend increased with increase of EPDM content. The degradation temperature of 80% PP, 50% PP and 20% PP blends was reported at 457.01 °C, 460.1 °C and 462.84 °C, respectively. This increase was due to increase in EPDM content which has higher thermal stability than PP itself (Ghosh et al., 1996) . Nevertheless, it can be noticed that upon irradiation of the blends (for both 40 kGy

and 80 kGy doses), there is no significant change in final degradation temperature, T_{dmax}. This again suggests that no prominent change in the net degradation took place in these samples. The thermal stability of a compound is strongly related to the network structure in the compound (Ghosh et al., 1996) . In irradiated PP/EPDM blends, some extent of chain scissions and crosslinking were occurring concurrently, leaving the net volume of the network almost similar to non-irradiated blends. Hence, no distinct changes were observed in final degradation temperatures of irradiated PP/EPDM blends.

5.8 Differential Scanning Calorimetry

The heating and cooling DSC thermo grams of PP and EPDM blends at different blend ratio are shown in Figure 5.8. Melting temperature (T_m), crystallization temperature (T_C), heat of fusion (ΔH_f) and crystallinity (X_c) of PP/EPDM blends before and after radiation were summarized in Table 5.3 Melting temperature (Tm), crystallization temperature (TC), heat of fusion (ΔHf) and crystallinity (Xc) of PP/EPDM blends before and after radiation. In this work, the heat of fusion (ΔH_f) and extent of crystallinity (X_c) of only the PP phase of the blends are studied. The endotherm curves exhibited a reduced melting slope for EPDM phase, making it not possible to calculate the area of the curve, due to its high amorphousness.

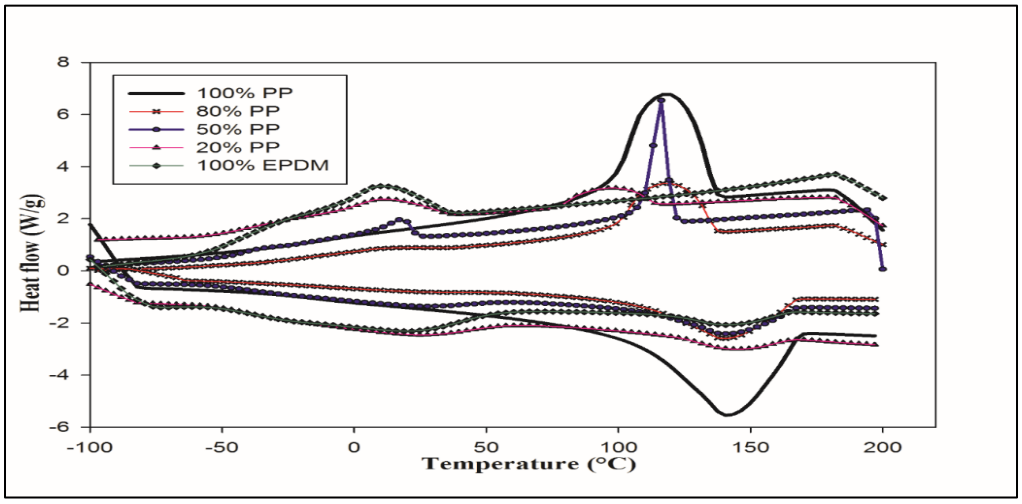


Figure 5.8 DSC Thermo grams for PP/EPDM blends before radiation

Table 5.3 Melting temperature (T_m), crystallization temperature (T_C), heat of fusion (ΔH_f) and crystallinity (Xc) of PP/EPDM blends before and after radiation

Samples	T_m (°C)		T_c (°C)		ΔH_f (J/g)	X_c (%)
	PP Phase	EPDM Phase	PP Phase	EPDM Phase	PP Phase	PP Phase
100% PP 0 kGy	151.05	-	120.17	-	57.49	27.50
100% PP 80 kGy	148.79	-	121.89	-	75.68	36.21
80% PP 0 kGy	150.64	32.32	120.11	18.69	54.52	26.08
80% PP 80 kGy	147.45	30.46	116.83	16.21	53.29	25.49
50% PP 0 kGy	149.89	33.31	116.06	18.38	27.86	13.33
50% PP 80 kGy	148.96	29.94	113.53	13.91	25.40	12.15
20% PP 0 kGy	144.55	33.78	96.49	18.07	13.93	6.66
20% PP 80 kGy	147.92	28.45	87.80	15.23	11.32	5.41
100% EPDM 0 kGY	-	33.27	-	17.25	-	-
100% EPDM 80 kGY	-	30.18	-	16.02	-	-

From Table 5.3, it can be noted that the neat PP prior to radiation exhibited a crystallization temperature (T_C) at 120.17°C. Meanwhile, the neat EPDM shows a reduced crystallization peak at 17.25°C due to its amorphous nature. PP/EPDM blends reveals two crystallization peaks, the first one corresponding to EPDM and the second peak corresponding to PP. From Table 5.3, it can be noticed that the crystallization temperature of PP/EPDM blend corresponding to the PP phase showed a marginal decrease in T_c with increase in EPDM content. T_c of the PP phase of these blend reduced to 116 °C and 96.9 °C when EPDM content was increased to 50% and 80%, respectively. However, the EPDM phase did not show a significant change in T_c, a decreasing trend was displayed as the EPDM content decreased. The decrease in crystallinity temperature is directly reflected by the heat of fusion (ΔH_f) and extent of crystallinity (X_c). The neat PP exhibited ΔH_f and crystallinity of 57.49 J/g and 27.50% respectively. As the content of the EPDM in the blend increased, the heat of fusion and thus the crystallinity decreased. The crystallinity percentage of PP phase in the blends slightly decreased to 26.08 % for 80% PP, while greatly decreased up to 13.3% and 6.6% for

50% PP and 20% blend respectively. This decrease in heat of fusion and crystallinity could be credited mainly due to dilution effects of EPDM (Xiao et al., 2002). The amorphous nature of EPDM hinders the crystallization of PP when mixed with the later. Similarly, it can be noticed that the pattern of changes in melting temperature was very much similar to the pattern of changes in crystallization temperature for blends with increasing EPDM content. Less the crystallites are formed, sooner is the melting of the crystals. Thus decrease in extent of crystallization reduces their melting temperature (T_m).

From Table 5.3, it can be witnessed that the T_c of pure PP increased slightly upon irradiation at 80 kGy dose. Additionally, upon radiation the neat PP showed a profound increase in the heat of fusion by 18 J/g and in X_c% by 8.7%. The increase in heat of fusion which implies the increase in crystallinity is attributed to the scission (evident from gel analysis) of extremely strained tie molecules leading to formation of small molecules which move freely and order themselves in solid phase, to form crystallites. On contrary, the melting temperature of PP showed a decreasing trend in spite of an increase in extent of crystallinity and T_c. Similar pattern was reported in literature for i-PP (Kostoski and Stojanović, 1995). This decrease could be because of the minimal crosslinking effect competing with the scission mechanism. The crosslinks hindered the movement of molecule resulting in breaking up or imperfection of crystallites, which requires comparatively less energy for melting. This result is in accordance with Sen and Kumar (1995) and Alariqi et al. (2015). The author reported that though chain scission is dominating in PP, existence of some crosslinks cannot be ruled out.

For 80% PP blend radiated at 80 kGy, T_c of the PP phase shows a decrease of 3°C. Similarly, for EPDM rich blend with 50% PP and 20% PP, there is an obvious decrease in T_c of PP phase up to 3.28°C and 8.69 °C, respectively. On the other hand, at the same dose, the T_c corresponding to EPDM phase of these blends also reduced by 4.47°C and 2.84 °C, respectively. In parallel, for blend with 80% PP (non-irradiated) the T_m of PP phase lies at 150.64 °C, whereas the melting peak is lowered to 147.85 °C at 80 kGy. Similarly, for 50% PP the T_m is reduced marginally by 1°C. T_m of EPDM phase of all the blends also decreased upon radiation. This decreasing trend in T_m and T_c of the blends is correlated to the presence of crosslinks which is evident from the gel analysis. The crosslinking taking place on irradiation, modifies the molecular structure and hinders the growth of crystal leading to its imperfection. Then again Khonakdar et al. (2006) reported that this decreasing trend could also be due to the decrease in the molecular weight between the crosslink junctions. On the

other hand, such a significant difference in crystallites size or hindrance of crystal formation is not reflected by the heat of fusion or crystallinity percentage. From Table 5.3, it can be seen that the heat of fusion and extent of crystallization show only a borderline decrease upon radiation. The network structures formed during the irradiation suppresses the crystallization of broken chains, leading to cause only a small change in the heat of fusion and thus the percentage of crystallinity (Gheysari et al., 2001). The existence of the networks formed due to radiations were witnessed in several EPDM blends (Chapiro, 1964, Dubey et al., 2006a).

5.9 Dynamic Mechanical Analysis

5.9.1 Tan delta/Damping factor curve

Figure 5.9 (A-F), shows the temperature dependence tan delta of 100% PP, 100% EPDM and PP/EPDM blends before and after irradiation, respectively. Tan delta indicates the damping factor, which is defined as the ratio of loss modulus to storage modulus, measuring the energy loss in relation to the recoverable energy. The tan delta curve shows distinct peaks ($T_{\delta max}$). The temperature corresponding to the maximum in tan delta is taken as glass transition temperature, T_g of the blend. Below the $T_{\delta max}$, the damping factor is less for all the blends (before and after radiation) and controls. The reduced damping factor is due to the insufficient thermal energy required for the segmental rotational and transnational movements. This affects the molecules to freeze, causing molecular slip resulting in reduced viscous flow. The tan delta curve exhibits increased damping factor resulting in a peak due to micro-Brownian motion of molecular chains. However, all the blends show low damping factor again after $T_{\delta max}$, due to the free movement of the molecular segments with minimal restrictions (George et al., 2007) . The damping factor of EPDM increases above 30°C, due to the contribution of the chain flow (Davenas et al., 2002a) . In this study, the position and the height of tan delta peak are indicative of the structure and the extent of crosslinking of the samples.

Figure 5.9 (B) shows T_g of 100% PP at 5.75 °C prior to radiation. It can be noticed that upon radiation T_g of PP decreased slightly to 4.7°C at 40 kGy radiation dose and to 4.5 °C at 80 kGy. The decrease in T_g upon irradiation could be attributed due to occurrence of chain scission (Luan et al., 2011). This is an indication of increase in crystallinity of PP due to the chain

scission as witnessed earlier in DSC analysis (Jafari and Gupta, 2000). On the other hand, the decrease in peak amplitude with increasing radiation dose is indicative of presence of some extent of crosslinks, restricting the molecular mobility. However, decrease in the $T_{\delta max}$ supported by the data from gel content analysis and increase in T_m of the PP proves the dominance of chain scission over crosslinking effect upon radiation. A similar results were reported by Steller et al. (2006), where the author concluded that few grades of commercially available PP underwent destruction of crystallites and crosslinking simultaneously under radiation.

The 100% EPDM control exhibits T_g at -31.8 °C. The damping factor for non-irradiated blend shows decreasing trend after the transition up to ≈30°C, followed by an increase in damping ratios. The increase of tan delta above 30°C is contributed by the molecular chain flow (Davenas et al., 2002a). Upon irradiation, the $T_{\delta max}$ remained at -31.8°C. Moreover, from Figure 5.9e the decrease in peak height could be witnessed upon radiation at 80 kGy. Upon radiation, the creep above 30°C also decreased drastically with increasing dose. The decrease in peak height and decrease in creep allied to chain flow above 30°C, mutually indicates the presence of crosslinks, which is in line with the results of the gel content and DSC analyses.

From Figure 5.9 (C), the blend with 80% PP shows two distinct peaks, where, the $T_{\delta max}$ of EPDM phase is at -41.284°C and $T_{\delta max}$ of PP phase is at 4.2°C. The appearance of two distinct peaks corresponding to the T_g of the individual polymers in the blend indicates that the blends are immiscible. The height of PP phase peak decreased noticeably (at 40kGy) similar to 100% PP indicating that some extent of crosslinking reaction at the interface hindered the molecular mobility (Jain et al., 2000).

Table 5.4 Glass transition temperatures and tan delta values for PP/EPDM blends before and after radiation

Sample	T_{gEPDM} (°C) (Corresponding to EPDM)	T_{gPP} (°C) (Corresponding to PP)	ΔT_g (T_{gPP}-T_{gEPDM}) (°C)	Tan delta (Corresponding to EPDM)	Tan delta (Corresponding to PP)
100% PP 0 kGy	-	5.7	3.5	-	0.0639
100% PP 40 kGy	-	4.7	3.5	-	0.0614
100% PP 80 kGy	-	4.5	3.5	-	0.0613
80% PP 0 kGy	-41.6	4.2	45.8	0.0314	0.0712
80% PP 40 kGy	-41.6	4.2	45.8	0.0317	0.0646
80% PP 80 kGy	-41.6	4.2	45.8	0.0301	0.0702
50% PP 0 kGy	-38.4	4.2	42.6	0.0908	0.0754
50% PP 40 kGy	-36.2	4.2	40.4	0.1096	0.0760
50% PP 80 kGy	-35.1	4.2	39.3	0.1008	0.0741
20% PP 0 kGy	-32.8	-	32.8	0.4806	-
20% PP 40 kGy	-32.8	-	32.8	0.4507	-
20% PP 80 kGy	-32.8	-	32.8	0.4507	-
100% EPDM 0 kGy	-31.8	-	31.8	0.5196	-
100% EPDM 40 kGy	-31.8	-	31.8	0.5158	-
100% EPDM 80 kGy	-31.8	-	31.8	0.4543	-

The 50% PP blend shows two distinct peaks, where, the $T_{\delta max}$ corresponding to EPDM is at -38.4 °C and $T_{\delta max}$ of PP phase is at 4.2 °C (Figure 5.9 D). From Table 5.4, it can be witnessed that, upon radiation, the T_g of EPDM phase was found to shift to higher temperature (-35.8°C)

while there was no significant change in the PP phase. From Table 5.5, it can also be witnessed that the ΔT_g (T_{gPP}-T_{gEPDM}) decreased upon increasing radiation. The inward shift of T_g is an indication of the improvement in the compatibility of the blend upon radiation due to radiation-induced crosslinking as evidenced by gel content results (Tang et al., 2004).

Further, the 20% PP blend which was rich in EPDM content shows only single peak at -32.8°C similar to the 100% EPDM blend (Figure 5.9 F). The higher quantity of EPDM in the blend masks the PP content resulting in only single peak (Sharma et al., 2015). On the other hand, from Figure 5.9 (C-E) it can be witnessed that blends are only partially miscible. From Table 5.4, it can be witnessed that there is no significant change in T_δ of the peak for 20%PP blend. However, the height of the peak decreased with radiation due to increase in crosslinking effect. The crosslinked structure restricts the molecular mobility, leading to decrease in the damping factor.

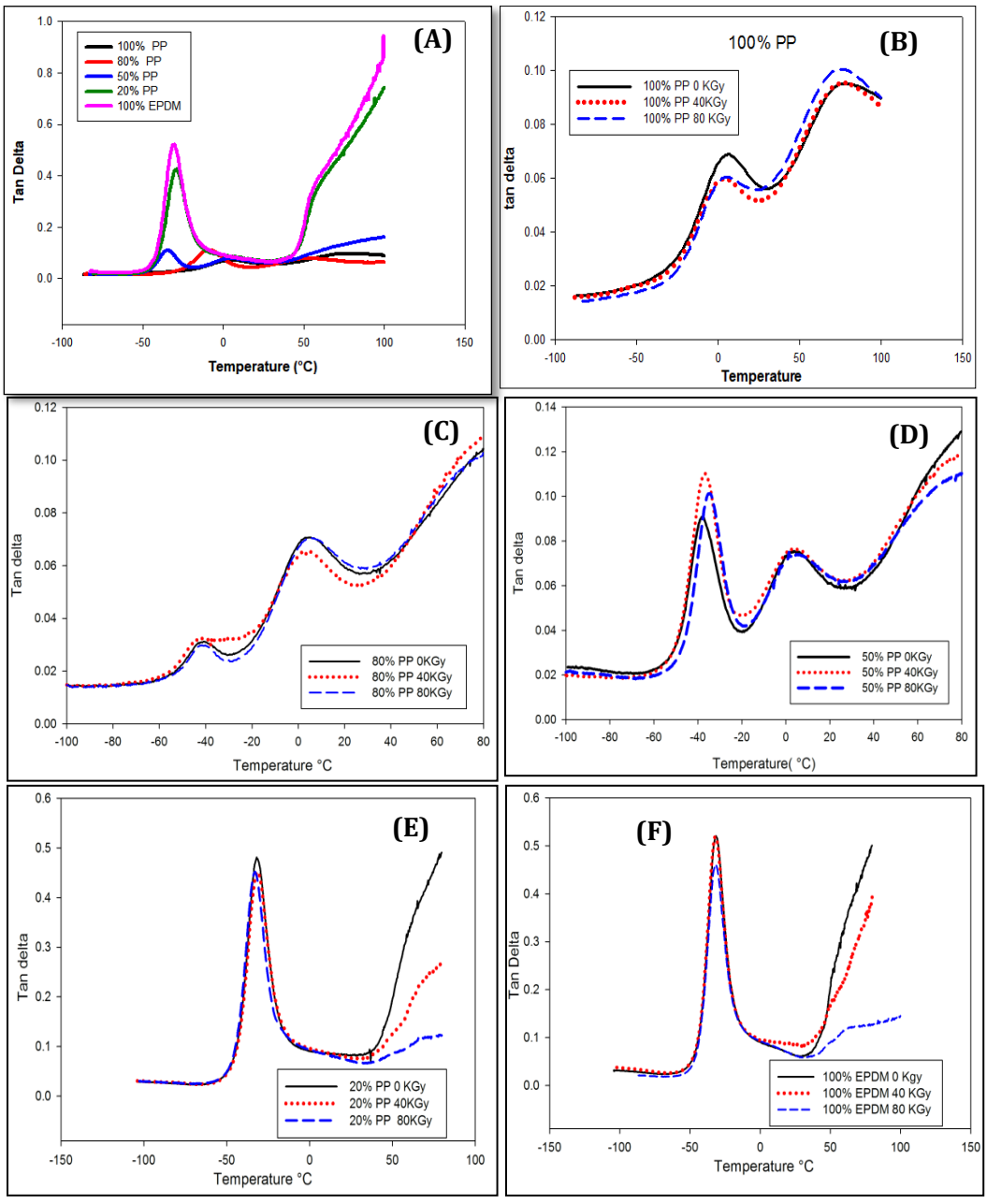


Figure 5.9 Temperature dependence of Tan delta curve – (A) PP/EPDM blends before radiation (B) 100% PP (C) 80% PP (D) 50% PP (E) 20% PP and(F) 100% EPDM

5.9.2 Storage Modulus

Storage modulus determines the dynamic rigidity of a material, which originates from the elastic response of the material. Figure 5.10 (A-E) shows the temperature dependence storage modulus of PP/EPDM blends and the respective neat polymers before and after radiation. Figure 5.10 (A-E) clearly indicates that PP, EPDM and their blends show three regions, namely, glass, transition and rubbery regions. The 100% EPDM showed a severe decrease in the transition region. The severity of decrement of storage modulus of 100% PP was less in comparison to the EPDM, because of its crystalline nature. The 100% EPDM with rubbery nature showed the least storage modulus value, while 100% PP had the highest throughout the change in temperature. The blends revealed intermediate storage modulus between 100% PP and 100% EPDM. The storage modulus decreased upon increasing the EPDM content, as the stiffness and rigidity of EPDM were less.

From Figure 5.10 (A), the storage modulus of 100% PP first increased at 40 kGy. This increase in storage modulus is due to the minimal crosslinking that exist at respective radiation dosage, which is well evident and explained in gel content analysis. However, this increase was not continuous, as the storage modulus slightly decreased with increasing irradiation to 80 kGy. Schulze et al. (2003) reported that the decrease in storage modulus with increasing radiation up to 90 kGy is due to loss of molecular weight caused by scission. On the other hand, 100% EPDM did not show any significant change in storage modulus at 40 kGy. However, upon increasing radiation dose to 80 kGy the EPDM sample showed a slight decrease in storage modulus in glass and transition regions. The reduction in storage modulus is due to the imperfect small PE crystallites that are formed in glass and transition regions. A similar result was reported previously (Harnischfeger et al., 1990). The reduction in perfectness of these crystallites due to extensive crosslinking is the main reason for decrease in storage modulus as stated by Harnischfeger et al. (1990). This is also evident from the DSC results as explained in previous sections. The 20% PP blend (Figure 5.10D), rich in elastomer content showed similar decrease in storage modulus upon radiation in glassy region for the same reasons. On the other hand, both EPDM and 20% PP blends showed no change in storage modulus in rubbery region.

In 80% PP blend (Figure 5.10B), upon irradiation at 40 kGy the storage modulus increased up to -21°C. Above this temperature, the radiated blend showed lower storage modulus compared to non-irradiated blend. While the improvement in the storage modulus of glassy region was associated with the irradiation induced grafting, the decrease upon reaching transition region was associated with the loss of crystalline zone of PP in the blend due to irradiation. In a semi-crystalline polymer, contribution to storage modulus, above the glass transition temperature is associated with the crystalline region of the polymer (John et al., 2003a). Alternatively, the blend at 80 kGy shows a substantial decrease in storage modulus along the entire temperature range due to chain scission, where the chain scissions act as crosslinks later to improve the grafting. Similarly 50% PP blend, upon radiation shows comparable trend to the blend with 80% PP (irradiated at 40 kGy) for the same reasons mentioned earlier. Furthermore, the application of the blend based product falling within the rubbery region (at 24°C), there is no significant change in storage modulus upon radiation. Therefore, the radiation effects would not affect the product performance in terms of storage modulus.

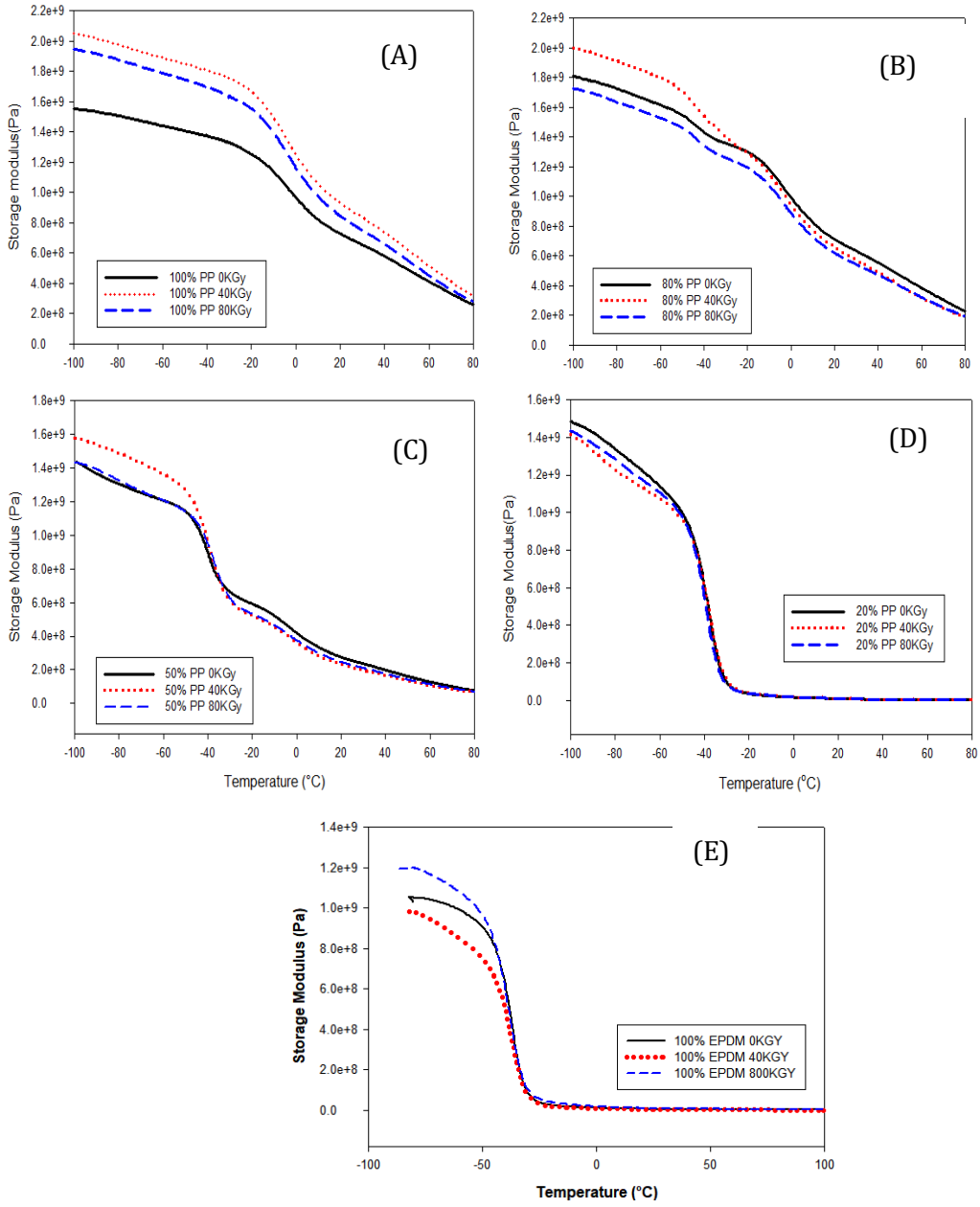


Figure 5.10 Temperature dependence of storage modulus of (A) 100% PP (B) 80% PP (C) 50% PP (D) 20% PP and (E) 100% EPDM

5.9.3 Loss Modulus

Figure 5.11a-e shows the temperature dependence of loss modulus of PP, EPDM and PP/EPDM blends. The loss modulus indicates the maximum heat dissipation per unit deformation. Neat PP had increasing loss modulus up to 60.7 Pa at -2.11 °C. Above this temperature, the loss modulus decreased. Similarly, pure EPDM showed an increase in loss modulus up to 106 Pa at -38.74°C. The decrease in the loss modulus beyond this temperature is due to rubbery nature of the polymer. The blends shows two distinctive peaks corresponding to PP and EPDM phase due to immiscibility of the blends.

The loss modulus increased upon irradiation of PP with increasing dose. The radiation induced break up of molecular chains reducing the degree of elasticity and thus the increase of loss. On the other hand, with radiation dose at 40 kGy the EPDM showed no difference in loss modulus. However, on increasing the dose to 80 kGy, the loss modulus decreased to 93.3 Pa. The crosslinking in polymer blends increased the elasticity but decreased the loss modulus at 80 kGy. Irradiation of 80% PP blend at 40 kGy had higher loss modulus up to -15.6°C in comparison to untreated blend due to scission in chains. However, above this temperature, crosslinking dominated which in turn reduced the loss modulus with respect to blend prior to radiation. However, the blend at 80 kGy shows a substantial decrease in loss modulus from 2°C blend throughout the temperature range. The decrease can again be contributed to crosslinking. With respect to 50% PP blend, the loss modulus peaks were at -39.6°C (77 Pa) and -1.756°C (31.5 Pa). However, upon radiation at 40 kGy, the peak increased until 94.05 Pa due to scission effects. Further dosage at 80 kGy, the peak substantially decreased to 79.77 Pa, as the chain scission was suppressed to some extent by the presence of crosslinking. At higher temperature, the peaks were lower in loss modulus. This decrease was due to less dissipation energy as a resultant of increase in crosslinking by radiation.

Unlike other blends, 20% PP exhibited only a single peak of 132.07 Pa at -1.756°C. This indicates that miscibility of the blends was improved remarkably. However, upon irradiation the peak remained at -1.756°C, the peak height reduced negligibly. The decrease was again due to the crosslinking induced by the radiation.

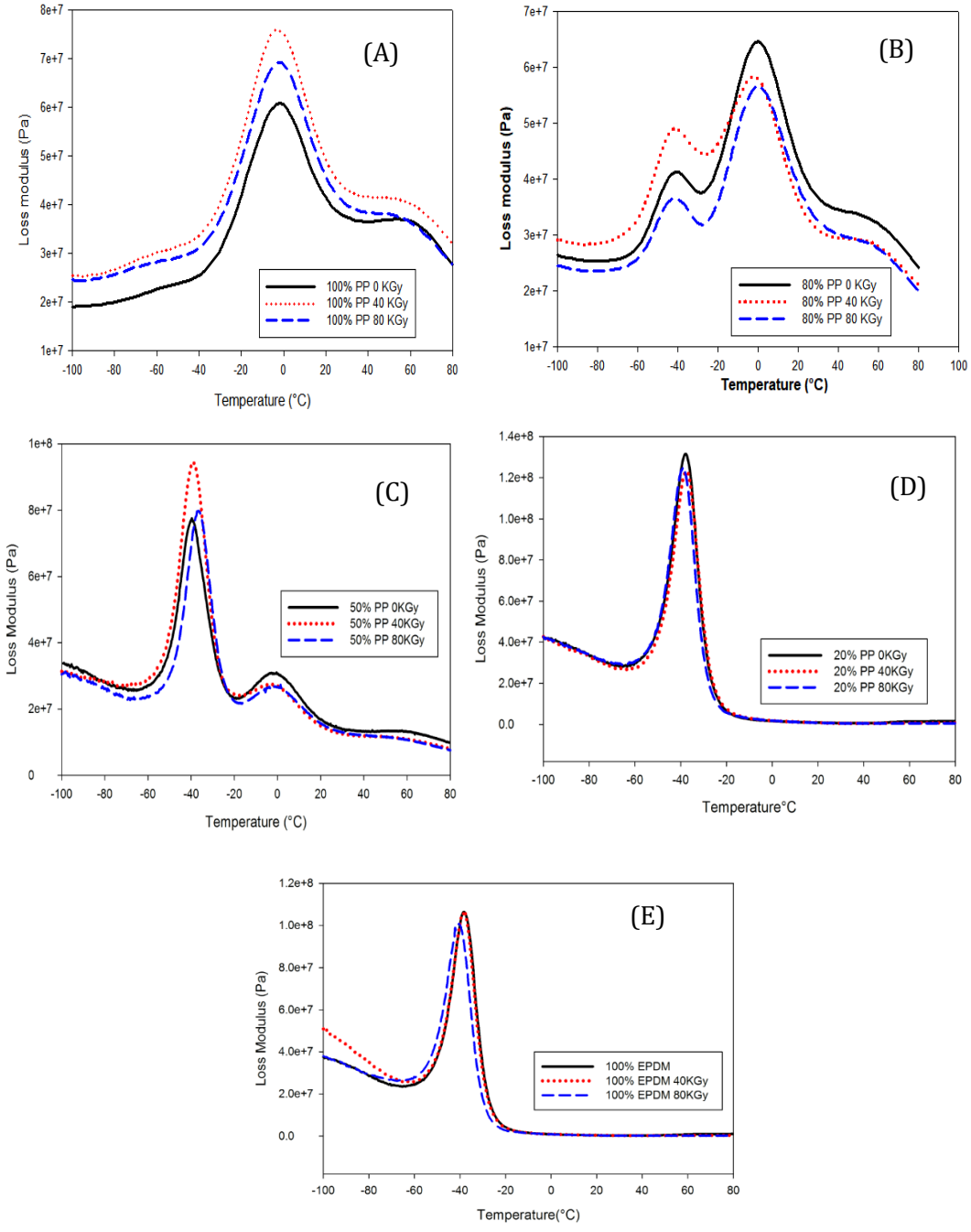


Figure 5.11 Temperature dependence of loss modulus of (A) 100% PP (B) 80% PP (C) 50% PP (D) 20% PP and (E) 100% EPDM

5.10 Scanning Electron Micrographs

Figure 5.12 (A-B) shows the SEM micrographs of 100% PP before and after radiation at 40 kGy respectively. It can be noted that 100% PP showed a semi-crystalline morphology before radiation, due to the amorphous content (poly-ethylene) in the co-polymer. However, upon radiation at 40 kGy, a few cracks (as indicated by the arrows in figure 5.12 (B)) in the matrix were witnessed. These cracks could be due to the degradation of the polymer matrix caused by the radiation-induced chain scission as well oxidation, making the polymer vulnerable to failure upon loading of energy. Figure 5.13 (A-B) show the cryogenically impact fractured fractographs of 100% PP before and after radiation. Also, from Figure 5.13 (A-B), it can be observed that 100% PP became more brittle after radiation, indicating the decrease in elongation at break as a result of the embrittlement. The increase in brittleness is due to increase in crystallinity caused by the E-beam radiation, which was well detailed in section 5.8.

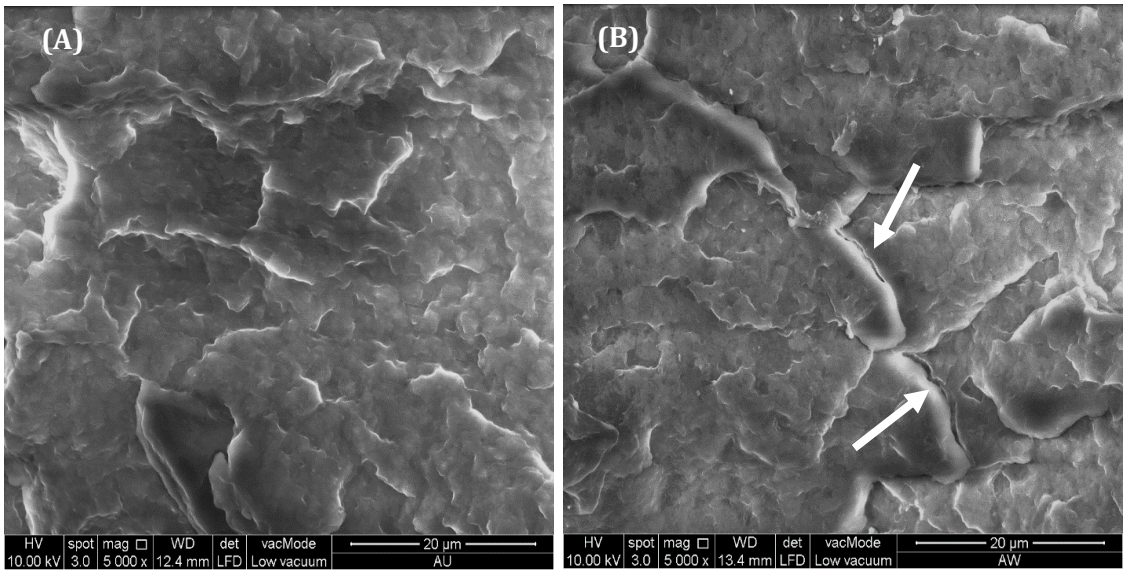


Figure 5.12 SEM image for 100% PP (A) before radiation and (B) after radiation at 40 kGy

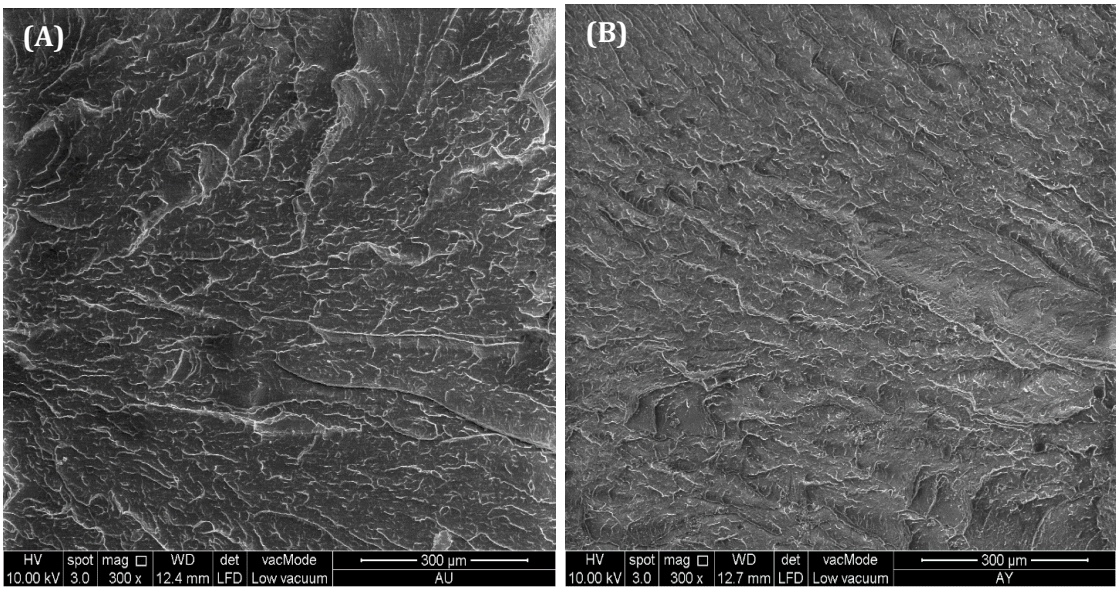


Figure 5.13 Impact fractograph for 100% PP (A) before radiation (B) radiated at 40 kGy

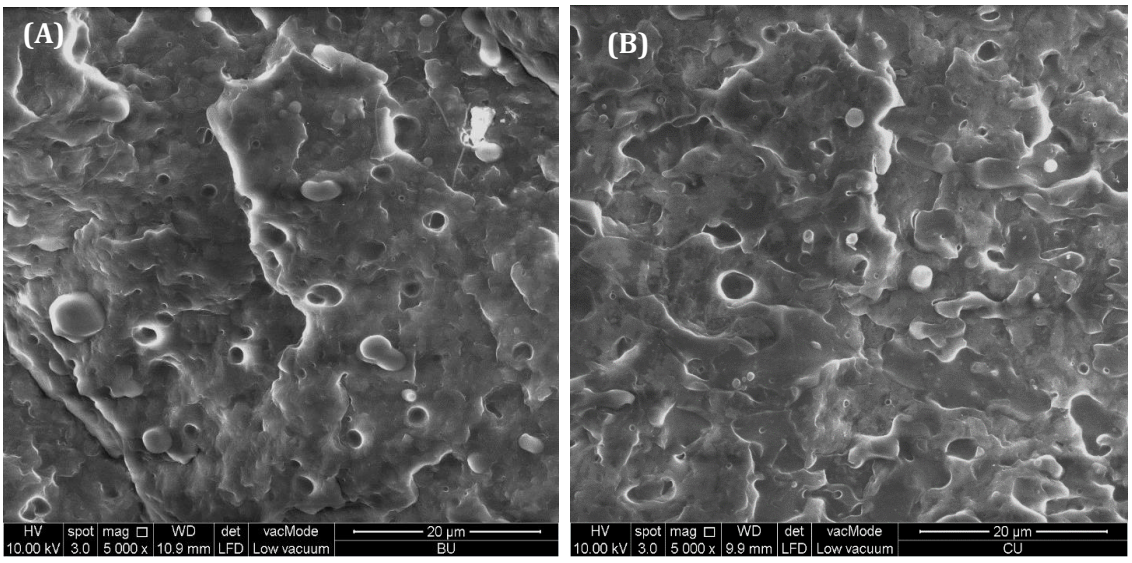


Figure 5.14 SEM images of blends before radiation (A) 80%PP and (B) 50%PP

Figure 5.14, it can be witnessed that more voids were formed in 80% PP and the elastomer was found to be dispersed as droplets in the PP matrix. Though few droplets of elastomer in matrix can be seen in 50% PP blend, they were fewer in comparison to 80% PP. The presence of more voids and elastomer as droplets improved the impact strength of 80% PP blend, which was explicitly explained in section 5.5.

Figure 5.15 (A-B) shows the SEM micrograph of 50% PP blends before and after radiation. Apparently, no significant changes were observed in 50 % PP blend upon radiation. However, in 20% PP blend a significant difference in the morphology upon radiation could be observed (Figure 5.16). After radiation, the continuous matrix covering or overlapping of the dispersed particles was achieved. This is an indication of enhancement of interfacial adhesion, as the PP was grafted to EPDM due to the radiation induced crosslinking. A similar interference was also reported in another literature, where crosslinking was achieved by various methods (Inoue and Suzuki, 1996, Jain et al., 2000). However, in this study the interfacial adhesion did not result in appreciable change in the mechanical properties of the blends. The continuous matrix overlaps or covers the dispersed phase, deterring them to act as stress concentrators. The continuous phase of PP simultaneously overlaps the voids, thus reducing the impact strength (Jain et al., 2000). The decrease in impact strength, elongation at break and tensile strength beyond optimum in radiated EPDM rich blends can also be related to the restriction of mobility of the macromolecules caused by the crosslinking. The macro-molecular immobility is well evident from the DMA analysis, which will be detailed in a separate study. This in turn reduces the elasticity and increases the stiffness and brittleness, which is evident in Figure 5.16. Figure 5.17 shows the impact fractographs of 20% PP blend before and after radiation at 80 kGy. It can be seen that energy was dissipated in the form of long fibrils, witnessing semi-ductile surface. However, upon radiation the morphology indicates semi-crystalline matrix, where brittleness is indicated by the increase in number of crazing formed and the roughness of the matrix.

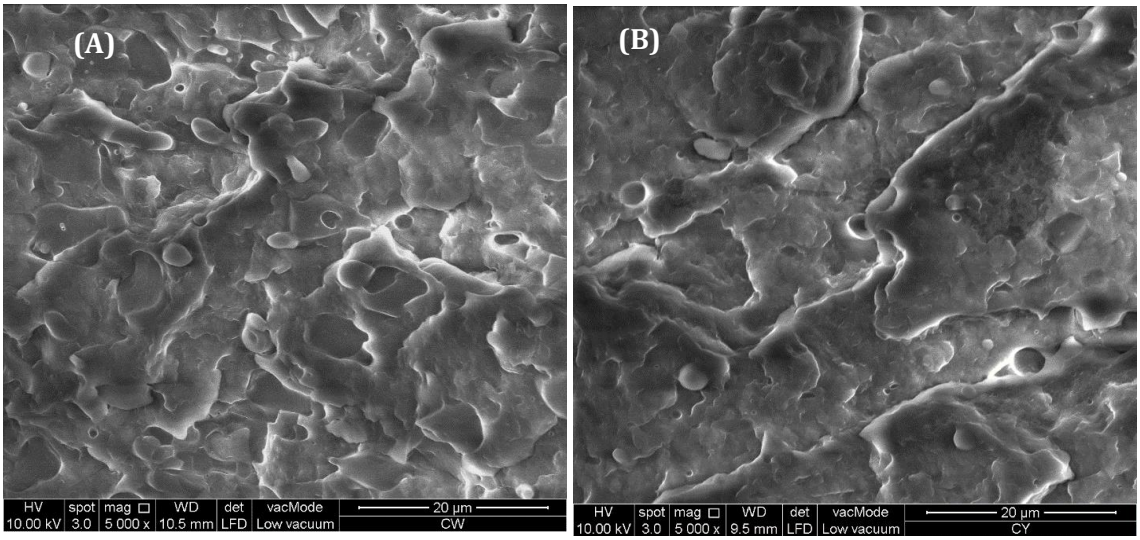


Figure 5.15 Morphology of 50%PP blend (A) radiation dose 40 kGY and (B) radiation dose 80 kGy

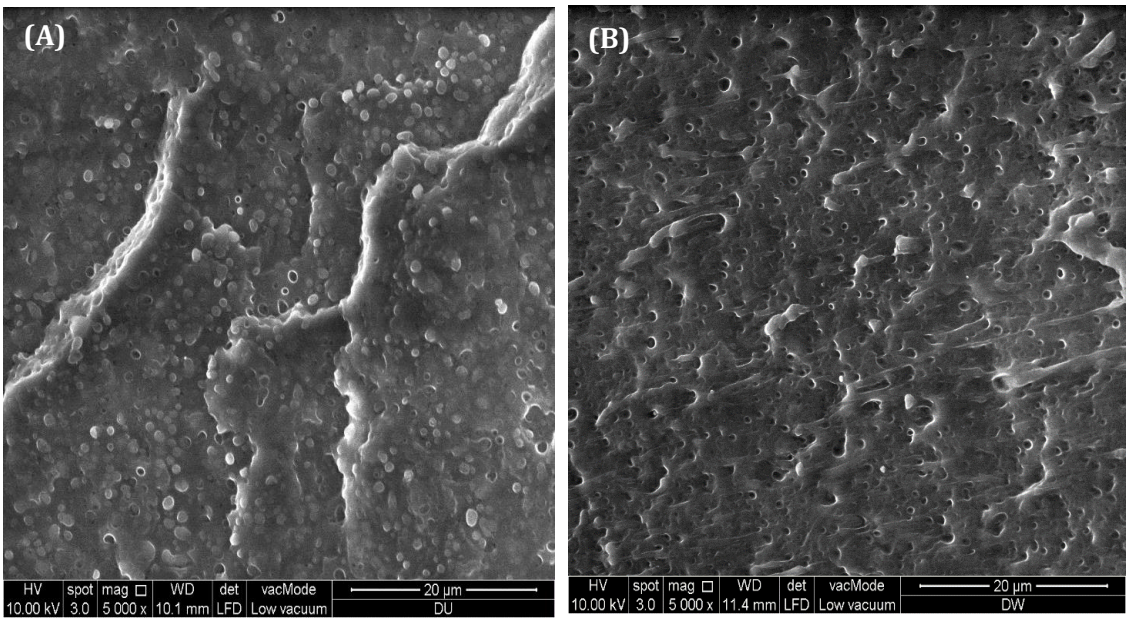


Figure 5.16 Morphology of 20% PP blend (A) before radiation (B) radiated at 40 kGy

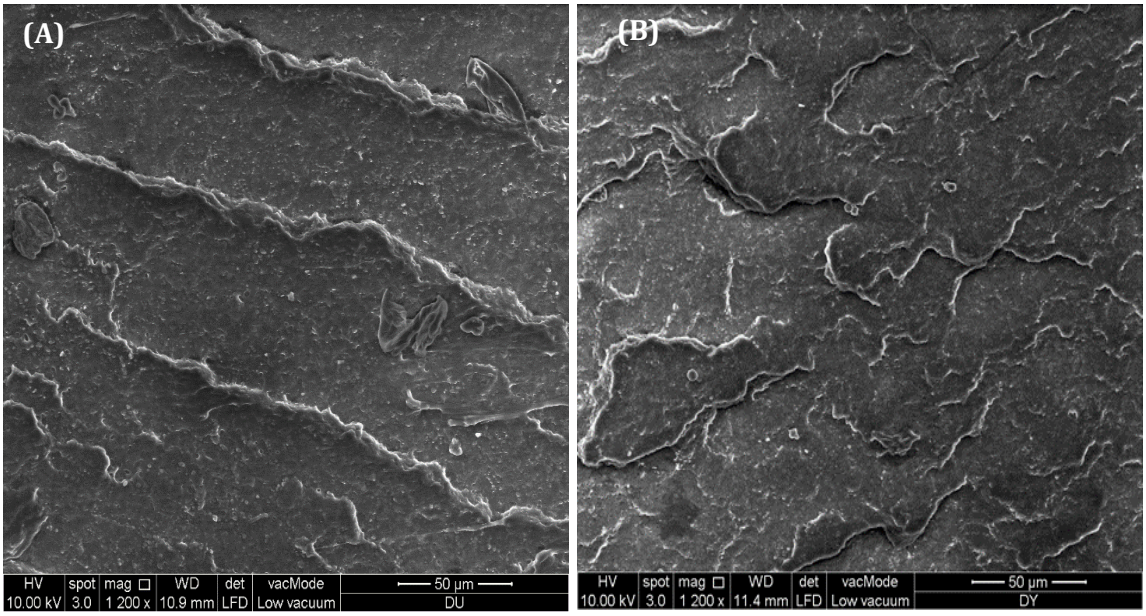


Figure 5.17 SEM micrographs of 20%PP (A) before radiation (B) 40 kGy

5.11 Fourier Transform Infrared Spectroscopy

The E-beam radiations is responsible for several structural changes leading to the modification of the physio-mechanical properties. The radiation induces crosslinks, chain scission and oxidation reactions within the polymer blends. The structural changes can be witnessed under the IR spectroscope of 80% EPDM blend in figure. The 20:80 PP/EPDM blend is considered for the FTIR study as they result in tremendous changes in the tensile strength upon irradiation (as discussed in section). From the Figure 5.18, it is evident that no new functional groups are formed upon irradiation. Nevertheless, the intensities of absorption of functional groups with increasing dosage varies marginally indicating the changes in the structure of blends, due to crosslinking and scission effects. (Elizabeth C. L. Cardoso, 2016, Majumder and Bhowmick, 1999) reported that upon radiation of EPDM, alkanes, alkenes, carbonyl and ether groups are affected. Further, (Urbaniak-Domagala, 2012) reported that , the major change in radiation of PP occurs only in the defiles of CH2- ; >CH- ; and –CH3 groups. The respective wavelengths of absorption of these functional groups along with the formation of –OH group is listed in Table 5.5. The change in absorption intensities of functional group are studied in terms of absorbance ratios of functional group, with respect to the methyl deformation of the respective blends.

From the figure4.12, it can be noticed that most of the changes occurs in the finger print region (700cm – 1500 cm-1). However, the absorbance ratios of the O-H bond increase with increasing dosage (0.028 for 0KGy and ≈ 0.04 for radiated blends). This indicates that the chain scission reaction has resulted in formation of more number of methyl groups as well as free hydrogen atoms (Deepalaxmi and Rajini, 2014). The free radicals are the active sites for increase in crosslinking, which is evident in the finger print region and at wavelengths from 2500-3000 cm-1. On the other hand, the free hydrogen cites can lead to increase in oxidation, leading to reduction in mechanical properties.

Table 5.5 Absorbance ratio and functional groups of 20% PP blend

Functional Group	**Absorption band**	**Reference**	**0kGy**		**40kGy**		**80kGy**		**100kGy**	
			WN	**Absorption %**	**WN**	**Absorption %**	**WN**	**Absorption %**	**WN**	**Absorption %**
Cis RCH=CHR	675-730	(Deepalaxmi and Rajini, 2014)	721	0.76	721.40	0.86	721.39	0.85	721.33	0.86
=C-H alkene, bending, strong	675-1000		809	0.18	809.20	0.30	809.21	0.21	809.18	0.20
			841	0.20	841.16	0.23	841.18	0.24	841.12	0.24
			899	0.11	899.36	0.12	899.36	0.13	899.34	0.14
			973	0.34	973.21	0.54	973.22	0.40	973.25	0.42
			997	0.26	997.8	0.32	997.81	0.31	997.65	0.32
-C=O, ethers	1000-1300	(Hornback, 2005)	1166.86	0.4	1166.90	0.64	1166.92	0.48	1166.80	0.50

CH3, alkanes	2850-3000		2966	0.57	2952	0.94	2938	0.97	2973	0.68
CH2 alkanes			2883	0.85	2871	0.90	2857	0.86	2861	0.73
-C=O, aldehydes	2700-2800	(Silverstein et al., 2014)	2722.94	0.38	2722.94	0.61	2722.98	0.45	2722.9	0.48
Hydrophilic (OH)	3200-3600	(Deepalaxmi and Rajini, 2014)	3345.44	0.028	3345.98	0.04	3347.53	0.04	3347.2	0.055
C=O, carbonyl	1670-1820	(Silverstein et al., 2014)	1691	0.04	1707.98	0.05	1691	0.05	1691.6	0.058

However, the absorbance ratios of cis RCH=CHR; =C-H alkene, bending (675-1000 cm-1); -C=O, ethers (1000-1300 cm-1), aldehydes (2700-2800 cm-1), carbonyl (1670-1820 cm-1) and CH_2 alkanes increases with increasing radiation. The increase of crosslinks upon radiation is line with the gel content analysis as mentioned in section. The upsurge in crosslinks can be corroborated to the increase in tensile strength up to 40KGy. However, from the Table 5.5 it can be witnessed that at higher dosage more crosslinks are formed which is beyond the sufficient range (necessary to increase tensile strength) making the blend more brittle. This in turn reduces the tensile strength and elongation at break of the PP/EPDM blend at high dosage. Moreover, the structural changes witnessed due to change in absorbance ratios are also responsible for the change in yellowing of the blends which is discussed in section. Indicating the connections axial strain of group C=C possibly due to the breaking of bonds terminal and favouring the formation of these new groups. Deformations in this group showed a significant crossing of chains causing crystallinity and hardening of the material.

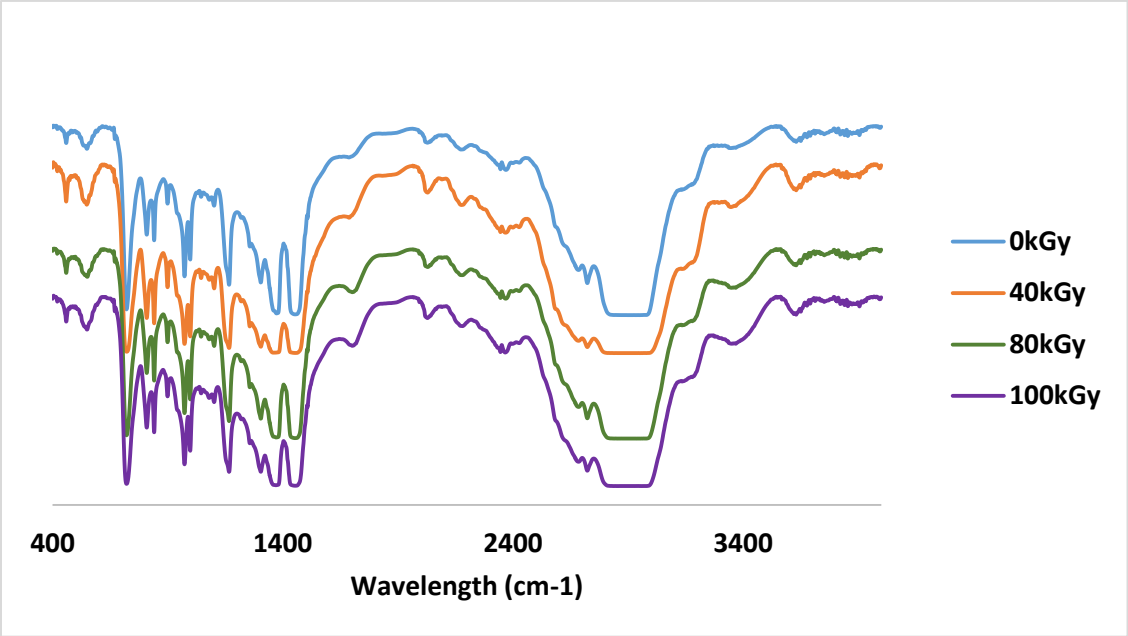


Figure 5.18 FTIR spectrum of 20PP/80EPDM blend at various radiation dose

5.12 Yellow Index

The Figure 5.19, represents yellow index of PP/EPDM blends upon irradiation. For translucent 100% PP and PP/EPDM blends, the 0kGy blend was considered as the blank. In order to standardize the results, for EPDM also, 0kGy EPDM sample was taken blank, even though they are transparent. The 100% PP deepens their yellow color upon irradiation. The radiation induced chain scission (as evident from gel content analysis) initiates free radicals. These free radicals undergo oxidation under their exposure to atmosphere. The oxidation in turn leads to formation of chromophores like –C=O and –COOH, responsible for yellowing of the material (Martakis et al., 1994, Luan et al., 2010). On the other hand 100% EPDM does not show significant change in the yellow index. The free radicals formed in EPDM under radiation are used maximum in crosslinking rather than oxidation. This reduces the formation of yellow coloured groups. The yellow index of 20% PP is at 0.65, upon irradiation at 20 kGy. This is significantly less than 100% PP at 20 kGy. The blend rich in EPDM causes higher crosslinks to be formed, rather than oxidation. This is in line with gel content analysis, where the crosslinks increase to 35% with radiation dosage of 20kGy for 20% PP blends. The yellow index drops to 0.59 at 40 kGy and further to 0.25 at 80kGy. This again is due to increase in crosslink formation with increasing radiation dose. This can also be verified from FTIR

analysis (section 5.11), where the absorbance ratios of –C=O (chromophore causing yellowness) for 20% PP at 40 kGy is 0.64 (Table 4.5). With increasing dosage to 80kGy the absorbance ratio dropped to 0.48. Thus the decrease in the formation of chromophore (due to increase in crosslinking) with increasing dosage reduces the yellowness index of the 20% PP blend.

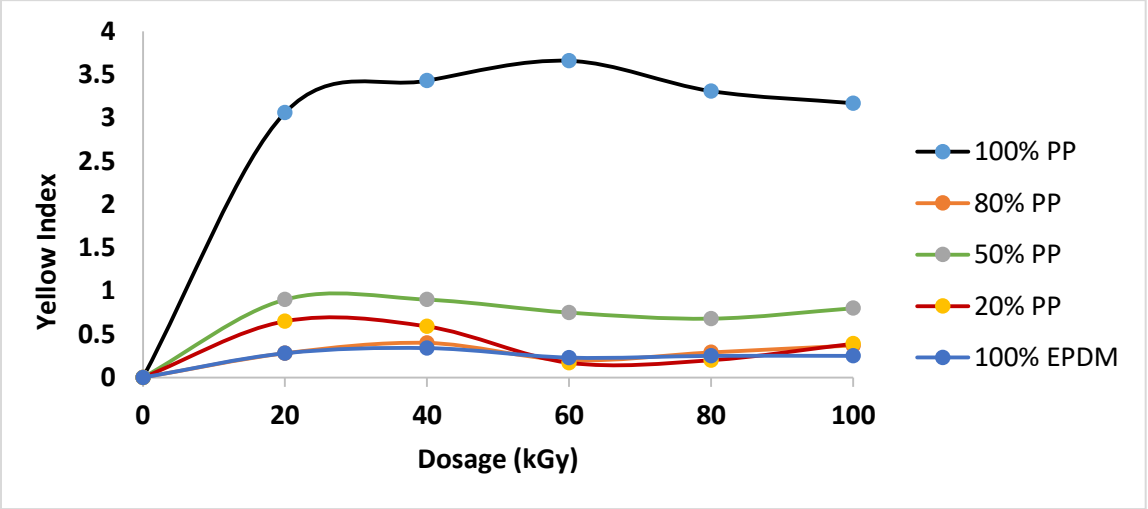


Figure 5.19 Yellow index of PP/ EPDM blend with increasing radiation dosage

5.13 Summary

The gel content analysis revealed that the E-beam radiated PP rich blends were dominated by the scission reaction, resulting in decreased mechanical and dynamical properties. Moreover, the yellowness of PP also increased upon irradiation, due to oxidation initiated by chain scissions. While for the blend with more than 50% EPDM, the crosslinking effect overruled the scission mechanism. With the increase in EPDM content, especially 20% PP blend, a noticeable improvement in mechanical and dynamic properties were recorded. Also, the crystallinity of blends was reduced with increasing dosage. While the PP rich blends were immiscible, the DMA results revealed that PP and EPDM phase in 20% PP blend showed better compatibility. Further, the yellowness of the sample also decreased remarkably. However, there was no significant change in the thermal stability of the all the blends.

6 PREDICTION OF MECHANICAL PROPERTIES OF POLYPROPYLENE (PP)/ ETHYLENE PROPYLENE DIENE MONOMER (EPDM) AND ETHYLENE VINYL ACETATE (EVA) TERNARY BLENDS USING DESIGN OF EXPERIMENTS

6.1 Introduction

In the previous chapter, it was noticed that only the EPDM rich blends showed improvement in tensile strength. On the other hand, the blend with 50% PP or higher showed a decrement in tensile strength and impact properties after treatment of E-beam dose at 20-100 kGy. In order to stabilize or improve the properties under radiation, an initiative to add ethylene vinyl acetate (EVA) in the polymer blend was carried out. Since three individual polymers were involved in a blend, more than 100 blend compositions are possible. It is a well-established fact that the mechanical properties significantly vary depending upon the blend composition. Hence, DOE was used to predict the mechanical property (tensile strength, elongation at break and impact strength) of every blend composition possible. The mechanical properties over the entire possible blend compositions with varied mixture proportions were predicted using the property charts generated by simplex centroid design. Different medical device products require different mechanical property specification. Therefore, different products are required to be manufactured with different blend ratios according to product specifications. The property charts generated, will help the researchers or industrialists instantly to predict the required blend proportion based on tensile properties and impact strength.

6.2 Experimental Design

The design sheets were generated using simplex centroid package under mixture design. The Statease Design expert 9.0.5 software was used in this chapter. A simplex-centroid design consists of all points that are equally weighted mixtures of 1 to q components. Included are permutations of: pure blends: (1, 0, ...,0), binary blends: (1/2, 1/2, 0, ...,0), tertiary blends: (1/3, 1/3, 1/3, 0, ...,0) and so on to the overall centroid: (1/q, 1/q, ..., 1/q). The default augmentation for the simplex-centroid design adds check points (half-way between the overall centre and each vertex). A range of 0 to 100% for all the three blend constituents was considered in this study. The general augmentation of the design or the structure of the equilateral triangle charts generated by DOE is shown in Figure 6.1. The design sheet considered for this study with various composition percentages is shown in Table 6.1. The tensile properties including tensile strength (MPa), elongation at break (%) and impact strength (J/m) were the responses predicted in this study using DOE.

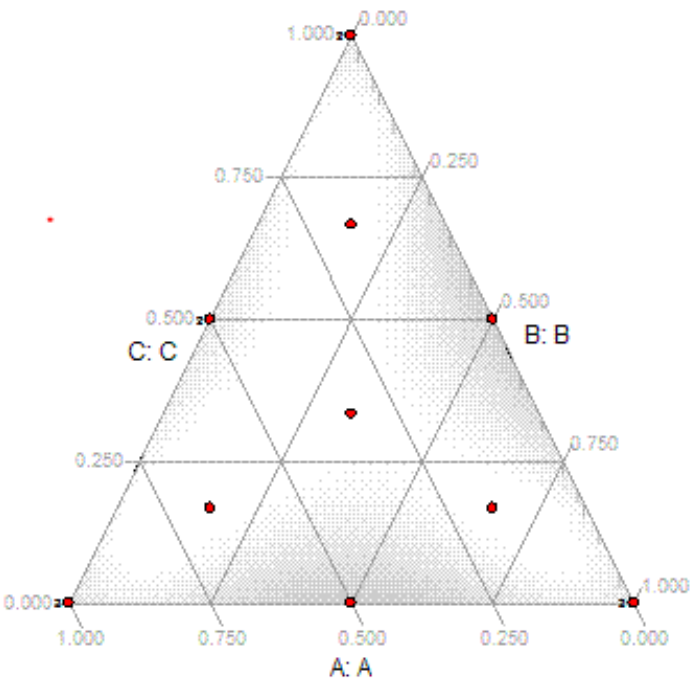


Figure 6.1 Three component simplex centroid design with extreme limits (augmented) (where A=EPDM, B=PP and C=EVA)

Table 6.1 Blend proportion designs generated by DOE

Run Number	Blend Proportion		
	A: EPDM (%)	B: PP (%)	C: EVA (%)
1	0	100	0
2	50	50	0
3	0	0	100
4	50	50	0
5	0	100	0
6	0	50	50
7	16.66	66.66	16.66
8	50	0	50
9	100	0	0
10	16.66	16.66	66.66
11	0	0	100
12	100	0	0
13	33.33	33.33	33.33
14	66.66	16.66	16.66

6.3 Fitting of model and Analysis of Variance (ANOVA)

The tensile properties and impact strength of the ternary blend were predicted using the simplex centroid mixture design. The property charts were generated with the following regression equations;

Tensile strength (MPa) = +4.09*A+32.53*B+10.01*C-4.18*AB+12.90*AC-45.77*BC-52.73*ABC *Eq 6.1*

Elongation at Break (%) = +1137.02*A+761.07*B+852.91*C-674.74*AB+869.71*AC+ 817.07*BC *Eq 6.2*

Impact strength (J/m) = +102.78*A+32.88*B+143.30*C-85.86*AB+948.02*AC-162.98*BC-468.66*ABC-6073.72*ABC^2 *Eq 6.3*

where, A= EPDM (%), B=PP (%) and C=EVA (%)

The above mentioned polynomial equations (Eq 6.1,6.2 and 6.3) with regression co-efficient (R^2) of 0.9496, 0.8032 and 0.9886 for tensile strength, elongation at break and impact strengths, respectively, were used to fit the regression models. The R^2 values reaching the integrity (≈1) indicates a high degree of model fitness. The adequate precision for tensile strength, elongation at break and impact strength are 13.14, 5.692 and 28.33, respectively. Adequate precision is a measure of signal to noise ratio. A ratio greater than 4 ensures that the model can be used to navigate the design spaces. The f and p values were determined by using the analysis of variance (ANOVA). The p-values for both the responses were less than 0.05, which indicates the model fitting was considered with 95% confidence limits. Further, the F-value for the models was 18.97, 4.90 and 62.04 respectively. This implies that there is only 0.05%, 3.94% and 0.01% chance that F-value this large for tensile strength and impact strength could occur due to noises. The p-value also assures that the models for both the responses pass the F-test. Further, the lack-of–fit for the both the response models were not significant due to low values of F-value and high p-values (>0.05), indicating that the ability of polynomial models to express the relationships for the independent and dependent variables within the domains of investigation. Figure 6.2 (A-C) represents the normal probability plot. In the figures, the data points are present around the normal line. This indicates that there is no abnormality in the data population and ensures that the data points follow normal distribution. In Figures 6.3 (A-C), it can be noticed that the data points scattered, which ensures constant variance along the hypothesis. Additionally, in Figures 6.4 (A-C), the distribution of experimental and predicted response values for tensile and impact strength confirms high correlation between these values. Thus, the statistical terms including R^2, adequate precision, F and p values, normal plots and residual plots display the robustness of the simplex centroid design used in generating the property chats for the ternary blends.

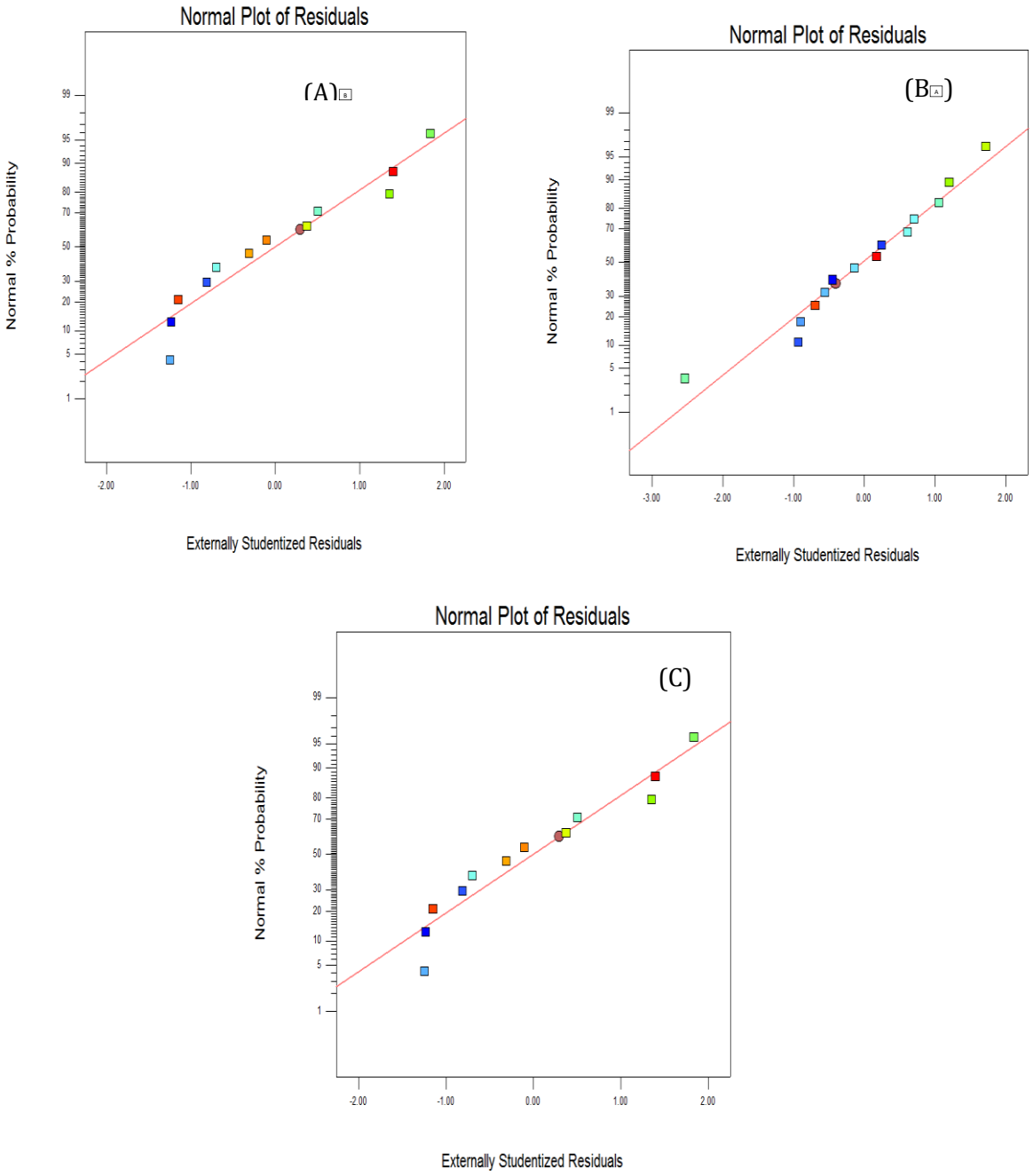


Figure 6.2 Normal Residual plots (A) Tensile strength (B) Elongation at break and (C) Impact strength

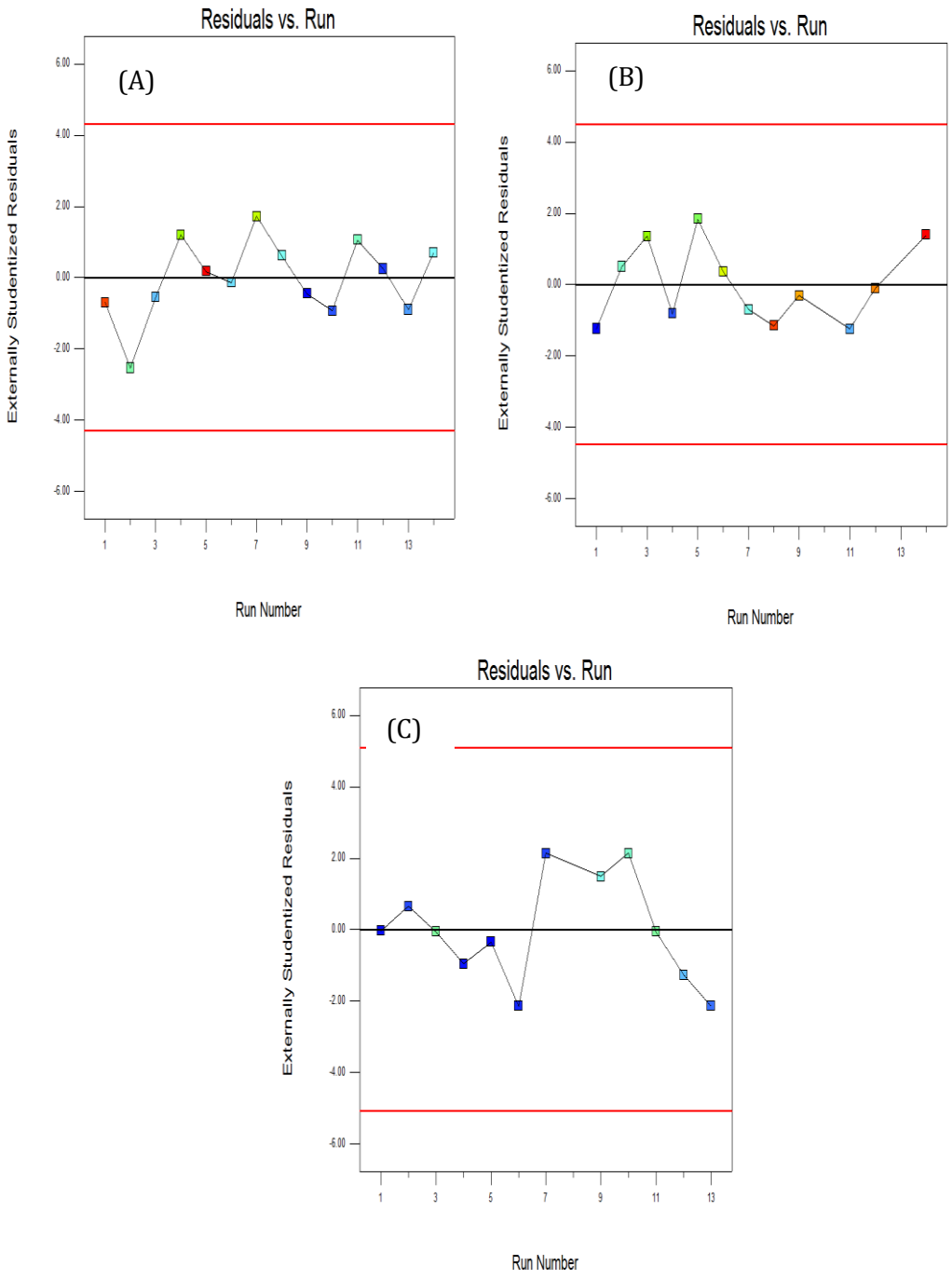


Figure 6.3 Residual vs runs plots (A) tensile strength (B) elongation at break and (C) impact strength

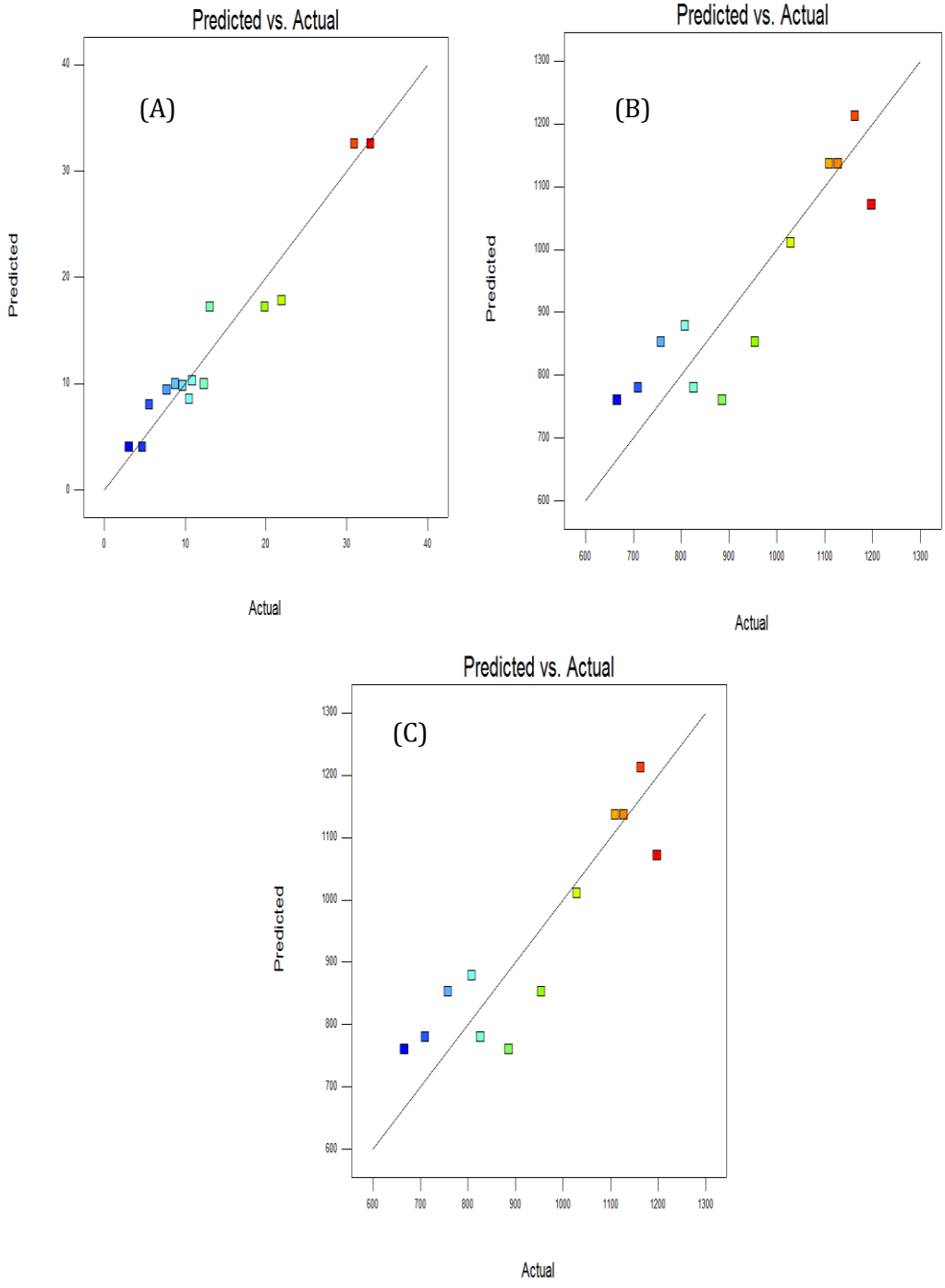


Figure 6.4 Actual vs. predicted plot (A) tensile strength (B) elongation at break and (C) impact strength

6.4 Tensile and Impact property profile of ternary blend obtained using Design of Experiments

Figure 6.5 represents the contour plot for tensile strength of the ternary blend. It can be witnessed that only 100% PP or PP greater than ≈85% showed a maximum tensile strength of 30 MPa in comparison to 100% EVA and 100% EPDM. Generally, the methyl groups attached to the successive carbon atom in the backbone of the polymer chains of PP, EPDM and EVA are short and rigid, restricting the rotational motion of the chain resulting in high tensile strength (Salih et al., 2013). The tensile strength of the blends decreased with increasing EPDM or EVA content. The increase in amorphousness after the addition of EVA and EPDM led to decrease of tensile properties of the ternary blends.

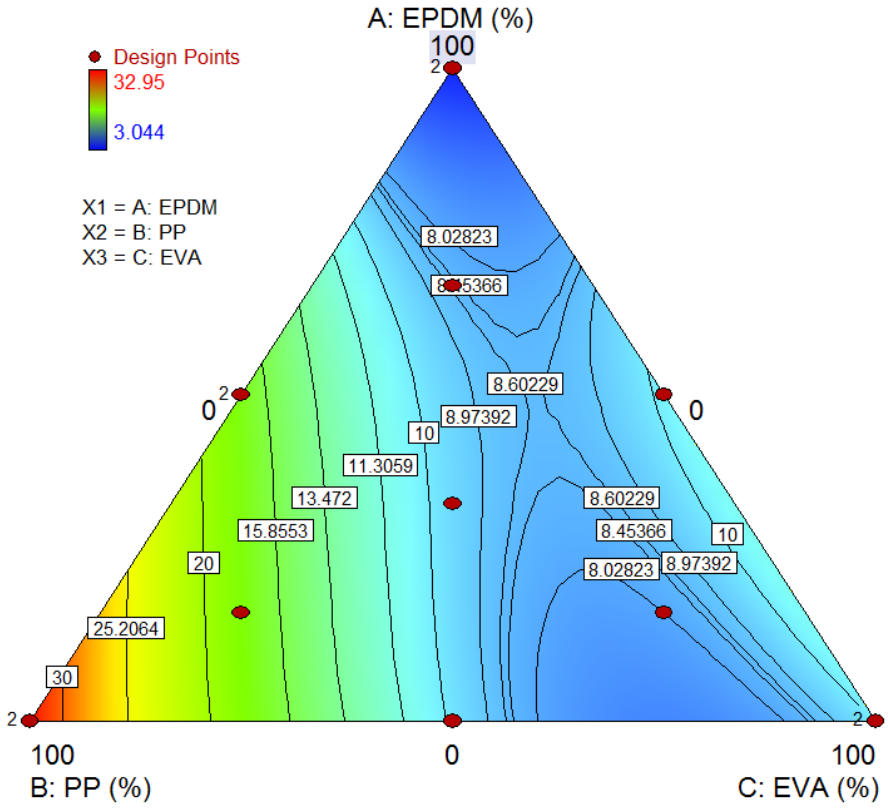


Figure 6.5 Tensile strength property chart for PP/EPDM/EVA blend

Figure 6.6 represents the elongation at break of the ternary mixture. As expected, PP exhibited the lowest elongation at break due to its inherent plasticizing nature, whereas the elastomers exhibited higher elongation at break. It can be noticed that addition of 20% EVA to PP increased the elongation at break remarkably by 25% (800-1000%). This could be due to dilution effects of amorphous EVA. However, more than 50% EPDM was necessary to modify the PP with elongation of break of this range. The maximum elongation at break for the blend could be witnessed in only a small region (marked in red colour), where least amount of PP and high content of EPDM with considerable amount of EVA was present.

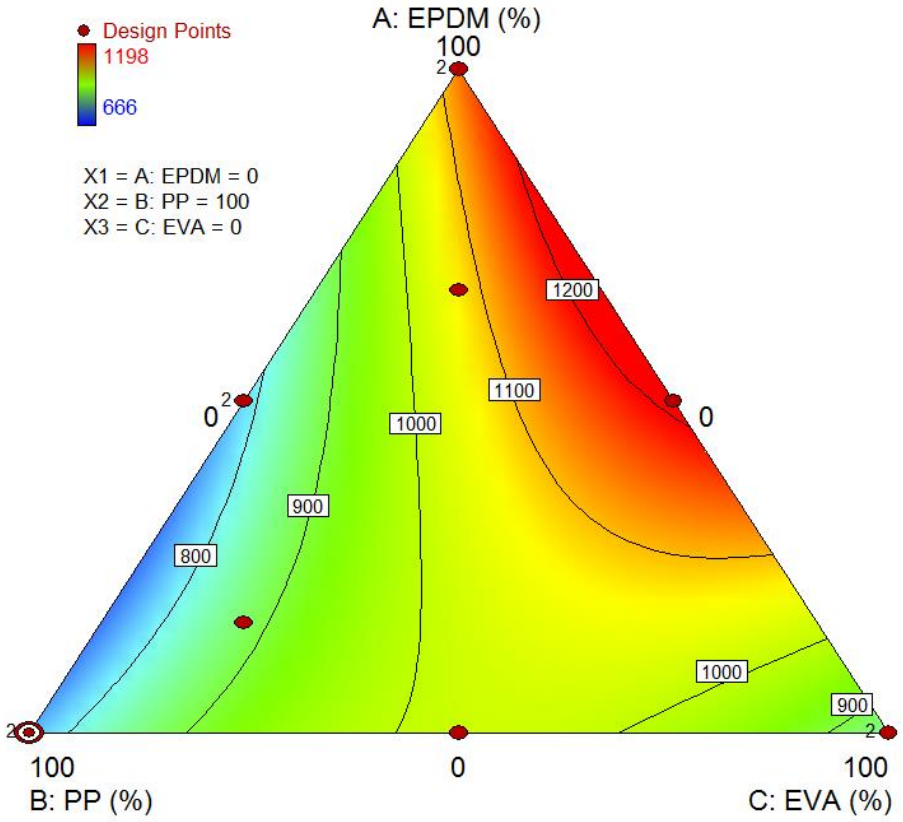


Figure 6.6 Elongation at break chart for PP/EPDM/EVA blend

Figure 6.7 represents the impact strength of the blends. As expected, it can be witnessed that the impact strength of the blend with high PP content decreased. On the other hand, the blends with more EVA and EPDM content showed higher impact strength. The binary blend of EVA and EPDM when blended with equal proportions resulted in the highest impact strength of 300 J/m. As the PP content decreased, the impact strength increased considerably.

It is well reported that the synthetic elastomers act as impact modifier in PP. It is interesting to note that only a small portion of the graph, where PP content of the blend is less than 25%, the blend can with withstand very high impact strength.

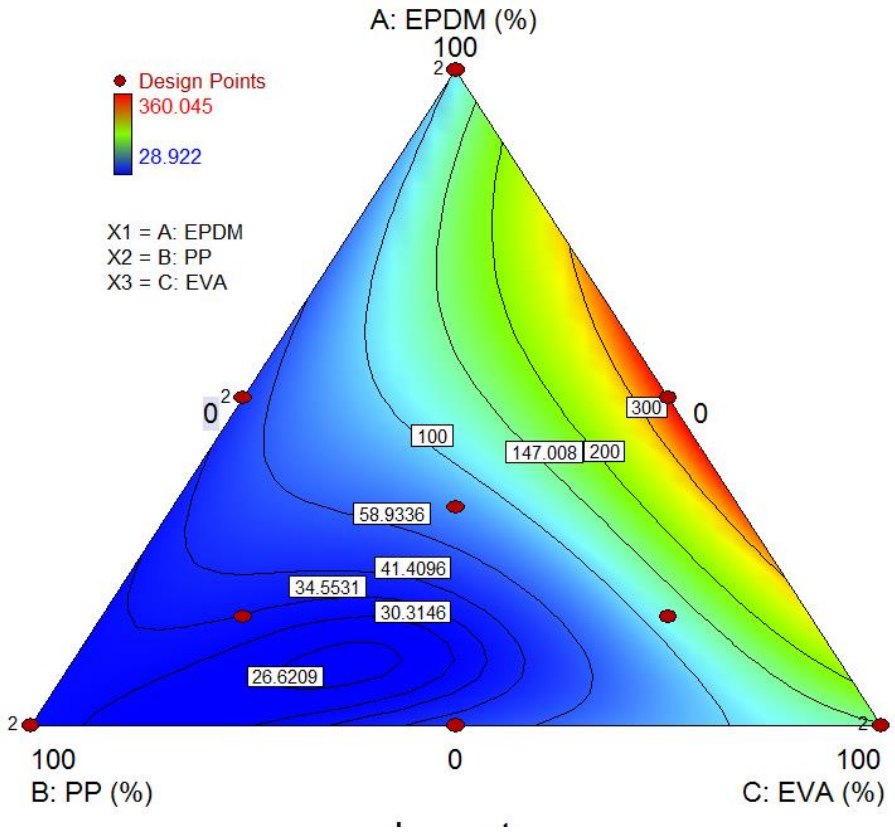


Figure 6.7 Impact strength chart for PP/EPDM/EVA blend

6.5 Validation of mechanical properties of ternary Blend:

To validate the property profile charts of ternary blend generated using DOE and to estimate the error percentage of the ternary blend's mechanical properties, three random compositions of the blends were mapped and listed in Table 6.2.

Table 6.2 Actual and predicted values of mechanical properties for PP/EPDM/EVA blends

Blend Composition (%)	**Tensile Strength**			**Elongation at Break**			**Impact Strength**		
	Actual Values (MPa)	***Predicted Values (MPa)***	***Error (%)***	***Actual Values (%)***	***Predicted Values (%)***	***Error (%)***	***Actual Values (J/m²)***	***Predicted Values (J/m²)***	***Error (%)***
50 PP: 25 EPDM: 25 EVA	13.464	12.703	5.65	875	950.16	8.58	51.56	44.008	17.11
25PP: 50 EPDM: 25 EVA	10.176	9.260	9.91	1010	1047.44	4.57	157.25	130.92	20.11
25 PP: 25 EPDM: 50 EVA	8.041	8.140	1.22	970	1069.65	10.2	106.42	88.781	19.8

It can be noticed from Table 6.2 that impact strength showed higher error percentage relatively in comparison to the actual impact strength of the ternary blends. Though composition of the mixture is important in determining the properties of the elastomer blends, there are other factors that also contribute to impact strength of the elastomer blends. In the blends with high PP content (>50%PP), the elastomers are present as dispersed phase. The SEM micrographs (Figure 6.8 A) shows that in PP/EPDM/EVA ternary blends also, the minor composition (the dispersed phase) was present in droplet form. The factors including

dispersed elastomer particle size, inter particle distances, spherulite size, spherulite boundary and degree of interfacial adhesion are some of the very important factors other than composition of the mixture that determines the properties of the blend (da Costa et al., 2010). This error percentage could also be contributed due to the non-homogeneity of the blends. Figure 6.8 (A and B) complemented the non-homogeneity of the blends. Apart from these factors, it is reported that some extent of crosslinking also took place during the melt blending process. Thus, the aforementioned factors collectively could have contributed to the changes in the actual impact strength of the polymer blends which could not be included while determining the properties using a statistical tool. However, for higher accuracy, the screened/selected blend composition from these charts should be further investigated and optimized by other means such as single factor analysis and Taguchi method.

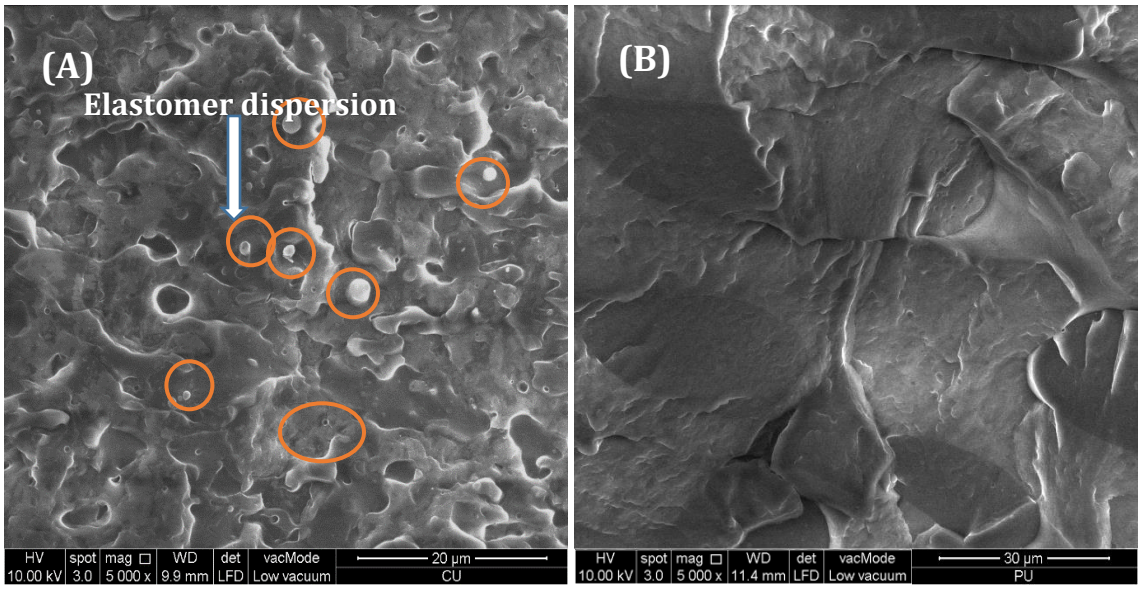


Figure 6.8 SEM micrographs of (A) 30EPDM/20EVA/50PP ternary blend and (B) 50PP/50EVA

6.6 Summary

The ternary blend consisting of various proportions of PP, EPDM and EVA were synthesized via melt blending. The property charts for the entire ternary blend proportions were generated using DOE. These charts enabled the researchers to predict the tensile strength elongation of the break and impact strength with ±10% error. However, the DOE predicted the impact strength property with 15-20% error. The accuracy for impact strength prediction needs further investigation considering the other factors like compatibility, interfacial adhesion, dispersion phase size and so on.

7 EFFECT OF E-BEAM IRRADIATION ON POLYPROPYLENE (PP)/ ETHYLENE PROPYLENE DIENE MONOMER (EPDM) AND ETHYLENE VINYL ACETATE (EVA) TERNARY BLENDS

7.1 Introduction

This chapter aims to address the fourth objective of the study. Chapter 7 gives an insight on how the mechanical properties of the ternary blend changed over different PP, EPDM and EVA composition in the ternary blend. From chapter 5, it was identified that E-Beam improved the mechanical properties only with higher EPDM loading (80EPDM/20 PP blend). Though crosslinking increased with increase in dosage for 50PP/50EPDM blend, there was no improvement in mechanical properties above 20 kGy dosage. However, the minimum dose required for effective sterilization is 25-40 kGy. Since one of the main objectives of the study was to improve the properties of the blend with higher PP content, 50PP/50 EPDM was taken as a base for this chapter. In order to improve its mechanical properties after radiation of above 25 kGy dose, EVA was amalgamated with PP/EPDM blend. For this study, the PP concentration was maintained constant at 50% as major phase. As the loading of EVA was increased in the blend, the content of EPDM was decreased in order to maintain a total of 100% volume in a ternary blend. The properties before and after radiation of ternary blends with mixing ratios of 10EVA/40EPDM/50PP, 20EVA/30EPDM/50PP, 30EVA/20 EPDM/50PP and 40EVA/10EPDM/50PP were investigated. Also, they were compared with 50PP/50EPDM and 50PP/50 EVA blends which were considered as controls. The addition of elastomers induced crosslinking in the ternary blend upon the absorption of irradiation. The self -crosslinking was possibly formed within the respective polymers and there lies the possibility of inter crosslinking between the polymer components. The plausible crosslinking mechanisms are illustrated in Figure 7.1 . Further, along with the crosslinking of the system on the whole, there existed scission mechanism as well. The crosslinking and scission existing side by side affected the properties of the blend depending upon the composition and radiation dose. The effect of radiation dose (over the range of 20-100 kGy) on mechanical, structural, thermal and dynamic mechanical properties of the PP/EPDM/EVA ternary blends are investigated in this chapter.

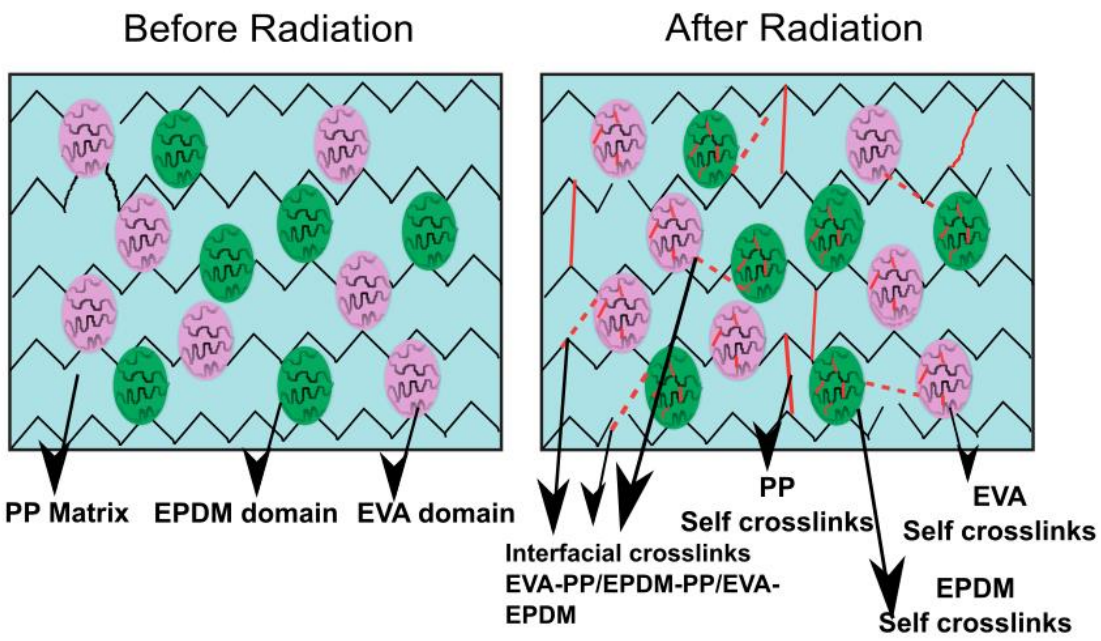


Figure 7.1 Schematic of inter and intra crosslinking of PP,EVA and EPDM

7.2 Gel Content

Figure 7.2 shows the influence of EVA loading and the effect of irradiation on gel content of PP/EVA/EPDM blends. It can be noticed that prior to radiation, pure EVA similar to neat EPDM and PP, was almost completely soluble in hot xylene and thus did not show formation of gel. It required more than 20 kGy dose to achieve a significant increase in gel content. Crosslinking further increased steadily with increasing radiation dose, exhibiting a maximum of 70% gel at 100 kGy. However, the neat EVA exhibited much lower gel content in relative to the neat EPDM, where the later exhibited a maximum of 90% gel content at 100 kGy. From Figure 7.2, it can be noticed that EPDM exhibited higher crosslinking while PP exhibited the lowest throughout all the radiation doses. The extent of gel content formation in this study followed the following order: EPDM >EVA >PP. EVA and EPDM exhibited higher crosslinking efficiency than PP because of their high amorphous nature and molecular structure in relative to semi-crystalline PP (Ray Chowdhury et al., 2016). Though EVA has higher ethylene content than EPDM (EVA ethylene content- 72% and EPDM has 68% ethylene content), EVA performs poorly with respect to EPDM in the studied range of irradiation dose. It was reported that ease of crosslinking of EPDM is very much higher in EPDM-EVA blends due to

the very large number of tertiary hydrogen atoms per chain present in EPDM backbone (Mishra et al., 1998) .

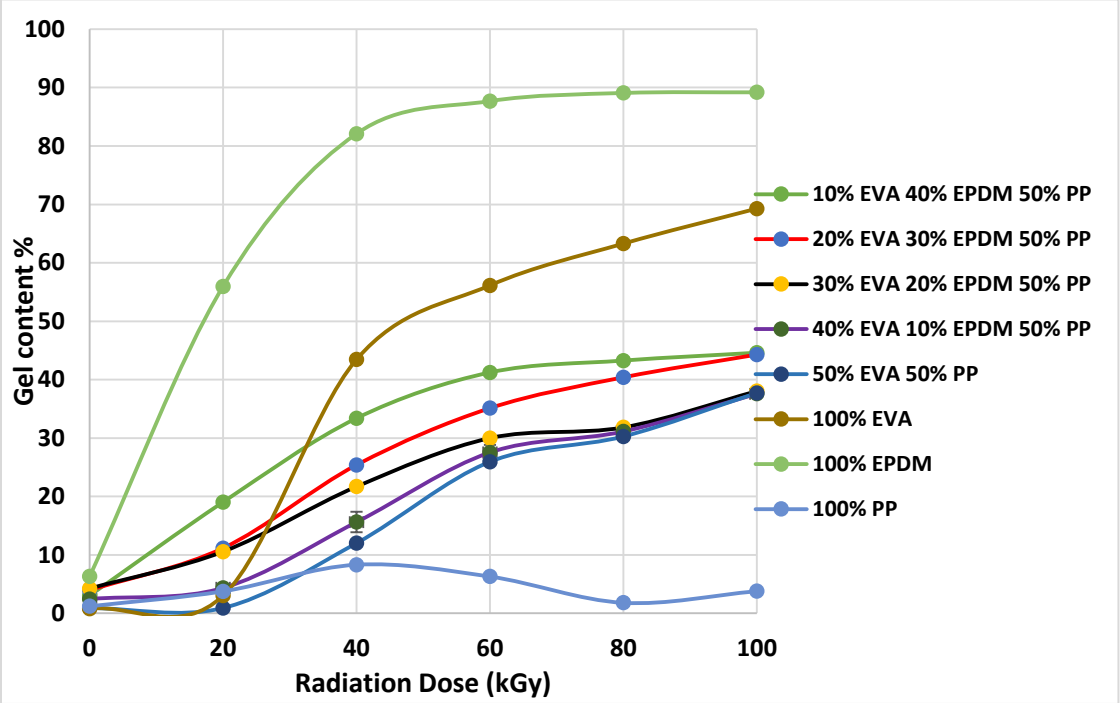


Figure 7.2 Gel content analysis of neat polymers, binary and ternary blends

Increase in crosslinking leads to decrease in the solubility of polymer blend in hot xylene, leading to higher formation of gel. Upon irradiation, free radicals were formed in both amorphous and crystalline regions. However, free radicals formed in amorphous regions favored crosslinking, while free radicals trapped in crystalline regions had a much lower mobility and a longer lifetime; such radicals can migrate slowly to amorphous region, where they subsequently react (Sabet and Soleimani, 2017).

From Figure 7.2, the blend with 10% EVA showed higher gel content than the blend with 50% EVA loading. This indicates that increase of the EVA loading in the blend resulted in decrement of gel formation at all radiation doses. Alternatively, it can be stated that the gel formation increased with increasing the EPDM content of the blend. EPDM in the ternary blends possessed more sensitive effect to gel formation than EVA. On the other hand, gel formation of all the ternary blends increased with increasing radiation.

Table 7.1 Crosslinking to scission ratio of the blends using Charles Pinner equation

Blend	**p_0/q_0**
10EVA/40EPDM/50PP	1.249
20EVA/30EPDM/50PP	1.29
30EVA/20EPDM/50PP	1.4031
40EVA/10EPDM/50PP	1.4023
50EVA/50PP	1.381
50EPDM/50PP	0.9865

Charles-Pinner equation was used to determine the crosslinking and chain scission yield of the blends. It can be seen in Table 7.1 that as the EVA content increased up to 30%, p_0/q_o increased, suggesting that crosslinking efficiency was aggravated. The more highly mobile methyl radicals from the acetoxy group in the PVA chains underwent scission and the free radicals led to oxidation decreasing the enhancement effect of EVA content on the crosslinking of the ternary blends (Charlesby and Pinner, 1959, Dalai and Wenxiu, 2002a) . However, with EVA more than 40%, the p_o/q_o decreased slightly showing increase in the crosslinking effect. The facts illustrate that PVA chains in the EVA had an enhancement effect on both radiation crosslinking and radiation oxidation, and the contradictory elements are reached to optimum equilibrium for radiation crosslinking in the 40 EVA/10 EPDM/50 PP and 50PP/50 EVA blend.

On the other hand, 50EPDM/50PP blend exhibited the lowest p_0/q_0 value of among all the EVA based blends, indicating that it had the highest crosslinking efficiency. This corroborates with the gel content data as discussed before. It could probably be due to more free radicals generated in the amorphous phase of EPDM favouring crosslinking (Sharif et al., 2000) . The crosslinking due to the amorphousness of EPDM may dominate the scission effect created by free radicals of EVA on the whole. Thus, it can be safely assumed that gel content or the crosslinks formed was the net result of the complex free radicals like PVA generated from EVA and from PE chains of PP,EPDM and EVA that either led to crosslinking or scission. The complex system was studied in detail further using TGA, morphological and DMA studies.

7.3 Tensile Properties

Figure 7.3 and Figure 7.4 show the tensile strength and elongation at break of EVA/EPDM/PP blends as a function of radiation dose. From these figures, it can be noticed that prior to radiation, the blend with 10% EVA showed a tensile strength of ≈15 MPa. As the EVA loading increased up to 30%, the tensile strength increased up to 18.41 MPa. However, with further increase in EVA loading the tensile strength decreased dramatically. Several studies reported that EVA (up to 30 wt%) dispersed in continuous PP phase provided compatibilizing effect, which in turn enhanced the mechanical properties of the PP blends (Thomas et al., 1987, Blom et al., 1996, Kocak et al., 2016). The tensile strength of 50PP/50 EVA dropped significantly to 10 MPa. Ajili et al. (2003) reported a similar trend in PP/EVA blend, where 70/30 or 30/70 blend composition had higher tensile strength than 50/50 blend due to the finer dispersion morphology leading to a reduction of the cohesive energy density in 50/50 PP/EVA phase.

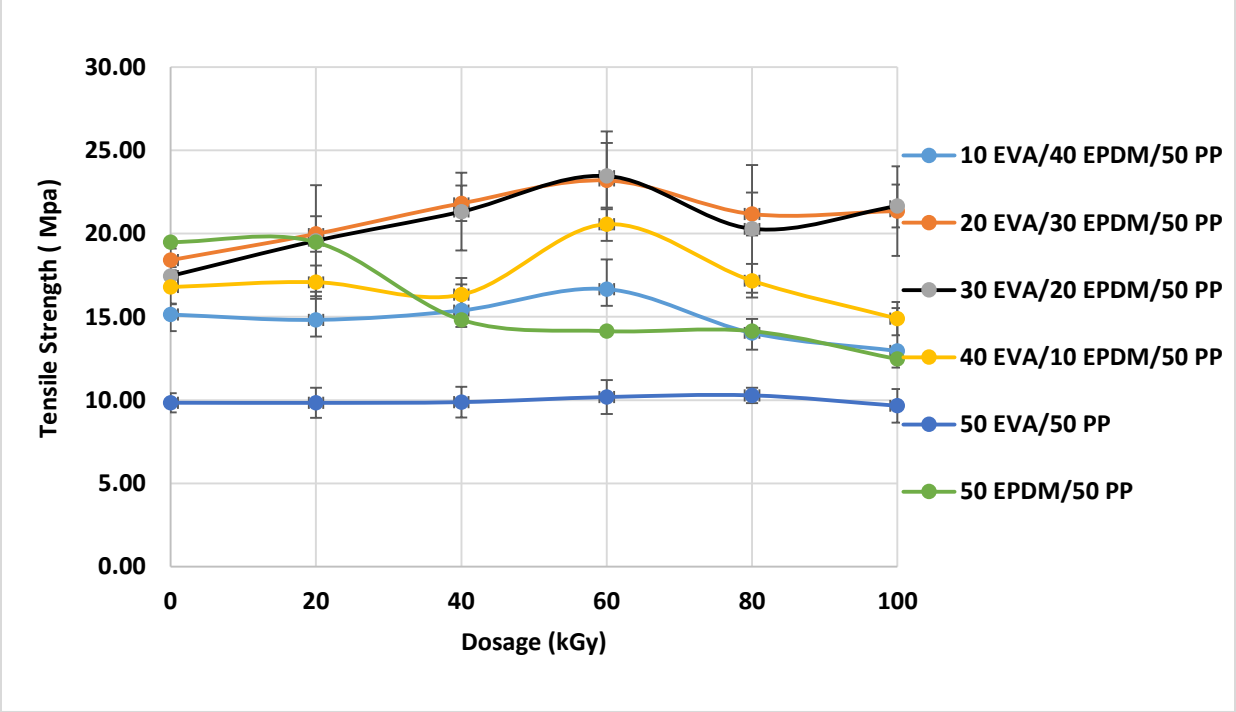


Figure 7.3 Tensile strength of PP/EVA and PP/EVA/EPDM blends as a function of radiation dose

The 50EVA/50PP blend upon irradiation up to 100 kGy, showed only a marginal change in both tensile strength and elongation at break (Figure 7.3 and Figure 7.4). However, the gel

content analysis shows that crosslinks increased with increasing radiation for 50/50 EVA/PP blend. This means that as the crosslinking processes continued to increase upon irradiation, a non-uniform distribution of the tension along the chains was created. The shorter segments, which are more strained, break down earlier and the tension is distributed between the other chains, gradually leading to their breaking as well (Zhao et al., 2016). Therefore, only a marginal change in tensile strength was observed in 50PP/50EVA blend even upon irradiation.

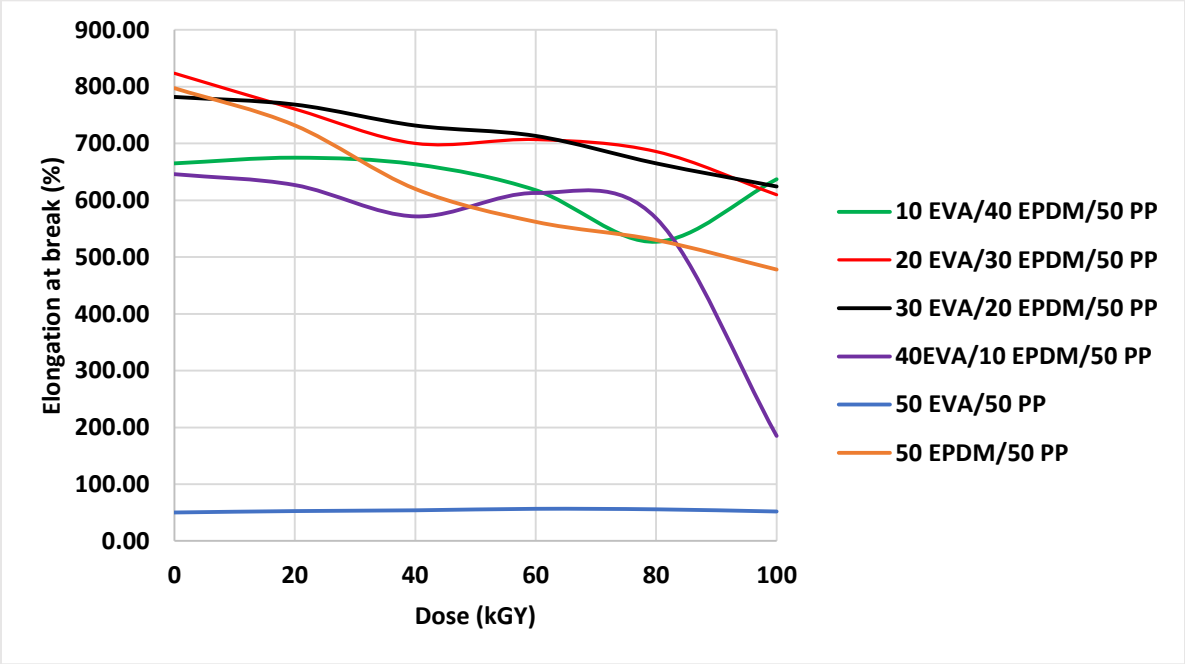


Figure 7.4 Elongation at break of PP/EVA and PP/EVA/EPDM blends as a function of radiation dose

On the other hand, blends with the presence of EPDM, the blends showed a different trend. Upon irradiation, the tensile strength of all the EVA/EPDM/PP blends increased significantly and reached a maximum at 60 kGy. While the blend with 10 EVA loading showed a maximum increase of 10% at 60 kGy, the blend with 20 EVA, 30 EVA and 40 EVA showed an increase in tensile strength up to 26%, 29% and 23%, respectively. It is to be noticed that the higher magnitude crosslinking was induced by EPDM in the blend, which plays a significant role in enhancement of overall tensile strength of the ternary blends. The presence of EPDM exhibited higher gel content in the ternary blend at a given dose as discussed in earlier section. High energy radiation of polymers creates free radicals by the scission of the weakest

bonds. These new entities react with each other forming crosslinks within the matrix (Hassan et al., 2007). Increasing the irradiation dose intensified the crosslinks formation as reflected in the improvement of tensile strength of ternary blends. It could be noted that increase in tensile strength due to increase in crosslinks was in relation to gel content analysis (Figure 7.2). Beyond 60 kGy, all the ternary blends showed a drop in tensile strength in spite of increase in gel content (crosslinks). This drop could be associated with the embrittlement of the blend caused by excessive formation of crosslinks above 60 kGy. In the initial state of irradiation, larger network structure is formed through radiation induced crosslinking resulting in an increase of the strength. However, later at higher irradiation doses, crosslinking are formed between the already crosslinked polymer chains breaking the larger network structure into smaller networks (microgel) and resulting in the embrittlement of the polymer matrix (Sharif et al., 2000, Salehi et al., 2004). A similar effect was observed in PP/EPDM binary blend as discussed in chapter 4.

From Figure 7.4, it can be noticed that for all the ternary blends, the elongation at break steadily decreased upon increasing radiation dose. Such a decline in elongation at break indicates that the compounds lost their elastic properties and became increasingly brittle. This in turn reduced the drawing of the blends as a consequence of the increase in cross-links upon irradiation (Sabet and Soleimani, 2017). A similar effect was reported in EVA blends upon irradiation (Thevy Ratnam et al., 2016).

7.4 Impact Strength

Figure 7.5 shows the impact strength of the PP/EPDM blends in the presence of EVA as a function of irradiation dosage. Prior to irradiation, it can be seen that the blends with higher content of EPDM (>20%) exhibited higher impact strength than EVA rich blends. It could be plausibly because of higher amorphousness of EPDM. Especially, the blends with 20EVA/30 EPDM and 30 EVA/20 EPDM showed high impact strength of 43.6 and 41.29 J/m respectively. As discussed in section 5.5, the polymers at these loadings when dispersed as droplets had the potential to absorb more impact energy. However, at more than 40 EVA loading, not many are dispersed as droplets having the tendency to reduce the capability of absorbing higher impact energy.

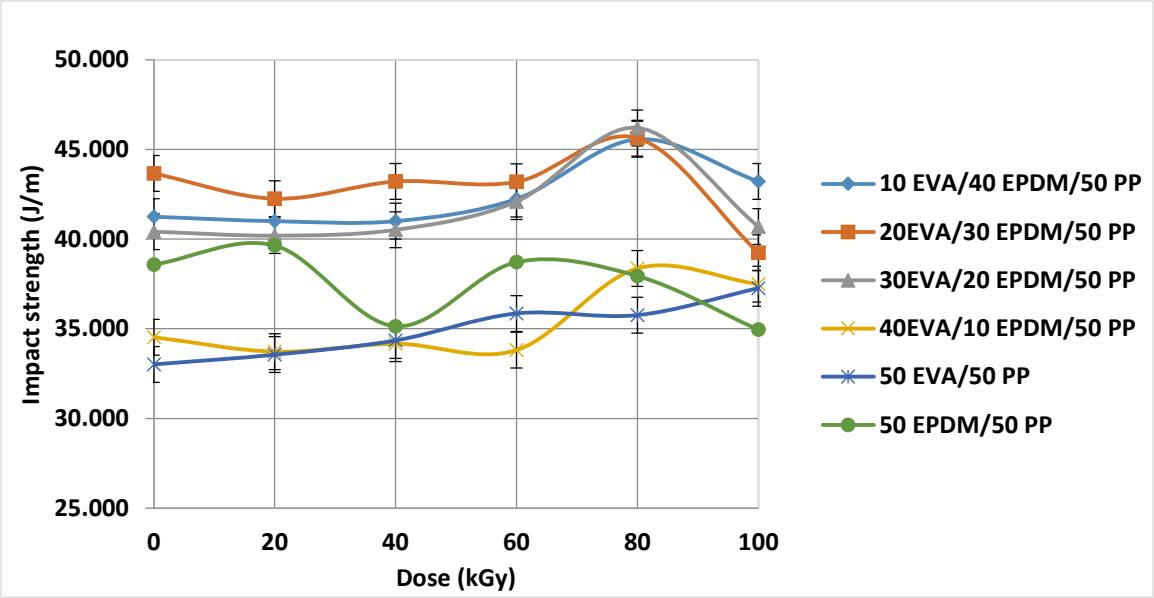


Figure 7.5 Impact strength of ternary blends upon radiation

Upon radiation, the ternary blend did not show significant change in impact strength until 60 kGy. However, all the ternary blends show an optimum increase in impact strength up to 12% at 80 kGy. This could possibly be due to the breaking of crosslinks due to excessive crosslinking induced by E-beam radiation. In previous section, it was reported that the tensile strength of the blends decreased at 80 kGy due to the formation of excessive crosslinks. The breaking of crosslinking reduces the restriction imposed on molecular movement caused by crosslinks. At 80 kGy, when the crosslinks are broken, the molecules relatively tend to move freely enhancing its capacity to absorb more impact energy. Alternatively, some studies reported that the impact strength in PP/Elastomer blend increased with radiation because of the improved compatibility between the blends upon irradiation (Tang et al., 2004, Singh, 2001). The effect of irradiation upon the compatibility and morphologies of the blend will be discussed in later sections.

7.5 Thermogravimetric Analysis

Figure 7.6 shows the mass loss and derivative TG thermogram for PP/EVA and PP/EPDM/EVA ternary blends. In general, two-step degradation process was observed for all the samples. The first degradation peak (T_1) is associated with the loss of acetic acid group of EVA and the second one (T_2) corresponds to the decomposition of polyethylene backbone from EPDM, EVA compounds and propylene backbone from polypropylene. As expected, from Figure 7.6, it can be witnessed that mass loss at T_1 (33-350°C) increased with increase in EVA loading. T_2 of the ternary blends with 10 EVA, 20 EVA, 30 EVA and 40 EVA lies at 449.46°C, 448.52°C, 454.25°C, 454.31°C, respectively. It is also observed that T_2 was delayed slightly with increase in EVA loading. This is mainly due to the higher final degradation temperature of EVA in comparison to EPDM and PP (Ray Chowdhury et al., 2016).

The change in T1 and T2 are listed in table 7.2. From the table, it can be witnessed that upon irradiation, both T1 and T2 increased slightly. This indicates that the thermal stability of the ternary blends enhanced upon radiation. It is supposed that increase in degradation temperature upon radiation is due to the crosslinking (Sabet and Soleimani, 2017). The increase in T1 indicates that EVA underwent self-crosslinking. The increase in T2 upon radiation could be due to the inter crosslinking between the three polymers in the blend. This specifies that many possible modes of crosslinking are possible upon radiation. For instance, increase in T2 could be due to self-crosslinking of EPDM alone. If that was the case and PP did not participate in crosslinking, the PP (being the major component degrading) due to scission upon radiation (evident from previous chapter and DSC analysis) would have lowered T2. However, in this study from the increase in T2, it is obvious that the crosslinking of EPDM and PE chains of EVA with PP, reduced the tendency of chain scission of PP during radiation. Thus, it is possible that self-crosslinking among EPDM, EVA and also the crosslinking between the PE chains of EVA and/or EPDM with PP in the blend-all together which showed increase in overall thermal stability of the material. Dalai and Wenxiu (2002b) carried a similar two-step analysis of TGA to predict the reaction mechanisms of PP/EVA blends. However, it was not conceivable to quantify which of these possible crosslinking mechanisms is the main reason for increase in thermal stability of the blend.

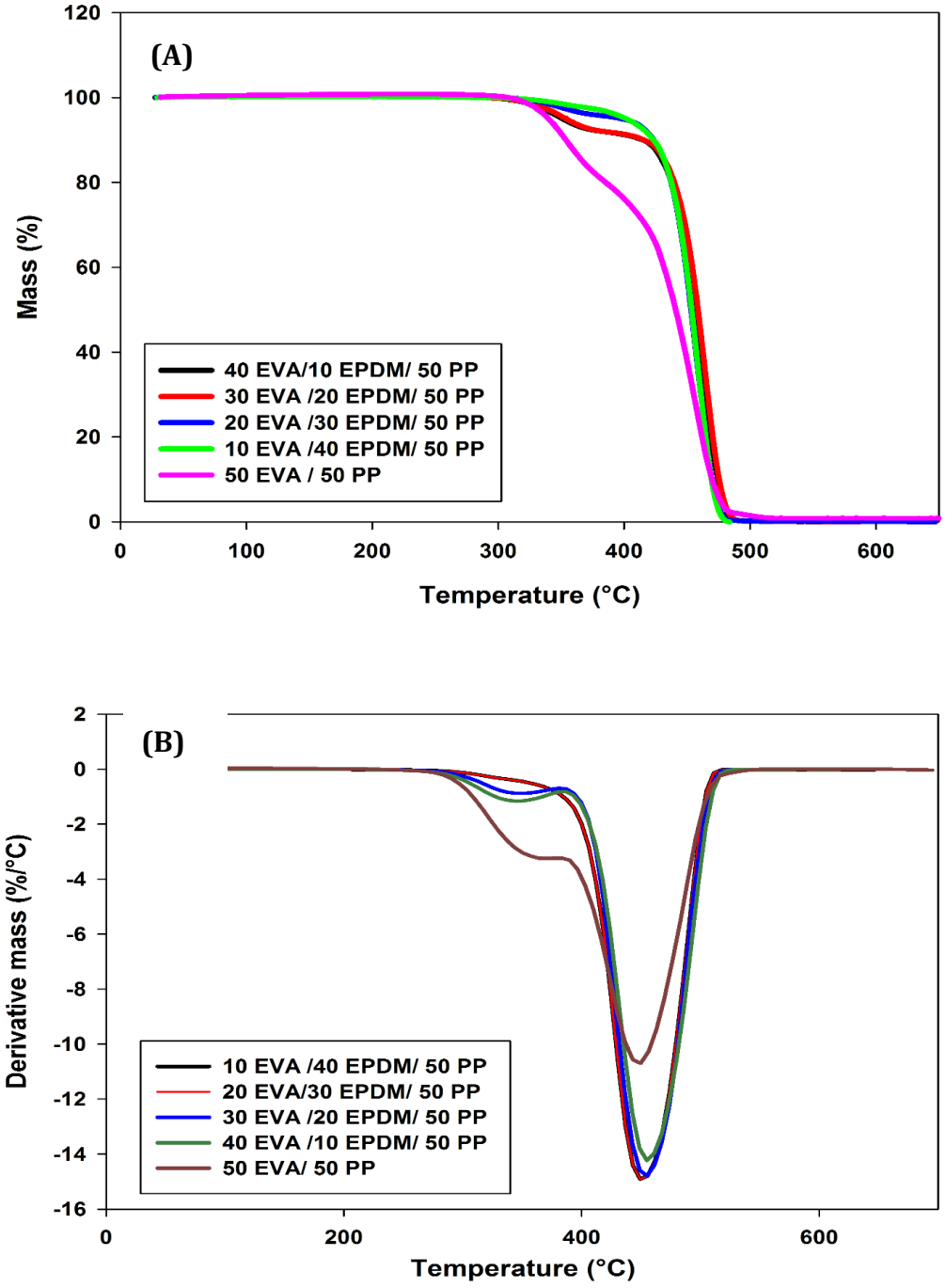


Figure 7.6 (A) TGA and (B) DTG thermograms of PP/EVA and PP/EVA/EPDM blends

Table 7.2 Effect of degradation temperatures of binary and ternary blends

Samples	Radiation dose	T_1	T_2
10 EVA/40 EPDM/50 PP	0	337.12	449.44
	60	337.24	450.36
	100	343.71	450.36
20 EVA/30 EPDM/50 PP	0	337.86	448.58
	60	338.33	452.25
	100	340.92	452.45
30 EVA/20 EPDM/50 PP	0	338.38	454.25
	60	344.46	455.89
	100	344.52	455.57
40 EVA/10 EPDM/50 PP	0	342.61	454.31
	60	343.55	455.57
	100	345.29	455.89
50 EVA/50 PP	0	343.71	455.1
	60	351.24	457.98
	100	351.76	457.98

7.6 Differential Scanning Calorimetry

The heating and cooling DSC thermograms of the 50/50 EVA/PP and EVA/EPDM/PP blends at different blend ratio are shown in Figure 7.7-7.10. From Figure 7.7, it can be seen that PP/EVA blend exhibited two distinct curves corresponding to PP and EVA phases individually. Similarly, it can be witnessed that under same heating and cooling rates, ternary blends exhibited three distinct peaks. The melting peak (T_m) of EPDM phase laid around 32°C and the T_m peaks for EVA and PP were 72°C and 144 °C respectively. Similarly, the crystallization peaks (T_c) of EPDM, EVA and PP was around 17°C, 55°C and 104 °C, respectively. The polymers may be thoroughly mixed in the molten state. But at slow cooling (during the crystallization process), liquid-liquid and liquid-solid phase separation caused

the macromolecular chain segments of respective polymer compounds to move away to their respective rich domains to form the crystal structures by regular arrangements of chain segments. Accordingly, distinct melting peaks are formed with respect to their crystallization peaks. The findings from the DSC thermograms (Figures 7.7-7.10) are tabulated in Table 7.3 for clear understanding.

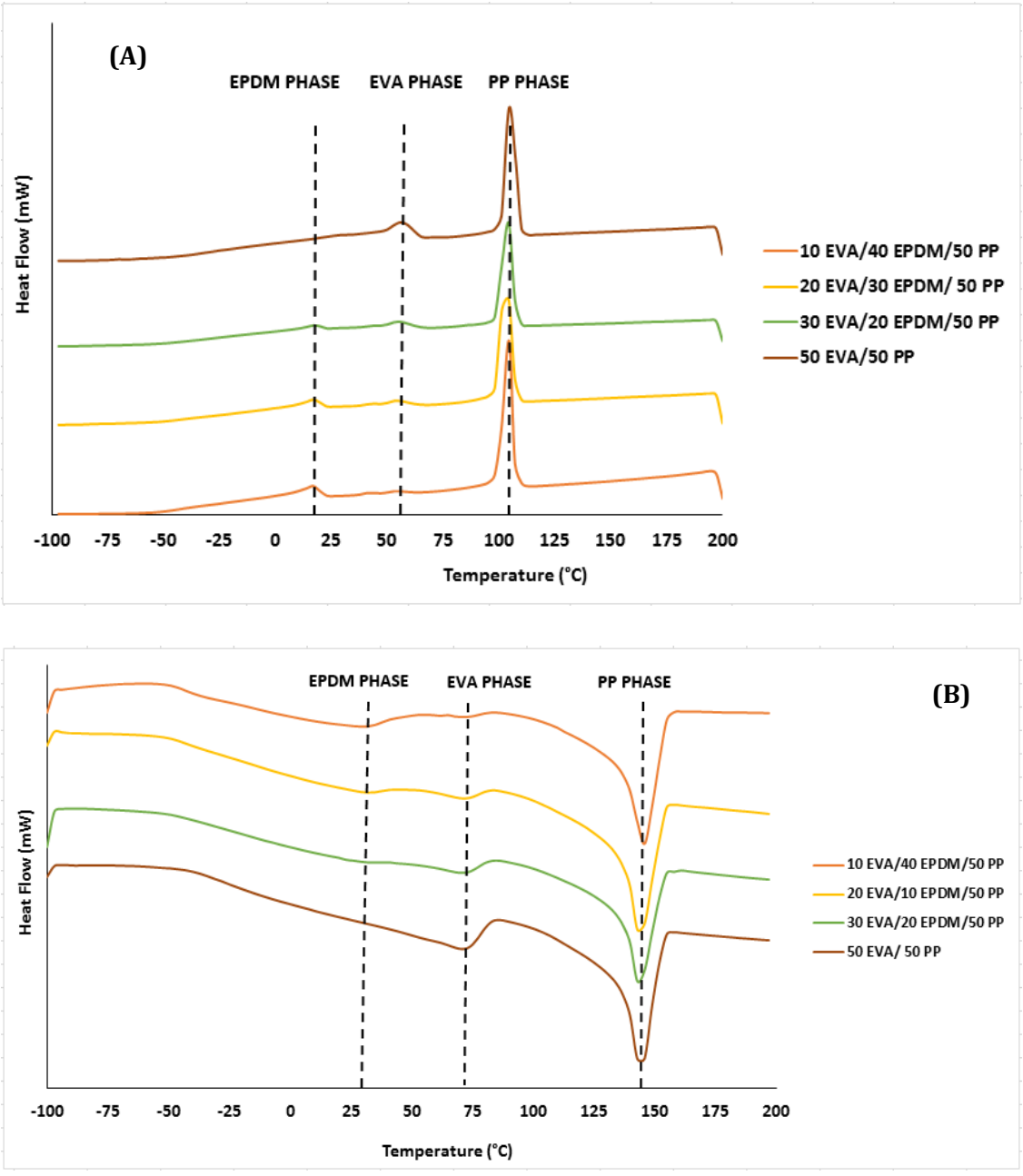


Figure 7.7 (A) Cooling and (B) heating curves of ternary blends prior to radiation

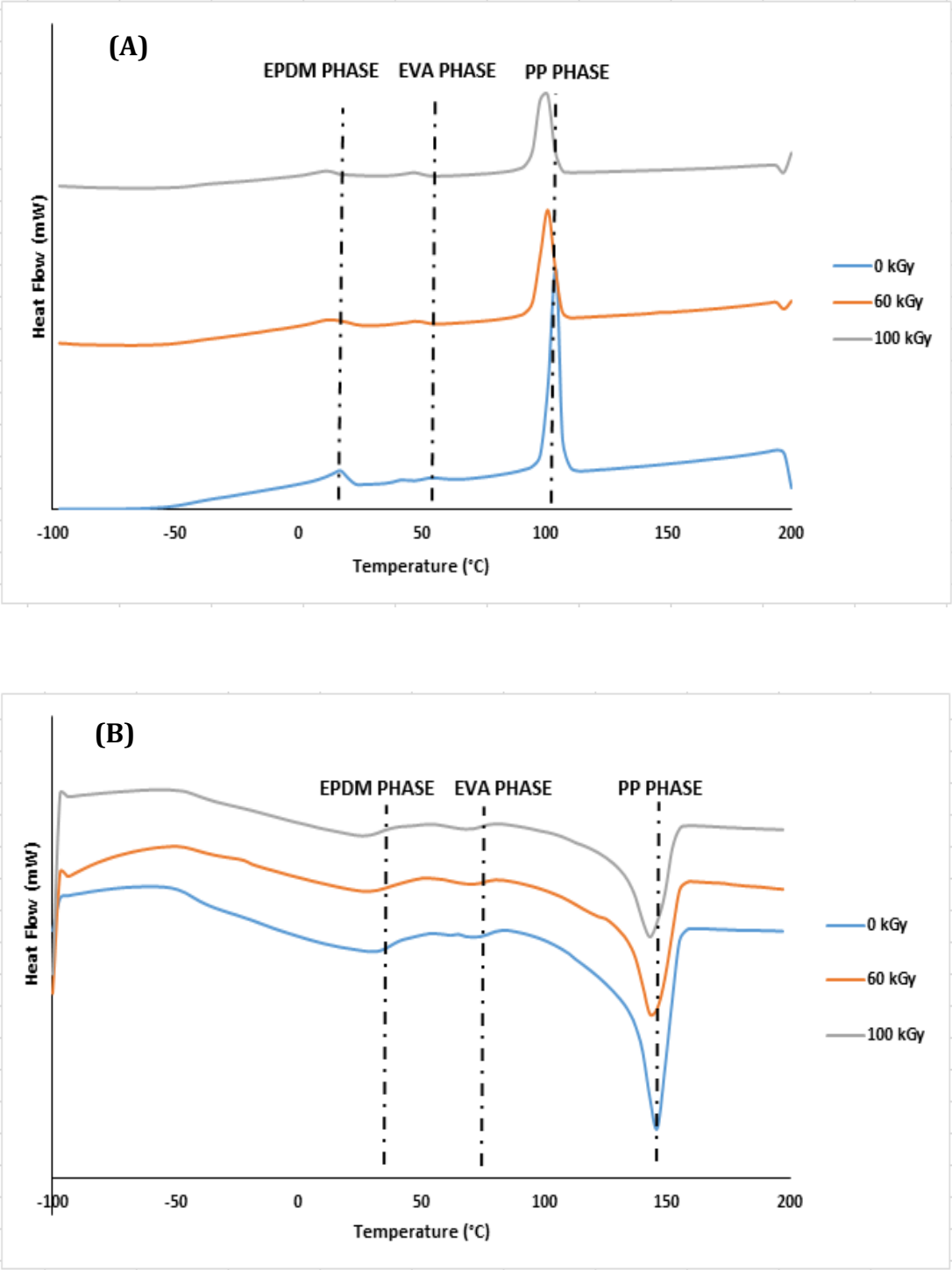
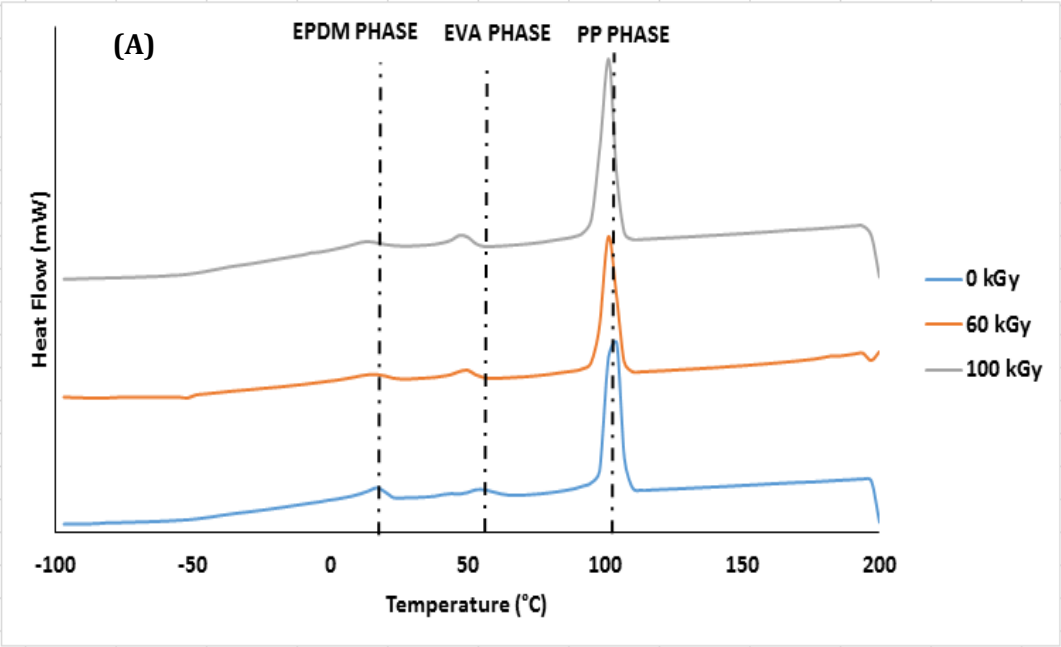


Figure 7.8 (A) Cooling and (B) heating curves of 10 EVA/40 EPDM/50 PP ternary blend at various radiation dose



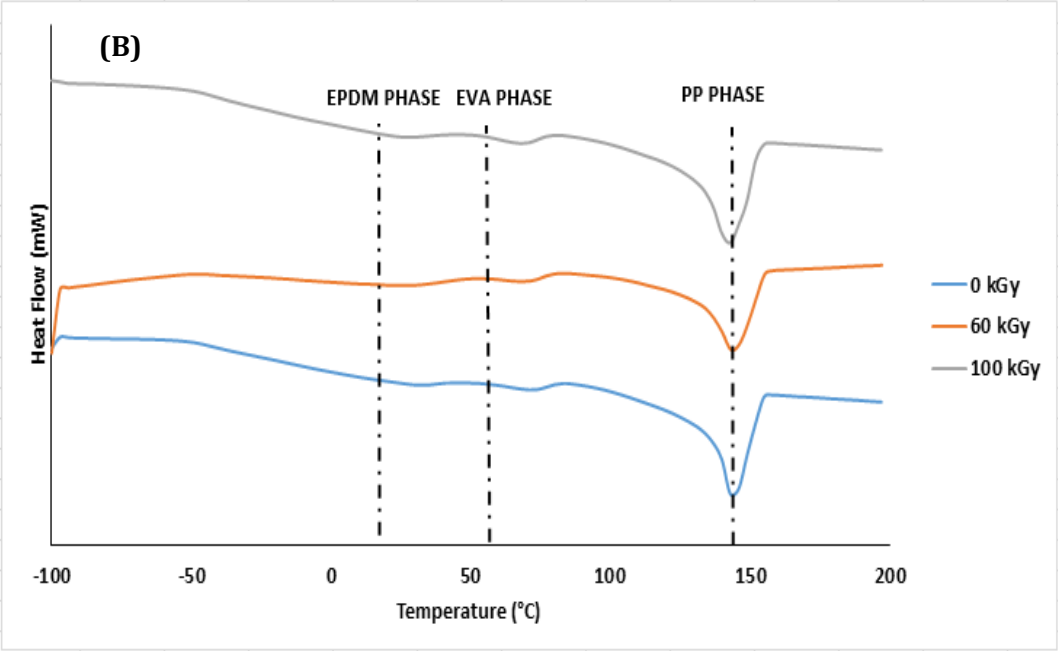


Figure 7.9 (A) Cooling and (B) heating curves of 20 EVA/30 EPDM/50 PP ternary blend at various radiation dose

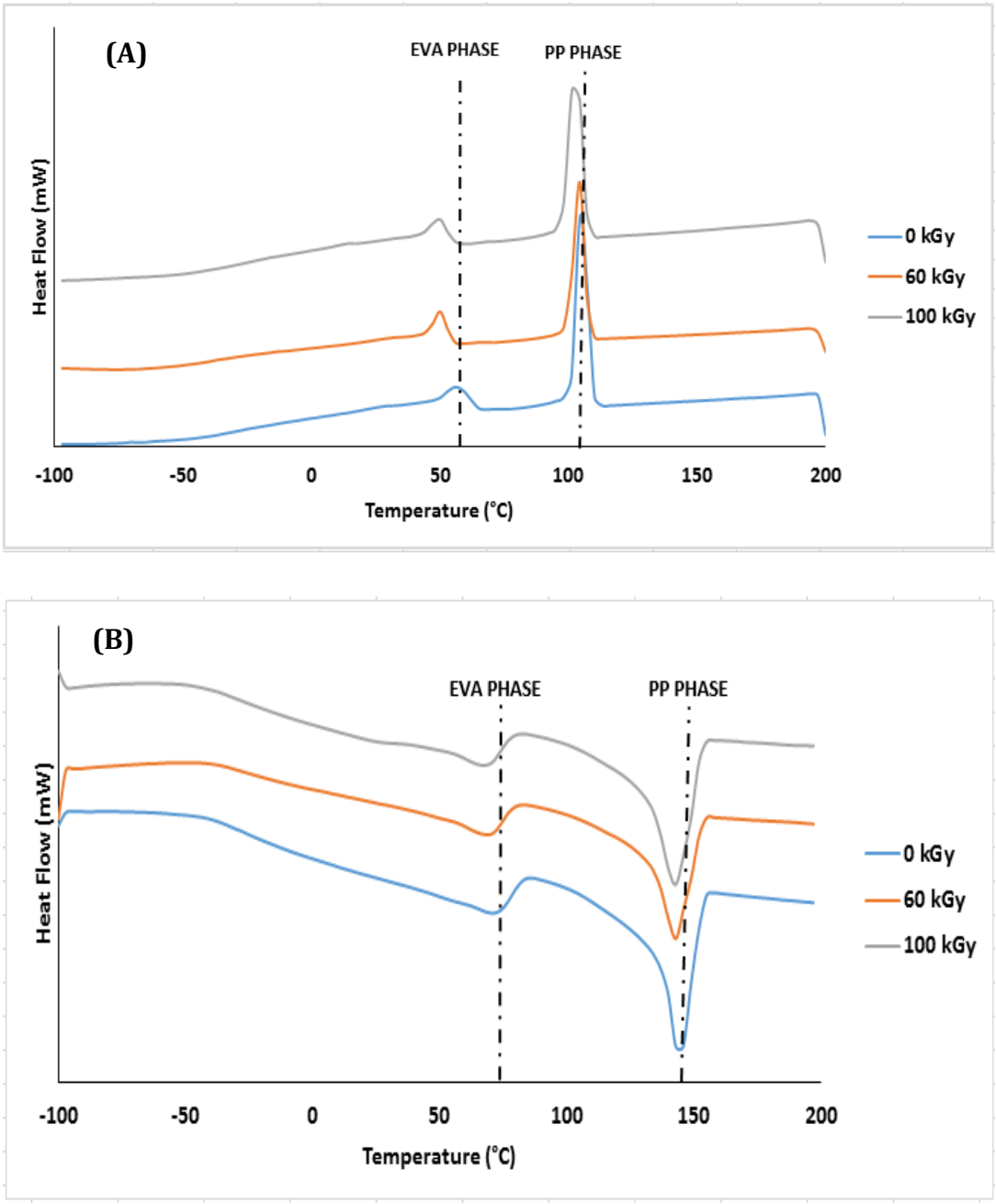


Figure 7.10 (A) Cooling and (B) heating curves of 50 EVA/50 PP blend at various radiation dose

From Table 7.3, prior to radiation it can be seen that with increase in EVA content in the blend, T_m of the EPDM phase slightly shifted to lower temperature. Also, from Figure 7.7, the peak height of EPDM reduced with increase in EVA content. It is mainly due to the reduction in EPDM percentage in the blend. Similarly, the T_m of PP phase also reduced slightly due to the delayed nucleation effect rendered by the elastomers or co-crystallization of ethylene backbones of all the three polymers (Zarandi and Bioki, 2013) . On the other hand, with increase in EVA content, the peak height of EVA phase increased, no significant change in T_m of EVA phase was observed.

Upon irradiation, the T_m of EPDM, EVA and PP phases reduced significantly by 2-6°C. As discussed in previous chapters, the crosslinks induced by the radiation causes the restriction of rearrangement of polymer chains leading to imperfection of crystallites with smaller sizes (Salehi et al., 2004). The magnitude of decrease in melting temperatures of the blends with increasing irradiation dose illustrates that more crosslinks are induced with increasing dosage. This is in correlation with the gel content analysis where crosslinking increased with increasing dosage.

The pattern of changes in T_c was very much similar to pattern of changes in T_m of the blends upon radiation. T_c of all the three phases decreased significantly upon irradiation. The imperfect crystallites with smaller sizes caused by radiation crosslinks, required less energy, hence a decrease in crystallization temperature of the blends was observed.

From Table 7.3, it can be witnessed that the crystallisable content (ΔH_f) and crystallinity of PP phase decreased with increase in EVA content. The decrease in the extent of crystallinity and heat of fusion upon addition of elastomers was due the delay of nucleation process. The inter-spherulitic interaction and the interaction of spherulites at the boundaries of three polymers affect the re-arrangement of molecular chains in the backbone of polymers. In addition to the spherulites of one polymer being covered by its own amorphous region, they are also covered with the amorphous phase of other polymers due to intermolecular interactions. These results could also suggest that the decrease in crystallinity upon increase in EVA loading because the presence of EVA would have enhanced these inter and intra spherulite interactions. A similar result was reported in various EVA blends (Zarandi and Bioki, 2013, Tashiro et al., 1992).

Table 7.3 Melting temperature (T_m), crystallization temperature (T_c) and extent of crystallinity of ternary blends before and after radiation

ample	Radiation Dose	T_c			T_m			ΔH_f	X_c
		EPDM Phase	EVA Phase	PP Phase	EPDM Phase	EVA Phase	PP Phase	PP Phase	PP Phase
10 EVA/40 EPDM/50 PP	**0**	**17.22**	**54.22**	**104.17**	**32.30**	**71.97**	**145.34**	**24.09**	11.52
	60	12.66	47.99	100.88	28.36	69.86	144.12	24.41	11.67
	100	11.32	46.98	99.65	27.03	69.54	142.97	24.17	11.56
20 EVA/30 EPDM/50 PP	**0**	**17.56**	**54.57**	**103.10**	**30.96**	**72.45**	**144.13**	**22.97**	10.99
	60	15.83	49.00	101.77	28.37	70.05	143.98	24.18	11.56
	100	12.30	48.25	101.28	26.12	68.43	142.12	22.87	10.94
30 EVA/20 EPDM/50 PP	**0**	**18.04**	**55.56**	**103.54**	**22.37**	**71.79**	**144.34**	**18.76**	8.97
50 EVA /50 PP	**0**		**56.26**	**105.50**		**72.61**	**144.30**	**18.05**	8.63
	60		49.91	104.18		69.44	142.71	22.22	10.63
	100		49.42	102.91		68.78	142.51	21.35	10.21

For both the binary blend with 50 PP/50 EVA and ternary blends with EPDM content, irradiation improved the heat of fusion and crystallinity up to 60 kGy was observed. This could be attributed to increase of intermolecular interaction caused by radiation which allows for closer packing of chains, hence increasing the crystallinity (Thevy Ratnam et al., 2016, Sujit et al., 1996). However, beyond the optimum irradiation dose (60 kGy in this case), the decrease in the crystallinity of all polymer blends was observed. It is because of rupturing of crystalline domains caused by crosslinking in the amorphous region. The amorphous and crystalline phases have some chains in common. That may reduce the crystallinity rupturing some crystal domains, as common chains are involved in crystalline as well as amorphous phase of polymer. Moreover, due to shrinkage of amorphous phase caused by crosslinking, the crystalline phase interacts with radiation which in turn may diminish the crystal domains and leads to reduction of crystallinity (Sharma et al., 2014).

7.7 Dynamic Mechanical Analysis

7.7.1 Tan delta/Damping factor curve

Figure 7.11 shows the temperature dependence of tan delta of the PP/EVA and PP/EPDM/EVA blends respectively. The tan delta and glass transition temperature from this figure were listed in Table 7.4 for better understanding. In section 5.9.1, T_g of PP phase laid at 5.75°C, T_g of 100% EPDM was at -31.68°C and also T_g of 100% EVA laid at -23.95°C. In Figure 7.11, 50PP/50 EVA exhibited first peak at -18.75°C corresponding to EVA phase and at 1.55°C corresponding to PP phase. It is interesting to note that both - EVA and PP phases in the blend are closer (from -23.95°C to -18.75°C for EVA phase and from 5.75°C to 1.55°C) with respect to their neat polymers. This indicates that some extent of compatibility exists between EVA and PP. Ramírez-Vargas et al. (2000) reported a similar trend where the compatibility of EVA/PP was increased with EVA loading, particularly with EVA content of more than 40%. However, Dutta and Naskar (2014) reported that since T_g of EVA and EPDM laid closely together, it did not indicate miscibility in true sense. The author also claimed that it can be considered as some level of only technological compatibility. This is evident from

storage modulus data, where 50 PP and 50 EVA blend did not show compatibility, which is explained in later section.

The ternary blends with the presence of EPDM also exhibited only two distinct peaks. However, unlike the binary blend, the first peak laid at -32.80°C (for 10 EVA/40 EPDM/50 PP) and at -31.75°C (for 20 EVA/30 EPDM/50 PP). The peaks at this temperature range correspond to T_g of EPDM phase. For both the ternary blends, the T_g of EVA peaks did not appear distinctively. It could be because of the lower concentrations of EVA loading with respect to EPDM and PP. Also, the T_g of EVA was masked by the tan delta of EPDM which was due to some interactions between the two amorphous polymer chains (Sharma et al., 2015). Kuila et al. (2009) reported a single tan delta peak exhibited by EVA/EPDM blend similar to our results. However, Acharya et al. (2008) reported that EVA and EPDM exhibited two distinctive peaks indicating no compatibility or immiscibility between two polymer chains. Nevertheless, their method (solvent casting) and the EVA and EPDM grade are different from our study. It can be concluded that the synthesis method and the polymer grade greatly determine the dynamic behaviour of the blends (Ramírez-Vargas et al., 2000).

Table 7.4 Tan delta peaks of ternary blends before and after radiation

Sample	**Radiation dose**	**Peak 1**		**Peak 2**	
		Tan delta	**T_g**	**T_g**	**Tan delta**
10EVA/40 EPDM/50 PP	0	0.090	-32.80	0.083	5.24
	60	0.091	-35.98	0.082	6.58
	100	0.094	-31.75	0.081	7.12
20EVA/30 EPDM/50 PP	0	0.079	-31.75	0.084	5.45
	60	0.079	-29.5	0.083	6.75
	100	0.079	-29.45	0.079	7.30
50 EVA/50 PP	0	0.100	-18.75	0.102	1.55
	60	0.112	-17.7	0.105	1.55
	100	0.096	-20.3	0.091	1.85

Upon radiation, the three blends showed different trends at different radiation dosage. For 10 EVA/40 EPDM/50 PP, the T_g of EPDM phase moved slightly away from -32.80°C to -35.98°C at 60 kGy. This may be due to the intraphase crosslinking of EPDM/EVA and/or crosslinking between EVA and EPDM rather than interphase crosslinking between EVA/EPDM and PP (Sharma et al., 2015). However, further increase in radiation dose of 100 kGy, the T_g of EPDM increased to -31.25°C due to crosslinking. On the other hand, upon radiation a slight broadening of peak at both EPDM and PP phases along with slight increase in peak height could be noticed. This might be due to increased free side chains as a result of scission or oxidation of EVA (Giri et al., 2012, Munusamy et al., 2012) and PP phase (Jafari and Gupta, 2000) (that occurs along with crosslinks) which introduced micro heterogeneity to the polymer blends.

For 20 EVA/30 EPDM/50 PP blend, the T_g of EPDM phase and PP phase increased at both 60 kGy and 100 kGy radiation dose due to crosslinking. Both T_g of EPDM phase and PP phase increased. Also, upon radiation the narrowing of peak and reduction in peak height was observed at PP phase. These could be attributed to inter and intra crosslinking between EPDM/EVA and PP polymer chains.

The shift in T_g temperature, change in peak height and area, all together again support the view that radiation induced a complex system of scission accompanied by crosslinking. Again a definitive conclusion cannot be reached in this to determine which mechanism dominates the glass transition temperatures of the blend upon radiation. However, the extent of scission and crosslinking competing each other shows only a slight difference at all the polymer phases.

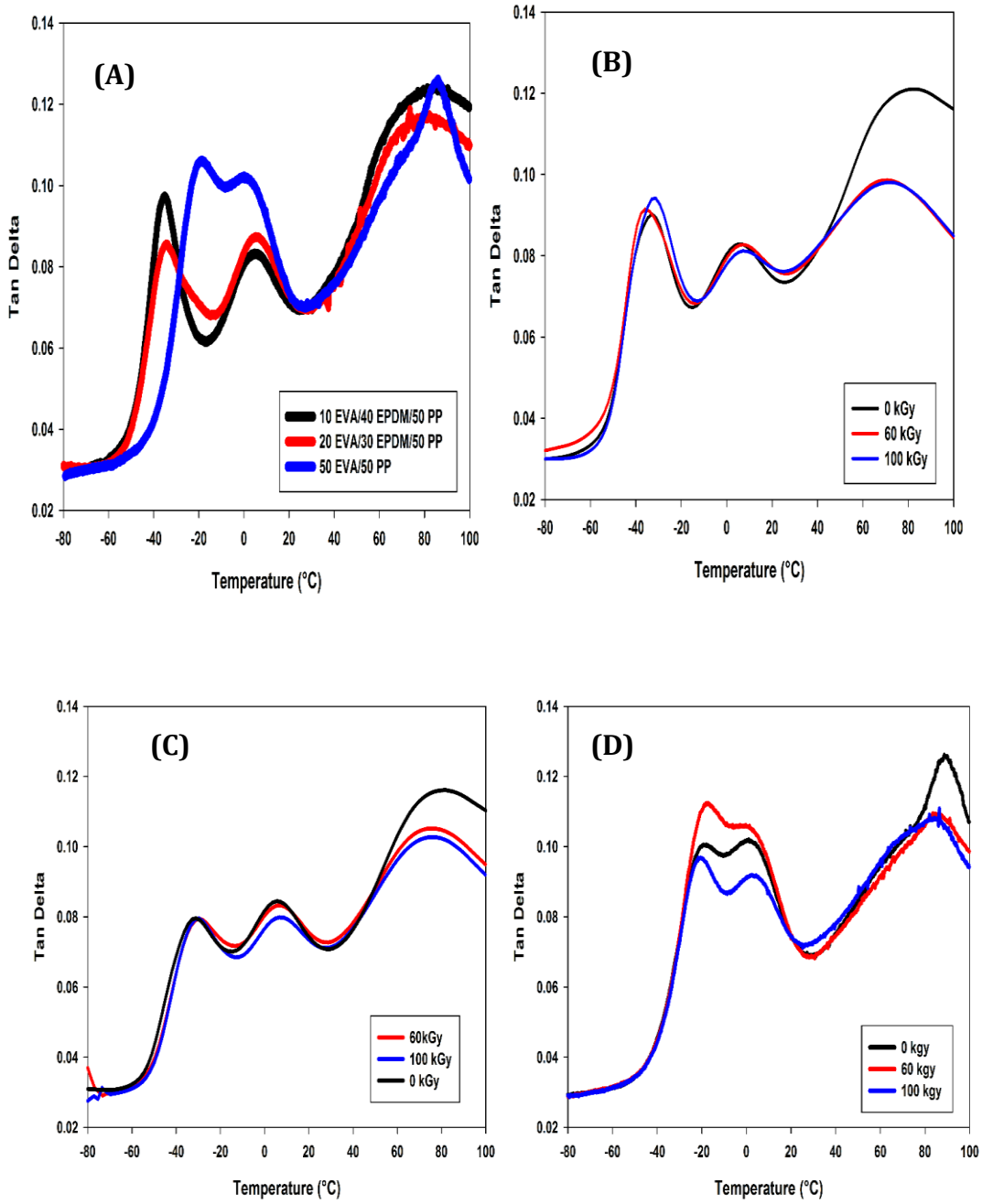


Figure 7.11 Tan delta curves of (A) ternary blends prior to radiation (B) 10EVA/40EPDM/50PP blend at various dose (C) 20EVA/30EPDM/50PP blend at various dose and (D) 50EVA/50 PP blend at various dose

7.7.2 Storage Modulus

Figure 7.12 shows the temperature dependence of storage modulus of the PP/EVA and the PP/EVA/EPDM ternary blend. Both the binary and ternary blends exhibited three regions (glass, transition and rubbery regions) like all other thermoplastic elastomers. In Figure 7.12, it can be witnessed that 50 PP/50 EVA exhibited the highest storage modulus throughout the temperature range, whereas 50PP/50EPDM exhibited the lowest. The storage modulus of the blends decreased when crystallinity decreased. This indicates that that EPDM is more amorphous than EVA used in this study. The storage modulus of the ternary blends decreased with increase in addition of EVA. In other words, the storage modulus decreased with increase in EPDM content due to amorphousness of EPDM. The 50PP/50 EPDM blend showed a single transition peak which was attributed to the co-continuous morphology of the blends (Jafari and Gupta, 2000, Aghjeh et al., 2015). Similarly, the ternary blends up to 30EVA loading showed a single transition indicating some extent of partial miscibility. This enhances the mechanical properties of the polymer as discussed earlier in the tensile strength section. At higher EVA loading (≥ 40%), the blends showed a broad transition with a shoulder in the middle. This indicates the presence of heterogeneous zones in the blend which is a result of poor interfacial adhesion between the polymer matrixes (Paul and Newman, 1978). This again led to decrease in the tensile properties when compared with the blends with up to 30% EVA loading. It can be noticed that at service temperature (room temperature to human body temperature) the stiffness of the blends increases with increase in EVA loading, as storage modulus is the measure of stiffness.

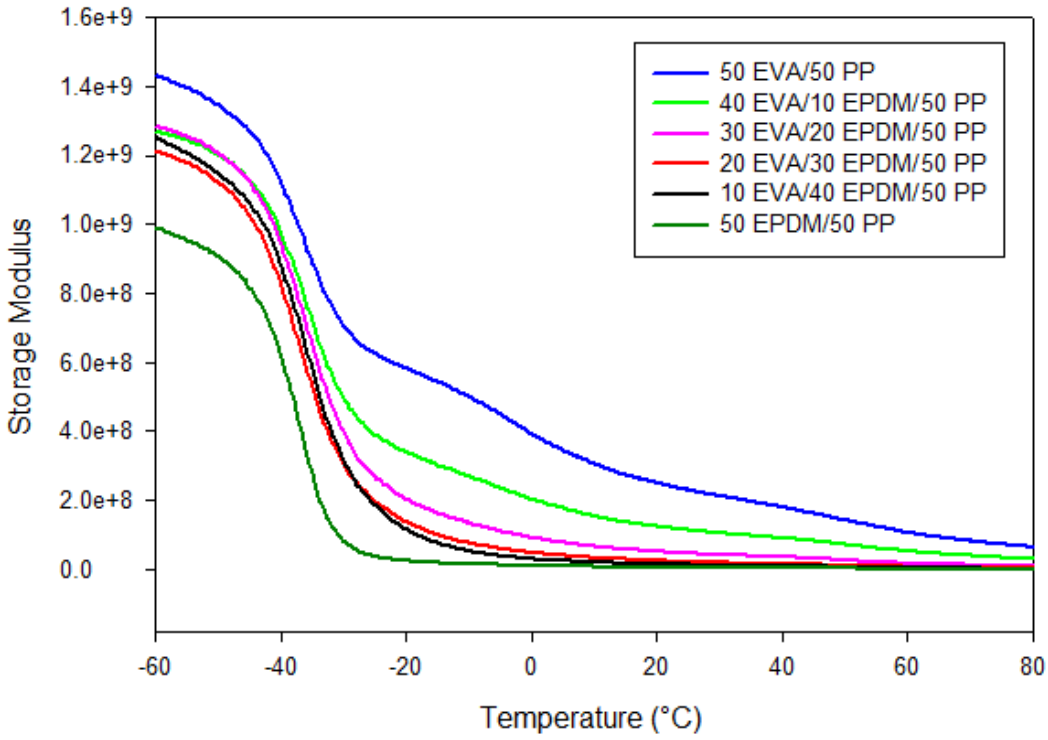


Figure 7.12 Storage modulus of ternary and binary blends

It could be noticed from Figure 7.13 that the binary blend with 50PP/50EVA, the radiation at 60 and 100 kGy caused the reduction in storage modulus in glass transition region. The decrease in storage modulus is mainly due to scission mechanism of the PP phase. The scission was very evident when crystallinity was improved in the PP/EVA blend as discussed earlier. This is also in line with gel content the 50PP/50 EVA showed the maximum scission and pinner equation (Eq 5.1) stated the scission mechanism dominated along with the existence of some crosslinks.

Upon radiation, the blends with lower EVA loading (for 10EVA/40EPDM/50PP) showed no significant change in storage modulus which was observed in transition and rubbery region. Upon irradiation for the blend with 20EVA/30EPDM/50 PP, storage modulus was improved with increasing radiation dose up to -45.5 °C. After which the irradiated blend showed slightly

lower storage modulus values compared to non-irradiated ternary blend. Such increase in glassy region's storage modulus of blend upon irradiation again validates the assumptions made in the gel content analysis where the gel content of the blends was found to increase more rapidly as the dose increased. After complete consumption of stabilizing and scavenging radicals, irradiation induced crosslinks are deemed to happen in the compounds. Radiation induced crosslinking in blend improves the ability of the blend to store elastic deformation, which translates to an increase in the storage modulus (Ratnam et al., 2001a). While the improvement in the storage modulus of glassy region was associated with the irradiation induced crosslinks, the decrease upon reaching transition region was associated with the loss of crystalline zone of EVA/EPDM/PP in the blend due to irradiation. These results well augment with the DSC analysis as explained before, where radiation crosslinks reduced the crystallinity of the blend. In a semicrystalline polymer, contribution to storage modulus, above the glass transition temperature is associated with the crystalline region of the polymer (Mohamad et al., 2006, George et al., 1997, John et al., 2003b). Irradiation induced redistribution of elastomer, decreases the crystallinity of blend, hence, a slight decrease in the storage modulus was noted.

Furthermore, the medical devices are mostly used in room conditions. It can be noticed that at room temperature, there was no significant changes were seen even upon radiation of these blends. Therefore, the effect of radiation in ternary blend would not affect the product performance in terms of stiffness, when the products are used at room temperature.

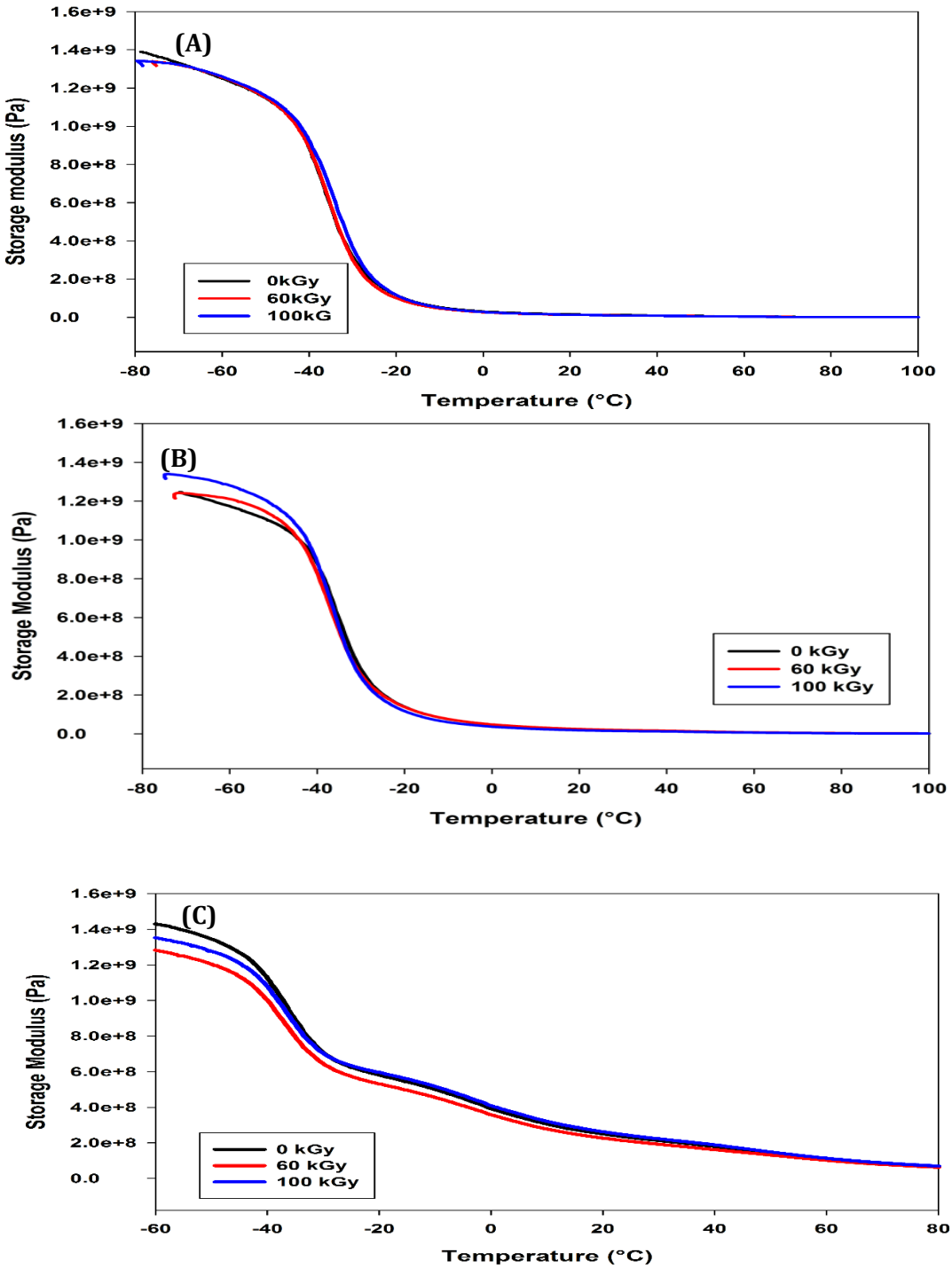


Figure 7.13 Storage modulus (A) 10EVA/40 EPDM/50 PP blend at various dose (B) 20EVA/30 EPDM/50 PP blend at various dose and (C) 50EVA/50PP blend at various dose

7.8 Scanning Electron Micrographs

Figure 7.14 (A-D) shows the morphology of 50 PP/50 EPDM, 10 EVA/40 EPDM50 PP, 20 EVA/30 EPDM/50 PP ternary blend and 50 PP/ 50 EVA blend. It can be noticed that the ternary blends with 10 EVA and 20 EVA loading (Figure 7.14 B and C) showed a similar morphology to 50 PP/ 50 EPDM (Figure 7.14 A). These blends showed a coarser morphology in comparison to 50 PP/50 EVA blend. A number of voids and the elastomers dispersed as droplets which contributed to the coarser morphology of the blends. On the other hand, 50 PP/50 EVA blends (Figure 7.14 D) shows a smoother co-continuous phase with much less voids. The presence of voids and elastomers dispersed as droplets in EPDM based blends acts as stress concentrators resulting in higher impact strength. This is again in accordance with section where, the ternary blends and 50PP/50 EPDM blend exhibited higher impact strength than 50 PP/50 EVA. However, all the blends showed two-phase morphology indicating that the blends are immiscible which is in accordance with distinctive separate tan delta peaks analysed using DMA studies. The 50PP/50 EVA blend having a smoother morphology tends to have better interfacial adhesion than the blends with EPDM.

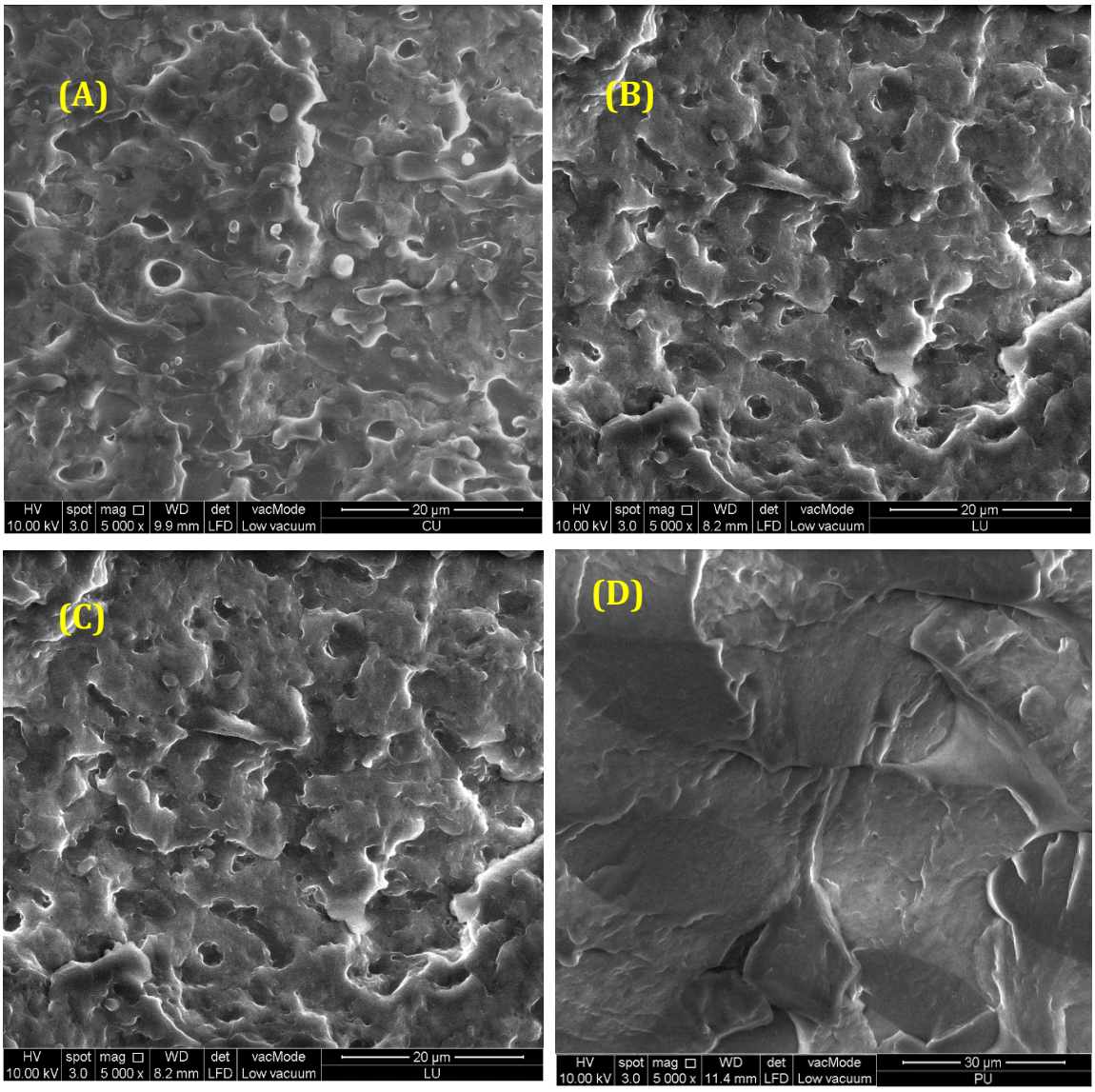


Figure 7.14 SEM micrographs (A) 50PP/50 EPDM (B) 10 EVA/40 EPDM/50PP (C) 20EVA/30 EPDM/50PP and (D) 50PP/50 EVA

Figure 7.15 (A-D) shows the morphology of 20EVA/30 EPDM/50 PP blends before radiation and after radiation at 60 kGy, 80 kGy and 100 kGy. It could be noticed that no significant improvement in morphology of the blends upon radiation was detected. DMA studies showed slight compatibility between the blends upon radiation. However, these slight changes were very hard to be differentiated and reflected in the SEM images.

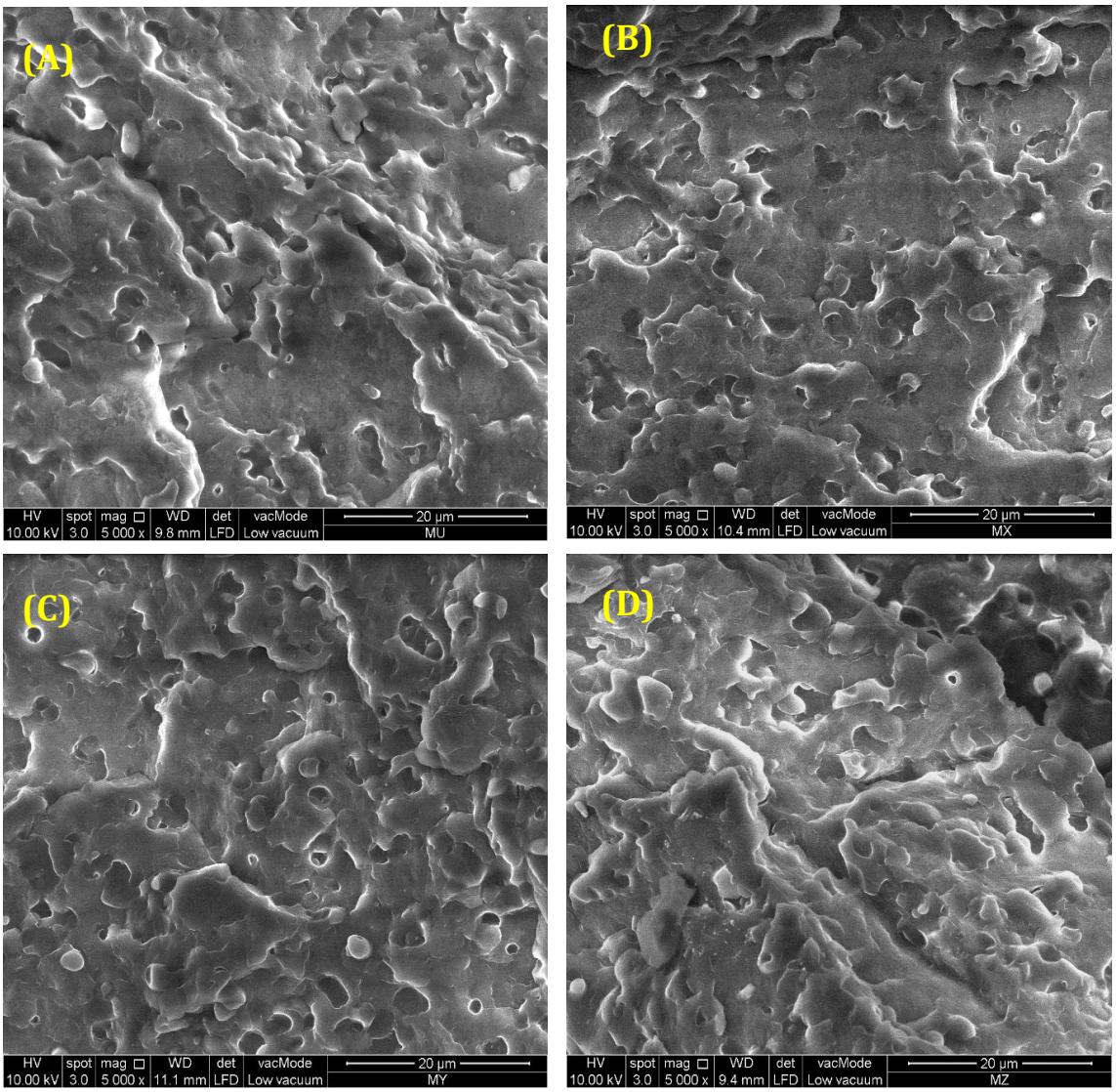


Figure 7.15 SEM of 20EVA/30EPDM/50PP blend at (A) 0 kGy (B) 60 kGy (C) 80 kGy and (D) 100 kGy

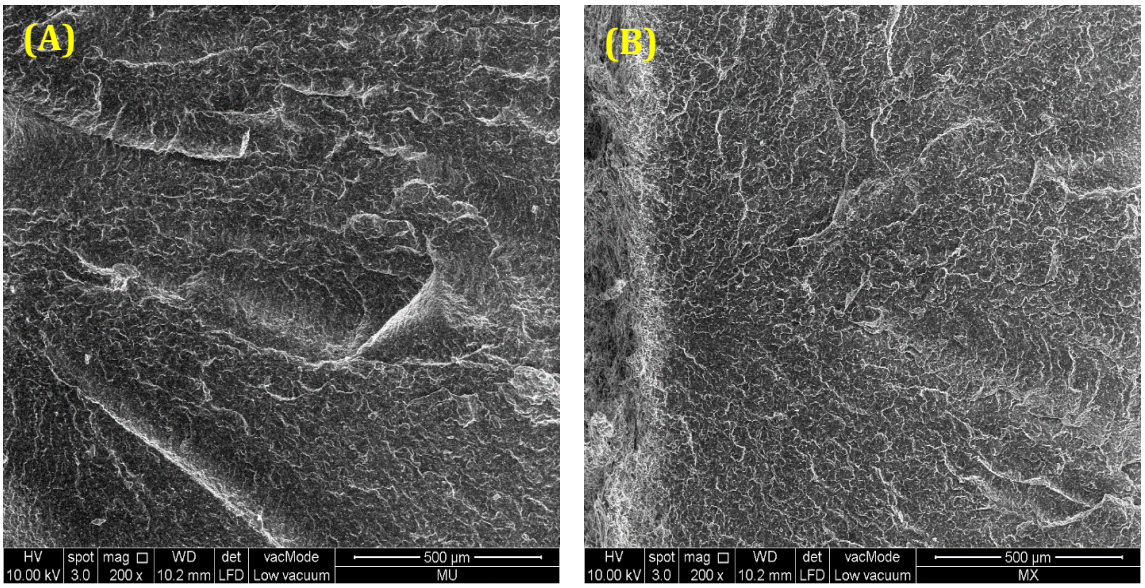


Figure 7.16 Surface morphology of cryo-factured 20EVA/30EPDM/50PP blend at (A) 0 kGy (B) 60 kGy

Figure 7.16 (A-B) shows the surface morphology of cryo- factured samples of 20EVA/30 EPDM/50 PP before and after radiation at 60 kGy. It can be observed that the blends exhibited a semi-crystalline morphology. In Figure 7.16 (A) the crazings were initiated upon the impact test from the notch. These crazings are in the form of fibrils traversing through long distances. However, more intense crazing were formed with rougher surfaces as shown in Figure 7.16(B). Also, the length of crazings was shortened indicating that the blends became comparatively brittle upon radiation. This is in accordance with tensile and impact properties, where at 60 kGy the tensile strength increased due to brittleness and hence the decrease in impact properties of the blends.

7.9 Visual Appearance

In section 5.12, the yellow discolouration in PP rich blend after radiation was discussed. However, the PP/EVA and the ternary blends did not show occurrence of yellowing before radiation. From figure 7.17, it can be noted that no significant change in the visual appearance or occurrence of yellowness was observed in these blends even after radiation. This gives us an insight that no significant oxidation due to scission occurred at the time of radiation. The yellow index of all the ternary blends was not detected by the colorimeter due to the absence of discolouration.

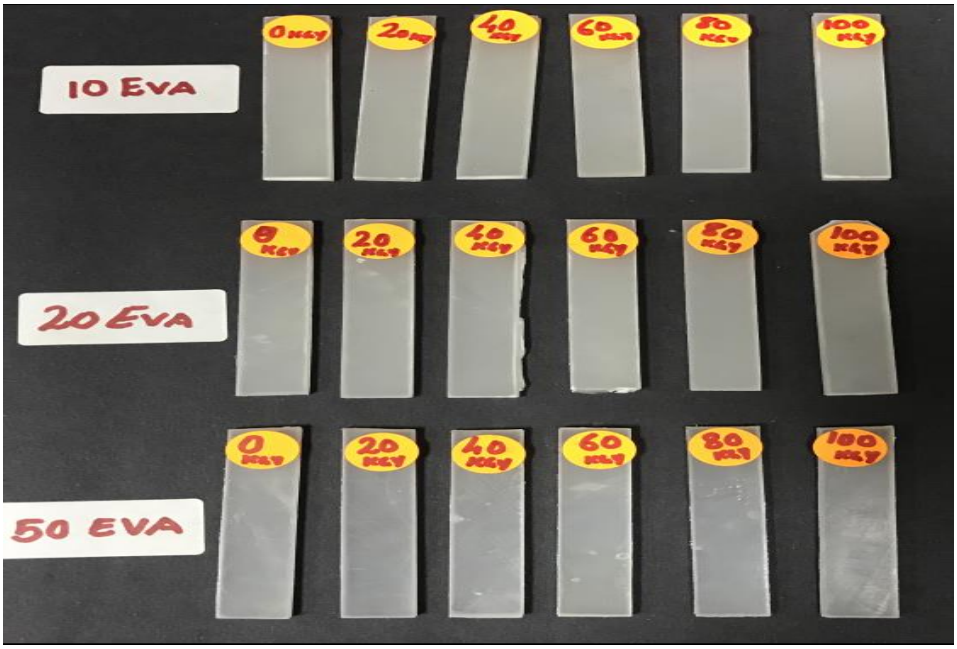


Figure 7.17 Visual appearance of polymer blends

7.10 Summary

Effect of E-beam radiation on the physical properties of PP/EVA/EPDM ternary blends was studied and compared with 50PP/50EVA and 50PP/ EPDM blends. The efficiency of crosslinking decreased with increase in EVA loading. However, the presence of EVA in ternary blend facilitated the induction of sufficient crosslinks leading to retention of good mechanical properties even at higher radiation dose. For 50 PP/50 EPDM blend, tensile strength decreased with increasing radiation above 20 kGY. However, tensile strength of the ternary blends retained up to 40 kGy and increment of up to ≈29% was observed at 60 kGy. On the other hand, there was slight decrease in impact strength of 50 PP/50 EPDM blend at 40kGy. However, impact strength of PP/EVA/EPDM was retained till 60 kGy and improvement of ≈15% was observed at 80 kGy. Slight improvement up to 2°C in thermal stability was also observed. Similarly, the crystallinity, melting and crystallization temperatures were also altered after crosslinking and chain scission caused by the radiation. However, the changes were very slight and was not reflected in the morphology studies. Overall, the ternary blends showed a capability to be sterilized up to 60 kGy under E-beam radiation, to retain and impact strength and improved tensile strength. Beyond which though the impact strength increased, the tensile strength decreased slightly. Among the ternary blends, 20 EVA/30 EPDM/50 PP blend showed the highest tensile and impact properties.

8 EFFECT OF E-BEAM ON POLYPROPYLENE (PP)/ ETHYLENE PROPYLENE DIENE MONOMER (EPDM) AND ETHYLENE VINYL ACETATE (EVA) TERNARY BLENDS CONTAINING SILVER NANOPARTICLES

8.1 Introduction

This chapter aims to study the mechanical, thermal and antimicrobial properties of PP/EVA/EPDM ternary blend upon addition of AgNP. For this study, 50PP/20EVA/30EPDM blend was chosen as control. From previous chapter, this ternary blend gave the best improvement in mechanical properties before and after irradiation (especially tensile properties). AgNP were varied at 0.3, 0.5 and 1 wt% loading. Ag nano-powders were melt blended along with the PP, EVA and EPDM at 165°C and 50 rpm for 10 min. The effect of Ag/ternary blend composite upon radiation at 60 kGy and 100 kGy was also discussed in this chapter.

8.2 SEM and Elemental Analysis

Energy Dispersive Spectroscopy (EDS) was used to perform the elemental analysis. EDS spectrograms along with SEM micrographs were used to study the dispersion of AgNP in the ternary blends. SEM Figures 8.1 (1A, 2A and 3A) shows the dispersion of Ag particles in ternary blend matrix. Similarly, the bright spots Figure 8.1 (1B, 2B and 3B) also confirms the presence of Ag nanoparticle dispersion in the polymer matrix. The elemental analysis proves that these bright spots belong to AgNP by the peaks at around 3.4 keV. Oliani et al. (2015) reported a similar result of peak corresponding to Ag at 3.40 keV in PP-Ag polymer composites. The intensity of the peak increased with increase in Ag loading percentage. However, in Figure 8.1, it can be noticed that AgNP agglomerates in polymer matrix irrespective of the loading concentration. It can also be noticed that the size of agglomeration clusters increased with increase in the concentration of AgNP. The agglomerated clusters formed in the polymer matrix were due to high surface energy of Ag nanoparticles (Liang et al., 2007).

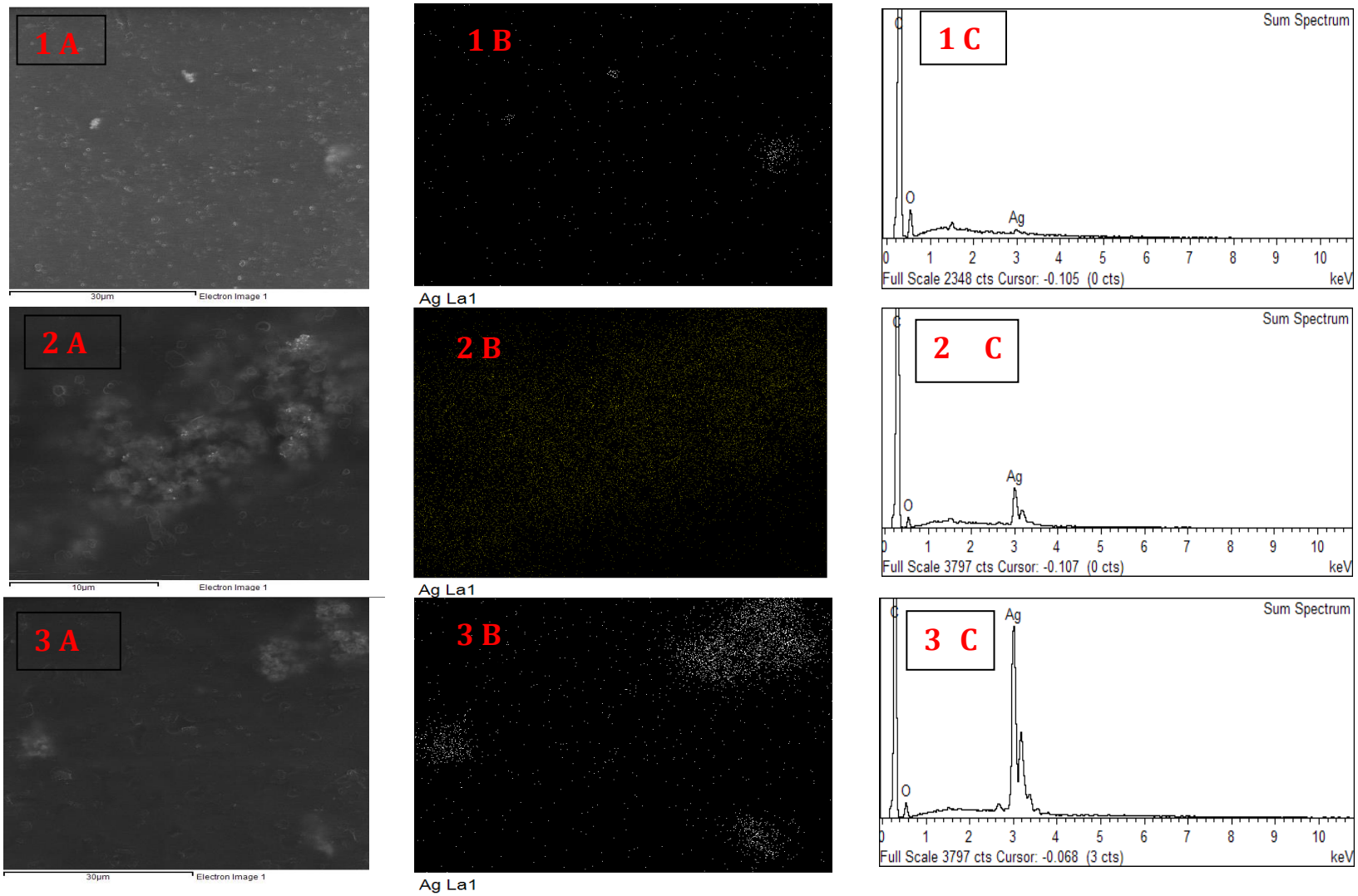


Figure 8.1 SEM and elemental analysis (1) 0.3% Ag (2) 0.5% Ag and (3) 1% Ag in 20 EVA/30 EPDM/50 PP blends

8.3 Gel Content Analysis

Figure 8.2 represents the gel formation analysis of the polymer blend composites at different AgNP loading as a function of radiation dose. It can be observed that the gel formation of all the blend composites increased with increase in radiation dosage. As mentioned in previous chapter, the increase in gel content illustrates that the formation of crosslinks formed increased with increasing radiation dosage. On the other hand, no significant difference in the intensity of gel percentage was observed when the concentration of AgNP was varied. This gives us an insight that Ag loading was neutral under these radiation conditions and did not render any significant contribution in enhancing the gel content. Also, it can be assumed that the increase in crosslinks content with increase in radiation dose is purely because of the polymeric chains.

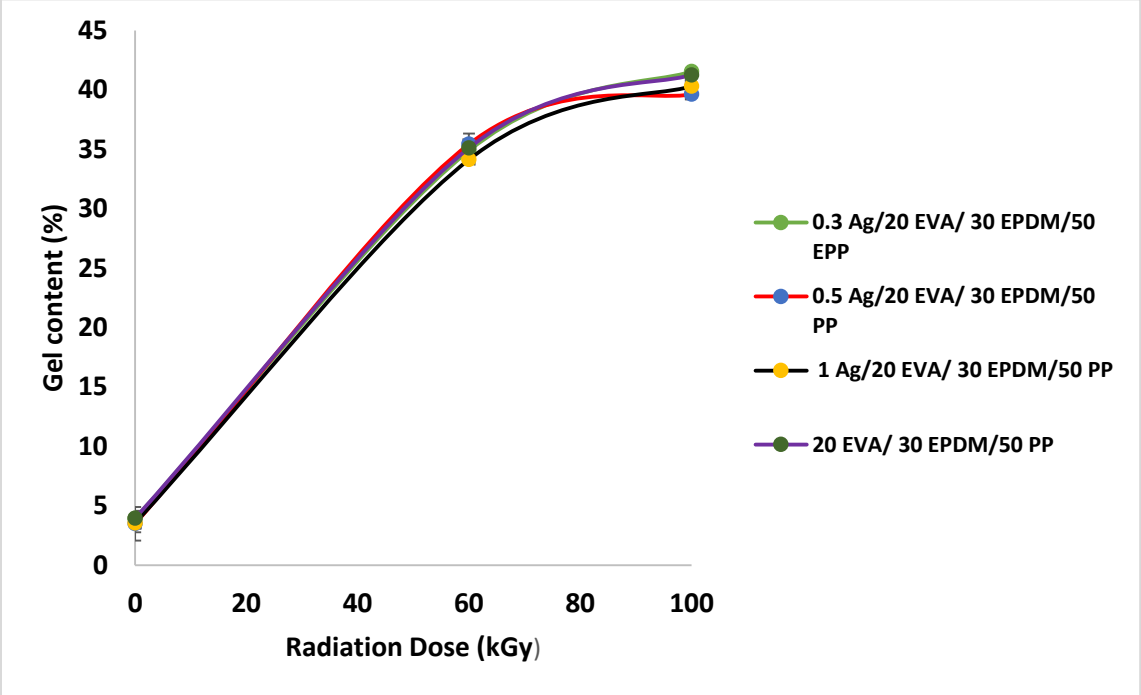


Figure 8.2 Gel content of Ag/ternary blend nanocomposite as a function of radiation dose

8.4 Tensile Strength

Figure 8.3 represents a tensile strength of Ag-ternary blend composites in comparison with 20EVA/30EPDM/50PP blend (considered as control). The change in tensile properties upon 60 kGy and 100 kGy radiation dose for the ternary blend and the blend-Ag composites are also illustrated in the same figure. Prior to radiation, it can be noticed that upon addition of AgNP, the tensile strength reduced remarkably. With addition of 0.3% AgNP, the tensile strength of the ternary blend decreased from 18.41MPa to 12.68 MPa. Further increase in Ag loading, the tensile strength of the composites fell to 13.0 MPa (for 0.5% Ag loading) and 13.06 MPa (for 1% Ag loading). The decrease in tensile properties was due to the poor adhesion or debonding of AgNP in the ternary blend. The debonding occurs due to the tendency of the polymers (particularly in semi crystalline polymers, for example, PP) to exclude AgNP as extraneous substance or impurities. The exclusion of nanoparticles leads to weakening of the polymeric system. Moreover, the presence of nanoparticle agglomerates causes hindrance in the mixing of polymers during melt mixing (Ginzburg, 2005) , which leads to reduced miscibility of between PP-EVA and EPDM polymers. Thus, the decrease in tensile strength is due to weakening of the system and reduction in miscibility of the polymers in the presence of AgNP.

Upon radiation, the ternary blend with 0.3% and 0.5% Ag loading showed a slight increase in tensile strength (up to 14.13MPa for 0.3% Ag loading and 14.17MPa for 0.5% Ag loading) at 60 kGy and then decreased marginally with increase in radiation dose (13.77MPa for 0.3% & 13.76 MPa for 0.5% Ag loading at 100 kGy). The trend of increase in tensile strength of the Ag polymer composites at 60 kGy and decrease at 100 kGy was similar to neat 20EVA/30EPDM/50PP blend. The increase was due to the formation of crosslinks in polymer matrix and the decrease was caused by excessive crosslinks as discussed in previous chapters. However, the intensity of increase was very much less compared to the ternary blend without AgNP. This illustrates that even though crosslinks are formed in Ag polymer composites (as discussed in gel content analysis), the weakening effect by Ag agglomerates creates more discontinuities upon the application of stress load. The AgNP absorbs the initial stress before the stress is transferred to the polymer matrix (Tjong and Bao, 2007). It could be that the discontinuities created by the Ag agglomerates leads to non-uniform distribution of stress in polymer matrix leading to breakage of the already formed crosslinks. Hence, the

intensity of improvement in tensile strength of Ag polymer composites is very much insignificant when compared to the ternary blends (without Ag) when exposed to radiation.

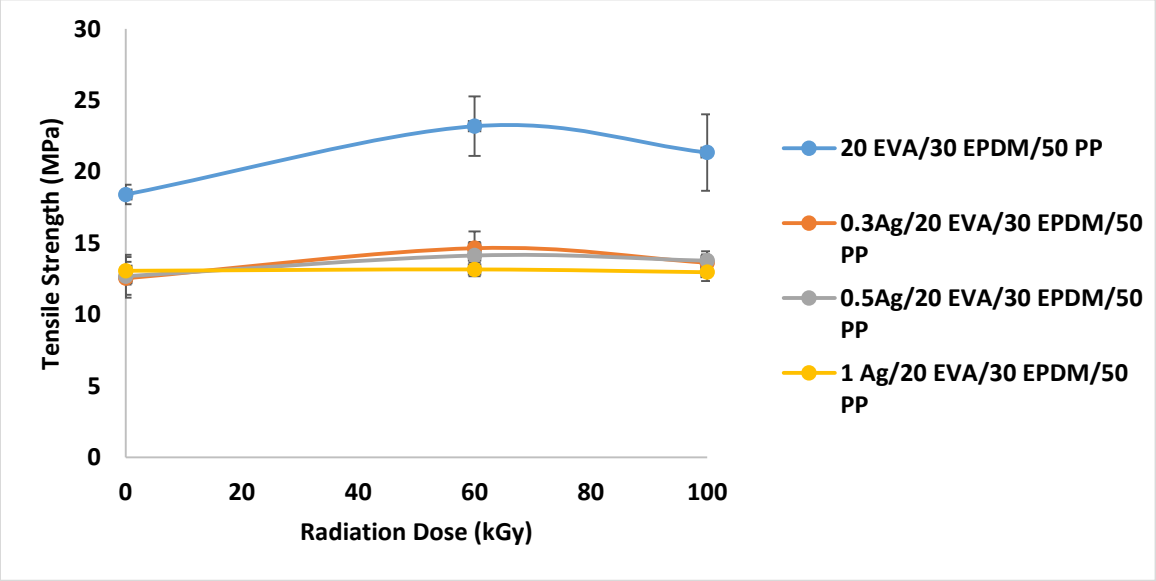


Figure 8.3 Tensile strength as a function of radiation dose for Ag/ternary blend nanocomposite

8.5 Elongation at Break

Figure 8.4 illustrates the elongation at break as function of radiation dose for neat 20EVA/30EPDM/50PP and the blends with different Ag nanoparticle loading. Prior to the radiation, it can be witnessed that the elongation at break of 20EVA/30EPDM/50PP was ≈825%. However, upon loading 0.3% AgNP the elongation at break reduced to 780% and to 525% at 0.5% Ag loading. It is well known that nanoparticles acts as stress concentrators in a polymer matrix. When a polymer composite is subjected to tensile tests, a triaxial stress is created around the Ag clusters. This leads to formation of voids due to the debonding of nanoparticles from the matrix. Hence, a decrease in elongation at break can be observed. With increase in Ag loading up to 1%, only a marginal drop of elongation at break to 515% was noticed. Ghosh and Maiti (1996) reported that when the loading of AgNP incorporated was more than 0.5%, matrix deformation was reduced in a pseudologratimic fashion by the metal

particles. Hence, only a marginal decrease was observed when 1% Ag was loaded to the ternary blends in this study.

Upon radiation, elongation at break of 0.3 Ag/20EVA/30EPDM/50PP was reduced to 480% at 60 kGy and 406% at 100 kGy. Likewise, elongation at break of the blends with 0.5% Ag and 1% Ag loading also decreased immensely upon radiation. The trend of decrease in elongation at break with increasing radiation is very much similar to the neat 20EVA/30EPDM/50P ternary blend. The decrease in elongation was again associated with decreased ductility due to the formation of radiation induced crosslinks (as discussed in previous chapters).

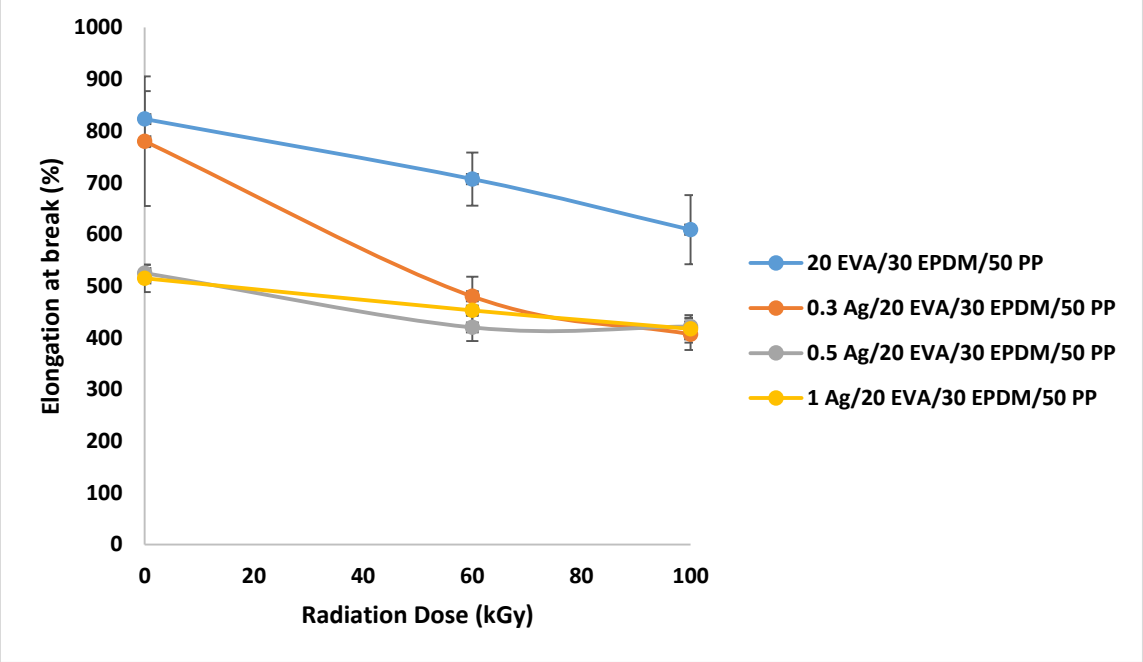


Figure 8.4 Elongation at break as a function of radiation dose for Ag/ternary blend nanocomposite

8.6 Impact Strength

Figure 8.5 shows the impact strength of Ag-ternary blend composites in comparison with the neat ternary blend. The variation of impact strength upon E-beam radiation is also presented in this figure. Prior to radiation, the impact strength of the blends increased from 41.65 J/m to 44.5 J/m upon addition of 0.3% Ag loading. With increase in Ag addition by 0.5% and 1% Ag, the impact strength slightly increased to 45.02J/m and 44.13 J/m, respectively. This slight increase in impact strength complements the reduction in tensile strength upon addition

AgNP. Addition of AgNP as nanofillers reduces the mobility of the polymer matrix leading to reduce in impact resistance. However, the agglomerates caused the stress to be concentrated around the nanoparticles, increasing the impact strength. Moreover, the debonding caused by the AgNP resulted in the formation of voids. As discussed in section 5.8, the presence of voids enhances the toughening effect of the polymer blends. The voids absorbs more impact energy before the energy is transferred to the surrounding matrix. In addition to the above postulates, the improvement in impact strength could also be due to the formation of β-form PP when AgNP were added (Tjong et al., 1996, Tjong and Bao, 2007).

Upon addition of 0.3% Ag, the impact strength slightly increased to 50.99 J/m at 60 kGy and decreased to 47.29 J/m at 100 kGy. Likewise, with increase in 0.5% and 1% Ag loading the impact strength increased at 60 kGy (49.12 J/m for 0.5% Ag and 50.99J/m for 1% Ag) and showed a slight decrease at 100 kGy (46.33 J/m for 0.5% Ag and 48.01 J/m for 1% Ag). The trend is very much in accordance with the trend exhibited by the neat ternary blend without AgNP, which is due to the crosslinking and scission effect induced upon irradiation (as disused in earlier chapters).

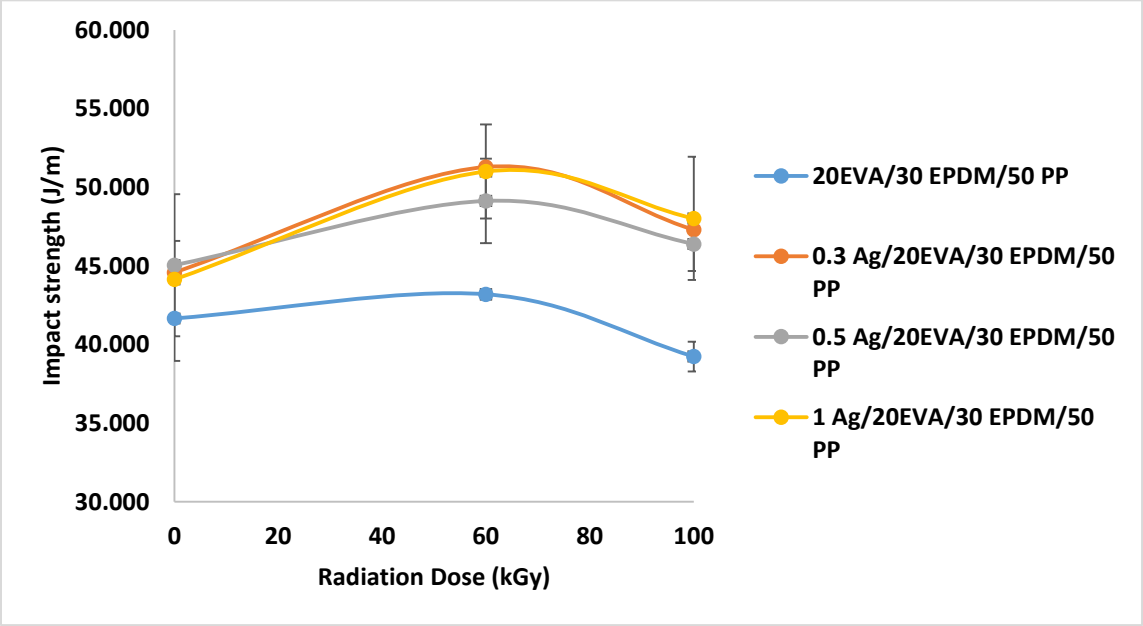


Figure 8.5 Impact strength of Ag/ternary blend nanocomposite as a function of radiation dose

8.7 Thermogravimetric Analysis

Figure 8.6 (A-B) depicts the weight loss and derivative TGA thermograms for 20 EVA/30 EPDM/50 PP ternary blend and the composites prepared with 0.3%, 0.5% and 1% AgNP. T_1 corresponds to the maximum degradation of first step and T_2 corresponds to the final degradation temperature of the ternary blends. The ternary blend composites exhibited two step degradation very much similar to the neat ternary blend. The first step corresponds to degradation of vinyl acetate in EVA polymeric chain and the second step corresponds to ethylene and propylene backbone of EVA, PP and EPDM matrix. T_1 of the ternary blend laid at 337.86°C and maximum degradation (T_2) was at 448.58°C. Upon the addition of 0.3% AgNP, both T_1 and T_2 shifted to 342.72°C and 453.68°C, respectively. Similarly, the addition of 0.5% and 1% AgNP also resulted in increase of T_1 and T_2 with respect to the neat ternary blend. The slight increase in the final degradation temperatures can be attributed to the restriction on the polymer chain mobility due to the presence of AgNP. This in turn led to slight improvement in the thermal stability of 20 EVA/30 EPDM/50 PP ternary blend with AgNP.

T_1 and T_2 of the ternary blends (with and without Ag addition) under the effect of radiation dose at 60 kGy and 100 kGy were listed in Table 8.1. However, it can be witnessed that upon radiation, the blends with AgNP did not show any significant change. This can directly be related to the effect of neat ternary blend upon radiation, where the radiation did not cause any change in polymer matrix as well.

Table 8.1 Degradation temperatures of ternary blends with different Ag loading

Samples	**Radiation dose (kGy)**	**T_1 (°C)**	**T_2 (°C)**
20 EVA/30 EPDM/50 PP	0	337.86	448.58
	60	338.33	452.25
	100	340.92	452.45
0.3 Ag 20 EVA/30 EPDM/50 PP	0	342.72	453.68
	60	342.57	454.12
	100	343.71	454.88
0.5 Ag 20 EVA/30 EPDM/50 PP	0	343.45	453.86
	60	344.12	454.42
	100	343.79	453.97
1 Ag 20 EVA/30 EPDM/50 PP	0	343.71	454.84
	60	344.64	454.91
	100	345.67	454.68

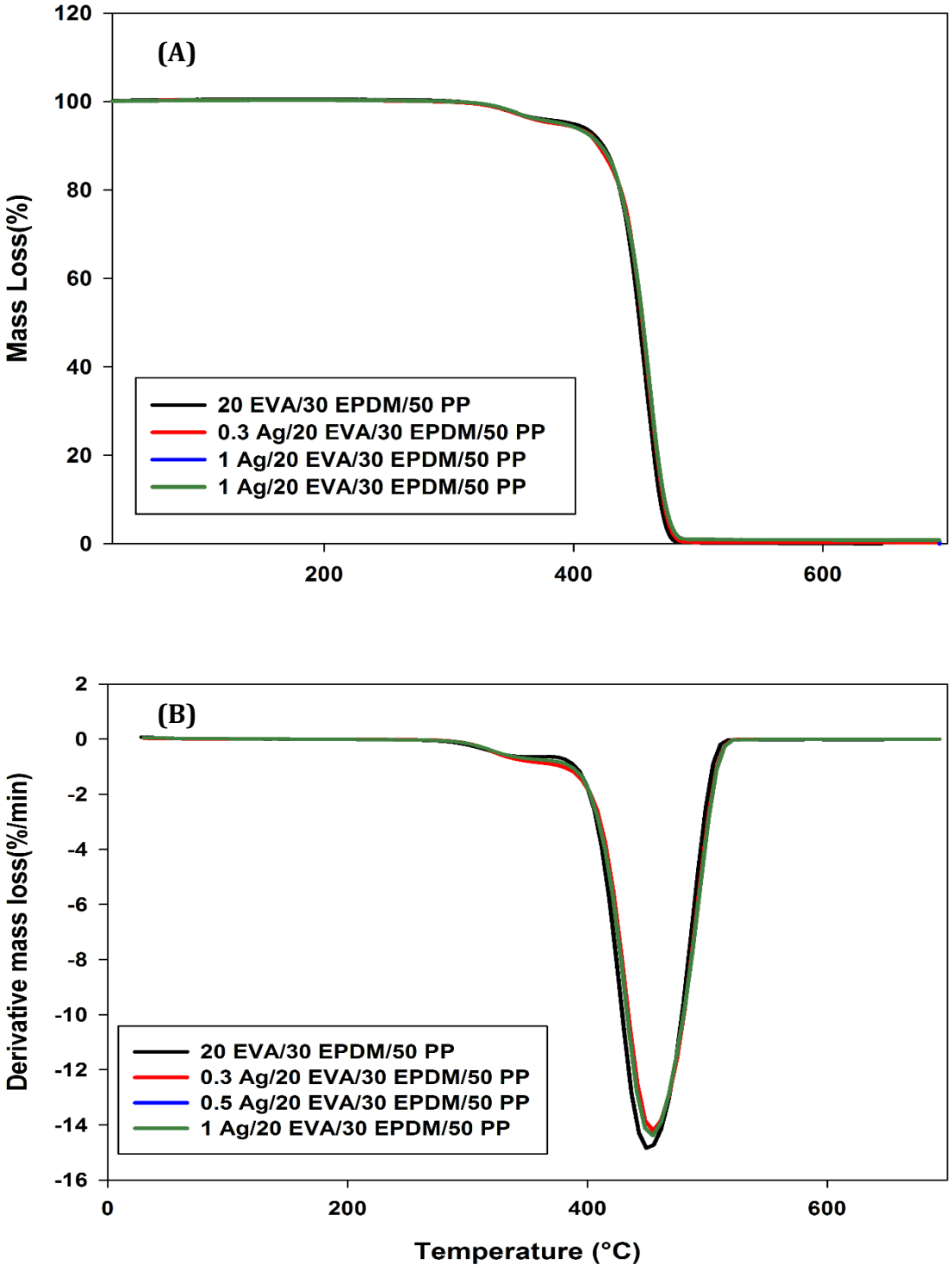


Figure 8.6 (A) TGA and (B) DTGA thermogram of ternary blend with different AgNP loading

8.8 Differential Scanning Calorimetry

Figure 8.7-8.10 (A-B) illustrates the heating and cooling curves DSC curves of Ag-ternary blend composites in comparison to neat ternary blend. The crystallization and melting temperatures of all the three phases from Figure 8.7-8.10 are listed in table 8.2 for further reference. From Figure 8.7 (A), it can be noticed that three crystallization peaks were exhibited by the neat 20 EVA/30 EPDM/50 PP blend. The crystallization temperatures (T_m) of EPDM exists at 30.96°C, T_m of EVA phase at 72.45°C and PP at 144.13°C. Upon the addition of AgNP, the composite blends exhibited T_m of EPDM phase at 25.23°C (for 0.3% Ag), 25.96°C (for 0.5% Ag) and 22.98°C (for 1% Ag). The T_m of EPDM phase decreased upon addition of AgNP. On the other hand, the T_m of EVA phase could not be identified as the melting peak of EVA phase overlapped by the formation of melting peaks corresponding to β-crystalline phase of PP. The addition of AgNP caused the formation of β-crytalline PP phase (which laid at ≈97°C), as the nucleating effects were rendered by AgNP (Camacho et al., 2017). Similar results, where, formation of β phase in addition to α phase (original melting peak of PP) upon the incorporation of AgNP into PP matrix were reported (Tjong and Bao, 2007, Camacho et al., 2017). The broad peaks of β phase lying close to the T_m of EVA (at 73°C) overlaps with later, making it not possible to differentiate the T_m of EVA phase separately. T_m of β-crystalline phase of PP for all the Ag-ternary composite blends laid around 97°C. No changes in both intensity and T_m of these peaks were found when the Ag loading was varied. Further, the α-crystalline phase of PP (resulted from the T_m of actual PP phase) laid at 151.81°C for ternary blends with 0.3%, 151.04°C for 0.5% Ag-ternary blend and at 152.21°C for 1% Ag-ternary blend. However, the T_m of α-crystalline phase of PP of the blends with Ag particles became much sharper than the ternary blend without AgNP. This indicates that some extent of uniformity was established in the crystals of PP α-phase upon the incorporation of AgNP into polymer matrix. Similar results were reported in PP/AgNP blend by Chae and Kim (2005). The addition of AgNP increased the T_m of PP α-phase from 143.13°C (for neat ternary blend) to ≈151°C (for blends with nanoparticles). The nucleating effect rendered by Ag causes the restriction in chain mobility of the polymer chains, reducing the T_m of α-phase.

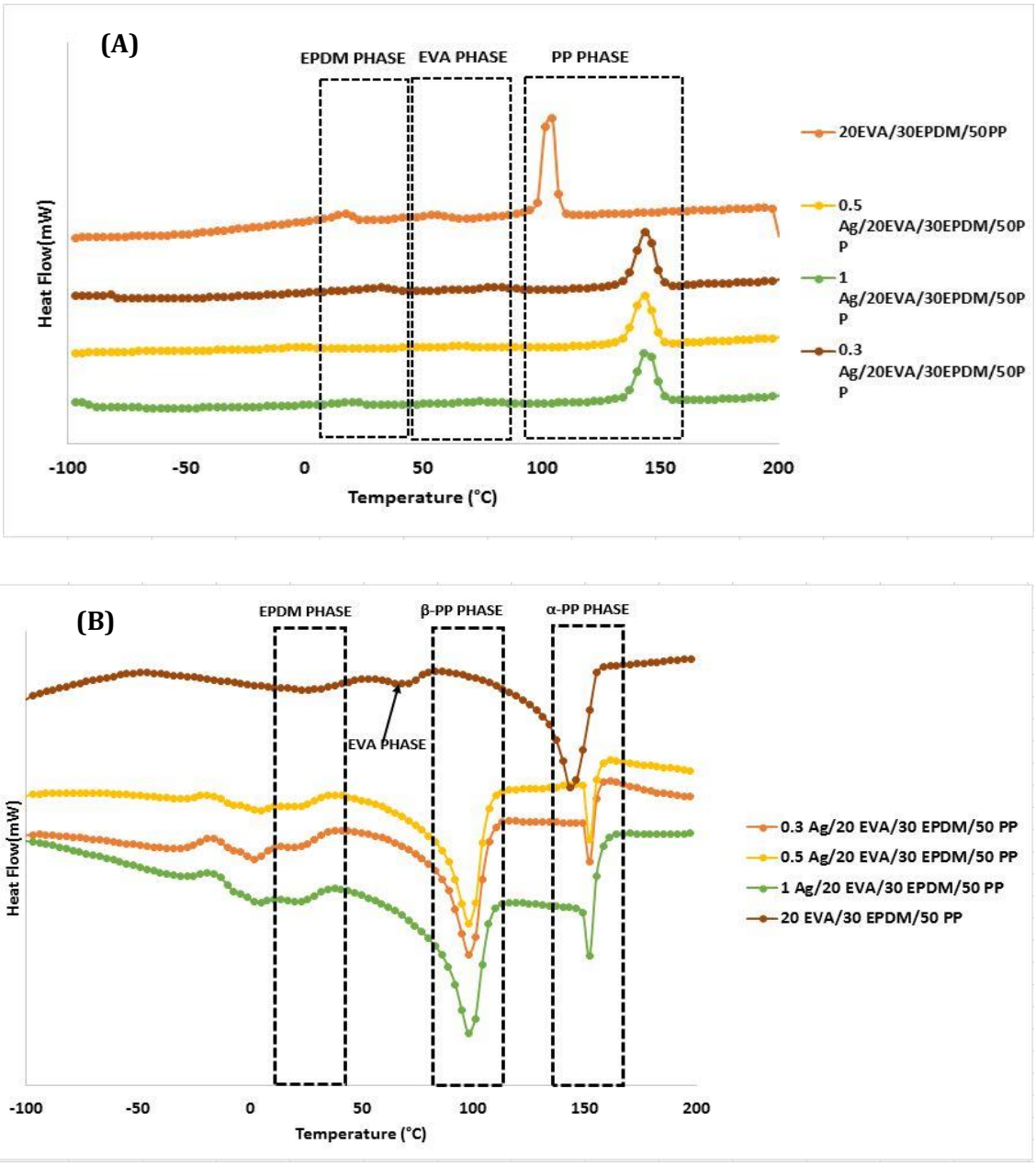


Figure 8.7 (A) Cooling and (B) heating curves of ternary blends with Ag loadings prior to radiation

Figure 8.7 (B) represents the cooling DSC thermographs of the ternary blends and blends with AgNP. It can be noticed that T_c of all the three phases were shifted to higher temperature upon addition of AgNP. The T_c of EPDM changed from 17.56°C (neat ternary blend) to 26.07°C (for 0.3% Ag loading), 29.74°C (for 0.5% Ag loading) and 23.02°C (for 1 % Ag loading). Similarly, T_c of EVA also increased to 68.06°C (for 0.3% Ag loading), 65.12°C (for 0.5% Ag

loading) and 74.30°C (for 1 % Ag loading) in comparison to neat ternary blend whose T_c is 74.30°C. Further, the T_c of PP phase also shifter to a higher temperature of ≈143°C (for all Ag loading) from 103.10°C (neat polymer blends). This indicates that AgNP act as nucleating agents, causing heterogeneous nucleation (Tjong and Bao, 2007), leading to increase in crystallization temperature in all three phases.

Table 8.2 Melting temperature (T_m) and crystallization temperature (T_c) of ternary blends with AgNP before and after radiation

Sample	Radiation Dose	T_c			T_m		
		EPDM Phase	EVA Phase	PP Phase	EPDM Phase	β - PP Phase	α - PP Phase
20 EVA/30 EPDM/50 PP	**0**	**17.56**	**54.57**	**103.10**	**30.96**	**-**	**144.13**
	60	15.83	49.00	101.77	28.37	-	143.98
	100	12.30	48.25	101.28	26.12	-	142.12
0.3 Ag/20 EVA/30 EPDM/50 PP	**0**	**26.07**	**68.06**	**143.36**	**25.23**	**97.68**	**151.81**
	60	23.62	68.93	143.48	25.91	97.77	150.42
	100	26.03	70.54	143.34	25.83	97.58	148.79
0.5 Ag/20 EVA/30 EPDM/50 PP	**0**	**29.74**	**65.12**	**143.2**	**25.96**	**97.86**	**151.04**
	60	29.52	62.00	143.27	25.97	97.92	148.45
	100	29.07	59.71	143.32	25.94	97.56	149.92
1 Ag/20 EVA/30 EPDM/50 PP	**0**	**23.02**	**74.30**	**143.26**	**22.98**	**97.87**	**152.98**
	60	20.04	68.05	143.41	22.89	97.67	152.21
	100	19.97	61.98	143.27	23.06	97.98	152.02

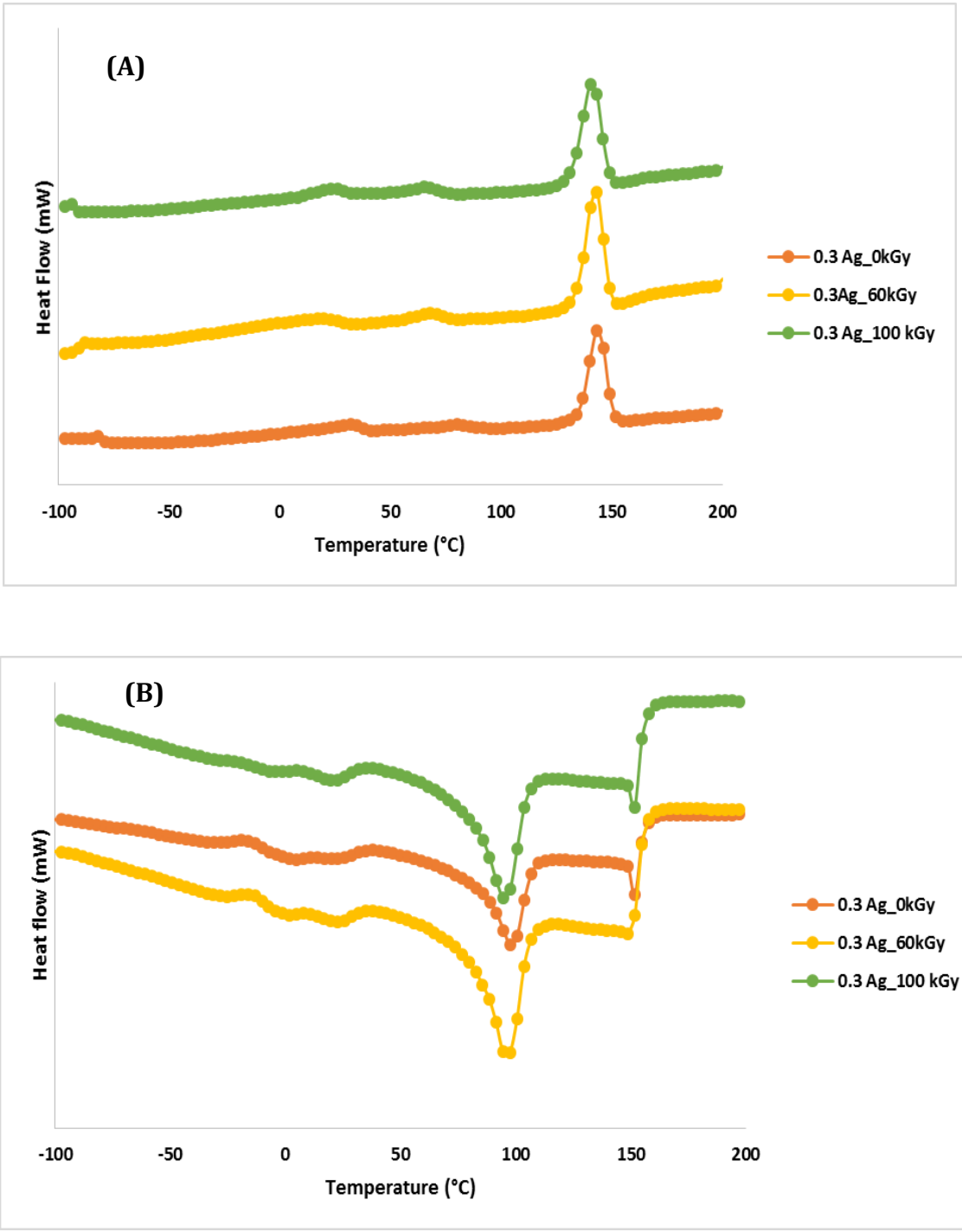
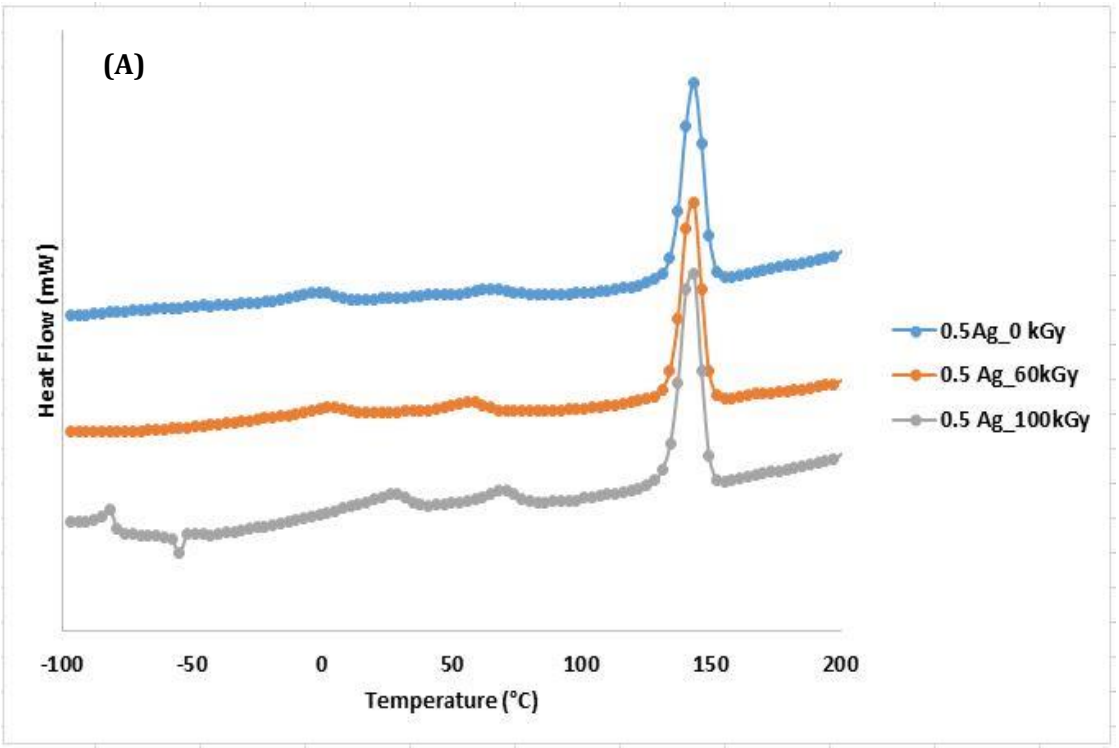


Figure 8.8 (A) Cooling and (B) Heating curves of ternary blend with 0.3 % Ag loading upon radiation



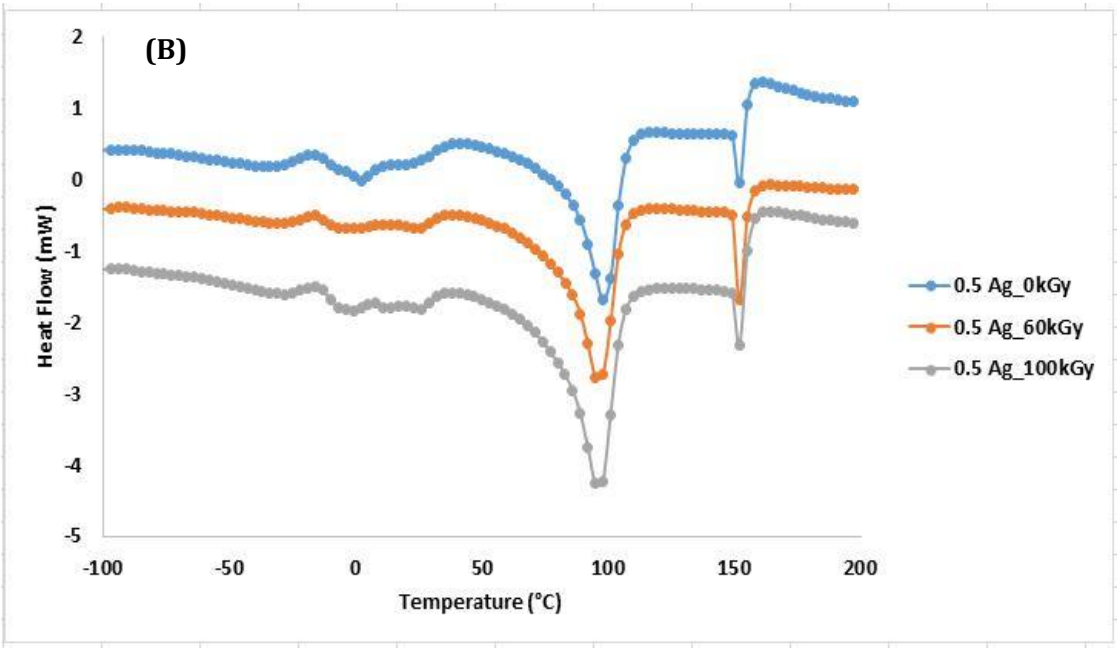


Figure 8.9 (A) Cooling and (B) Heating curves of ternary blend with 0.5 % Ag loading upon radiation

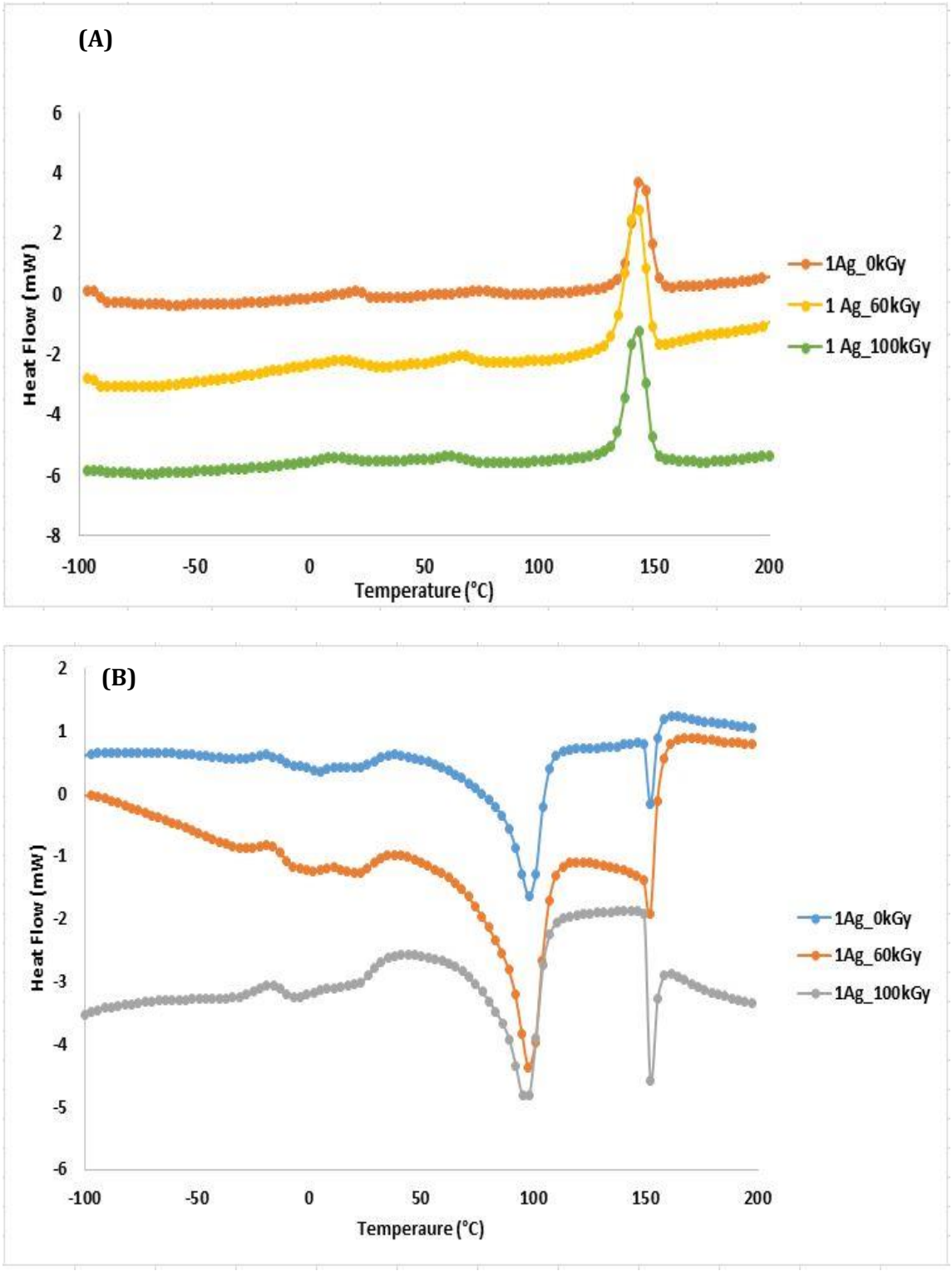


Figure 8.10 (A) Cooling and (B) Heating curves of ternary blend with 1 % Ag loading upon radiation

The effect of irradiation at 60 kGy and 100 kGy on T_c and T_m temperatures of the blends are summarized in Table 8.2. It can be noticed that upon radiation, in Ag-ternary blend composites the T_c and T_m of all three phases tend to decrease slightly. This decreasing trend of peak temperature in Ag-ternary blends upon irradiation was similar to the effect of radiation on neat polymers. Again, this slight decrease can be attributed completely to the crosslinks formed by radiation in the polymer matrix (as discussed in previous chapter). This in turn was in line with gel analysis, where AgNP did not interrupt the formation of crosslinks even under radiation.

8.9 *In-vitro* Analysis

The biocompatibility of the ternary blends and the Ag-ternary polymer blends was evaluated using *in-vitro* assays including cell adhesion test and cell proliferation test (MTT assay). HaCaT cells were used in this study for the biocompatibility evaluation of the ternary blends. HaCaT cells are human keratinocyte cells that are usually used to study skin biology, dermal toxicity and differentiation (Wilson, 2014).

8.9.1 Cell Adhesion Test

Cell adhesion tests were used to analyze the tendency of the HaCaT cells to get adhered to the ternary blend composites. The morphology of the cells on 50 PP/50 EPDM binary blend, 20 EVA/30 EPDM/50 PP ternary blend and the blends with 0.3%, 0.5% and 1% AgNP after 4-h, 3 day and 7 day incubation periods was studied. Also, the blends radiated at 60 kGy and 100 kGy were also examined in the *in-vitro* assay. FESEM images (Figure 8.11 to Figure 8.15) shows contact of HaCaT cells on neat blends and blends with nanoparticles at pre-determined incubation periods. It can be noticed that most of the blends (with and without nanoparticles) the morphology of cells were spherical showing microvilli projections at 4h incubation. This indicates that the cells were less favourable for adhesion, as they still existed at cell fixation stage. However, after 3 days and 7 days of incubation, the cells showed different morphologies. In most cases, the morphology of the cells became flattened. These drastic changes in the morphology of the cells indicates that the HaCaT cells showed improvement in adhesion on all the blends with and without AgNP. The improvement adhesion indicates that cell growth is favourable on the ternary blends which confirms that MTT assay can be performed to evaluate the biocompatibility of the ternary blends.

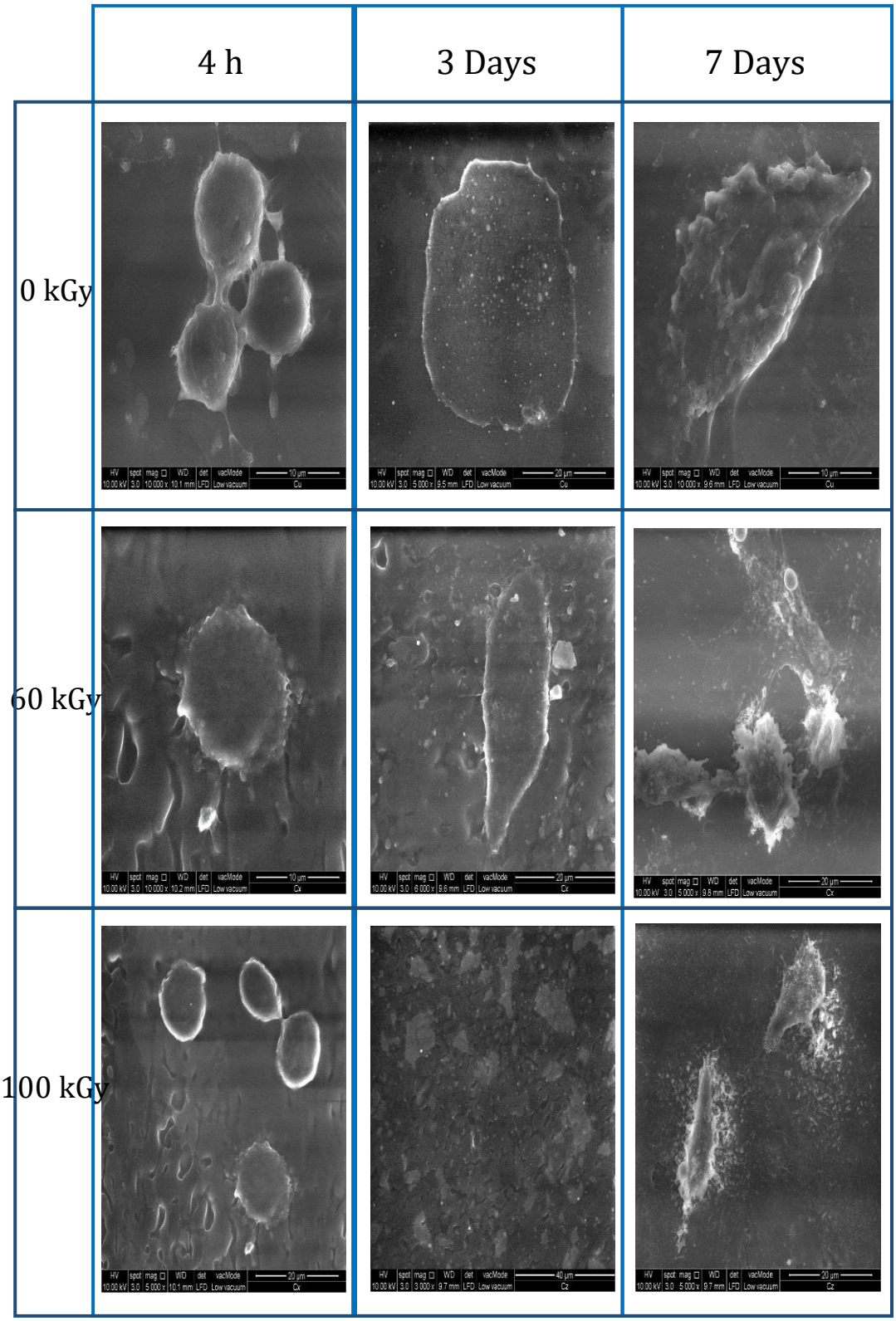


Figure 8.11 SEM images showing the morphology of the cells on 50PP/50EPDM blends at different radiation dose after 4 h, 3 days and 7 days of culture

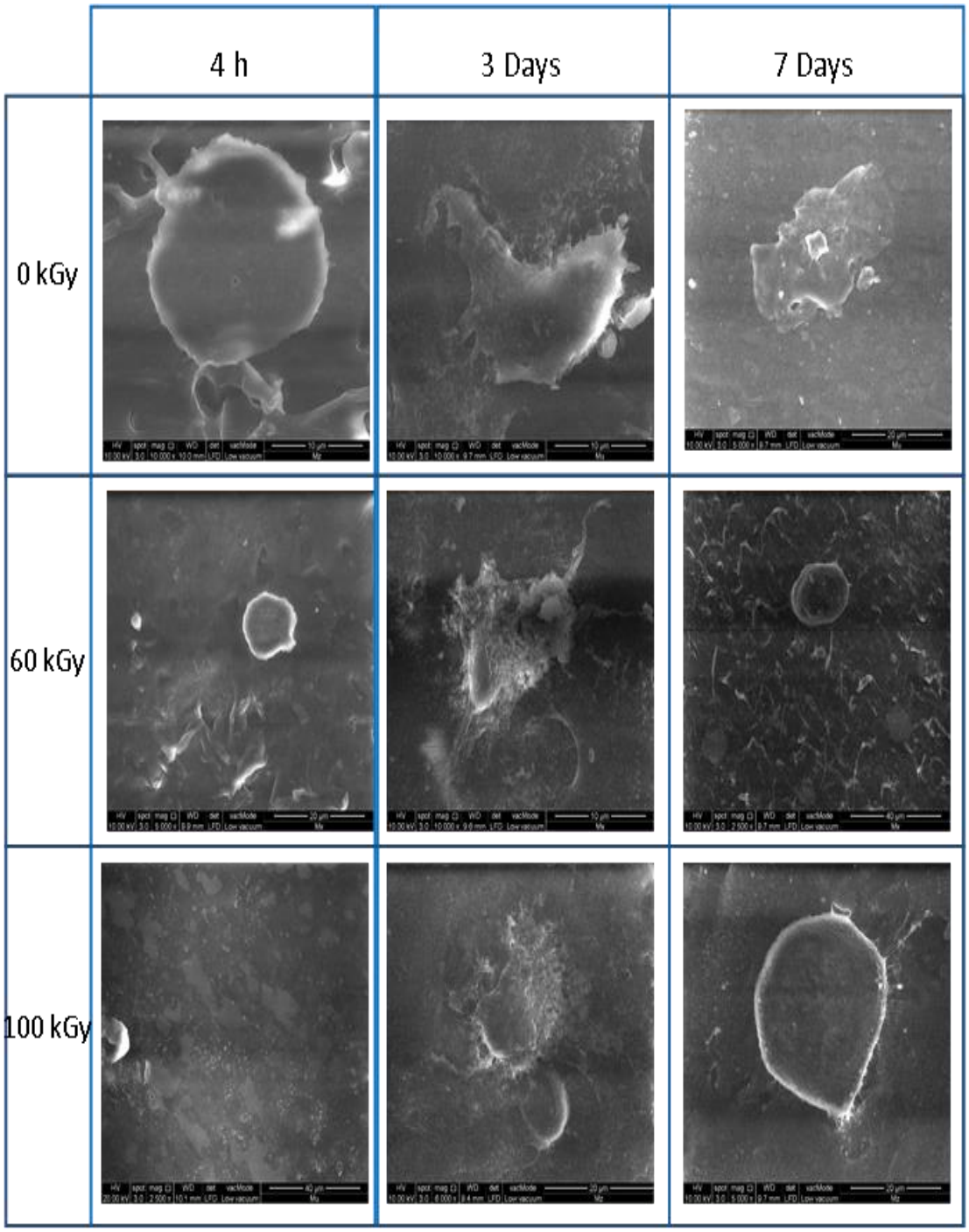


Figure 8.12 SEM images showing the morphology of the cells on 20 EVA/30 EPDM/50 PP blends at different radiation doses after 4 h, 3 days and 7 days.

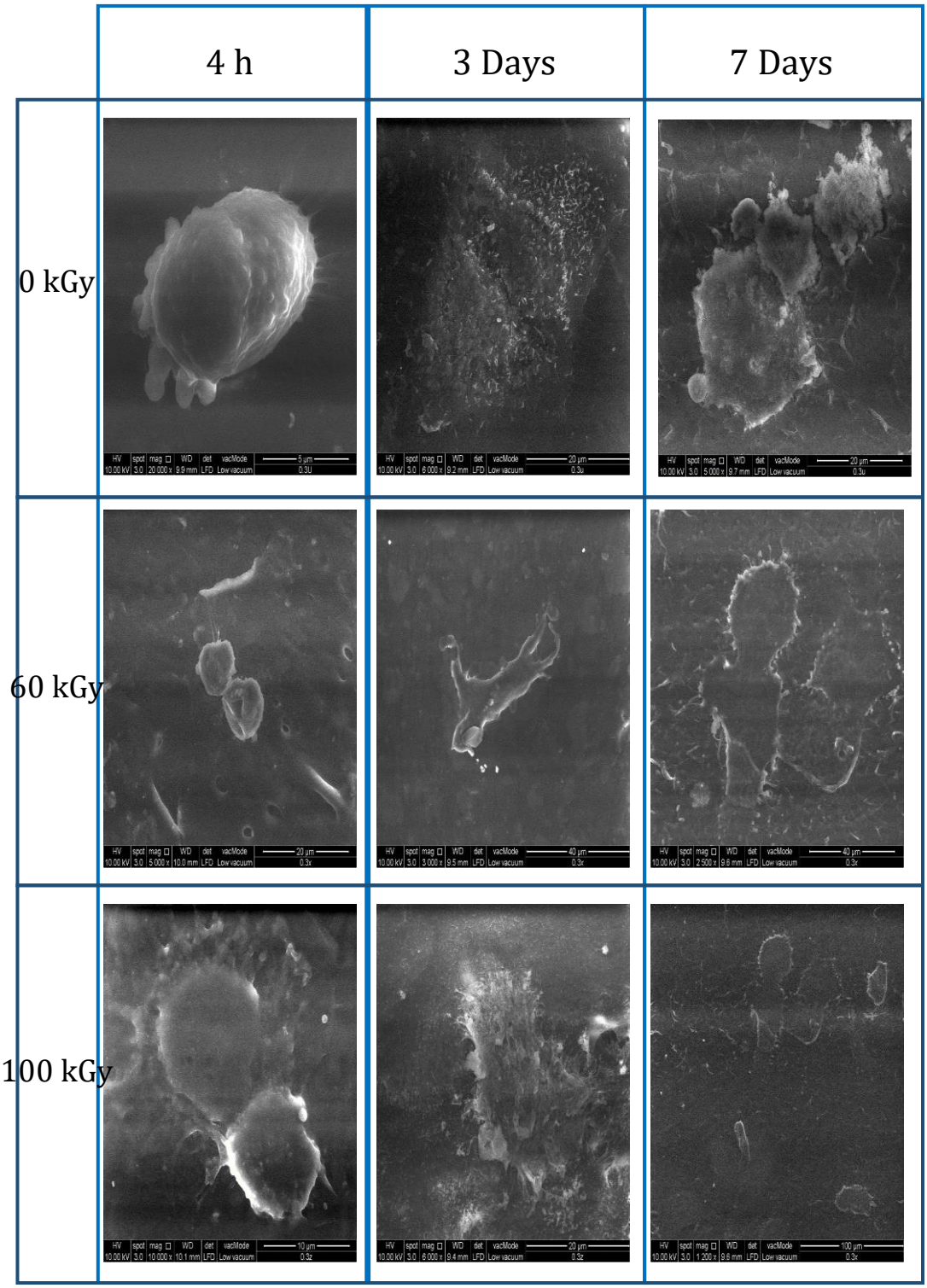


Figure 8.13 SEM images showing the morphology of the cells on 20 EVA/30 EPDM/50 PP blend with 0.3 wt% Ag

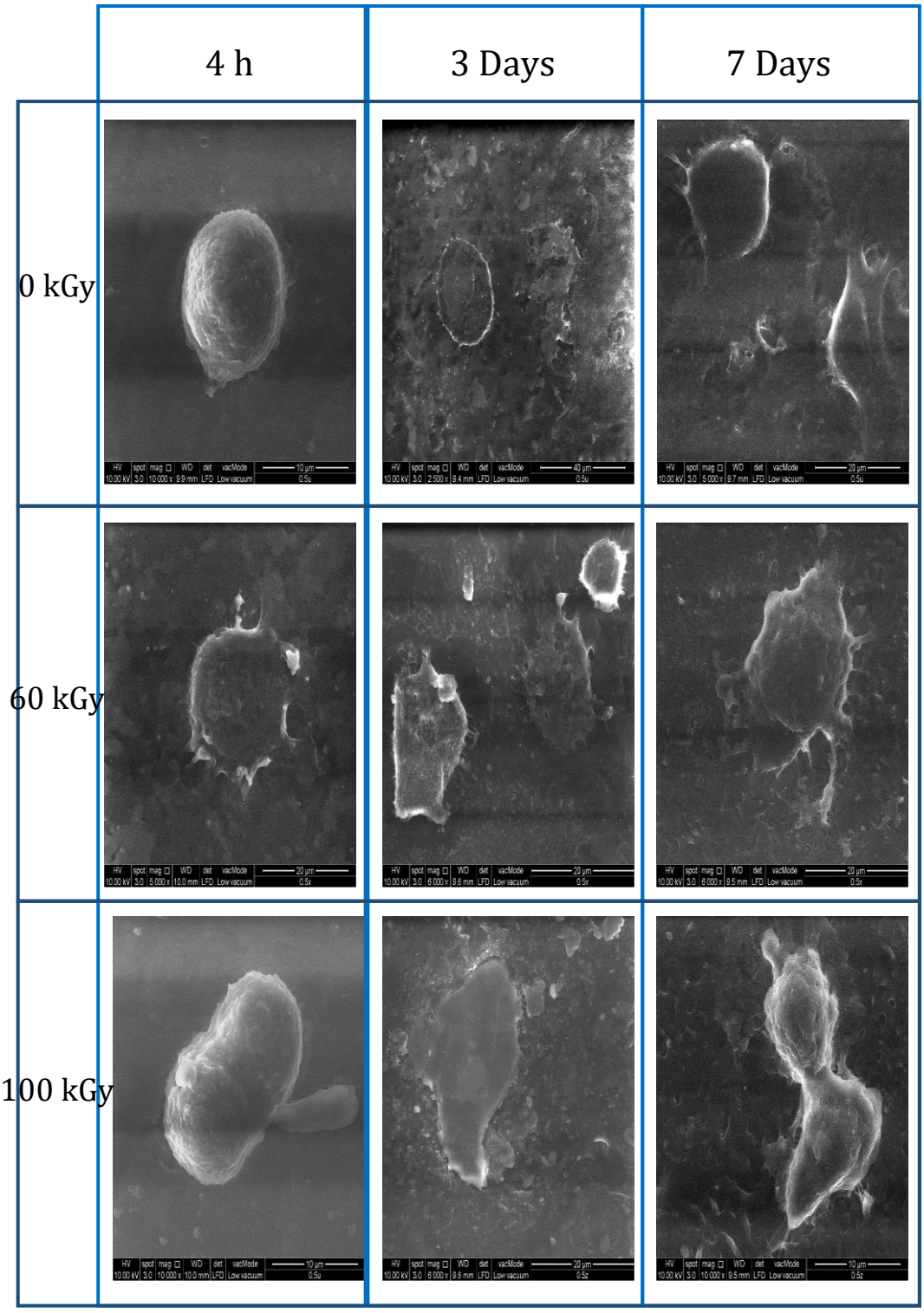


Figure 8.14 SEM images showing the morphology of the cells on 20 EVA/30 EPDM/50 PP blend with 0.5 wt% Ag

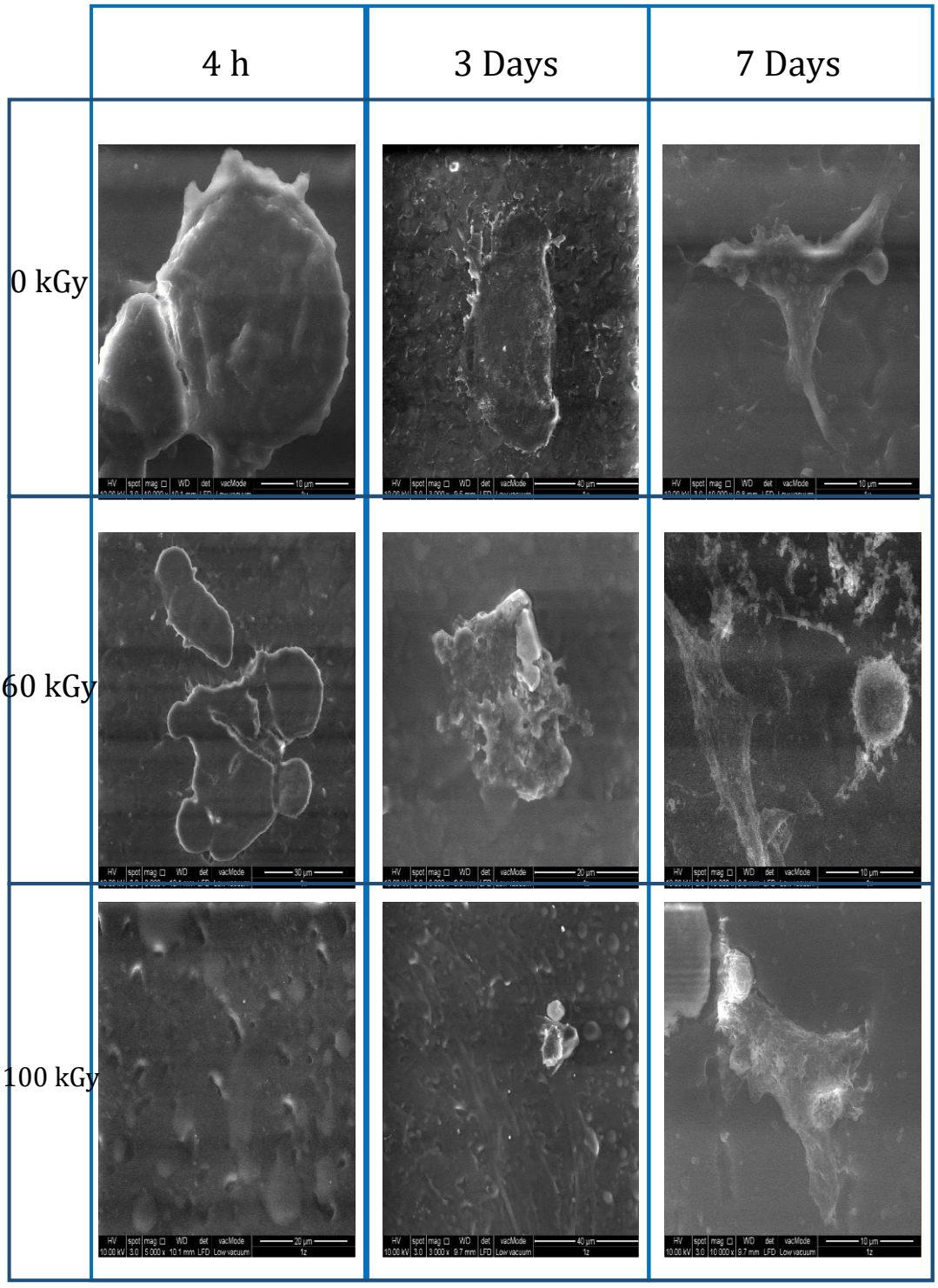


Figure 8.15 SEM images showing the morphology of the cells on 20 EVA/30 EPDM/50 PP blend with 1 wt% Ag

8.9.2 MTT assay

The *in vitro* biocompatibility of all polymer blends and polymer blends with different Ag loading was evaluated by using MTT assay. The MTT was performed for 3 incubation periods – 1 day, 3 days and 7 days. The cell viability or the cell growth during all the incubation periods of all the blends considered for the study are represented in Figure 8.16 to Figure 8.20. From Figure 8.16 to Figure 8.20, it can be noticed that all the polymer blends promoted cell viability of greater than 70%. This indicates that the 50PP/50EPDM, 20 EVA/30 EPDM/50 PP ternary blend and the blends with 0.3%, 0.5% and 1% AgNP showed no cytotoxicity. Materials supporting cell viability of more than 70% are considered safe to be used in medical devices (Reis and Cunha, 2000, Bhatia and Yetter, 2008, Liu et al., 2009). Additionally, from Figure 8.16 to Figure 8.20, it can be seen that all the blends even after exposing to radiation at 60 kGy and 100 kGy, supported the cell viability of greater than 70%. This shows that there no toxic degraded compounds was formed due to scission mechanism caused by E-beam radiation that retarded the cell growth. Hence, products manufactured using ternary blends can be safely sterilized under E-beam radiation, which fulfils the main objective of our study. Thus, the cell adhesion images and MTT assay verified that these blends are dermatologically safe to be manufactured as healthcare devices.

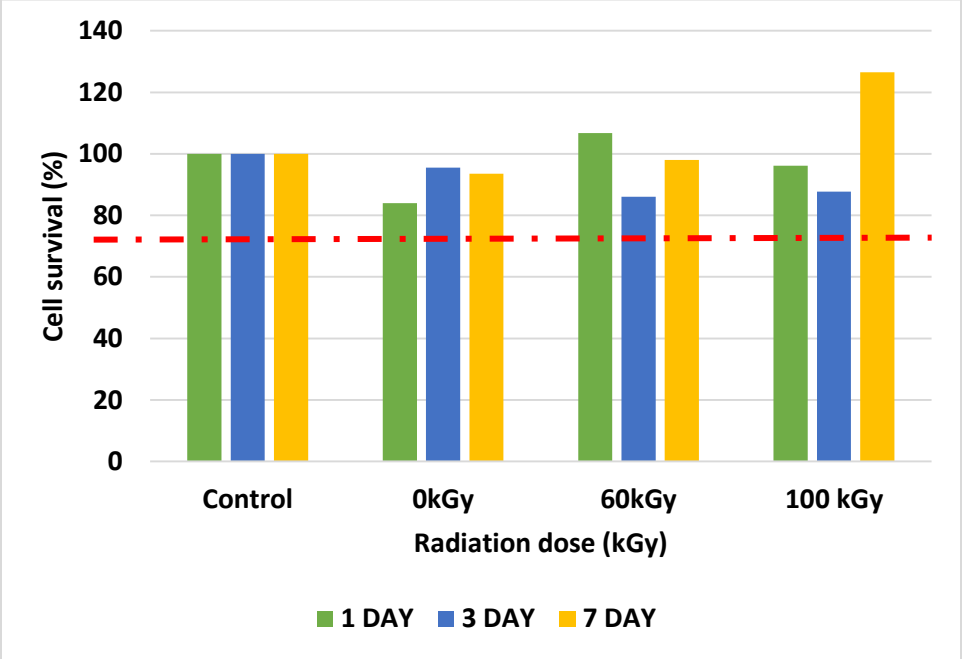


Figure 8.16 Proliferation of HaCaT cells on 50PP/50EPDM blend

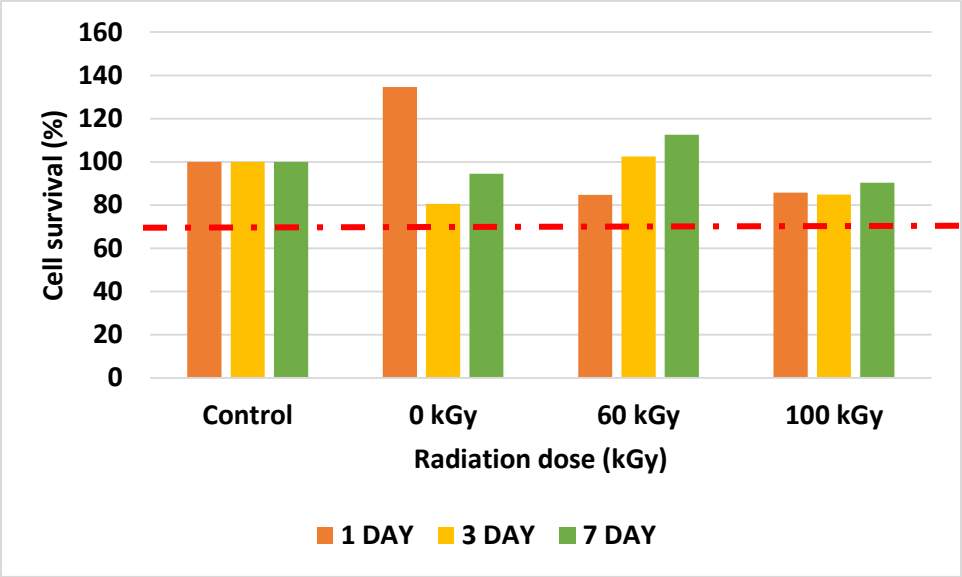


Figure 8.17 Proliferation of HaCaT cells on 20 EVA/30 EPDM/50PP blend

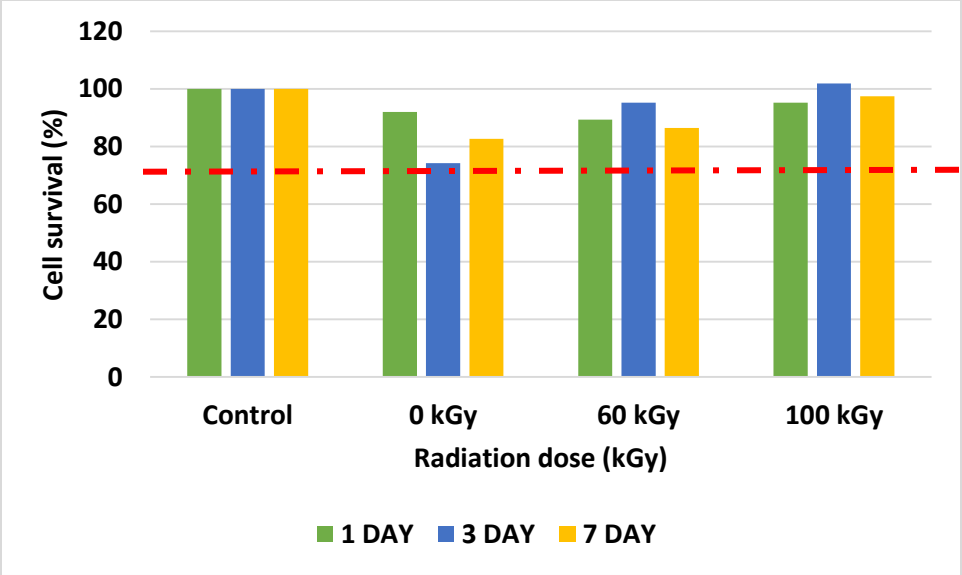


Figure 8.18 Proliferation of HaCaT cells on 20 EVA/30 EPDM/50PP blend with 0.3% Ag loading

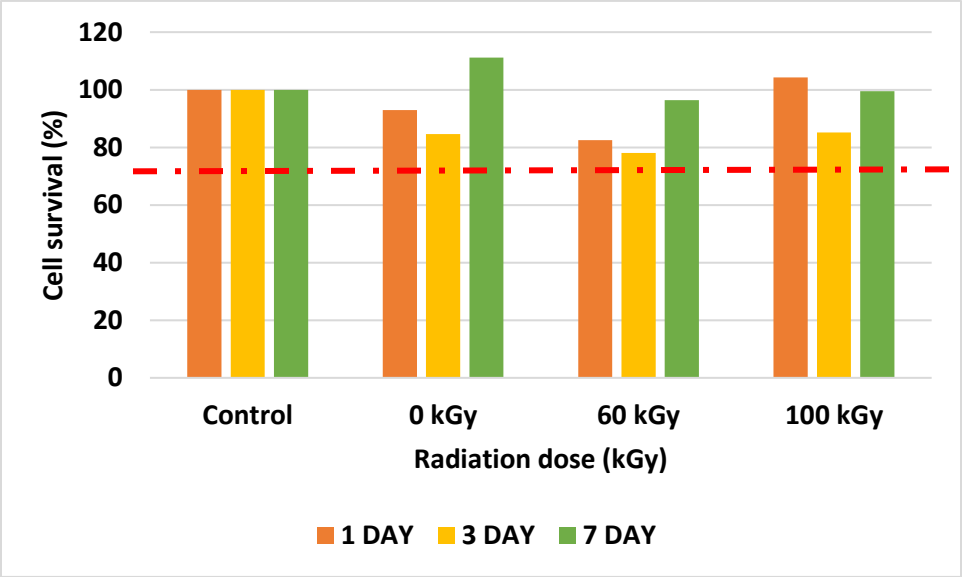


Figure 8.19 Proliferation of HaCaT cells on 20 EVA/30 EPDM/50PP blend with 0.5% Ag loading

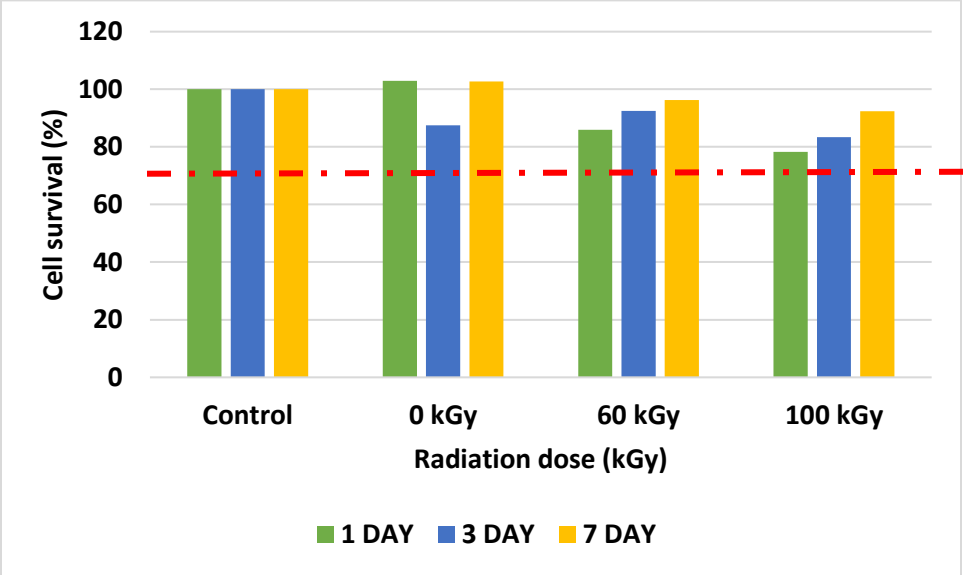


Figure 8.20 Proliferation of HaCaT cells on 20 EVA/30 EPDM/50PP blend with 1% Ag loading

8.10 Antimicrobial Studies

The biocide action of AgNP in the blend was tested using viable bacterial colony counting method. These tests were performed on 1% Ag/20 EVA/30 EPDM/50 PP and compared with the neat 20 EVA/30 EPDM/50 PP which was used as control. The antibacterial property of 1% Ag/20 EVA/30 EPDM/50 PP radiated at 60 kGy was also included. The tests were performed on a gram negative bacteria-Pseudomonas aeruginosa and on a gram positive bacteria-Staphylococcus aureus. These two strains are commonly occurring bacterial biofilms on biomaterials leading to various hospital infections (Salomoni et al., 2017, Lara et al., 2010). Since they can survive in harsh environments, they were then used as model study to test the effect of biocide actions of the synthesized materials. The viable bacteria found on agar plate after 24-h incubation period are shown in Figure 8.21. Figure shows the bacterial viability of Staphylococcus aureus. It can be seen that upon addition of Ag nanoparticle the bacterial viability reduced by 66% from $8.8x10^4$ cfu/ml (control) to $3x10^4$ cfu/ml. Similarly for the radiated Ag-ternary blend also showed 66% decrease in bacterial growth. Though bacterial growth of Staphylococcus aureus was reduced after the addition of AgNP into the polymer blends, a significant amount of bacterial colonies was still observed in the agar plates. The bacterial growth can be seen from Figure 8.23-8.24. Hence, the ternary blend with 1% AgNP showed only bacteriostatic effects rather than bactericidal effects, as complete growth of bacteria was not achieved. A similar effect was also observed in AgNP/chitosan and AgNP/LDPE blend on E.coli (Abdelgawad et al., 2014, Jokar et al., 2012, Torres-Giner et al., 2009). Further, the viability of Pseudomonas aeruginosa was shown in Figure 8.22 . No significant change was observed in biocidal effect on this particular gram negative bacteria. Several similar works were published, where AgNP when ionized in presence of water showed inhibitory effects (Rai et al., 2012, Durairaj et al., 2012). In our study, no significant inhibition of the bacterium growth was found. This could plausibly be due to the agglomeration of AgNP in the matrix. The agglomerates hindered the migration of nanoparticles which led to poor contact with the bacteria strain. Additionally, the localization caused by agglomeration could also have reduced the efficiency of AgNP migration. Thus, a detailed study on AgNP dispersion in polymer matrix has to be adopted to make use of the biocide potential of AgNP against P. aeruginosa strain.

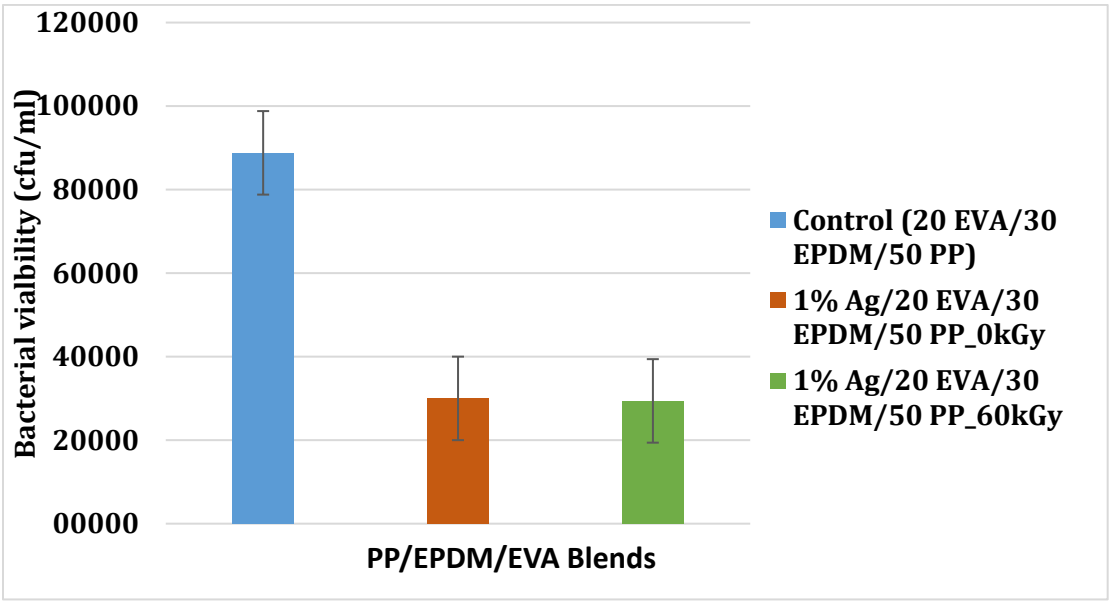


Figure 8.21 Proliferation of Staphylococcus aureuson on ternary blend with or without AgNP radiated at 60 kGy

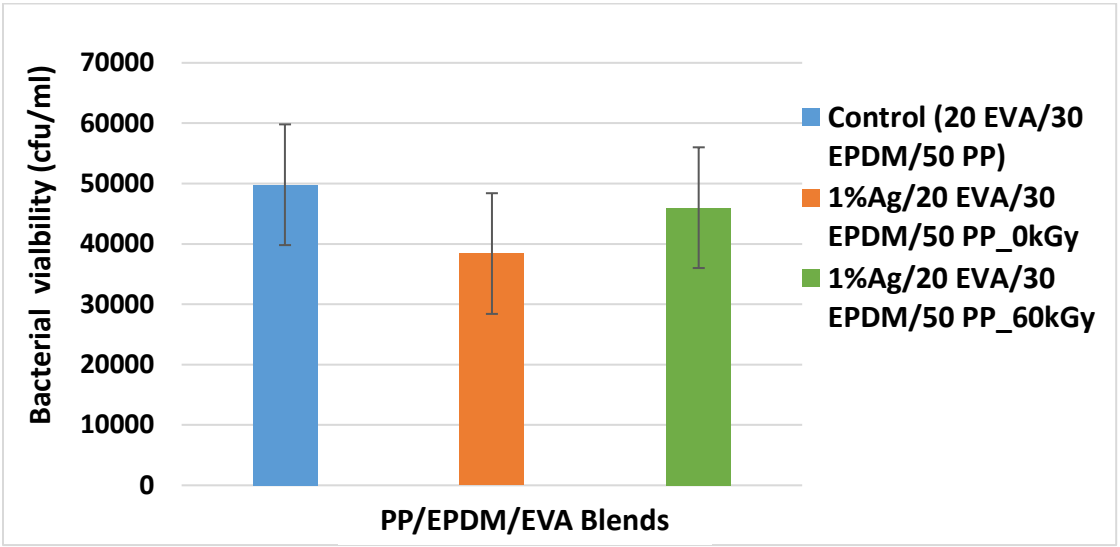


Figure 8.22 Proliferation of Pseudomonas aeruginosa on ternary blend with or without AgNP radiated at 60 kGy

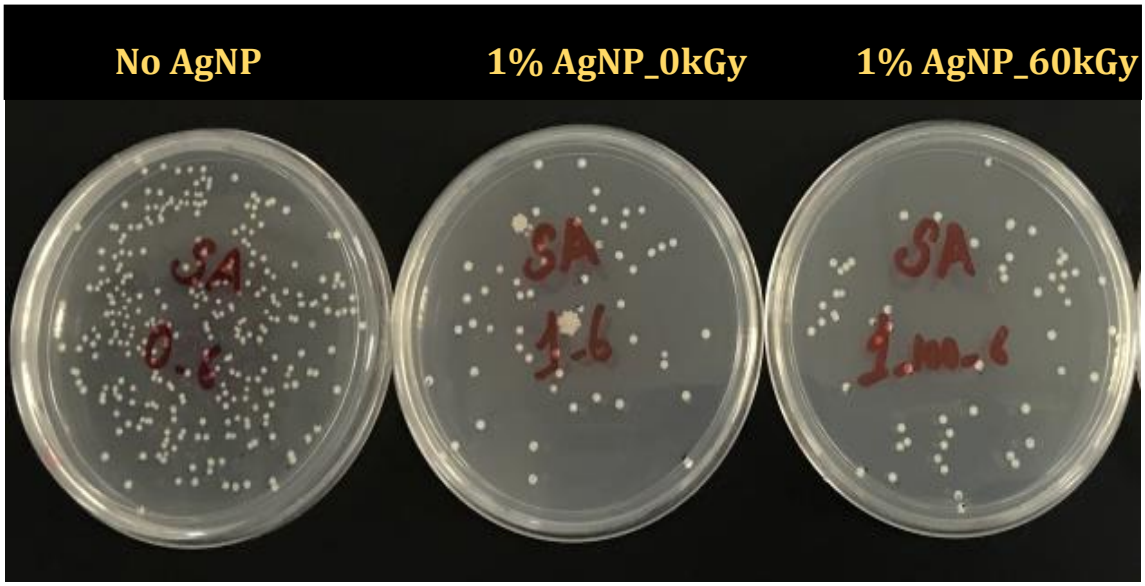


Figure 8.23 Growth of Staphylococcus aureuson after 6x dilution on different polymer blends

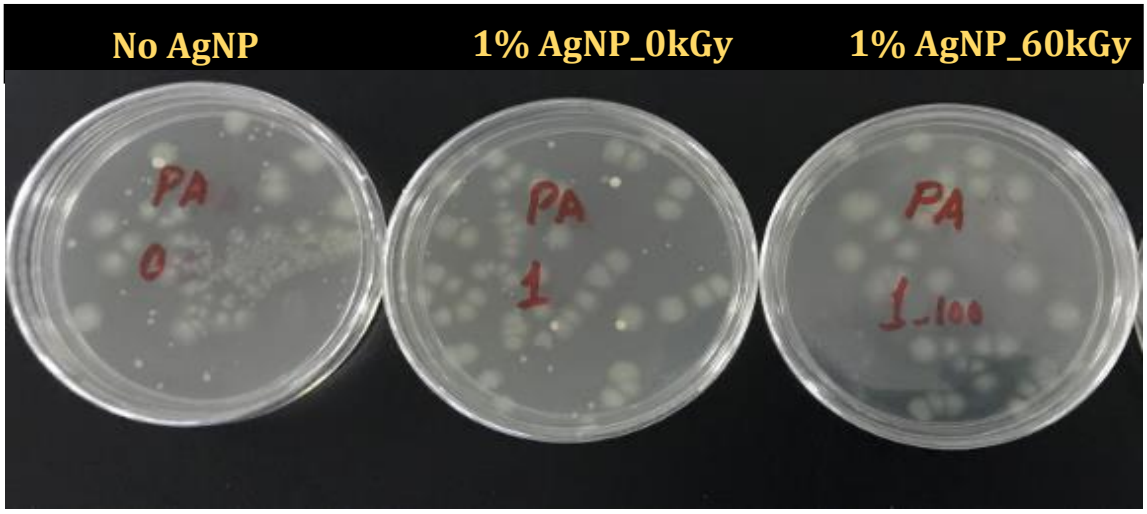


Figure 8.24 Growth of Pseudomonas aeruginosa after 6x dilution on different polymer blends

8.11 Visual Appearance

The thermoplastics elastomers based on PP/EVA/EPDM blends were white and translucent before and after radiation. From Figure 8.25, it can be noticed that the addition of AgNP resulted in changing the colour of the blends from white to dark. The intensity of darkness increased with increase in Ag content. The change in colour could be attributed mainly to the presence of AgNP in the polymer matrix. Stará et al. (2011), Eisa et al. (2012) and many others reported a similar trend of in-situ blend composites where the colour the polymers change was due to the dark nature of AgNP. This could serve as a serious limitation of using melt blended AgNP-ternary blends in manufacturing of food packaging products and healthcare products where administration of flow of fluids or the quantity of the fluids present is necessary (for example blood bags, storage vials and syringe barrels). However, it could be used in manufacturing drainage tubes, urinary catheters, dialysis tubes, stoppers, sealants, O-rings, coatings and gaskets where regular administration is not required.



Figure 8.25 Colour of ternary blends with AgNP

8.12 Summary

The addition of AgNP to ternary blend polymeric matrix resulted in the decrement of tensile and impact properties. The decrease in properties could mainly be attributed to the poor dispersion or localisation effect caused by the agglomeration of nanoparticles in polymer matrix. E-beam radiation on ternary blends/Ag nanocomposites did not show any significant change in thermal, mechanical and antimicrobial properties. This indicates products manufactured using AgNP incorporated ternary blends can be safely sterilized by E-beam. In the *in-vitro* analysis, it found that the all the blends (with and without AgNP) did not show any significant toxicity on HaCaT cells even upon radiation at 60 kGy and 100 kGy. While, the ternary blends with 1% Ag showed bacteriostatic effect on Staphylococcus aureus, no significant inhibition was found on Pseudomonas aeruginosa. On the other hand, the addition of AgNP changed the colour of polymer blends making them dark and opaque.

9 PRINCIPLE FINDINGS AND RECOMMENDATIONS FOR FURTURE WORK

9.1 Principal Findings

This thesis has enunciated the possibility of improving the properties of the PP/EPDM and PP/EPDM/EVA thermoplastic elastomers by E-beam radiation. Apart from improving the blend properties, E-beam also offers a dual advantage of sterilization. Both sterilization of products and improvement in properties can be achieved by single step process. Three different PP/EPDM blends with 30, 50 and 70% EPDM were compounded, characterized and compared with neat PP and EPDM polymers. All the blends were melt blended with optimized process parameters with a temperature of 165°C at 50 rpm for 10 min. The blends displayed intermediate mechanical and dynamic mechanical properties between neat PP and EPDM. No significant change in thermal stability was observed. The mere presence of EPDM decreased the crystallinity of the blends. Both PP and EPDM exist as partially miscible blends.

The gel content analysis indicated that EPDM cross-linked upon radiation and the extent of crosslinking increased with increasing radiation dose. However, on the other hand PP did not show significant crosslinking effect as chain scission dominated over crosslinking effect. The blends show intermediate crosslinking, where the extent of crosslinking increased with increasing EPDM content and radiation dose. The blends with ≤ 50% PP showed reduction in tensile strength upon radiation. Further, the blend with 80% EPDM showed an improvement of 36% at dose rate of 40 and 60 kGy, followed by a significant drop. However, the elongation at break and crystallinity of this blend showed a decreasing trend upon radiation due to crosslinking. No prominent improvement in stiffness, impact strength and other dynamic mechanical properties was recorded.

In order to improve or retain the properties of the blend with high PP content under radiation, an initiative to add EVA in 50 PP/50 EPDM was performed. Addition of EVA improved the impact strength significantly. A maximum of 11% increase in impact strength and 13% improvement in elongation at break was observed upon addition of 20% EVA. The crystallinity and stiffness of the blends reduced with EVA addition. Nevertheless, no prominent change in thermal stability was observed.

E-beam radiation was also conducted on the ternary blends. The addition of EVA decreased the extent of crosslinking in the blends, merely due to its lower crosslinking efficiency in comparison with EPDM. However, the crosslinking was just sufficient to retain the mechanical properties of ternary blend up to 40 kGy. In fact, an increase in tensile strength up to 29% was observed at 60 kGy. Further, the ternary blends could also retain their impact properties up to 60 kGy and increment of 15% was observed at 80 kGy. However, the tensile and impact properties were improved at an expense of elongation at break, where the ductility of the blend was reduced due to crosslinking. No conspicuous changes were observed on thermal stability, stiffness and morphology of the blends when radiated. Though the T_m and T_c decreased due to restriction imposed by crosslinking, there was no prominent change in crystallinity of the blends. Among all the ternary blends, 20EVA/30 EPDM/50PP showed maximum improvement in tensile strength and impact strength and retained all other properties when radiated within a dose range of 20-100 kGy. Thus, the ternary blends of PP/EPDM/EVA, especially the blend with 20 EVA can withstand the radiation sterilization which is performed at 25-40 kGy without losing its major properties. Further, if one is in the need to improve the properties, the blends should be radiated at 60 or 80 kGy depending upon product requirement.

Further as a step ahead, the PP/EPDM/EVA blend with Ag composites were compounded and characterized. The blend composites were prepared with 0.3 wt%, 0.5 wt% and 1 wt% Ag nanoparticle loading. The ternary blend-Ag nanocomposites exhibited improved impact strength and thermal properties with Ag loading. In contrast to impact strength, the tensile strength were observed to deteriorate even at 0.3wt% Ag loading. In addition, blend matrix had poor interfacial adhesion with the AgNP. All the changes could be attributed to the agglomeration of AgNP in the blend matrix. The E-beam did not help in the dispersion of AgNP and no significant change was observed. This gives us an insight that melt blending of AgNP at the studied process conditions are not effective. The purpose of adding AgNP is to impart antimicrobial properties to the material, which was studied using Pseudomonas aeruginosa and Staphylococcus aureus strains. The studies revealed that the blend composites showed bacteriostactic effects on Staphylococcus aureus which restricted the bacteria migration. However, no effect of bacterial inhibition was observed on Pseudomonas aeruginosa.

Finally, *in-vitro* analysis was used to aid in the final objective of this study. The biocompatibility of the prepared nanocomposites was determined based on their ability to

attach with HaCaT cell; thus allowing the cells to proliferate, and enhance their ability to differentiate. FESEM images of the cells-blend composites, as well as results of the MTT confirmed that the blends before and after radiation showed no significant toxicity.

The findings of this study suggesting the aim to enhance or retain at least few properties of PP based thermoplastic elastomer were achieved. It also leads to a possibility to replace PP or EPDM with PP/EPDM/EVA thermoplastic elastomer that could be improved and sterilized using E-beam radiation, bridging the gap between thermoset and thermoplastic materials while providing plastic like processing and rubber like properties. Subsequently, contributing to the current body of knowledge for developing E-beam sterilizable thermoplastic elastomers.

9.2 Future Prospects

This study, though profoundly contributes to the knowledge and feasibility of E-beam sterilizable PP/EPDM/EVA blends, it also gives rise to some limitations that could probably affect the commercialization of these blends. In most cases, the limitations are drawn from the lack of resources or the need for completion of project within the stipulated time. However, these limitations also serve as open leeway for future research.

Firstly, properties reported in this study were confined to processing, mechanical and thermal characterization. It is a known fact; this alone could not push the door to commercialization of these materials. More studies addressing the fatigue, kink resistance, flexural strength, reaction against medical fluids should be based on the product requirement. Now that the blends have shown to withstand radiation dose of 25-40 kGy by retaining its tensile, impact, dynamic mechanical and thermal properties, the odds of the other properties such as elongation at break and hardness being studied will increase. One of the important uplifting in the study is that the E-beam is a safe mode of sterilizing agent of the ternary blends as *in-vitro* studies showed no signs of significant toxicity. However, a detailed study on *in-vivo* procedures such as acute toxic system, MEM elution and dermal sensitization test must be carried to push these blends for commercialization.

Moreover, from the literature review it could be understood that the properties of the blends changes over the days due to oxidation (of scavenging free radicals created by radiation). This

could significantly affect the shelf life of the products manufactured using the PP/EPDM/EVA ternary blends. A detailed ageing and tests on mechanical properties should be performed to evaluate the shelf life of the products.

Another important finding was that the poor dispersion of AgNP in the thermoplastic elastomer blends. This will lead to future studies of enhancing the dispersion using various non-toxic dispersants. However, it should be taken to consideration that the additives used must be biocompatible and not prone to leaching effects. Apart from usage of additives, other physical methods such as sputtering and vapour deposition should be considered to improve its antibacterial efficacy. Though there are past studies related to these techniques, none ventured into synergetic effects of radiation when AgNP are sputtered or coated to polymeric blends by other means to fulfil the needs of sterilization.

REFERENCES

ABDELGAWAD, A. M., HUDSON, S. M. & ROJAS, O. J. 2014. Antimicrobial wound dressing nanofiber mats from multicomponent (chitosan/silver-NPs/polyvinyl alcohol) systems. *Carbohydrate Polymers,* 100**,** 166-178.

ABIONA, A. A. & OSINKOLU, A. G. 2010. Gamma-irradiation induced property modification of polypropylene. *International Journal of Physical Sciences,* 5**,** 960-967.

ABOLHASANI, M., AREFAZAR, A. & MOZDIANFARD, M. 2010. Effect of dispersed phase composition on morphological and mechanical properties of PET/EVA/PP ternary blends. *Journal of Polymer Science Part B: Polymer Physics,* 48**,** 251-259.

ABOLHASANI, M. M., AZAR, A. A. & SHOKOOHI, S. 2009. PET/EVA/PP ternary blends: An investigation of extended morphological properties. *Journal of applied polymer science,* 112**,** 1716-1728.

ABOU ZEID, M. M., RABIE, S. T., NADA, A. A., KHALIL, A. M. & HILAL, R. H. 2008. Effect of gamma irradiation on ethylene propylene diene terpolymer rubber composites. *Nuclear Instruments and Methods in Physics Research Section B: Beam Interactions with Materials and Atoms,* 266**,** 111-116.

ABRAHAM, A. C., CZAYKA, M. A. & FISCH, M. R. 2010. Electron beam irradiations of polypropylene syringe barrels and the resulting physical and chemical property changes. *Radiation Physics and Chemistry,* 79**,** 83-92.

ACHARYA, H., KUILA, T., SRIVASTAVA, S. & BHOWMICK, A. 2008. Effect of layered silicate on EPDM/EVA blend nanocomposite: Dynamic mechanical, thermal, and swelling properties. *Polymer Composites,* 29**,** 443-450.

ACTON, Q. A. 2013. *Advances in Bacterial Physiological Phenomena Research and Application: 2013 Edition: ScholarlyPaper*, ScholarlyEditions.

ADJEI, A. A., KUMA, G. K., TETTEY, Y., AYEH-KUMI, P. F., OPINTAN, J., APEAGYEI, F., ANKRAH, J. O., ADIKU, T. K. & NARTER-OLAGA, E. G. 2009. Bacterial contamination of blood and blood components in three major blood transfusion centers, Accra, Ghana. *Jpn J Infect Dis,* 62**,** 265-9.

AGARWALA, M., BARMAN, T., GOGOI, D., CHOUDHURY, B., PAL, A. R. & YADAV, R. 2014. Highly effective antibiofilm coating of silver–polymer nanocomposite on polymeric medical devices deposited by one step plasma process. *Journal of Biomedical Materials Research Part B: Applied Biomaterials,* 102**,** 1223-1235.

AGHJEH, M. R., KHONAKDAR, H. A. & JAFARI, S. H. 2015. Application of mean-field theory in PP/EVA blends by focusing on dynamic mechanical properties in correlation with miscibility analysis. *Composites Part B: Engineering,* 79**,** 74-82.

AJILI, S. H., EBRAHIMI, N. G. & KHORASANI, M. T. 2003. Study on thermoplastic polyurethane/polypropylene (TPU/PP) blend as a blood bag material. *Journal of Applied Polymer Science,* 89**,** 2496-2501.

ALARIQI, S. A., AL-AREQI, N. A. & ALAGHBARI, E. S. 2015. γ-Radiation-Induced Crystallinity Changes and Thermal Behavior of Low-Crystalline Polypropylene Films. *American Journal of Chemistry and Application,* 2**,** 12-16.

ANDERSON, M. J. 2001. A new method for non-parametric multivariate analysis of variance. *Austral Ecology,* 26**,** 32-46.

ANTUNES, C., VAN DUIN, M. & MACHADO, A. 2012. Effect of crosslinking on morphology and phase inversion of EPDM/PP blends. *Materials Chemistry and Physics,* 133**,** 410-418.

APREM, A. S., JOSEPH, K. & THOMAS, S. 2005. Recent developments in crosslinking of elastomers. *Rubber chemistry and technology,* 78**,** 458-488.

ARNOLD, K., AVERY, L., BENNETT, R., BRINSLEY-RAINISCH, K., BOYTER, M., COFFIN, N., DESHPANDE, S., DUDECK, M. A., EDWARDS, J. R. & FULLER, S. National and state healthcare-associated infections progress report.

BAK, J., LADEFOGED, S. D., TVEDE, M., BEGOVIC, T. & GREGERSEN, A. 2009. Dose requirements for UVC disinfection of catheter biofilms. *Biofouling,* 25**,** 289-296.

BALAJI, A. B., KHALID, M. & RATNAM, C. T. 2016. Characteristics of E-beam Sterilized PP/EPDM blends for Medical Applications. *한국고분자학회 학술대회 연구논문 초록집* 41**,** 322-322.

BHATIA, S. K. & YETTER, A. B. 2008. Correlation of visual in vitro cytotoxicity ratings of biomaterials with quantitative in vitro cell viability measurements. *Cell biology and toxicology,* 24**,** 315-319.

BIEDERMANN, M., CASTILLO, R., RIQUET, A.-M. & GROB, K. 2014. Comprehensive two-dimensional gas chromatography for determining the effect of electron beam treatment of polypropylene used for food packaging. *Polymer Degradation and Stability,* 99**,** 262-273.

BLOM, H., TEH, J. & RUDIN, A. 1996. iPP/HDPE blends. II. Modification with EPDM and EVA. *Journal of applied polymer science,* 60**,** 1405-1417.

BORGGREVE, R., GAYMANS, R. & SCHUIJER, J. 1989. Impact behaviour of nylon-rubber blends: 5. Influence of the mechanical properties of the elastomer. *Polymer,* 30**,** 71-77.

BOUCHART, V., BHATNAGAR, N., BRIEU, M., GHOSH, A. & KONDO, D. 2008. Study of EPDM/PP polymeric blends: mechanical behavior and effects of compatibilization. *Comptes Rendus Mecanique,* 336**,** 714-721.

BOURGES, F., BUREAU, G. & PASCAT, B. 1993. Effects of electron beam irradiation on the migration of antioxidants and their degradation products from commercial polypropylene into food simulating liquids. *Food Additives & Contaminants,* 10**,** 443-452.

BRECHER, M. E. & HAY, S. N. 2005. Bacterial contamination of blood components. *Clinical microbiology reviews,* 18**,** 195-204.

BUSFIELD, W. & O'DONNELL, J. 1979. Effects of gamma radiation on the mechanical properties and crystallinity of polypropylene film. *European Polymer Journal,* 15**,** 379-387.

CAMACHO, P. H., MORALES-CEPEDA, A. B., SALAS-PAPAYANOPOLOS, H., BAUTISTA, J. E., CASTRO, C., LOZANO, T., SANCHEZ-VALDES, S. & LAFLEUR, P. G. 2017. Crystallization behavior of polypropylene/silver nanocomposites using polyethylene glycol as reducing agent and interface modifier. *Journal of Thermoplastic Composite Materials,* 30**,** 662-677.

CARDOSO, E. C., SCAGLIUSI, S. R. & LUGÃO, A. B. 2016. Gamma-Radiation Effect on Mechanical Properties of Pp/Epdm Polymeric Blends.

CHAPIRO, A. 1964. Radiation chemistry of polymers. *Radiation Research Supplement,* 4**,** 179-191.

CHARLESBY, A. & PINNER, S. H. 1959. Analysis of the Solubility Behaviour of Irradiated Polyethylene and Other Polymers. *Proceedings of the Royal Society of London. Series A. Mathematical and Physical Sciences,* 249**,** 367-386.

CHATTOPADHYAY, S., CHAKI, T. & BHOWMICK, A. 2001. Electron beam modification of thermoplastic elastomeric blends made from polyolefins. *Journal of materials science,* 36**,** 4323-4330.

CHEN, Y., XU, C., CAO, L. & CAO, X. 2013. Highly toughened polypropylene/ethylene–propylene-diene monomer/zinc dimethacrylate ternary blends prepared via peroxide-induced dynamic vulcanization. *Materials Chemistry and Physics,* 138**,** 63-71.

CHENNAKESAVULU, K., BASARIYA, M. R., SREEDEVI, P., BHASKAR RAJU, G., PRABHAKAR, S. & RAO, S. S. 2011. Study on thermal decomposition of calix[4]arene and its application in thermal stability of polypropylene. *Thermochimica Acta,* 515**,** 24-31.

CORAN, A. Y. & PATEL, R. 1980. Rubber-thermoplastic compositions. Part I. EPDM-polypropylene thermoplastic vulcanizates. *Rubber Chemistry and Technology,* 53**,** 141-150.

DA COSTA, H. M., RAMOS, V. D., DA SILVA, W. S. & SIRQUEIRA, A. S. 2010. Analysis and optimization of polypropylene (PP)/ethylene–propylene–diene monomer (EPDM)/scrap rubber tire (SRT) mixtures using RSM methodology. *Polymer Testing,* 29**,** 572-578.

DA COSTA, H. M., RAMOS, V. D. & ROCHA, M. C. 2006. Analysis of thermal properties and impact strength of PP/SRT, PP/EPDM and PP/SRT/EPDM mixtures in single screw extruder. *Polymer Testing,* 25**,** 498-503.

DAI, T., TEGOS, G. P., ST. DENIS, T. G., ANDERSON, D., SINOFSKY, E. & HAMBLIN, M. R. 2011. Ultraviolet-C Irradiation for Prevention of Central Venous Catheter-related Infections: An In Vitro Study. *Photochemistry and Photobiology,* 87**,** 250-255.

DALAI, S. & WENXIU, C. 2002a. Radiation effects on HDPE/EVA blends. *Journal of applied polymer science,* 86**,** 553-558.

DALAI, S. & WENXIU, C. 2002b. Radiation effects on poly (propylene)(PP)/ethylene–vinyl acetate copolymer (EVA) blends. *Journal of applied polymer science,* 86**,** 3420-3424.

DALLAS, P., SHARMA, V. K. & ZBORIL, R. 2011. Silver polymeric nanocomposites as advanced antimicrobial agents: classification, synthetic paths, applications, and perspectives. *Adv Colloid Interface Sci,* 166**,** 119-35.

DATTA, P., RANI, H., CHAUHAN, R., GOMBAR, S. & CHANDER, J. 2014. Health-care-associated infections: Risk factors and epidemiology from an intensive care unit in Northern India. *Indian journal of anaesthesia,* 58**,** 30.

DATTA, S., NASKAR, K., JELENIC, J. & NOORDERMEER, J. 2005. Dynamically vulcanized PP/EPDM blends by multifunctional peroxides: Characterization with various analytical techniques. *Journal of applied polymer science,* 98**,** 1393-1403.

DAVENAS, J., STEVENSON, I., CELETTE, N., CAMBON, S., GARDETTE, J., RIVATON, A. & VIGNOUD, L. 2002a. Stability of polymers under ionising radiation: the many faces of radiation interactions with polymers. *Nuclear Instruments and Methods in Physics Research Section B: Beam Interactions with Materials and Atoms,* 191**,** 653-661.

DAVENAS, J., STEVENSON, I., CELETTE, N., CAMBON, S., GARDETTE, J. L., RIVATON, A. & VIGNOUD, L. 2002b. Stability of polymers under ionising radiation: The many faces of radiation interactions with polymers. *Nuclear Instruments and Methods in Physics Research Section B: Beam Interactions with Materials and Atoms,* 191**,** 653-661.

DE RISI, F. & NOORDERMEER, J. W. 2007. Effect of methacrylate co-agents on peroxide cured PP/EPDM thermoplastic vulcanizates. *Rubber chemistry and technology,* 80**,** 83-99.

DEEPALAXMI, R. & RAJINI, V. 2014. Property enhancement of SiR-EPDM blend using electron beam irradiation. *Journal of Electrical Engineering and Technology,* 9**,** 984-990.

DOPICO-GARCÍA, M., LOPEZ-VILARINO, J. & GONZÁLEZ-RODRÍGUEZ, M. 2007. Antioxidant content of and migration from commercial polyethylene, polypropylene, and polyvinyl chloride packages. *Journal of agricultural and food chemistry,* 55**,** 3225-3231.

DOWLING, D., DONNELLY, K., MCCONNELL, M., ELOY, R. & ARNAUD, M. 2001. Deposition of anti-bacterial silver coatings on polymeric substrates. *Thin Solid Films,* 398**,** 602-606.

DROBNY, J. G. 2012. *Ionizing Radiation and Polymers: Principles, Technology, and Applications*, Elsevier Science.

DUBEY, K., BHARDWAJ, Y., CHAUDHARI, C., BHATTACHARYA, S., GUPTA, S. & SABHARWAL, S. 2006a. Radiation effects on SBR–EPDM blends: A correlation with blend morphology. *Journal of Polymer Science Part B: Polymer Physics,* 44**,** 1676-1689.

DUBEY, K., BHARDWAJ, Y., CHAUDHARI, C., KUMAR, V., GOEL, N. & SABHARWAL, S. 2009. Radiation processed ethylene vinyl acetate-multiple walled carbon nanotube nano-composites: effect of MWNT addition on the gel content and crosslinking density. *eXpress Polymer Letters,* 3**,** 492-500.

DUBEY, K., BHARDWAJ, Y., CHAUDHARI, C. & SABHARWAL, S. 2006b. Role of blend morphology in the radiation processing of SBR-EPDM blends. *BARC NEWSLETTER,* 273**,** 92.

DURAIRAJ, R., AMIRULHUSNI, A. N., PALANISAMY, N. K., MOHD-ZAIN, Z. & PING, L. J. 2012. Antibacterial effect of silver nanoparticles on multi drug resistant Pseudomonas aeruginosa. *World Acad Sci Eng Technol,* 6**,** 210-213.

DUTTA, J. & NASKAR, K. 2014. Investigation of morphology, mechanical, dynamic mechanical and thermal behaviour of blends based on ethylene vinyl acetate (EVA) and thermoplastic polyurethane (TPU). *RSC Advances,* 4**,** 60831-60841.

EDER, A. F., KENNEDY, J. M., DY, B. A., NOTARI, E. P., WEISS, J. W., FANG, C. T., WAGNER, S., DODD, R. Y. & BENJAMIN, R. J. 2007. Bacterial screening of apheresis platelets and the residual risk of septic transfusion reactions: the American Red Cross experience (2004‐2006). *Transfusion,* 47**,** 1134-1142.

EISA, W. H., ABDEL-MONEAM, Y. K., SHABAKA, A. & HOSAM, A. E. M. 2012. In situ approach induced growth of highly monodispersed Ag nanoparticles within free standing PVA/PVP films. *Spectrochimica Acta Part A: Molecular and Biomolecular Spectroscopy,* 95**,** 341-346.

ELIZABETH C. L. CARDOSO, S. R. S., ADEMAR B. LUGÃO. 2016. Gamma-Radiation Effect on Mechanical Properties of Pp/Epdm Polymeric Blends. *Journal of Materials Sciences and Applications,* Vol. 2**,** 1-9.

ETO, H., ONO, Y., OGINO, A. & NAGATSU, M. 2008. Low‐Temperature Internal Sterilization of Medical Plastic Tubes Using a Linear Dielectric Barrier Discharge. *Plasma Processes and Polymers,* 5**,** 269-274.

EZZATI, P., GHASEMI, I., KARRABI, M. & AZIZI, H. 2008. Rheological behaviour of PP/EPDM blend: the effect of compatibilization. *Iran Polym J,* 17**,** 670-679.

FAGES, E., PASCUAL, J., FENOLLAR, O., GARCÍA-SANOGUERA, D. & BALART, R. 2011. Study of antibacterial properties of polypropylene filled with surfactant-coated silver nanoparticles. *Polymer Engineering & Science,* 51**,** 804-811.

FENG, W., YUAN, L. H., ZHENG, S. Y., HUANG, G. L., QIAO, J. L. & ZHOU, Y. 2000. The effect of p-tert-butylcalix[n]arene on γ-radiation degradation of polypropylene. *Radiation Physics and Chemistry,* 57**,** 425-429.

FINTZOU, A. T., BADEKA, A. V., KONTOMINAS, M. G. & RIGANAKOS, K. A. 2006. Changes in physicochemical and mechanical properties of γ-irradiated polypropylene syringes as a function of irradiation dose. *Radiation Physics and Chemistry,* 75**,** 87-97.

FINTZOU, A. T., KONTOMINAS, M. G., BADEKA, A. V., STAHL, M. R. & RIGANAKOS, K. A. 2007. Effect of electron-beam and gamma-irradiation on physicochemical and mechanical properties of polypropylene syringes as a function of irradiation dose: Study under vacuum. *Radiation Physics and Chemistry,* 76**,** 1147-1155.

FIOL, A. G., HORVATH, R., SCHOENBERG, C., AHMED, N., DHAR, S. K. & LE, V. 2016. Comparison of Changes in Tensile Strength in Three Different Flexible Epidural Catheters Under Various Conditions. *Anesthesia & Analgesia,* 123**,** 233-237.

FISCHER, J. P., BECKER, U., VON HALASZ, S. P., MÜCK, K. F., PÜSCHNER, H., RÖSINGER, S., SCHMIDT, A. & SUHR, H. H. The preparation and characterization of surface‐grafted plastic materials designed for the evaluation of their tissue and blood compatibility. Journal of Polymer Science: Polymer Symposia, 1979. Wiley Online Library, 443-463.

FRAGA, A., RUSECKAITE, R. A. & JIMÉNEZ, A. 2005. Thermal degradation and pyrolysis of mixtures based on poly (3-hydroxybutyrate-8%-3-hydroxyvalerate) and cellulose derivatives. *Polymer Testing,* 24**,** 526-534.

FROUNCHI, M., DADBIN, S. & PANAHINIA, F. 2006. Comparison between electron-beam and chemical crosslinking of silicone rubber. *Nuclear Instruments and Methods in Physics Research Section B: Beam Interactions with Materials and Atoms,* 243**,** 354-358.

FUNKE, W., OKAY, O. & JOOS-MÜLLER, B. 1998. Microgels-Intramolecularly Crossünked Macromolecules with a Globular Structure. *Microencapsulation Microgels Iniferters.* Springer.

FURNO, F., MORLEY, K. S., WONG, B., SHARP, B. L., ARNOLD, P. L., HOWDLE, S. M., BAYSTON, R., BROWN, P. D., WINSHIP, P. D. & REID, H. J. 2004. Silver nanoparticles and polymeric medical devices: a new approach to prevention of infection? *Journal of Antimicrobial Chemotherapy,* 54**,** 1019-1024.

GAO, J., LU, Y., WEI, G., ZHANG, X., LIU, Y. & QIAO, J. 2002. Effect of radiation on the crosslinking and branching of polypropylene. *Journal of applied polymer science,* 85**,** 1758-1764.

GEISSLER, W., ZOTT, H. & HEUSINGER, H. 1978. Investigations on the mechanism of radiation induced crosslinking in ethylene-propylene-diene terpolymers. *Die Makromolekulare Chemie,* 179**,** 697-705.

GEORGE, K., KOMALAN, C., KUMAR, P., VARUGHESE, K. & THOMAS, S. 2007. Dynamic mechanical analysis of binary and ternary polymer blends based on nylon copolymer/EPDM rubber and EPM grafted maleic anhydride compatibilizer.

GEORGE, S., NEELAKANTAN, N. R., VARUGHESE, K. T. & THOMAS, S. 1997. Dynamic mechanical properties of isotactic polypropylene/nitrile rubber blends: Effects of blend ratio, reactive compatibilization, and dynamic vulcanization. *Journal of Polymer Science Part B: Polymer Physics,* 35**,** 2309-2327.

GHEYSARI, D., BEHJAT, A. & HAJI-SAEID, M. 2001. The effect of high-energy electron beam on mechanical and thermal properties of LDPE and HDPE. *European polymer journal,* 37**,** 295-302.

GHOSH, K. & MAITI, S. N. 1996. Mechanical properties of silver-powder-filled polypropylene composites. *Journal of Applied Polymer Science,* 60**,** 323-331.

GHOSH, P., CHATTOPADHYAY, B. & SEN, A. K. 1996. Thermal and oxidative degradation of PE-EPDM blends vulcanized differently using sulfur accelerator systems. *European polymer journal,* 32**,** 1015-1021.

GINZBURG, V. V. 2005. Influence of nanoparticles on miscibility of polymer blends. A simple theory. *Macromolecules,* 38**,** 2362-2367.

GIRI, R., NASKAR, K. & NANDO, G. B. 2012. Effect of electron beam irradiation on dynamic mechanical, thermal and morphological properties of LLDPE and PDMS rubber blends. *Radiation Physics and Chemistry,* 81**,** 1930-1942.

GROSU, E., RÂPĂ, M., TOMESCU, A., NEMEŞ, E., ZAHARESCU, T., JIPA, S., SETNESCU, R. & VASILE, C. 2003. Radiation processing of elastomer materials for medical uses. *Nuclear Instruments and Methods in Physics Research Section B: Beam Interactions with Materials and Atoms,* 208**,** 220-224.

HA, C. S., IHM, D. J. & KIM, S. C. 1986. Structure and properties of dynamically cured EPDM/PP blends. *Journal of Applied Polymer Science,* 32**,** 6281-6297.

HAMMAD, A. 2008. Microbiological aspects of radiation sterilization. *Trends in radiation sterilization of health care products.*

HAN, D.-H., JANG, J.-H., CHO, B.-G., KIM, B.-N. & SEO, G.-S. 2006. Melt complex viscosity and molecular weights for homo-polypropylene modified by grafting bifunctional monomers under electron beam irradiation. *Polymer,* 47**,** 6592-6597.

HARNISCHFEGER, P., KINZEL, P. & JUNGNICKEL, B. J. 1990. The influence of electron irradiation on the mechanical properties of polypropylene/EPDM rubber blends. *Macromolecular Materials and Engineering,* 175**,** 157-168.

HASSAN, M. M., MAHMOUD, G. A., EL‐NAHAS, H. H. & HEGAZY, E. S. A. 2007. Reinforced material from reclaimed rubber/natural rubber, using electron beam and thermal treatment. *Journal of Applied Polymer Science,* 104**,** 2569-2578.

HEGAZY, E. S. A., SEGUCHI, T., ARAKAWA, K. & MACHI, S. 1981. Radiation‐induced oxidative degradation of isotactic polypropylene. *Journal of Applied Polymer Science,* 26**,** 1361-1372.

HILLYER, C. D., JOSEPHSON, C. D., BLAJCHMAN, M. A., VOSTAL, J. G., EPSTEIN, J. S. & GOODMAN, J. L. 2003. Bacterial Contamination of Blood Components: Risks, Strategies, and Regulation Joint ASH and AABB Educational Session in Transfusion Medicine. *ASH Education Program Book,* 2003**,** 575-589.

HORNBACK, J. M. 2005. *Organic Chemistry*, Cengage Learning.

IBA 2014. REVIEW OF RADIATION STERILIZATION TECHNOLOGIES FOR MEDICAL DEVICES.

INOUE, T. & SUZUKI, T. 1995. Selective crosslinking reaction in polymer blends. III. The effects of the crosslinking of dispersed EPDM particles on the impact behavior of PP/EPDM blends. *Journal of applied polymer science,* 56**,** 1113-1125.

INOUE, T. & SUZUKI, T. 1996. Selective crosslinking reaction in polymer blends. IV. The effects on the impact behavior of PP/EPDM blends (2). *Journal of applied polymer science,* 59**,** 1443-1450.

IVERSON, A., KIM, S. & SOJIPHAN, K. 2004. Materials Selection Analysis: Bag for Viable Blood Storage.

JAFARI, S. & GUPTA, A. 2000. Impact strength and dynamic mechanical properties correlation in elastomer‐modified polypropylene. *Journal of applied polymer science,* 78**,** 962-971.

JAIN, A. K., NAGPAL, A. K., SINGHAL, R. & GUPTA, N. K. 2000. Effect of dynamic crosslinking on impact strength and other mechanical properties of polypropylene/ethylene-propylene-diene rubber blends. *Journal of Applied Polymer Science,* 78**,** 2089-2103.

JIA, H., WANG, H. & CHEN, W. 2007. The combination effect of hindered amine light stabilizers with UV absorbers on the radiation resistance of polypropylene. *Radiation Physics and Chemistry,* 76**,** 1179-1188.

JOHN, B., VARUGHESE, K., OOMMEN, Z., PÖTSCHKE, P. & THOMAS, S. 2003a. Dynamic mechanical behavior of high‐density polyethylene/ethylene vinyl acetate copolymer blends: The effects of the blend ratio, reactive compatibilization, and dynamic vulcanization. *Journal of Applied Polymer Science,* 87**,** 2083-2099.

JOHN, B., VARUGHESE, K. T., OOMMEN, Z., PÖTSCHKE, P. & THOMAS, S. 2003b. Dynamic mechanical behavior of high-density polyethylene/ethylene vinyl acetate copolymer blends: The effects of the blend ratio, reactive compatibilization, and dynamic vulcanization. *Journal of Applied Polymer Science,* 87**,** 2083-2099.

JOKAR, M., RAHMAN, R. A., IBRAHIM, N. A., ABDULLAH, L. C. & TAN, C. P. 2012. Melt production and antimicrobial efficiency of low-density polyethylene (LDPE)-silver nanocomposite film. *Food and bioprocess technology,* 5**,** 719-728.

JONES, N., RAY, B., RANJIT, K. T. & MANNA, A. C. 2008. Antibacterial activity of ZnO nanoparticle suspensions on a broad spectrum of microorganisms. *FEMS microbiology letters,* 279**,** 71-76.

KALDANY, A. 1993. Biocompatible tube of polyurethanes and polybutadiene with hard cured sections and soft flexible uncured sections for ease of adjustment and conformation in medical equipment. Google Patents.

KAMPOURIS, E. & ANDREOPOULOS, A. 1989. Gel content determination in cross-linked polyethylene. *Biomaterials,* 10**,** 206-208.

KARPUZ, M. & ÖZER, A. Y. 2016. Syringes As Medical Devices. *FABAD J. Pharm. Sci,* 41**,** 27-37.

KELLY, M., MACDOUGALL, K., OLABISI, O. & MCGUIRE, N. 2017. In vivo response to polypropylene following implantation in animal models: a review of biocompatibility. *International urogynecology journal,* 28**,** 171-180.

KHALID, M., RATNAM, C. T., LUQMAN, C., SALMIATON, A., CHOONG, T. S. Y. & JALALUDIN, H. 2009. Thermal and dynamic mechanical behavior of cellulose-and oil palm empty fruit bunch (OPEFB)-filled polypropylene biocomposites. *Polymer-Plastics Technology and Engineering,* 48**,** 1244-1251.

KHONAKDAR, H., JAFARI, S., WAGENKNECHT, U. & JEHNICHEN, D. 2006. Effect of electron-irradiation on cross-link density and crystalline structure of low-and high-density polyethylene. *Radiation Physics and Chemistry,* 75**,** 78-86.

KIM, B. C., HWANG, S. S., LIM, K. Y. & YOON, K. J. 2000. Toughening of PP/EPDM blend by compatibilization. *Journal of applied polymer science,* 78**,** 1267-1274.

KIM, J. S., KUK, E., YU, K. N., KIM, J.-H., PARK, S. J., LEE, H. J., KIM, S. H., PARK, Y. K., PARK, Y. H., HWANG, C.-Y., KIM, Y.-K., LEE, Y.-S., JEONG, D. H. & CHO, M.-H. 2007. Antimicrobial effects of silver nanoparticles. *Nanomedicine: Nanotechnology, Biology and Medicine,* 3**,** 95-101.

KLEMCHUK, P. P. 1993. Protecting polymers against damage from gamma radiation. *Radiation Physics and Chemistry,* 41**,** 165-172.

KNETSCH, M. L. & KOOLE, L. H. 2011. New strategies in the development of antimicrobial coatings: the example of increasing usage of silver and silver nanoparticles. *Polymers,* 3**,** 340-366.

KOCAK, D., AKALIN, M. & MERDAN, N. 2016. Investigation of the mechanical, thermal, and morphological properties of isotactic polypropylene/linear low-density polyethylene/ethylene vinyl acetate polymer blends and their fibers. *Journal of Industrial Textiles,* 45**,** 879-895.

KONDO, M. & DOLE, M. 1966. Radiation Chemistry of Isotactic and Atactic Polypropylene. III. Radiolysis in the Presence of Nitrous Oxide1. *The Journal of Physical Chemistry,* 70**,** 883-889.

KOSTOSKI, D. & STOJANOVIĆ, Z. 1995. Radiation-induced crystallinity changes and melting behavior of drawn isotactic polypropylene. *Polymer degradation and stability,* 47**,** 353-356.

KRAUSE, S. 1972. Polymer compatibility. *Journal of Macromolecular Science—Reviews in Macromolecular Chemistry,* 7**,** 251-314.

KREBS, M. C., BÉCASSE, P., VERJAT, D. & DARBORD, J. C. 1998. Gas–plasma sterilization: relative efficacy of the hydrogen peroxide phase compared with that of the plasma phase. *International Journal of Pharmaceutics,* 160**,** 75-81.

KRUPA, I. & LUYT, A. 2001. Thermal properties of isotactic polypropylene degraded with gamma irradiation. *Polymer Degradation and Stability,* 72**,** 505-508.

KUILA, T., SRIVASTAVA, S. & BHOWMICK, A. K. 2009. Ethylene vinyl acetate/ethylene propylene diene terpolymer‐blend‐layered double hydroxide nanocomposites. *Polymer Engineering & Science,* 49**,** 585-591.

LARA, H. H., AYALA-NÚNEZ, N. V., TURRENT, L. D. C. I. & PADILLA, C. R. 2010. Bactericidal effect of silver nanoparticles against multidrug-resistant bacteria. *World Journal of Microbiology and Biotechnology,* 26**,** 615-621.

LEE, K.-H. & CHU, C.-C. 1996. Gamma irradiation sterilizing of biomaterial medical devices or products, with improved degradation and mechanical properties. Google Patents.

LEVERNIER, J. S. 2010. Surgical covering material. Google Patents.

LIANG, G., BAO, S. & TJONG, S. C. 2007. Microstructure and properties of polypropylene composites filled with silver and carbon nanotube nanoparticles prepared by melt-compounding. *Materials Science and Engineering: B,* 142**,** 55-61.

LIU, Q., WU, J., TAN, T., ZHANG, L., CHEN, D. & TIAN, W. 2009. Preparation, properties and cytotoxicity evaluation of a biodegradable polyester elastomer composite. *Polymer Degradation and Stability,* 94**,** 1427-1435.

LOPEZ-MANCHADO, M., TORRE, L. & KENNY, J. M. 2000. Kinetic analysis of the thermal degradation of PP-EPDM blends. *Rubber chemistry and technology,* 73**,** 694-705.

LOPEZ-MANCHADO, M. A., ARROYO, M. & KENNY, J. M. 2001. New Developments in Dynamically Cured PP—EPDM Blends. *Rubber chemistry and technology,* 74**,** 211-220.

LÓPEZ MANCHADO, M. A. & KENNY, J. M. 2001. Use of Benzene-1, 3-Bis (Sulfonyl) Azide as Crosslinking Agent of TPVs Based on EPDM Rubber—Polyolefin Blends. *Rubber chemistry and technology,* 74**,** 198-210.

LUAN, S., SHI, H., YAO, Z., WANG, J., SONG, Y. & YIN, J. 2010. Effect of electron beam irradiation sterilization on the biomedical poly (octene-co-ethylene)/polypropylene films. *Nuclear Instruments and Methods in Physics Research Section B: Beam Interactions with Materials and Atoms,* 268**,** 1474-1477.

LUAN, S., YANG, H., SHI, H., ZHAO, J., WANG, J. & YIN, J. 2011. Stabilization of polypropylene, polypropylene blends with poly (styrene-b-(ethylene-co-butylene)-b-styrene) under irradiation: a comparative investigation. *Nuclear Instruments and Methods in Physics Research Section B: Beam Interactions with Materials and Atoms,* 269**,** 94-99.

LUGÃO, A. B., CARDOSO, E. C. L., LIMA, L. F. C. P., HUSTZLER, B. & TOKUMOTO, S. 2003. Characterization study of gamma-irradiated, high melt-strength polypropylene. *Nuclear Instruments and Methods in Physics Research Section B: Beam Interactions with Materials and Atoms,* 208**,** 252-255.

LUGÃO, A. B., HUTZLER, B., OJEDA, T., TOKUMOTO, S., SIEMENS, R., MAKUUCHI, K. & VILLAVICENCIO, A.-L. C. 2000. Reaction mechanism and rheological properties of polypropylene irradiated under various atmospheres. *Radiation Physics and Chemistry,* 57**,** 389-392.

MAJUMDER, P. S. & BHOWMICK, A. K. 1999. Surface-and bulk-properties of EPDM rubber modified by electron beam irradiation. *Radiation Physics and Chemistry,* 53**,** 63-78.

MAKI, D. G. & TAMBYAH, P. A. 2001. Engineering out the risk for infection with urinary catheters. *Emerging Infectious Diseases,* 7**,** 342-347.

MAKUNI, N., SIMANGO, C. & MAVENYENGWA, R. T. 2015. Prevalence of bacterial contamination in blood and blood products at the National Blood Service Zimbabwe. *The Journal of Infection in Developing Countries,* 9**,** 421-424.

MANCHADO, M. L., BIAGIOTTI, J., TORRE, L. & KENNY, J. 2000. Polypropylene crystallization in an ethylene-propylene-diene rubber matrix. *Journal of thermal analysis and calorimetry,* 61**,** 437-450.

MANSHAIE, R., NOURI KHORASANI, S., JAHANBANI VESHARE, S. & REZAEI ABADCHI, M. 2011. Effect of electron beam irradiation on the properties of natural rubber (NR)/styrene–butadiene rubber (SBR) blend. *Radiation Physics and Chemistry,* 80**,** 100-106.

MARKARIAN, J. 2008. Thermoplastic elastomer compounds continue upward trend. *Plastics, Additives and Compounding,* 10**,** 38-43.

MARTAKIS, N., NIAOUNAKIS, M. & PISSIMISSIS, D. 1994. Gamma‐sterilization effects and influence of the molecular weight distribution on the postirradiation resistance of polypropylene for medical devices. *Journal of applied polymer science,* 51**,** 313-328.

MCDONNELL, G. 2012. Gas Plasma Sterilization. *Russell, Hugo & Ayliffe's: Principles and Practice of Disinfection, Preservation and Sterilization, 5th Edition***,** 333-342.

MCKEEN, L. W. 2012. *The Effect of Sterilization on Plastics and Elastomers*, Elsevier Science.

MEENAKUMARI, S., ARUNACHALAM, K. D. & KUMAR, A. S. 2013. Screening and characterisation of silver nanoparticles for the prevention of biofilm in urinary catheters. *Asian Journal of Chemistry,* 25**,** S347-S349.

MENDES, G. C., BRANDAO, T. R. & SILVA, C. L. 2007. Ethylene oxide sterilization of medical devices: a review. *American journal of infection control,* 35**,** 574-581.

MIHAILOVA, M., KRESTEVA, M., AIVAZOVA, N., KRESTEV, V. & NEDKOV, E. 1999. X-ray investigation of polypropylene and poly (ethylene-co-vinyl acetate) blends irradiated with fast electrons. *Radiation Physics and Chemistry,* 56**,** 581-589.

MIHAYLOVA, M., KRESTEVA, M., PEREÑA, J. & PHILLIPS, P. 2001. Dynamic mechanical properties of polymer blends of polypropylene and poly (ethylene-co-vinyl acetate) irradiated with fast electrons. *Bulgarian Journal of Physics,* 28**,** 85-94.

MIORINI, T. Sterilization of Medical Devices.

MISHEVA, M., MIHAYLOVA, M., DJOURELOV, N., KRESTEVA, M., KRESTEV, V. & NEDKOV, E. 2000. Positron annihilation lifetime spectroscopy studies of irradiated poly(propylene-co-ethylene)/poly(ethylene-co-vinyl acetate) blends. *Radiation Physics and Chemistry,* 58**,** 39-47.

MISHRA, S., BALAKRISHNAN, S. & CHANDRA, R. 1998. Thermal stability of ethylene–vinyl acetate and ethylene–propylene–diene (EVA–EPDM) blends. *Journal of applied polymer science,* 70**,** 1829-1835.

MITTAL, V. 2016. *Functional Polymer Blends: Synthesis, Properties, and Performance*, CRC Press.

MOHAMAD, Z., ISMAIL, H. & RATNAM, C. T. 2006. Characterization of epoxidized natural rubber/ethylene vinyl acetate (ENR-50/EVA) blend: Effect of blend ratio. *Journal of Applied Polymer Science,* 99**,** 1504-1515.

MOHAMMAD, M. A., MUHAMMAD, M., DEW, S. K. & STEPANOVA, M. 2012. Fundamentals of electron beam exposure and development. *Nanofabrication.* Springer.

MUKHERJEE, A., SADIQ, L., PRATHNA, T. & CHANDREASEKARAN, N. 2011. Antimicrobial activity of aluminium oxide nanoparticles for potential clinical applications. *Science against*

microbial pathogens: communicating current research and technological advances, 1**,** 245-251.

MUÑOZ-BONILLA, A. & FERNÁNDEZ-GARCÍA, M. 2012. Polymeric materials with antimicrobial activity. *Progress in Polymer Science,* 37**,** 281-339.

MUNUSAMY, Y., ISMAIL, H. & RATNAM, C. T. 2012. Effect of organoclay loading on the crosslinking and degradation of irradiated ethylene(vinyl acetate) copolymer/natural rubber nanocomposites. *Journal of Reinforced Plastics and Composites,* 31**,** 946-958.

NADERI, G., LAFLEUR, P. G. & DUBOIS, C. 2007. Microstructure-properties correlations in dynamically vulcanized nanocomposite thermoplastic elastomers based on PP/EPDM. *Polymer Engineering & Science,* 47**,** 207-217.

NASKAR, K. 2007. Thermoplastic elastomers based on PP/EPDM blends by dynamic vulcanization. *Rubber Chemistry and Technology,* 80**,** 504-519.

NASKAR, K., KOKOT, D. & NOORDERMEER, J. W. M. 2004. Influence of various stabilizers on ageing of dicumyl peroxide-cured polypropylene/ethylene-propylene-diene thermoplastic vulcanizates. *Polymer Degradation and Stability,* 85**,** 831-839.

NASKAR, K. & NOORDERMEER, J. W. 2004. Dynamically Vulcanized PP/EPDM Blends: Multifunctional Peroxides as Crosslinking Agents—Part I. *Rubber chemistry and technology,* 77**,** 955-971.

NHAN, D. D., QUYNH, T. M. & QUY, N. H. 2014. A DSC/TGA STUDY OF THE HETEROGENEOUS NUCLEATION OF CRYSTALLIZATION IN POLYPROPYLENE COPOLYMER. *Vietnam Journal of Chemistry,* 45**,** 652.

NICOLINI, A., DE CAMPOS ROCHA, T. L. Á. & MALDANER JACOBI, M. A. 2008. Dynamically vulcanized PP/EPDM blends: Influence of curing agents on the morphology evolution. *Journal of Applied Polymer Science,* 109**,** 3093-3100.

NING, N., LI, S., WU, H., TIAN, H., YAO, P., HU, G.-H., TIAN, M. & ZHANG, L. 2017. Preparation, microstructure, and microstructure-properties relationship of thermoplastic vulcanizates (TPVs): A review. *Progress in Polymer Science*.

NWABUNMA, D. K., T. 2008. Polyolefin Blends. 474.

O'DONNELL, J. H. & WHITTAKER, A. K. 1985. The radiation crosslinking and scission of ethylene‐propylene copolymers studied by solid‐state nuclear magnetic resonance. *Polymer International,* 17**,** 51-55.

OLIANI, W., PARRA, D., FERMINO, D., RIELLA, H., LIMA, L. & LUGAO, A. 2013. Study of gel formation by ionizing radiation in polypropylene. *Radiation Physics and Chemistry,* 84**,** 20-25.

OLIANI, W. L., PARRA, D. F., LIMA, L. F. C. P., LINCOPAN, N. & LUGAO, A. B. 2015. Development of a nanocomposite of polypropylene with biocide action from silver nanoparticles. *Journal of Applied Polymer Science,* 132**,** n/a-n/a.

OTAGURO, H., DE LIMA, L., PARRA, D., LUGAO, A., CHINELATTO, M. & CANEVAROLO, S. 2010a. High-energy radiation forming chain scission and branching in polypropylene. *Radiation Physics and Chemistry,* 79**,** 318-324.

OTAGURO, H., DE LIMA, L. F. C. P., PARRA, D. F., LUGÃO, A. B., CHINELATTO, M. A. & CANEVAROLO, S. V. 2010b. High-energy radiation forming chain scission and branching in polypropylene. *Radiation Physics and Chemistry,* 79**,** 318-324.

PALZA, H. 2015. Antimicrobial polymers with metal nanoparticles. *International journal of molecular sciences,* 16**,** 2099-2116.

PATERMANN, S. & ALTSTÄDT, V. PP/EPDM-blends by dynamic vulcanization: Influence of increasing peroxide concentration on mechanical, morphological and rheological characteristics. AIP Conference Proceedings, 2014. AIP, 516-519.

PAUL, D. & NEWMAN, S. 1978. Polymer Blends, Vol. 1, Ch. 7. Academic Press, New York.

PHAM, H. 2006. *Springer handbook of engineering statistics*, Springer Science & Business Media.

PISSUWAN, D., CORTIE, C. H., VALENZUELA, S. M. & CORTIE, M. B. 2010. Functionalised gold nanoparticles for controlling pathogenic bacteria. *Trends in biotechnology,* 28**,** 207-213.

PRABHU, S. & POULOSE, E. K. 2012. Silver nanoparticles: mechanism of antimicrobial action, synthesis, medical applications, and toxicity effects. *International Nano Letters,* 2**,** 32.

PRUT, E., MEDINTSEVA, T. & DREVAL, V. Mechanical and Rheological Behavior of Unvulcanized and Dynamically Vulcanized i‐PP/EPDM Blends. Macromolecular symposia, 2006. Wiley Online Library, 78-85.

PRZYBYTNIAK, G., MIRKOWSKI, K., RAFALSKI, A., NOWICKI, A. & KORNACKA, E. 2007. Radiation degradation of blends polypropylene/poly (ethylene-co-vinyl acetate). *Radiation Physics and Chemistry,* 76**,** 1312-1317.

PURNIMA, D., MAITI, S. & GUPTA, A. 2006. Interfacial adhesion through maleic anhydride grafting of EPDM in PP/EPDM blend. *Journal of applied polymer science,* 102**,** 5528-5532.

RADHESHKUMAR, C. & MÜNSTEDT, H. 2006. Antimicrobial polymers from polypropylene/silver composites—Ag+ release measured by anode stripping voltammetry. *Reactive and Functional Polymers,* 66**,** 780-788.

RAI, M. K., DESHMUKH, S. D., INGLE, A. P. & GADE, A. K. 2012. Silver nanoparticles: the powerful nanoweapon against multidrug-resistant bacteria. *Journal of Applied Microbiology,* 112**,** 841-852.

RAMARAD, S., KHALID, M., RATNAM, C., CHUAH, A. L. & RASHMI, W. 2015a. Waste tire rubber in polymer blends: A review on the evolution, properties and future. *Progress in Materials Science,* 72**,** 100-140.

RAMARAD, S., RATNAM, C. T., KHALID, M. & CHUAH, A. L. 2015b. Improving the properties of reclaimed waste tire rubber by blending with poly (ethylene‐co‐vinyl acetate) and electron beam irradiation. *Journal of Applied Polymer Science,* 132.

RAMÍREZ-FUENTES, Y. S., BUCIO, E. & BURILLO, G. 2007. Radiation-induced grafting of N-isopropylacrylamide and acrylic acid onto polypropylene films by two step method. *Nuclear Instruments and Methods in Physics Research Section B: Beam Interactions with Materials and Atoms,* 265**,** 183-186.

RAMÍREZ‐VARGAS, E., NAVARRO‐RODRÍGUEZ, D., HUERTA‐MARTÍNEZ, B., MEDELLÍN‐RODRÍGUEZ, F. & LIN, J. 2000. Morphological and mechanical properties of polypropylene [PP]/poly (ethylene vinyl acetate)[EVA] blends. I. Homopolymer PP/EVA systems. *Polymer Engineering & Science,* 40**,** 2241-2250.

RAMSTEINER, F., MCKEE, G. & BREULMANN, M. 2002. Influence of void formation on impact toughness in rubber modified styrenic-polymers. *Polymer,* 43**,** 5995-6003.

RATNAM, C. T., NASIR, M., BAHARIN, A. & ZAMAN, K. 2000. Electron beam irradiation of epoxidized natural rubber. *Nuclear Instruments and Methods in Physics Research Section B: Beam Interactions with Materials and Atoms,* 171**,** 455-464.

RATNAM, C. T., NASIR, M., BAHARIN, A. & ZAMAN, K. 2001a. Effect of electron‐beam irradiation on poly (vinyl chloride)/epoxidized natural rubber blend: dynamic mechanical analysis. *Polymer international,* 50**,** 503-508.

RATNAM, C. T., NASIR, M., BAHARIN, A. & ZAMAN, K. 2001b. Electron‐beam irradiation of poly (vinyl chloride)/epoxidized natural rubber blends in presence of trimethylolpropane triacrylate. *Journal of Applied Polymer Science,* 81**,** 1926-1935.

RAVISHANKAR RAI, V. & JAMUNA BAI, A. 2011. Nanoparticles and their potential application as antimicrobials. *Science against microbial pathogens: communicating current research and technological advances. FORMATEX***,** 197-209.

RAY CHOWDHURY, S., SHARMA, B. K., MAHANWAR, P. & SARMA, K. S. 2016. Vinyl acetate content and electron beam irradiation directed alteration of structure, morphology, and associated properties of EVA/EPDM blends. *Journal of Applied Polymer Science,* 133**,** n/a-n/a.

REIS, R. & CUNHA, A. 2000. New degradable load-bearing biomaterials composed of reinforced starch based blends. *Journal of applied medical polymers,* 4**,** 1-5.

RIVATON, A., LALANDE, D. & GARDETTE, J.-L. 2004. Influence of the structure on the γ-irradiation of polypropylene and on the post-irradiation effects. *Nuclear Instruments and Methods in Physics Research Section B: Beam Interactions with Materials and Atoms,* 222**,** 187-200.

ROGERS, W. 2012. Sterilisation techniques for polymers. *Sterilisation of Biomaterials and Medical Devices.* Elsevier.

ROSIAK, J., ULANSKI, P. & KADŁUBOWSKI, S. 2005. Emerging Applications of Radiation in Nanotechnology. Conventional and radiation synthesis of polymeric nanoand microgels and their possible applications. The proceeding of a technical meeting. IAEA-TECDOC-1438, 22–25 March, 2005, Bologna, Italy, 99–120.

ROSIAK, J. M. 1998. Gel/sol analysis of irradiated polymers. *Radiation Physics and Chemistry,* 51**,** 13-17.

RUTALA, W. A., WEBER, D. J. & CONTROL, C. F. D. 2008. Guideline for disinfection and sterilization in healthcare facilities, 2008. Centers for Disease Control (US).

SABET, M. & SOLEIMANI, H. The impact of electron beam irradiation on Low density polyethylene and Ethylene vinyl acetate. IOP Conference Series: Materials Science and Engineering, 2017. IOP Publishing, 012005.

SALEHI, S., MIRJALILI, G. & AMROLLAHI, J. 2004. Effects of high‐energy electron beam on low‐density polyethylene materials containing EVA. *Journal of applied polymer science,* 92**,** 1049-1052.

SALIH, S. E., HAMOOD, A. F. & ALSABIH, A. H. 2013. Comparison of the characteristics of LDPE: PP and HDPE: PP polymer blends. *Modern Applied Science,* 7**,** 33.

SALOMONI, R., LÉO, P., MONTEMOR, A., RINALDI, B. & RODRIGUES, M. 2017. Antibacterial effect of silver nanoparticles in Pseudomonas aeruginosa. *Nanotechnology, science and applications,* 10**,** 115.

SAWAI, J., KOJIMA, H., IGARASHI, H., HASHIMOTO, A., SHOJI, S., SAWAKI, T., HAKODA, A., KAWADA, E., KOKUGAN, T. & SHIMIZU, M. 2000. Antibacterial characteristics of magnesium oxide powder. *World Journal of Microbiology and Biotechnology,* 16**,** 187-194.

SCAGLIUSI, S. R., CARDOSO, E. C. L., ZAHARESCU, T. & LUGÃO, A. B. Influence of gamma radiation on EPDM compounds properties for use in nuclear plants. AIP Conference Proceedings, 2016. AIP Publishing, 080015.

SCHREZENMEIER, H., WALTHER‐WENKE, G., MÜLLER, T. H., WEINAUER, F., YOUNIS, A., HOLLAND‐LETZ, T., GEIS, G., ASMUS, J., BAUERFEIND, U. & BURKHART, J. 2007. Bacterial contamination of platelet concentrates: results of a prospective multicenter study comparing pooled whole blood–derived platelets and apheresis platelets. *Transfusion,* 47**,** 644-652.

SCHULZE, D., TRINKLE, S., MÜLHAUPT, R. & FRIEDRICH, C. 2003. Rheological evidence of modifications of polypropylene by β-irradiation. *Rheologica acta,* 42**,** 251-258.

SELLKE, T., BAYARRI, M. & BERGER, J. O. 2001. Calibration of ρ values for testing precise null hypotheses. *The American Statistician,* 55**,** 62-71.

SEN, K. & KUMAR, P. 1995. Influence of gamma‐irradiation on structural and mechanical properties of polypropylene yarn. *Journal of applied polymer science,* 55**,** 857-863.

SEVIL, U. & GÜVEN, O. 1995. Spectroscopic, viscometric and mechanical characterization of γ-irradiated isotactic polypropylene syringes. *Radiation Physics and Chemistry,* 46**,** 875-878.

SHAMSHAD, A. & BASFAR, A. A. 2000. Radiation resistant polypropylene blended with mobilizer,: antioxidants and nucleating agent. *Radiation Physics and Chemistry,* 57**,** 447-450.

SHARIF, J., AZIZ, S. H. S. A. & HASHIM, K. 2000. Radiation effects on LDPE/EVA blends. *Radiation Physics and Chemistry,* 58**,** 191-195.

SHARMA, B. K., CHOWDHURY, S. R., MAHANWAR, P. & SARMA, K. 2014. Influence of electron beam treatment on the crystallization and thermal stability of LDPE/EPDM blends. *American Journal of Engineering and Applied Sciences,* 7**,** 338.

SHARMA, B. K., CHOWDHURY, S. R., MAHANWAR, P. A. & SARMA, K. S. S. 2015. Structure-Property Relationship in Terms of Dynamic Mechanical Properties of High Energy Radiation Treated Industrially Important Thermoplastic Elastomer Blend. *Advances in Materials Physics and Chemistry,* 5**,** 383.

SHIN, J. S., SUSAN EM 2014. Food packaging. *Food Processing: Principles and Applications, Second Edition***,** 249-273.

SHISHIDO, K., MATSUOKA, M., ISHIHARA, N. & TAMURA, M. 2000. Medical bag. Google Patents.

SHRIVASTAVA, S. 2004. *Medical Device Materials: Proceedings from the Materials & Processes for Medical Devices Conference 2003, 8-10 September 2003, Anaheim, California*, ASM International.

SILINDIR, M. & OZER, A. 2009. Sterilization methods and the comparison of E-Beam sterilization with gamma radiation sterilization. *FABAD J Pharm Sci,* 34**,** 43-53.

SILVERSTEIN, R. M., WEBSTER, F. X., KIEMLE, D. J. & BRYCE, D. L. 2014. *Spectrometric identification of organic compounds*, John Wiley & Sons.

SIMMONS, A. 2012. Future trends for the sterilisation of biomaterials and medical devices. *Sterilisation of Biomaterials and Medical Devices***,** 310.

SINGH, A. 2001. Irradiation of polymer blends containing a polyolefin. *Radiation Physics and Chemistry,* 60**,** 453-459.

SIRAJUDDIN, D. & FOSTER, J. E. 2007. Plasma Sterilization.

SONDI, I. & SALOPEK-SONDI, B. 2004. Silver nanoparticles as antimicrobial agent: a case study on E. coli as a model for Gram-negative bacteria. *Journal of colloid and interface science,* 275**,** 177-182.

SONNIER, R., MASSARDIER, V., CLERC, L., LOPEZ-CUESTA, J. M. & BERGERET, A. 2010. Reactive compatibilization of polymer blends by γ-irradiation: Influence of the order of processing steps. *Journal of Applied Polymer Science,* 115**,** 1710-1717.

STARÁ, H., STARÝ, Z. & MÜNSTEDT, H. 2011. Silver Nanoparticles in Blends of Polyethylene and a Superabsorbent Polymer: Morphology and Silver Ion Release. *Macromolecular Materials and Engineering,* 296**,** 423-427.

STELLER, R., ŻUCHOWSKA, D., MEISSNER, W., PAUKSZTA, D. & GARBARCZYK, J. 2006. Crystalline structure of polypropylene in blends with thermoplastic elastomers after electron beam irradiation. *Radiation Physics and Chemistry,* 75**,** 259-267.

STOIMENOV, P. K., KLINGER, R. L., MARCHIN, G. L. & KLABUNDE, K. J. 2002. Metal oxide nanoparticles as bactericidal agents. *Langmuir,* 18**,** 6679-6686.

SUJIT, K., BHOWMICK, A., CHAKI, T., MAJALI, A. & DESPANDE, R. 1996. Electron beam initiated modification of ethylene vinyl acetate using TMPTA. *Polymer,* 37**,** 45-55.

SULJOVRUJIC, E. 2009. The influence of molecular orientation on the crosslinking/oxidative behaviour of iPP exposed to gamma radiation. *European Polymer Journal,* 45**,** 2068-2078.

SULTANA, Y. 2007. Pharmaceutical Microbiology and Biotechnology Sterilization Methods and Principles'. *New Delhi: Jamia Hamdard*.

SVOBODA, P. 2015. Influence of Branching Density in Ethylene-Octene Copolymers on Electron Beam Crosslinkability. *Polymers,* 7**,** 2522-2534.

SYED, M. A., BABAR, S., BHATTI, A. & BOKHARI, H. 2009. Antibacterial effects of silver nanoparticles on the bacterial strains isolated from catheterized urinary tract infection cases. *Journal of biomedical nanotechnology,* 5**,** 209-214.

TAMBYAH, P. A., HALVORSON, K. T. & MAKI, D. G. 1999. A Prospective Study of Pathogenesis of Catheter-Associated Urinary Tract Infections. *Mayo Clinic Proceedings,* 74**,** 131-136.

TANG, L., QU, B. & SHEN, X. 2004. Mechanical properties, morphological structure, and thermal behavior of dynamically photocrosslinked PP/EPDM blends. *Journal of applied polymer science,* 92**,** 3371-3380.

TASHIRO, K., STEIN, R. S. & HSU, S. L. 1992. Cocrystallization and phase segregation of polyethylene blends. I: Thermal and vibratonal spectroscopic study by utilizing the deuteration technique. *Macromolecules,* 25**,** 1801-1808.

THEVY RATNAM, C., RAMARAD, S., SIDDIQUI, M. K., ABIDIN, A. S. Z. & CHUAH, L. T. 2016. Irradiation cross-linking of ethylene vinyl acetate/waste tire dust: Effect of multifunctional acrylates. *Journal of Thermoplastic Composite Materials,* 29**,** 464-478.

THOMAS, S., GUPTA, B. & DE, S. 1987. Mechanical properties, surface morphology and failure mode of γ-ray irradiated blends of polypropylene and ethylene-vinyl acetate rubber. *Polymer degradation and stability,* 18**,** 189-212.

TJONG, S., SHEN, J. & LI, R. 1996. Mechanical behavior of injection molded β - crystalline phase polypropylene. *Polymer Engineering & Science,* 36**,** 100-105.

TJONG, S. C. & BAO, S. 2007. Structure and mechanical behavior of isotactic polypropylene composites filled with silver nanoparticles. *e-Polymers,* 7**,** 1618-1634.

TON-THAT, T. M. & JUNGNICKEL, B. J. 1999. Water diffusion into transcrystalline layers on polypropylene. *Journal of Applied Polymer Science,* 74**,** 3275-3285.

TORRES-GINER, S., OCIO, M. J. & LAGARON, J. M. 2009. Novel antimicrobial ultrathin structures of zein/chitosan blends obtained by electrospinning. *Carbohydrate Polymers,* 77**,** 261-266.

TPEMARKET, R. 2016. Thermoplastic Elastomers (TPE) Market Analysis By Product (Styrenic Block Copolymers (SBC, SBS, SIS, HSBC), Thermoplastic Polyurethanes (TPU), Thermoplastic Polyolefins (TPO), Thermoplastic Vulcanizates (TPV), Copolyester Elastomers (COPE)), By Application (Automotive, Footwear, Construction, Medical, Electronics, Industrial, Advanced Materials) And Segment Forecasts To 2022. *Market Research Report*.

TRIACCA, V., GLOOR, P., ZHU, S., HRYMAK, A. & HAMIELEC, A. 1993. Free radical degradation of polypropylene: random chain scission. *Polymer Engineering & Science,* 33**,** 445-454.

TRIEBEL, C., VASYLYEV, S., DAMM, C., STARA, H., ÖZPıNAR, C., HAUSMANN, S., PEUKERT, W. & MÜNSTEDT, H. 2011. Polyurethane/silver-nanocomposites with enhanced silver ion release using multifunctional invertible polyesters. *Journal of Materials Chemistry,* 21**,** 4377-4383.

UEDA, Y., TANAKA, T., OHNISHI, T. & OKAMOTO, S. Retardation effect of additives on radiation degradation of EPDM. Electrical Insulation and Dielectric Phenomena, 1992. Annual Report. Conference on, 1992. IEEE, 719-724.

URBANIAK-DOMAGALA, W. 2012. *The use of the spectrometric technique FTIR-ATR to examine the polymers surface*, INTECH Open Access Publisher.

VAN DUIN, M. Recent Developments for EPDM‐Based Thermoplastic Vulcanisates. Macromolecular symposia, 2006. Wiley Online Library, 11-16.

VARMA, R. 2007. *New TPEs Provide Material Flexibility* [Online]. Available: https://www.mddionline.com/new-tpes-provide-material-flexibility [Accessed 23/12/17.

VORONOV, A., KOHUT, A. & PEUKERT, W. 2007. Synthesis of Amphiphilic Silver Nanoparticles in Nanoreactors from Invertible Polyester. *Langmuir,* 23**,** 360-363.

WAGNER, J. R. 2016. *Multilayer Flexible Packaging*, Elsevier Science.

WANG, H. & CHEN, W. 2006. Radiation-induced grafting of binary monomers containing HALS onto polypropylene. *Radiation Physics and Chemistry,* 75**,** 138-148.

WANG, L., HU, C. & SHAO, L. 2017. The antimicrobial activity of nanoparticles: present situation and prospects for the future. *International journal of nanomedicine,* 12**,** 1227.

WEI, X., YANG, Z., WANG, Y., TAY, S. L. & GAO, W. 2014. Polymer antimicrobial coatings with embedded fine Cu and Cu salt particles. *Appl Microbiol Biotechnol,* 98**,** 6265-74.

WILSON, V. G. 2014. Growth and differentiation of HaCaT keratinocytes. *Epidermal Cells: Methods and Protocols***,** 33-41.

WOO, L. & SANDFORD, C. L. 2002. Comparison of electron beam irradiation with gamma processing for medical packaging materials. *Radiation Physics and Chemistry,* 63**,** 845-850.

XIAO, H. W., HUANG, S. Q., JIANG, T. & CHENG, S. Y. 2002. Miscibility of blends of ethylene‐propylene‐diene terpolymer and polypropylene. *Journal of applied polymer science,* 83**,** 315-322.

XIE, D.-S., LAI, R.-P. & NIE, S.-F. 2011. Surveys of catheter-associated urinary tract infection in a university hospital intensive care unit in China. *Brazilian Journal of Infectious Diseases,* 15**,** 296-297.

YEO, S. Y. & JEONG, S. H. 2003. Preparation and characterization of polypropylene/silver nanocomposite fibers. *Polymer International,* 52**,** 1053-1057.

YOUSEFI, A. & KATBAB, A. 1994. Post irradiation degradation of polypropylene radiation durability of polypropylene stabilized with phenolic stabilizer (II). *Radiation Physics and Chemistry,* 44**,** 645-649.

ZAHARESCU, T. & BUDRUGEAC, P. 2002. Radiation processing of EPDM/PP blends. *Polymer Bulletin,* 49**,** 297-303.

ZAHARESCU, T., CHIPARĂ, M. & POSTOLACHE, M. 1999. Radiation processing of polyolefin blendsII. Mechanical properties of EPDM-PP blends. *Polymer degradation and stability,* 66**,** 5-8.

ZAHARESCU, T., JIPA, S., SETNESCU, R., SANTOS, C., GIGANTE, B., MIHALCEA, I., PODINĂ, C. & GORGHIU, L.-M. 2002. Thermal stability of additivated isotactic polypropylene. *Polymer Bulletin,* 49**,** 289-296.

ZAHARESCU, T., SETNESCU, R., JIPA, S. & SETNESCU, T. 2000. Radiation processing of polyolefin blends. I. Crosslinking of EPDM–PP blends. *Journal of Applied Polymer Science,* 77**,** 982-987.

ZARANDI, M. B. & BIOKI, H. A. 2013. Thermal and mechanical properties of blends of LDPE and EVA crosslinked by electron beam radiation. *The European Physical Journal-Applied Physics,* 63.

ŻENKIEWICZ, M. & DZWONKOWSKI, J. 2007. Effects of electron radiation and compatibilizers on impact strength of composites of recycled polymers. *Polymer Testing,* 26**,** 903-907.

ZHANG, Z., YU, F., ZHOU, N. & ZHANG, H. 2015. Compatibilization by olefin block copolymer (OBC) in Polypropylene/Ethylene-Propylene-Diene Terpolymer (PP/EPDM) blends. *Journal of Macromolecular Science, Part B,* 54**,** 159-176.

ZHAO, J., YU, P. & DONG, S. 2016. The Influence of Crosslink Density on the Failure Behavior in Amorphous Polymers by Molecular Dynamics Simulations. *Materials,* 9**,** 234.

ZIELIŃSKA, A. J., NOORDERMEER, J. W. M., TALMA, A. G. & VAN DUIN, M. 2011. Di-azides cross-linked, iPP/EPDM-based thermoplastic vulcanizates. *European Polymer Journal,* 47**,** 2311-2320.

ZIMLICHMAN, E., HENDERSON, D., TAMIR, O., FRANZ, C., SONG, P., YAMIN, C. K., KEOHANE, C., DENHAM, C. R. & BATES, D. W. 2013. Health care–associated infections: a meta-analysis of costs and financial impact on the US health care system. *JAMA internal medicine,* 173**,** 2039-2046.

ZOU, K. H., WARFIELD, S. K., BHARATHA, A., TEMPANY, C. M. C., KAUS, M. R., HAKER, S. J., WELLS III, W. M., JOLESZ, F. A. & KIKINIS, R. 2004. Statistical validation of image segmentation quality based on a spatial overlap index1: scientific reports. *Academic Radiology,* 11**,** 178-189.

ZOUTMAN, D. E., FORD, B. D., COMMITTEE, C. H. E. & PROGRAM, C. N. I. S. 2005. The relationship between hospital infection surveillance and control activities and antibiotic-resistant pathogen rates. *American journal of infection control,* 33**,** 1-5.